Author/s:
Nguyen, Thi Hong Hanh

Title:
Characterisation of bromodomain proteins in the malaria parasite Plasmodium falciparum

Date:
2020

Persistent Link:
https://hdl.handle.net/11343/241688

Characterisation of bromodomain proteins in the malaria parasite *Plasmodium falciparum*

Thi Hong Hanh Nguyen

Submitted in total fulfilment of the requirements for the degree of

Doctor of Philosophy

April 2020

Department of Medicine (Royal Melbourne Hospital)

Faculty of Medicine, Dentistry, and Health Sciences

The University of Melbourne

Abstract

Plasmodium falciparum is a protozoan parasite that is responsible for the most severe and fatal form of human malaria. In addition to the canonical histones, the parasite possesses divergent and Apicomplexa-specific histone variants. The N-terminal tails of histones in *P. falciparum* are extensively acetylated and carry unique acetylation marks. *P. falciparum* relies on this network of histone post-translational modifications and interactive, chromatin-associated proteins to modulate its gene expression. Integral to this process are bromodomain (BRD) histone reader proteins which interact with acetylated lysine. The rapid emergence and development of human BRD inhibitors for the treatment of many diseases prompted our project to study *P. falciparum* BRD proteins (PfBDPs) and assess their value as potential, novel, antimalarial therapies.

There are eight bromodomain proteins in *P. falciparum*. *P. falciparum* bromodomain protein 1 (PfBDP1) is critical for the coordinated regulation of invasion genes and is essential for parasite survival. In addition, a *piggyBac* transposon mutagenesis forward-genetic screen in *P. falciparum* showed that PfBDP2, PfGCN5 and PfTAF2 are essential for the parasite during the blood, asexual life cycle. Recent studies showed that PfBDPs can interact with histone acetylations and transcription factors as well as other chromatin-associated proteins to form a network of histone reader complexes.

This thesis investigates the functions of PfBDP4 and PfBDP3 and their importance to parasite survival. Conditional disruption of PfBDP4 caused a growth defect from which an essential role in the blood stage, asexual life cycle was inferred. Chromatin immunoprecipitation sequencing (ChIP-seq) indicated that PfBDP4 was enriched upstream of highly expressed genes, especially genes that are important for parasite invasion. In addition, PfBDP4 shares genomic localisation with an Apicomplexa-specific transcription factor AP2-I and the BRD protein PfBDP1, confirming their interaction in a complex as observed in previous studies. PfBDP4 was also enriched upstream of genes that are involved in metabolic pathways such as proteolysis and phosphorylation which demonstrates that PfBDP4 likely regulates multiple critical pathways of the parasite. In contrast, parasite growth was not inhibited by knockdown of PfBDP3, which is consistent with previous studies. In trophozoites, PfBDP3 was enriched in heterochromatin or compact chromatin, where genes are generally silenced. As PfBDP3 has two BRDs, PfBDP3 may act as a scaffold for proteins that are associated with heterochromatin.

Finally, hit compounds from collaborators biochemical screens of recombinant PfBDP BRDs were tested for *P. falciparum in vitro* growth inhibition. Potent hit compounds were identified. These confirmed hits should now be tested for specificity and selectivity to confirm that they are acting on-target and do not cause cytotoxic effects in human cells.

Overall, this study showed that PfBDP4 is associated with active promoters of select processes and its BRD is essential for the parasite survival while PfBDP3 is associated with heterochromatin and is non-essential during the asexual life cycle. This work also highlighted PfBDPs as novel drug targets in *P. falciparum* and demonstrated the feasibility of identifying potent PfBDP inhibitors as candidates for future investigation.

Declaration

This is to certify that:

i. the thesis comprises of on my original work towards the PhD except where indicated in the Preface,
ii. due acknowledgement has been made in the text to all other material used,
iii. the thesis is fewer than 100 000 words in length, exclusive of tables, maps, bibliographies and appendices.

Preface

I duly acknowledge the work and assistance of others which contributed to the completion of this thesis.

Chapter 1.4 in the Introduction is a published review article which I have written

- Nguyen, H.H.T., Yeoh, L.M., Chisholm, S.A., and Duffy, M.F. (2020). Developments in drug design strategies for bromodomain protein inhibitors to target *Plasmodium falciparum* parasites. Expert Opinion on Drug Discovery 15, 415-425.

Dr. Lee Yeoh generated the 3D7-PfBDP4-*loxP-glmS* parasite line from the 3D7 DiCre parental parasite line, which was a gift from Professor Alan Cowman laboratory. The 3D7-PfBDP4-*loxP-glmS* parasite line was used to study the essentiality of PfBDP4 in Chapter 4.

Dr. Michaela Petter, Dr. Gabrielle Josling and Dr. Jingyi Tang generated the Ty-tagged parasite lines that were used to determine protein localisation and ChIP-seq in Chapter 5.

Dr Danny Wilson gifted us the CS2-GFP parasite line which was used for the *in vitro* growth inhibition assay in Chapter 6.

Acknowledgement

First and foremost, I would like to thank my supervisor, Dr. Michael Duffy, for allowing me to join his lab. None of this would have been possible without his guidance and encouragement in the six years I have spent in his laboratory and I am extremely grateful for his support and understanding during my personally difficult times.

I would like to acknowledge my co-supervisor Dr. Michaela Petter who has helped me overcome many challenges during my candidature. Her dedication and creativity have been inspiring, and I am truly privileged to have had her as a mentor. I would like to thank my external committee members, Professor Stephen Rogerson and Dr. Darren Creek, who have been very supportive over the past years.

I would also like to thank Dr. Lee Yeoh and Dr. Scott Chisholm. Their mentorship and friendship have helped me navigate through my experiments and tough times in the lab when nothing seems to work. Furthermore, it has been such a joy to work with members of the Day/Duffy group, especially my dear friends Dr. Evelyn Chou, Dr. Jingyi Tang and Mohd Suffian Azizan.

I am very grateful for my partner, Michael Ho, who has been extremely patient, supportive and a source of comfort when I need to get away from it all. His positivity constantly motivates me to keep moving forward.

Last but not least, to my Mum, Dad, Sister, Jarred and Alexie, your love has gotten me through everything, and I love you all very dearly. I am forever indebted to my dad who taught me to always be inquisitive and persistent. My mum and dad sacrificed everything they had to give me a better education and a better future. This is possible because of you.

Contents

List of Figures

List of Tables

List of abbreviations

% (v/v)	percent volume per volume
% (w/v)	percent weight per volume
5mC	cytosine methylation
ACT	artemisinin combination therapy
AlphaScreen	Amplified Luminescent Proximity Homogenous Assay Screen
AMA1	apical membrane antigen 1
ApiAP2	apicomplexan apetala 2
aslncRNA	antisense long non-coding RNA
ATAC-seq	Assay for Transposase-Accessible Chromatin by sequencing
BDF	bromodomain factors
BET	bromo- and extra-terminal domain
BRD	bromodomain
BSA	bovine serum albumin
$CaCl_2$	calcium chloride
CDS	coding sequence
ChIP	chromatin immunoprecipitation
CM	cerebral malaria
CRISPR	clustered regularly interspaced short palindromic repeats
DAPI	4′,6-diamidino-2-phenylindole

DHFR	dihydrofolate reductase
DiCre	dimerisable Cre recombinase
DMSO	dimethyl sulphoxide
DNA	Deoxyribonucleic acid
dNTP	deoxynucleotide triphosphates
DSF	differential scanning fluorimetry
DTT	dithiothreitol
EBL	erythrocyte binding-like ligand
EDTA	ethylenediaminetetraacetic acid
EGTA	egtazic acid
FRET	Förster/fluorescence resonance energy transfer
gDNA	genomic DNA
GFP	green fluorescent protein
GlcN	glucosamine
glmS	glucosamine-6-phosphate activated ribozyme
GO	gene ontology
GTF	general transcription factors
HA	hemagglutinin
HAT/KAT	histone/lysine acetyltransferase
HDAC	histone deacetylase

HEPES	4-(2-hydroxyethyl)-1-piperazineethanesulfonic acid
HKMT	histone lysine methyltransferase
HMGB	high mobility group box
HP1	heterochromatin protein 1
hpi	hours post invasion
HRP	horse radish peroxidase
HSP	heat shock protein
IC_{50}	half-masimal growth inhibition concentration
IDC	intraerythrocyte cycle
IE	infected erythrocyte
iRBC	infected red blood cell
IFA	immunofluorescence assay
JmJC	Jumonji domain-containing histone demethylase
kb	kilobase
kDa	kilo Dalton
KCl	potassium chloride
KO	knockout
KU	Kunitz units
LSD	lysine-specific demethylase
LysoPC	lysophosphatidylcholine

M	molar
mg	milligram
mL	millilitre
mM	millimolar
µg	microgram
µL	microlitre
µM	micromolar
Mnase	micrococcal nuclease
mRNA	messenger RNA
MSP	merozoite surface protein
MSPDBL	MSP Duffy-binding-like
$NaHCO_3$	sodium bicarbonate
NAP	nucleosome remodelling factors
ncRNA	non-coding RNA
PAGE	polyacrylamide gel electrophoresis
PAM	protospacer adjacent motif
PBS	phosphate-buffered saline
PCR	polymerase chain reaction
PDB	protein data bank
Pf	*Plamodium falciparum*

PfBDP	*P. falciparum* bromodomain protein
PfEMP1	*P. falciparum* erythrocyte membrane protein 1
PHD	plant homeodomain
PIC	pre-initiation complex
PKG	cGMP-dependent protein kinase
Plk1	polo-like kinase 1
PRMT	protein arginine methyltransferase
PTEX	Plasmodium translocon of exported proteins
PTM	post-translational modification
PV	parasitophorous vacuole
PVM	parasitophorous vacuole membrane
qPCR	quantitative polymerase chain reaction
qRT-PCR	quantitative reverse transcriptase PCR
RBC	red blood cell
RDT	rapid diagnostic test
Rh	reticulocyte binding-like homolog proteins
RhopH	high molecular weight rhoptry protein
RIF	repetitive interspersed families of polypeptides
RNA	Ribonucleic acid
RNAP	RNA polymerase

RON	rhoptry neck protein
RPMI	Roswell Park Memorial Institute
rRNA	ribosomal RNA
RT	room temperature
RUVBL3	RuvB-like protein 3
SBP1	skeleton-binding protein 1
SDS	sodium dodecyl sulphate
SEM	standard error of mean
SERA	serine-rich antigen
SGC	the Structural Genomic Consortium
SIP2	SPE2-interacting protein 2
Sir2	sirtuin enzyme
STEVOR	subtelomeric variant open reading frame
STF	specific transcription factor
SUB	subtilisin-like protein
TAF	TBP-associated factor
TBP	TATA-binding protein
TBS	Tris-buffered saline
TBS-T	Tris-buffered saline with 0.05% Tween
TE	Tris-EDTA buffer

TFIIA/B/D/E/F/H	transcription factor II A/B/D/E/F/H
TSS	transcription start site
WHO	the World Health Organisation
X-linked	crosslinked

1. Introduction

1.1. Malaria

Malaria remains one of the major infectious diseases of the world despite much effort since the initiation of the malaria eradication program more than 60 years ago. According to the World malaria report 2019, there were approximately 228 million malaria cases and 405 000 deaths globally in 2018. Around 213 million cases occurred in sub-Saharan Africa and the most vulnerable group is children aged under 5 years who accounted for 67% of malaria deaths worldwide (WHO, 2019).

Malaria is caused by *Plasmodium* parasites, which belong to the Apicomplexa phylum. The Apicomplexa consists of a large number of parasitic protists of human and veterinary importance such as *Toxoplasma*, *Theileria*, *Cyclospora* and *Eimeria*. The six known parasite species that cause malaria in humans are *Plasmodium falciparum*, *P. vivax*, *P. malariae*, *P. ovale* as well as the simian species *P. knowlesi* and *P. simium*, which were found to infect humans in some forested areas (Brasil et al., 2017; Singh and Daneshvar, 2013). Among these, *P. falciparum* is responsible for the highest number of mortalities. After initial infection, the incubation time of *P. falciparum* varies from 9 to 30 days before clinical symptoms appear. Malaria clinical symptoms include fever, headache, dizziness, anorexia, nausea and chills (Bartoloni and Zammarchi, 2012). *P. falciparum* infection can lead to severe malaria with multiple serious clinical manifestations such as severe anaemia, cerebral malaria, renal failure, acute respiratory distress syndrome, jaundice and placental malaria (reviewed in (Beeson and Brown, 2002)).

During the 2000s, the global mortality rate of malaria dropped significantly. However, in recent years between 2014 and 2018, the rate of decrease in global malaria cases has diminished indicating that the progress in controlling malaria is stalling. Furthermore, the world is also facing the problem of parasites that are resistant to the current first-line treatment for malaria in many regions in the world – artemisinin combination therapy (ACT). Drug resistance is a recurring issue for malaria as Chloroquine resistance was first recorded during the late 1950s and early 1960s in areas of South-east Asia and has spread globally since then. Resistance to other drugs, including sulfadoxine/pyrimethamine and mefloquine, was also reported (Roper et al., 2004; Wongsrichanalai et al., 2002) leaving the world with limited options for antimalarials. In addition, the malaria rapid diagnostic test (RDT) relies on the detection of histidine-rich proteins. Recently, there have been reports of deletion of *hrp2* and *hrp3* in

parasites which can result in false negative tests (Berhane et al., 2017; Koita et al., 2012; Thomson et al., 2019). Therefore, in order to achieve the goal of global malaria eradication, there is a need for an efficacious vaccine, rapid and accurate diagnostic tools and novel antimalarial therapies to reduce infection by targeting blood stage parasites and to prevent transmission.

1.2. The life cycle of *Plasmodium falciparum*

The *P. falciparum* life cycle is complicated and involves a human host and a female *Anopheles* mosquito vector (figure 1.1). The infection starts when a female *Anopheles* mosquito carrying *P. falciparum* parasites bites a human during a blood meal. Sporozoites enter the bloodstream and travel to the liver where they traverse through several hepatocytes before invading a hepatocyte to establish asexual replication or schizogony. After around 5 days, the liver stage merozoites are released into the bloodstream leading to the intraerythrocytic developmental cycle (IDC) where parasite asexual reproduction occurs approximately every 48 hours (figure 1.1) (Bartoloni and Zammarchi, 2012). Inside the red blood cell (RBC), the parasite becomes a ring stage before maturing into trophozoite and schizont stages. Finally, the infected erythrocyte (IE) ruptures, releasing merozoites, which can infect new RBCs. This blood phase is associated with all of the malaria symptoms. To survive inside different hosts, the parasite possesses invasion pathways (Cowman et al., 2017) and families of clonally variant surface antigen genes (Kraemer and Smith, 2003) and nutrient transporters (Cortés et al., 2007; Mira-Martínez et al., 2013; Nguitragool et al., 2011; Pillai et al., 2012). By epigenetic mechanisms, the parasites heritably switch expression between gene family members to generate phenotypic variation between clonal progeny. This bet-hedging strategy enables parasite survival in human host environments that can vary in available erythrocyte invasion receptors, existing immunity and available nutrients.

For transmission between hosts, some parasites exit the IDC and differentiate into sexual forms called gametocytes. The development of gametocytes lasts between 9 to 12 days before they are taken up by a female *Anopheles* mosquito during a blood meal. In the mosquito midgut, the gametocytes develop into male and female gametes followed by fertilisation to form a zygote that develops into a motile ookinete within approximately 20 hours. The ookinetes cross the midgut epithelial layer and form oocysts, which produce sporozoites. After around 2 weeks, mature sporozoites are released from the oocysts and travel to the salivary gland to infect humans during the next blood meal (Aly et al., 2009; Bennink et al., 2016; Ghosh and Jacobs-Lorena, 2009; Han et al., 2000; Jin et al., 2007).

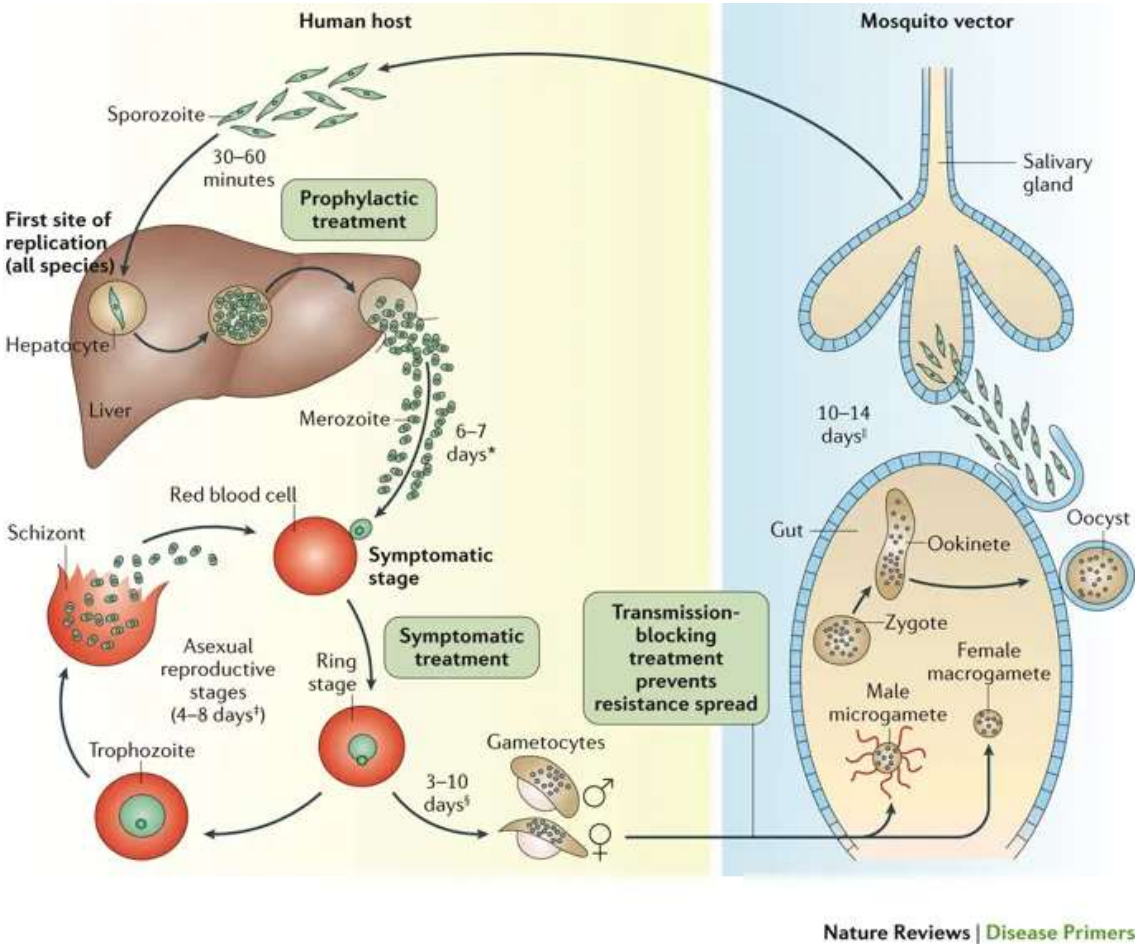

Figure 1.1 *Plasmodium falciparum* life cycle in human and mosquito (figure obtained from (Phillips et al., 2017), license number 4804060101021) showing the liver and intra-erythrocytic (asexual) cycles as well as gametocytes (sexual forms) and mosquito stages.

1.2.1. Invasion and egress of the IDC

Invasion and egress of erythrocytes are critical processes that allow the parasite to maintain infection of the human host during the IDC. RBC invasion allows the parasite to establish an infection. The initial and low affinity interaction between a merozoite and the erythrocyte surface is mediated by proteins on the surface of the merozoites (MSPs) (Cowman and Crabb, 2006; Goel et al., 2003). Subsequently, the merozoite reorientates such that its apex is in contact with the erythrocyte membrane. During this stage, the parasite has direct and high affinity interactions with receptors on the host cell membrane (Tham et al., 2012). After that, the parasite inserts a protein complex into the host membrane to form a 'tight junction' before penetrating using an actin-myosin motor (Farrow et al., 2011; Keeley and Soldati, 2004; Shen

and Sibley, 2012). As the parasite penetrates the host erythrocyte, many proteins on the surface on the merozoite are shed (Harris et al., 2005). Finally, the membrane of the host cell envelops the parasite creating a parasitophorous vacuole membrane (PVM) (Weiss et al., 2015).

Many proteins and complexes are responsible for the modulation of this brief but precise invasion process that is essential for the survival of the malaria parasite. MSPs are abundant on the merozoite surface coat and are shed when the parasite enters the erythrocyte (Harris et al., 2005). There is interest in using these surface antigens as vaccine candidates as they are exposed to the human immune system (Blank et al., 2020; Ogutu et al., 2009; Sheehy et al., 2012). There are many family members of MSPs including MSP1 to MSP9. In particular, MSP1 forms a complex with MSP3, MSP6, MSP7 and MSPDBL1 and -2 (MSP Duffy-binding-like) (Kauth et al., 2006; Lin et al., 2016b; Lin et al., 2014; Pachebat et al., 2001; Stafford et al., 1996; Trucco et al., 2001), which interacts with the surface of human erythrocyte during the initial stage of invasion (Lin et al., 2016b). Merozoite invasion can be inhibited by human antibodies against MSP1 and MSP2 (Boyle et al., 2015). However, recent evidence shows that merozoites lacking MSP1 can still successfully invade RBC indicating that MSP1 may not be required for invasion (Das et al., 2015).

Like other apicomplexans, *P. falciparum* merozoites has specific secretory organelles (micronemes and rhopstries) in its apical complex which helps the parasite orientate, attach and invade the host cell (figure 1.2). The erythrocyte binding-like antigens/ligands (EBAs/EBLs) and the reticulocyte binding-like homolog proteins (Rhs) are two gene families that are important in the next phase of invasion for the high affinity interaction between the apical tip of merozoites and the surface of host RBC. Intracellular signalling that involves fluctuation of cytoplasmic calcium (Gao et al., 2013; Singh et al., 2010) possibly lead to the release of micronemal proteins such as EBA175 onto the surface of the merozoite (Singh et al., 2010). Each member of the EBA and Rh families displays affinity towards different host receptors on the surface of the RBC (figure 1.2), which allows the parasite to use redundant pathways to invade the RBC (DeSimone et al., 2009; Duraisingh et al., 2003; Lopaticki et al., 2011; Stubbs et al., 2005). Following the tight attachment of merozoites, the content of the rhoptries is released into the RBC to assist the 'tight junction' formation and penetration. Central to this process are the apical membrane antigen 1 (AMA-1) and the rhoptry neck protein (RON) (Alexander et al., 2006; Besteiro et al., 2011; Riglar et al., 2011; Tonkin et al., 2011).

Egress is the process in which an IE ruptures and releases merozoites into the bloodstream. The regulation of egress is highly accurate to ensure the timely release of merozoites (Collins et al., 2017; Collins et al., 2013b; Raj et al., 2014). Central to this process is the proteolytic activity of the parasite in the minutes prior to egress (Blackman, 2008), as protease inhibitors can successfully disrupt egress (Wickham et al., 2003). *P. falciparum* has four secreted subtilisin-like proteins (SUBs) and SUB-1 is the most studied member (Collins et al., 2013b; Suarez et al., 2013; Tawk et al., 2013; Thomas et al., 2018; Withers-Martinez et al., 2012). SUB-1 is released into the lumen of the parasitophorous vacuole (PV) through the activation of a parasite cGMP-dependent protein kinase (PKG) (Collins et al., 2013b). Here, SUB-1 is responsible for cleaving soluble parasite proteins including members of the serine-rich antigen (SERA) family as well as the MSPs (Agarwal et al., 2013; Koussis et al., 2009; Ruecker et al., 2012; Yeoh et al., 2007). The function of SUB-1 is essential for the parasite as indicated by previous gene disruption, mutagenesis and inhibition studies (Collins et al., 2017; Das et al., 2015; Tarr et al., 2020; Thomas et al., 2018). The SUB-1 protein cleaves and activates SERA-4, -5 and -6 proteins prior to egress (Collins et al., 2017; Ruecker et al., 2012; Thomas et al., 2018). Previously, functional studies showed that disruption of SERA-5 and -6 was detrimental for parasite growth (Collins et al., 2017; Ruecker et al., 2012). SERA-5 plays key roles in regulating the timely rupture of the RBC as disruption of SERA-5 caused impaired egress by accelerating schizont rupture (Collins et al., 2017).

Other proteins from the rhoptry bulb are released after invasion including the high molecular weight rhoptry proteins (RhopHs). There are three members of RhopHs, which are RhopH1, RhopH2 and RhopH3 that forms a complex that is inserted into the PVM after the parasite invasion (Ling et al., 2004; Sam-Yellowe et al., 1995). The RhopH complex is responsible for nutrients uptake and is critical for parasite survival (Nguitragool et al., 2011; Sherling et al., 2017). RhopH3 is required for the correct localisation of RhopH1 and RhopH2 and therefore is important for the formation of the RhopH complex (Sherling et al., 2017). The RhopH1 or Clag3 protein is encoded by a multigene family that is mutually exclusively expressed via epigenetic regulation (Chung et al., 2007; Comeaux et al., 2011; Cortés et al., 2007).

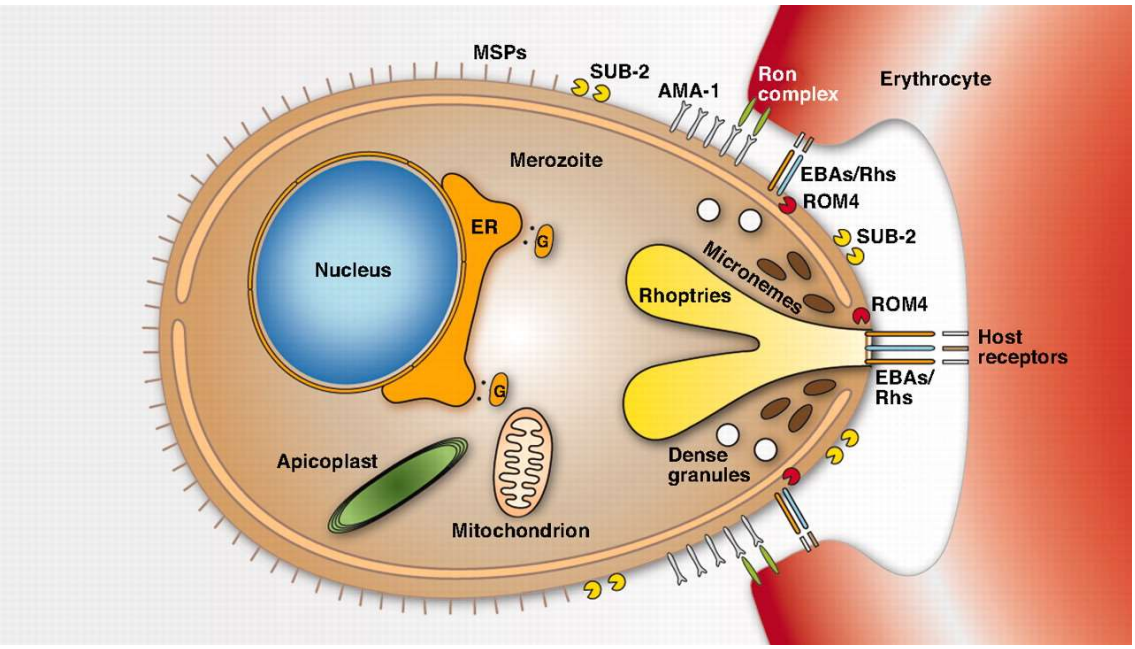

Figure 1.2 Merozoite attaching to the RBC (sourced from (Kappe et al., 2010), licence 4804040802380). Merozoite organelles and proteins on the surface of the merozoite are depicted in the figure.

1.2.2. Cytoadhesion and antigenic variation

A hallmark of *P. falciparum* pathogenesis is the parasite's ability to sequester in the microvasculature, which can lead to many clinical signs and symptoms, some of which are severe (Idro et al., 2010; Rogerson et al., 2007). As the parasite matures into a trophozoite, variant surface antigens are expressed on the surface of the IEs that allow the parasite to adhere to various host receptors expressed on the endothelial layer of the blood vessels (reviewed in (Beeson and Brown, 2002; Rowe et al., 2009)). The immunodominant, parasite, variant surface antigen expressed on the surface of the IE is the *P. falciparum* erythrocyte membrane protein 1 (PfEMP1) (Chan et al., 2012). PfEMP1 is responsible for the cytadhesion of *P. falciparum* IEs (Baruch et al., 1995; Smith et al., 1995; Su et al., 1995).

PfEMP1 is encoded by the diverse *var* multigene family with each parasite possessing approximately 60 members. The expression of *var* genes is mutually exclusive meaning that only one *var* gene is expressed at a given time (Biggs et al., 1991; Scherf et al., 1998) and the parasite can switch the expression of *var* gene to a different variant to evade the host immune

system and maintain chronic infections (Dzikowski et al., 2006; Voss et al., 2006). The expression of *var* genes is discussed in more detail in chapter 1.3.2.7. *Var* genes are classified by their promoter and orientation with the subgroups named UpsA, UpsB, UpsC and UpsE (Lavstsen et al., 2003) and conserved domain cassettes (Rask et al., 2010). They are found in regions where chromatin is compact (heterochromatin) at the subtelomeric regions (UpsA and UpsB) and certain intrachromosomal regions (UpsC). The expression of PfEMP1 on the surface of the IE allows mature parasites to sequester away from the peripheral circulation and thus avoid splenic clearance. Parasite sequestration in vital organs, such as the brain or lungs can lead to serious and fatal outcomes (Brewster et al., 1990; Miller et al., 2013; Newton and Krishna, 1998; Newton et al., 1997; Rogerson et al., 2007). For example, cerebral malaria is most deadly in young children aged between 1 and 4 and can lead to impaired consciousness, coma and long-term sequelae (Brewster et al., 1990; Idro et al., 2006; Idro et al., 2010; Newton and Krishna, 1998). Parasites can also sequester in the placenta impairing foetal development and causing infant mortality. Thus, the parasite has evolved a sophisticated strategy to alter exposed cytoadhesins to survive the immune system of the host.

1.3. Gene regulation in *P. falciparum*

Gene transcription of *P. falciparum* is tightly regulated with around 60% of the genes cyclically activated and silenced in a continuous transcriptional cascade during the asexual blood stage (Bozdech et al., 2003). Recently, single-cell RNA-seq suggested that for a subset of genes this transition is more abrupt with simultaneous activation in trophozoites (Reid et al., 2018). Regardless of timing, a sophisticated underlying network of regulatory mechanisms is required to achieve such a highly ordered and stage-specific pattern of gene transcription. This chapter will discuss the different mechanisms that the malaria parasite uses to regulate its gene expression.

1.3.1. Transcriptional regulation in *P. falciparum*

The *P. falciparum* genome consists of 80% AT in coding sequences and > 90% AT in intergenic regions (Gardner et al., 2002). Identification of conserved general transcription factors in *P. falciparum* was challenging, possibly due to the evolutionary divergence of the parasite from yeast and metazoans as well as its AT-rich genome. As a result, different approaches of sequence analysis were employed to identify conserved transcription factors in *P. falciparum* (Callebaut et al., 2005; Coulson and Ouzounis, 2003).

1.3.1.1. Basal transcription machinery and general transcription factor

In eukaryotes, transcription requires the assembly of the pre-initiation complex (PIC), which consist of the RNA polymerase (RNAP) and general transcription factors (GTFs), at the promoter region 5' upstream of the transcriptional start site (Lanzer et al., 1992). RNAP II is responsible for the transcription of genes into messenger RNA; GTFs are required to stabilise and correctly position RNAPII for the initiation of transcription (Woychik and Hampsey, 2002). The assembly of the PIC starts with the interaction between the RNAP II, transcription factor II D (TFIID), TFIIA and TFIIB and the DNA at the promoter region. After that, TFIIE and TFIIH are recruited to the PIC via the binding of TFIIF to TFIIB and a subunit of the TFIID (Woychik and Hampsey, 2002).

The TFIID is comprised of the TATA-binding protein (TBP), which makes direct contact with the TATA box, and the TBP-associated factors (TAFs) (Chen and Hampsey, 2002). The metazoan TAFII250 subunit of TFIID contains two bromodomains at its C-terminal end that can recognise acetylated lysines on histones (Jacobson et al., 2000) while these features are absent in the *Saccharomyces cerevisiae* orthologue TAF145 (Matangkasombut et al., 2000). Instead, there are two bromodomain proteins (BDF1 and BDF2) in *S. cerevisiae,* which fulfil the function of the missing domains, and have other roles that are independent of the TFIID (García-Oliver et al., 2017; Matangkasombut et al., 2000; Sanders et al., 2002). Some redundancy was observed for these two proteins, as only one of the BDFs is required for the survival of *S. cerevisiae*. These proteins localise to different locations of the genome of *S. cerevisiae*, but BDF2 can compensate for the loss of BDF1 (Fu et al., 2013; Liu et al., 2007).

In *P. falciparum*, the RNAP I, II, III (Fox et al., 1993; Li et al., 1989; Li et al., 1991) as well as many GTFs and their components were identified by various approaches of DNA and protein sequence analysis (Aravind et al., 2003; Bischoff and Vaquero, 2010; Callebaut et al., 2005; Coulson and Ouzounis, 2003). Of particular relevance to the study of bromodomains is the *P. falciparum* TAF1, which is a homologue of the metazoan TAF250 within the TFIID complex (Callebaut et al., 2005). Like TAF250, PfTAF1 has a C-terminal bromodomain (Callebaut et al., 2005). There are conflicting reports regarding PfTAF1 essentiality during the blood asexual life cycle which will be discussed in greater details in section 1.4.

During the IDC, Gopalakrishnan et al. showed that components of the PIC were enriched upstream of a few tested genes regardless of whether the cognate gene was transcribed in the asexual blood stage (Gopalakrishnan et al., 2009). Therefore, although many components of the basal transcription machinery were identified in *P. falciparum*, differing temporal activation of subsets of genes requires other mechanisms.

1.3.1.2. Specific transcription factor in *P. falciparum*

The identification of specific transcription factors (STFs) in *P. falciparum* was more challenging than the basal transcription machinery. Between *Plasmodium* species, transcription factors evolved more rapidly than other processes such as invasion or mRNA decay and processing (Essien et al., 2008). In addition, the evolution of eukaryotic STFs is lineage-specific (Coulson and Ouzounis, 2003; de Mendoza et al., 2013; Iyer et al., 2008; Lespinet et al., 2002; Nowick and Stubbs, 2010) and many eukaryotic STF domains are not detected in apicomplexans (Aravind et al., 2003; Coulson and Ouzounis, 2003; Templeton et al., 2004).

1.3.1.2.1. ApiAP2 – the Apicomplexa-specific STF

Although early attempts to identify orthologues of STFs from model organisms were not very successful in the evolutionary divergent *Plasmodium* (Hedges, 2002), a family of apicomplexan Apetala 2 (ApiAP2) proteins was identified (Balaji et al., 2005). These ApiAP2 proteins have at least one AP2 domain and can recognise one or multiple specific DNA motifs, which are commonly found 5' upstream of the genes that they regulate (Campbell et al., 2010; De Silva et al., 2008). Additionally, their expression is stage-specific and matches well with the observed transcriptional transition between developmental stages (Bozdech et al., 2003).

Multiples studies have now shown that different ApiAP2 STFs regulate different guilds of proteins that are required for transition between stages and/or survival of specific stages. AP2-I regulates gene expression during the asexual stage and is critical for parasite survival (Modrzynska et al., 2017; Santos et al., 2017; Zhang et al., 2018). In *P. falciparum*, AP2-I is enriched in the promoters of a subset of invasion genes including members of the *msp*, *rap* and *rhopH* gene families (Santos et al., 2017). While the same DNA binding motif was predicted for both AP2-I and another AP2 protein – SIP2 (Campbell et al., 2010), ChIP-sequencing analysis showed that these proteins are enriched at different regions in the genome suggesting that there might be interactive partners or surrounding components that also determine the positioning of these ApiAP2 proteins. An interactive partner protein of AP2-I is *P. falciparum* bromodomain protein 1 (PfBDP1) (Hoeijmakers et al., 2019; Josling et al., 2015; Santos et al.,

2017) and together they regulate the transcription of invasion genes. It was shown that in the absence of PfBDP1, AP2-I can still recognise the target DNA (Santos et al., 2017), suggesting that AP2-I positioning is not dependent on PfBDP1 although both proteins are required for normal parasite invasion during the asexual stage (Josling et al., 2015; Santos et al., 2017).

In *Plasmodium* parasites, the production of sexual forms (gametocytogenesis) is critical for viable transmission and only a small proportion of the parasite population commits to become gametocytes (Taylor and Read, 1997). The processes that determine the decision of sexual commitment remain mostly unclear although there is evidence showing that the parasite can sense and respond to external stimuli to regulate sexual conversion (Brancucci et al., 2015; Brancucci et al., 2017). The regulation of gametocytogenesis is better understood with the recent identification of AP2-G as the master regulator of gametocyte production in multiple *Plasmodium* species (Kafsack et al., 2014; Sinha et al., 2014). Transcription of AP2-G leads to a downstream cascade of gametocyte-specific gene transcription (Poran et al., 2017) while disruption of AP2-G completely abolished the parasite's ability to produce gametocytes indicating that AP2-G is crucial for gametocytogenesis (Modrzynska et al., 2017). An additional ApiAP2 protein called AP2-G2 is important for the formation of mature gametocytes (Modrzynska et al., 2017; Yuda et al., 2015) but does not affect sexual commitment, early gametocyte formation or sex differentiation (Modrzynska et al., 2017; Yuda et al., 2015). Interestingly, AP2-G2 may function as a repressor, as AP2-G2 is enriched upstream of silent genes which are only expressed in other non-erythrocytic stages (Yuda et al., 2015).

ApiAP2 proteins also regulate mosquito and exoerythrocytic forms. AP2-O, AP2-O2, AP2-O3 and AP2-O4 are crucial for the normal development of *P. berghei* ANKA strain ookinetes and oocysts in the mosquito midgut (Kaneko et al., 2015; Yuda et al., 2009). In addition, AP2-SP, AP2-SP2 and AP2-SP3 are essential for sporogony (Modrzynska et al., 2017; Yuda et al., 2010) and one ApiAP2 protein (AP2-L) is important for liver stage maturation (Iwanaga et al., 2012). Disruption of any of these genes led to significant defect at various stages during the development of ookinete, oocyst, sporozoite and liver stage (Modrzynska et al., 2017) highlighting their importance to the parasite biology. Interestingly, AP2-L is also expressed during the trophozoite stage in *P. berghei*, and during late ring and early trophozoite stages in *P. falciparum* (Lopez-Barragan et al., 2011; Otto et al., 2010) but is dispensable for asexual blood stage parasites. While the function of AP2-L during the asexual stage is unclear, this observation suggests that it may be redundant during the asexual stage, and that one ApiAP2 protein may have more than one regulatory function. In addition to acting as specific

transcription factors, members of the ApiAP2 family are also implicated in telomere maintenance and have been suggested to regulate the expression of RIF and STEVOR multigene families expressed in asexual blood stage parasites (Flueck et al., 2010; Martins et al., 2017; Sierra-Miranda et al., 2017). Overall, these studies emphasise the important and diverse processes in different life stages of the parasite that are regulated by ApiAP2 proteins.

1.3.1.2.2. Other STFs in *P. falciparum*

A few other STFs were also identified in *Plasmodium* including the helix-turn-helix protein Myb1 and two high mobility group box (HMGB) proteins (Boschet et al., 2004; Briquet et al., 2006). Disruption of Myb1 led to dysregulation of gene expression and Myb1 is enriched upstream of genes that are directly involved in chromatin structure and transcription regulation such as histone 3, histone 2A, TBP as well as proliferating cell nuclear antigen (Gissot et al., 2005). The HMGB proteins can bind and induce bending of DNA, which is presumed to allow recruitment of the PIC to the promoter region (Briquet et al., 2006; Gissot et al., 2008). In humans, HMGB proteins can be released from a variety of cell types (Andersson et al., 2000; Wang et al., 1999a; Wang et al., 1999b) and interact with receptors on the cell surface as well as stimulate the release of many other pro-inflammatory cytokines (Andersson et al., 2002; Andersson et al., 2000; Li et al., 2003; Yang et al., 2005). Interestingly, like the human HMGB protein, the release of *P. falciparum* HMGB 1 and 2 can also induce pro-inflammatory cytokines (Kumar et al., 2008) and is associated with cerebral malaria in mice (Briquet et al., 2015) and severe malaria in clinical patients (Angeletti et al., 2013; Higgins et al., 2013).

1.3.2. Epigenetic regulation in *P. falciparum*

In addition to the use of specific transcription factors, the malaria parasite heavily depends on epigenetic mechanisms to regulate its gene expression. This section will review the epigenetic processes that *P. falciparum* uses and how the parasite utilises these processes to regulate vital pathways.

Epigenetic regulation refers to heritable modulations of gene expression that are caused by changes in the chromatin structure and its associated proteins without alteration of the DNA sequence (Berger et al., 2009). For the particular discussion of gene regulation in *P. falciparum*, this work is extending the classical developmental definition of epigenetic regulation to encompass that component of cyclical gene regulation that occurs in every IDC of the parasite that is mediated by chromatin structure rather than by TFs.

In eukaryotes, cytosine methylation (5mC) is a major epigenetic mechanism that regulates gene expression by acting as a gene transcription repressive mark at the gene promoters (Hashimoto et al., 2015). Indeed, CpG methylation is well-studied in human for its role in cancer biology (Kulis and Esteller, 2010). Thus far, very little evidence of DNA methylation was found in *Plasmodium* species, which is possibly due to the high A-T content of their genomes. Low levels of non-CG methylation have been demonstrated in *P. falciparum* (Ponts et al., 2013) and *P. berghei* (McInroy et al., 2016) and one functional DNA methyltransferase was identified in *P. falciparum* (Ponts et al., 2013).

1.3.2.1. Chromatin landscape and nucleosome assembly in *P. falciparum*

DNA wrapped around histone octamers forms the nucleosome, which is the fundamental architectural unit of chromatin. Chromatin can exist in a relaxed form as euchromatin, which allows the basal transcriptional machinery and other chromatin-associated proteins to access DNA regulatory regions. In contrast, heterochromatin is the compact form of chromatin in which DNA accessibility is restricted and genes are repressed.

In *P. falciparum*, approximately 147 bp of DNA are wrapped around the histone octamer in a nucleosome (Ay et al., 2015). Mass spectrometric analyses detected four canonical histones (H2A, H2B, H3 and H4) and four variant histones (H2A.Z, H2B.Z, H3.3 and CenH3) in *P. falciparum* asexual stages (Miao et al., 2006). The linker histone H1 is absent in apicomplexans (Sullivan et al., 2006) indicating less chromatin compaction. Indeed, during the IDC, 90% of the *P. falciparum* genome is in euchromatin (Salcedo-Amaya et al., 2009) with the few heterochromatin clusters found mostly in the subtelomeric regions and a few intra-chromosomal locations (Lopez-Rubio et al., 2009). Deposition and removal of canonical and alternative histones can influence chromatin structure by changing the physiochemical properties of nucleosomes, and through recruiting protein complexes via their post translationally modified N-terminal tails.

Histone chaperones are indispensable and fundamental for the assembly and disassembly of nucleosomes by coordinating appropriate interaction between histone, DNA and other chromatin remodelling factors. *P. falciparum* has two essential orthologues of eukaryotic nucleosome assembly proteins (NAPs), PfNAPL and PfNAPS (Chandra et al., 2005; Gill et al., 2010; Gill et al., 2009). While both proteins are expressed during the IDC, they have distinct cellular localisation and do not interact with each other. PfNAPS interacts directly with histone

tetramers and octamers in the nucleus while PfNAPL is localised to the cytoplasm suggesting a role in histone shuttling (Navadgi et al., 2006).

1.3.2.2. Nucleosome occupancy and positioning in *P. falciparum*

Nucleosome occupancy is an important factor for determining whether the transcriptional machinery and other DNA-binding proteins can access DNA. In *P. falciparum*, genome-wide nucleosome occupancy is lowest during the early trophozoite stage which coincides with the start of DNA replication during the asexual blood stage (Ponts et al., 2010). Heterochromatin has the highest level of nucleosome occupancy (Ponts et al., 2010; Westenberger et al., 2009) which is likely due to the compaction of chromatin. For example, high levels of nucleosome occupancy were observed at the transcriptional start site (TSS) of the silenced var gene (Ponts et al., 2010). More recently, the nucleosome occupancy of the whole P. falciparum genome was explored by MNase (micrococcal nuclease)-sequencing (Bunnik et al., 2014; Kensche et al., 2016). In brief, the naked and exposed DNA in the genome is digested leaving nucleosomal DNA that which is subsequently sequenced on a next-generation sequencing platform. Nucleosomes were most strongly positioned at the TSS + 1 nucleosome position although nucleosome occupancy at the TSS did not correlate with gene transcription (Kensche et al., 2016). In addition, nucleosomes were also well-positioned around the exon-intron boundaries (Kensche et al., 2016) as well as the start and the end of CDS (Bunnik et al., 2014; Kensche et al., 2016). However, the depletion of nucleosomes in the intergenic regions remains controversial. MNase-sequencing data from Bunnik et al. showed that nucleosome occupancy was lowest in the regions 5' upstream of the ATG- of the CDS, especially, of highly expressed genes in comparison to the CDS (Bunnik et al., 2014). However, Kensche et al. demonstrated that nucleosomes were not depleted in the intergenic region, rather there were locally nucleosome depleted regions that were observed immediately upstream of the TSS of active genes which might represent the binding site of the RNAP II pre-initiation complex (Kensche et al., 2016). The DNA of *P. falciparum* is inherently inflexible due to the extremely high AT-content of its genome (Gardner et al., 2002; Tillo and Hughes, 2009). Despite this, *P. falciparum* nucleosomes did not display a binding preference for AT-rich sequences but nucleosome positioning in *P. falciparum* is influenced by A-T boundaries which are normally adjacent to the TSS as well as in the intergenic regions (Silberhorn et al., 2016).

Furthermore, the pattern of chromatin accessibility is highly dynamic throughout the parasite asexual life cycle (Toenhake et al., 2018). A total of around 4000 regulatory regions was detected by ATAC-seq and most of them are within 2kb upstream of genes (Toenhake et al., 2018).

1.3.2.3. Histone Variants

In addition to the canonical histones, *P. falciparum* possesses the variant histones PfH2A.Z, PfH2B.Z, PfCen3 and PfH3.3 (Miao et al., 2006; Trelle et al., 2009). H2A.Z is a histone variant of H2A that is conserved in many eukaryotes and is important for their biology (Faast et al., 2001; Guillemette et al., 2005; Kumar and Wigge, 2010; Raisner et al., 2005; Zilberman et al., 2008). H2A.Z-containing nucleosomes exhibit higher mobility, which allows sliding along the DNA (Flaus et al., 2004). A crystal structure study showed that H2A.Z-containing nucleosome binds to a metal ion and predicted a destabilised interaction between the H3-H4 tetramer and H2A.Z-H2A dimer (Suto et al., 2000). However, biochemical and biophysical assays suggested that a nucleosome with unmodified H2A.Z is more stable than a H2A-containing nucleosome (Park et al., 2004; Thambirajah et al., 2006) although a recent study used Förster resonance energy transfer (FRET) to show that the altered stability between of H2A.Z- and H2A-containing nucleosomes was marginal (Hoch et al., 2007). More importantly, acetylation on the N-terminal tail of H2A.Z destabilises the nucleosome core particle (Ishibashi et al., 2009). Impaired H2A.Z acetylation by mutating all lysine residues on the H2A.Z N-terminal tail was lethal for *Tetrahymena thermophila* (Ren and Gorovsky, 2001). In *P. falciparum*, PfH2A.Z has eight unique lysine acetylation sites on its N-terminal, which is divergent in sequence from the H2A.Z of other organisms (Miao et al., 2006; Trelle et al., 2009). These acetylations can recruit chromatin-associated proteins such as members of the *P. falciparum* bromodomain proteins as indicated by protein pulldowns of acetylated H2A.Z peptides (Hoeijmakers et al., 2019).

PfH2B.Z (previously known as PfH2Bv) (Talbert et al., 2012) is an Apicomplexan-specific histone variant of H2B which also carries unique acetylation sites in *P. falciparum* (Miao et al., 2006; Trelle et al., 2009). In *P. falciparum*, PfH2A.Z and PfH2B.Z dimerise to form a double-variant nucleosome that is enriched in the intergenic regions of euchromatin, irrespective of transcription level (Bártfai et al., 2010; Petter et al., 2011; Petter et al., 2013). The dimer also colocalises with the euchromatic histone marks H3K4me3 and H3K9ac in promoter regions (Bártfai et al., 2010). Recently, a publication investigating the dynamics of TSSs across the asexual stage revealed that H2A.Z and H2B.Z dimers are enriched at TSS +1

nucleosome positions across the asexual life cycle (Adjalley et al., 2016). This publication also confirmed the enrichment of the dimer in the intergenic regions and promoters.

PfH3.3 is a H3 variant in *P. falciparum* which is very similar to H3. Generally, PfH3.3 is stably enriched in GC-rich regions including CDS and subtelomeric repetitive regions. The localisation of PfH3.3 did not correlate with transcription levels (Fraschka et al., 2016), but in trophozoites, H3.3 dynamically marked the intergenic region upstream of CDSs (Fraschka et al., 2016). CenH3 together with H2A.Z demarcates the centromeric regions of *P. falciparum* chromosomes throughout the asexual life cycle (Hoeijmakers et al., 2013). It is colocalised with components of the kinetochore protein complex CENP-C at distinct spots at the nuclear periphery with a potential role in chromosome segregation (Verma and Surolia, 2013).

Overall, unique histone variants were identified in *P. falciparum* with distinct roles in epigenetic regulation. Furthermore, they probably contribute to an additional layer of epigenetic modulation as they also possess unique sites on their N-terminal tail that can be modified post-translationally.

1.3.2.4. Histone post-translational modification

The N-terminal tails of canonical histones and their variants are subject to a range of post-translational modifications (PTMs) such as acetylation, methylation and phosphorylation (Dastidar et al., 2013; Issar et al., 2008; Miao et al., 2006; Ponts et al., 2011; Trelle et al., 2009). PTMs are important for gene regulatory mechanisms and may influence the physicochemical properties of the nucleosome and therefore, the architecture of chromatin. They can also act as sites for the recruitment of other chromatin-associated proteins that form regulatory complexes. Histone acetylation is generally associated with gene activation, partially because the positive lysine charges are neutralised leading to a less stable interaction with the negatively charged DNA and hence a more open form of chromatin. Histone methylation can be associated with both gene silencing and activation.

P. falciparum possesses a large complement of histone PTMs including PTMs on the H2B.Z histone variant N-terminal tail that are unique to *Plasmodium* suggesting their importance in the malaria parasite's regulation of gene expression (Miao et al., 2006). Over the past decade, many studies have investigated *P. falciparum* histone PTMs. Acetylation and methylation are the most abundant modifications although sites of phosphorylation, SUMOylation and ubiquitination were also reported (Dastidar et al., 2013; Issar et al., 2008; Ponts et al., 2011).

The dynamic landscape of histone PTM's has been described by two main features: their genomic localisation and association with transcription. *P. falciparum* heterochromatin is enriched with the repressive histone 3 lysine 9 trimethylation (H3K9me3) mark (Lopez-Rubio et al., 2009). On the other hand, much evidence showed that histone 3 lysine 9 acetylation (H3K9ac) and histone 3 lysine 4 trimethylation (H3K4me3) broadly marked the intergenic regions of the *P. falciparum* genome (Lopez-Rubio et al., 2009; Salcedo-Amaya et al., 2009; Westenberger et al., 2009), especially 5' of open reading frames (ORFs) of highly expressed genes during the schizont stage (Bártfai et al., 2010; Gupta et al., 2013; Karmodiya et al., 2015; Petter et al., 2011). Other PTMs that are also enriched in the promoter or at the TSS and positively correlate with transcription are H4K8ac, H4K16ac, H3K56ac, H4K20me1 and tetra-acetylated histone H4 (also known as H4ac4), which is acetylated at lysine residue 5, 8, 12 and 15, by ChIP-on-chip (Gupta et al., 2013); and H3K14ac, H3K4me2 and H3K4me1 by ChIP-seq (Karmodiya et al., 2015). Notably, the enrichment of H4K8ac and H3K4me3 had the most dynamic changes in levels of enrichment between different stages across the asexual life cycle, followed by H3K56ac, H3K9ac, H4ac4, H4K16ac, H4K12ac, H4K20me1 and H4K20me3. On the other hand, H4R3me2, H3K14ac, H3K79me3 and H4K5ac showed the least change in their enrichment profile throughout the asexual life cycle (Gupta et al., 2013). Finally, enrichment of H4K20me3, H4K12ac and H3K79me3 in the ORFs and histone 4 arginine 3 dimethylation (H4R3me2) in the intergenic regions did not correlate with gene transcription (Gupta et al., 2013; Karmodiya et al., 2015).

In *P. falciparum*, the N-terminal tails of the histone variants H2A.Z and H2B.Z carry many unique acetylation sites (Miao et al., 2006; Trelle et al., 2009). Recently, the presence of acetylated H2A.Z and H2B.Z was confirmed during the asexual IDC (Saraf et al., 2016) although their genomic localisations remain unclear. In humans, H2A.Z is found near the TSS of both active and poised genes but H2A.Z is only acetylated at the TSS of active genes and hyperacetylation of H2A.Z led to the activation of genes in cancer cells (Valdes-Mora et al., 2012).

1.3.2.5. Histone PTM modifying proteins

1.3.2.5.1. Histone acetylation modifying proteins

Histone acetylations are mediated by histone acetyltransferase (HATs). There are eight putative HATs predicted in *P. falciparum* (Bischoff and Vaquero, 2010). Two HATs were previously

characterised; PfGCN5, which is an orthologue of the yeast GCN5 (Fan et al., 2004) and PfMYST, which belongs to the MYST family of HATs (Miao et al., 2010).

PfGCN5 and its transcriptional coactivator ADA2 acetylate H3K9 and H3K14, and exhibit some acetylation activity towards H4 although the target has not been determined (Cui et al., 2007b; Fan et al., 2004). ChIP-on-chip experiment showed that in trophozoites, the enrichment patterns of GCN5 and H3K9ac were similar and around 60% of the identified GCN5-enriched sites were associated with transcription (Cui et al., 2007b). A more recent ChIP-seq study indicated that PfGCN5 is enriched throughout the genome with 51% of the signal was found in gene promoters (Bhowmick et al., 2020). The PfGCN5 full-length protein is processed in the cytoplasm near the food vacuole before it is transported into the nucleus (Bhowmick et al., 2020). Inhibition of the proteolytic processing of PfGCN5 using compound MG132 (Prasad et al., 2013) led to a decrease in global H3K9ac in the parasite (Bhowmick et al., 2020) implicating PfGCN5 processing in its HAT activity. However, as MG132 has a broad activity that can inhibit haemoglobin degradation and the ubiquitin proteasomal system in the parasite (Prasad et al., 2013), the effect of inhibition of PfGCN5 processing may not be directly related to the decrease of histone acetylation.

PfMYST acetylates H4K5, K8, K12 and K16 (Miao et al., 2010). It is associated with the TSSs of active *var* genes during the immature stage and overexpressing PfMYST disturbed the level of H4 acetylation and caused a parasite growth defect during the schizont stage (Miao et al., 2010). Different observations were reported regarding the localisation of PfMYST in ring-stage parasites with evidence showing PfMYST co-localised to the nucleus (Miao et al., 2010) or localised to the parasitophorous vacuole outside of the nucleus (Sen et al., 2018). The latter study also showed that PfMYST interacts with RuvB-like protein 3 (RUVBL3), which possesses ATPase, oligomerisation and DNA cleaving activity, and their cellular localisation was dynamic during the IDC and was only associated with the nucleus in trophozoites (Sen et al., 2018).

Histone deacetylases (HDACs) antagonise HATs by removing the acetyl groups from histones. Five HDACs were predicted in *P. falciparum* (Bischoff and Vaquero, 2010). The most studied HDAC in *P. falciparum* is the sirtuin enzyme (PfSir2) which belongs to class III HDACs (Duraisingh et al., 2005). PfSir2A is involved in chromatin compaction and is responsible for the silencing of the *var* genes/virulent genes that allow the parasite to maintain mutually exclusive *var* gene expression and evade the host immune system (Duraisingh et al., 2005; Freitas-Junior et al., 2005; Merrick et al., 2010; Merrick et al., 2015). Each PfSir2 paralogue

has specific targets and is responsible for the regulation of different groups of *var* genes based on their promoter type (Tonkin et al., 2009). PfSir2A deacetylates H3K9ac, H3K14ac and H4K16ac (French et al., 2008) and the removal of the acetyl group on H3K9 allows the sites to be methylated leading to gene silencing (Lopez-Rubio et al., 2009). In addition, PfSirA also regulates the growth rate of *P. falciparum* by deacetylating histones at ribosomal RNA genes (Mancio-Silva et al., 2013). PfSir2 knockout in different parasite strains (NF54, 3D7 and IT4/FCR3) had variable effects on dysregulation of *var* genes (Merrick et al., 2015), suggesting that *var* gene regulation differs between parasite strains and PfSir2 is not the sole factor responsible for *var* gene silencing.

P. falciparum class I HDAC, PfHDAC1, is homologous to class 1 human HDACs (Joshi et al., 1999; Le Roch et al., 2003) and PfHda2 is a class II HDAC (Bischoff and Vaquero, 2010). A recent study showed that PfHda2 regulates the expression of virulence genes (Coleman et al., 2014). Knockdown of PfHda2 disturbed the integrity of heterochromatin and also led to a higher gametocyte conversion rate (Coleman et al., 2014).

1.3.2.5.2. Histone methylation modifying proteins

Lysine and Arginine residues on the N-terminal tails of the histones are subjected to methylations, which are associated with both silent and active genes in *P. falciparum* (Lopez-Rubio et al., 2009; Salcedo-Amaya et al., 2009). At least ten histone lysine methyltransferases (HKMTs) that contain a SET domain were predicted by bioinformatic analysis in *P. falciparum* (Cui et al., 2008; Volz et al., 2010; Volz et al., 2012). The targets of some of these PfSET proteins were predicted and a few have been functionally described. PfSET2/PfSETvs, PfSET4, PfSET5 and PfSET8 could be knocked out suggesting that they are dispensable during the asexual life cycle *in vitro*, while PfSET1, PfSET3, PfSET6, PfSET 7 and PfSET9 were essential for the parasite (Jiang et al., 2013). Interestingly, PfSET2/PfSETvs methylates H3K36 and disruption of this protein led to the activation of all the *var* genes showing that PfSET2/PfSETvs is important for the silencing of *var* genes (Jiang et al., 2013; Ukaegbu et al., 2014). PfSET3 localised to the nuclear periphery and was predicted to be responsible for the silencing mark H3K9me3 in heterochromatin (Lopez-Rubio et al., 2009), however, experimental proof is still missing. PfSET5 and PfSET6 localised to the mitochondria and nuclear periphery, respectively (Volz et al., 2010; Volz et al., 2012). Meanwhile, PfSET7 is found outside of the nucleus during the IDC, sporozoite and liver stages, raising the possibility that it may have non-histone substrates (Chen et al., 2016). In *T. gondii*, SET8 mono-, di- and tri-methylates H4K20 (Sautel et al., 2007). (Sautel et al., 2007). In addition, many of these

PfSET proteins have other functional domains, for example, PfSET1 has one bromodomain and three plant homeodomain fingers (PHD fingers) domains (Cui et al., 2008), which can mediate interaction with the chromatin. Therefore, these PfSET proteins can probably interact with other proteins and potentially form complexes that regulate gene expression. Finally, protein arginine methyltransferase 1 (PfPRMT1) is the only known *P. falciparum* enzyme that can methylate arginine (Fan et al., 2009). Recombinant PfPRMT1 was able to methylate H4 and H2A as well as substrates involved in RNA metabolism (Fan et al., 2009).

Histone demethylases remove methylations from the histone N-terminal tail. Bioinformatic analyses identified five *P. falciparum* demethylases including lysine-specific demethylases 1 (LSD1) and Jumonji domain-containing histone demethylase 1 and 2 (JmJC1 and JmJC2) (Cui et al., 2008). JmJC1 and 2 can demethylate H3K36 (Ukaegbu et al., 2014). Knockout of LSD1 and JmJC1/2 was not lethal for the parasite (Jiang et al., 2013) but no other functional data have been reported for these proteins.

1.3.2.6. Epigenetic regulation of invasion

The malaria parasite has evolved to be highly adaptive to the host environment, especially during invasion when surface proteins on the merozoites are exposed to the host immune system. Invasion-related genes such as EBA and Rh, which are important for the tight adhesion between the apical tip of the merozoite and the surface of the RBC (DeSimone et al., 2009; Duraisingh et al., 2003; Lopaticki et al., 2011; Stubbs et al., 2005), exist in multigene families (Cortés et al., 2007; Rovira-Graells et al., 2012). This allows redundant mechanisms for invasion in the parasite to contend with diversity in available host receptors and to avoid detection by the host immune system. The expression of members of these multigene families is epigenetically regulated (Comeaux et al., 2011; Cortés et al., 2007; Crowley et al., 2011). The silent locus is marked with the repressive histone PTM H3K9me3 and heterochromatin protein 1 (HP1) whereas, the active locus is enriched with H3K9ac, H3K14ac and H4ac in its promoter region (Comeaux et al., 2011; Crowley et al., 2011; Flueck et al., 2009).

Soon after invasion, the parasite inserts the RhopH complex into the PVM, which is important for nutrients uptake (Nguitragool et al., 2011). In this complex, the RhopH1/Clag3 has two variant genes called *clag3.1* and *clag3.2*, which are epigenetically regulated (Cortés et al., 2007). Parasites can become resistant to low concentrations of blasticidin S drug when the transcription of *clag3.2* switches to *clag3.1* and increased H3K9me3 was observed at the promoter of the silent *clag* gene (Comeaux et al., 2011; Crowley et al., 2011). Silencing of both

clag3.1 and *clag3.2* led to a decrease in solute uptake in the parasites allowing them to become resistant to higher concentrations of blasticidin S (Mira-Martínez et al., 2013; Sharma et al., 2013). This example of epigenetic regulation of invasion genes highlights the importance of histone PTMs in activation of gene expression but also as epigenetic memory markers.

1.3.2.7. Epigenetic regulation of *var* genes

Regulation of *var* gene expression via epigenetic mechanisms has been extensively studied due to the significance of *var* genes in malaria pathogenesis. In addition, this is a good model to understand the epigenetic regulation in malaria as *var* genes expression is mutually exclusive and parasites can be enriched for the different cytoadhesion phenotypes encoded by different *var* genes. Therefore, the features of both active and inactive *var* loci can be investigated. Overall, the mechanisms of *var* gene regulation discussed in this section can be summarised into three main categories: 1) subnuclear localisation, 2) DNA regulatory elements and 3) histone PTMs, epigenetic memory and chromatin-associated proteins.

1) Sub-nuclear localisation

The nucleus of the *P. falciparum* parasite inside the IE consists of functional compartments and active and inactive *var* genes are found in distinct locations (Dzikowski et al., 2007). *Var* genes, which are inactive or silenced, form clusters in the nuclear periphery. There are two different models explaining the sub-nuclear localisation of a *var* gene when it is activated. The first model suggests that the one active *var* gene is removed from the cluster and relocate to distinct areas in the nuclear periphery (Mok et al., 2008; Ralph et al., 2005) via direct interaction between actin-1 and the *var* gene intron (Zhang et al., 2011). On the other hand, there is also evidence supporting a second model that a *var* gene can be activated while remaining within the same telomeric clusters as other inactive *var* genes (Brolin et al., 2009; Duffy et al., 2017; Lemieux et al., 2013; Marty et al., 2006; Voss et al., 2006).

2) DNA regulatory elements

Each *var* gene has one intron, which has a conserved structure in the majority of *var* gene members (Calderwood et al., 2003; Lavstsen et al., 2003). The *var* intron has bi-directional promoter activity that can transcribe non-coding RNA (Deitsch et al., 2001b). However, there is an ongoing debate as to whether these introns contribute to *var* gene silencing. Previously, a study showed that the pairing of *var* promoter and intron of UpsC *var* genes led to the silencing of a reporter gene in episomes (Deitsch et al., 2001b). Several subsequent studies also supported this model (Calderwood et al., 2003; Dzikowski et al., 2006; Gannoun-Zaki et al.,

2005; Swamy et al., 2011) although it is worth noting that these studies used episomes and transgenes. More recently, antisense long non-coding RNA (aslncRNA) from the intron promoter to the exon 1 of a *var* gene was suggested to be responsible for the activation of the specific corresponding *var* gene (Amit-Avraham et al., 2015; Jing et al., 2018). In contrast, there was also evidence that subtelomeric UpsB *var* gene promoters are epigenetically silenced by default regardless of *var* intron activity (Voss et al., 2007). These authors suggested that local chromatin compaction of the SPE2 elements (Voss et al., 2003) is involved in *var* gene silencing (Voss et al., 2007). More recently, CRISPR-Cas9 was used to directly edit and remove the intron of *var2csa,* which is the *var* gene that codes for the PfEMP1 variant that causes placental malaria (Bryant et al., 2017). Mutant parasites with intron-less *var2csa* were able to silence and re-activate *var2csa* indicating that it is likely that the switching of this particular *var* gene does not require activity from the *var* intron (Bryant et al., 2017). Further work using the CRISPR-Cas9 approach can potentially be used to query the role of the *var* intron in *var* gene regulation with respect to the different *var* gene groups. Nevertheless, it is clear that the regulation of *var* genes is complex and involves the interplay of many different mechanisms.

3) Histone PTMs, epigenetic memory and chromatin-associated proteins

Histone PTMs and associated proteins also play critical roles in regulating the expression of *var* genes. As *var* genes are found mainly in heterochromatic regions, inactive *var* genes are extensively marked with H3K9me3 as well as the HP1 protein (Flueck et al., 2009; Jiang et al., 2013; Lopez-Rubio et al., 2009; Perez-Toledo et al., 2009) while active histone marks such as acetylated H4 are depleted from these regions (Freitas-Junior et al., 2005). The histone deacetylase Sir2A is important for this process as disruption of Sir2A disrupts the mutually exclusive *var* gene expression (Duraisingh et al., 2005; Tonkin et al., 2009). PfSET2 methylates H3K36 and deletion of PfSET2 also led to dysregulation of mutually exclusive expression of *var* genes (Jiang et al., 2013). Furthermore, H3K36me3 was enriched in the promoter and intron regions of inactive *var* loci in one study (Jiang et al., 2013) but another study only detected H3K36me3 in the CDS of *var* genes regardless, of transcriptional status (Ukaegbu et al., 2014).

The silencing histone PTMs are replaced with H3K9ac, H3K4me3 and H3K27ac in active *var* loci (Bártfai et al., 2010; Duffy et al., 2017; Lopez-Rubio et al., 2009; Salcedo-Amaya et al., 2009). Interestingly, evidence of epigenetic memory was discovered when H3K4me2 was enriched at transiently repressed *var* genes during the schizont stage (Lopez-Rubio et al., 2007),

potentially to mark its activation in the next cycle. PfSET10 is responsible for mono- and di-methylation of H3K4me3 and therefore, is implicated the activation of repressed *var* genes (Volz et al., 2012). The histone variants H2A.Z and H2B.Z are dynamically enriched at the promoter of the single active *var* gene (Petter et al., 2011; Petter et al., 2013), but only while it is transcribed during the ring stage. H2A.Z and H2B.Z are later evicted by a Sir2A dependent mechanisms when the active *var* gene is transiently repressed in mature stages of the parasite (Petter et al., 2011). In contrast, H2A.Z is stably enriched in the introns of both active and silent *var* genes (Petter et al., 2011).

1.3.2.8. Epigenetic regulation of gametocytogenesis

In order to successfully combat malaria and reach the goal of eradication, it is important to understand the biology of the sexual stage. While the asexual, intra-erythrocytic stage is responsible for malaria pathogenesis and clinical symptoms, transmission can only occur when an Anopheles mosquito ingests sexual forms (gametocytes) from an infected person during a blood meal. One of the factors that are important for sexual commitment in the parasite is external stimuli. For example, the presence of host-derived lysophosphatidylcholine (LysoPC) inhibits parasite sexual commitment and depletion of LysoPC induce transcriptional changes that are typical for sexual transition (Brancucci et al., 2017).

The ApiAP2 protein AP2-G was confirmed as a master regulator of gametocytogenesis by several genetic screens in *P. falciparum*, *P. berghei* and *P. yoelii* (Kafsack et al., 2014; Modrzynska et al., 2017; Zhang et al., 2018). In asexual parasite, AP2-G is epigenetically silenced by the activity of Hda2 and the enrichment of HP1 and H3K9me3 (Coleman et al., 2014). The protein GDV1 can remove HP1 from the *ap2-g* locus and allow the transcription of AP2-G (Filarsky et al., 2018). A recent single-cell transcriptomic study showed that AP2-G transcription leads to a cascade of altered gene expression including two other ApiAP2 genes along with genes involved in chromatin remodelling, the histone acetylase HDA1 and the demethylase LSD2 (Poran et al., 2017). These changes suggest that ApiAP2 activates other transcriptional machinery in preparation for the transition to sexual stage.

Interestingly, putative AP2-G binding sites were found upstream of the *ap2-g* locus (Campbell et al., 2010; Josling et al., 2020) and there is evidence suggesting that AP2-G also positively regulates its expression starting in the schizonts that have been committed to gametocytogenesis of its progeny (Bancells et al., 2019; Josling et al., 2020). Mutation of the putative AP2-G binding sites led to reduced transcription of ap2-g and a subset of genes

expressed early during gametocyte development (Josling et al., 2020). This did not change the overall progress of gametocyte development, but it decreased the commitment rate (Josling et al., 2020). AP2-G might have additional roles during gametocyte development beyond initiating gametocytogenesis as the transcription of AP2-G persisted even in stage I gametocyte (Bancells et al., 2019; Josling et al., 2020).

1.4. Bromodomain protein in *P. falciparum* and developments in drug design strategies to target PfBDPs (accepted publication (Nguyen et al., 2020))

Taylor & Francis
Taylor & Francis Group

Expert Opinion on Drug Discovery

ISSN: 1746-0441 (Print) 1746-045X (Online) Journal homepage: https://www.tandfonline.com/loi/iedc20

Developments in drug design strategies for bromodomain protein inhibitors to target *Plasmodium falciparum* parasites

Hanh H. T. Nguyen, Lee M. Yeoh, Scott A. Chisholm & Michael F. Duffy

To cite this article: Hanh H. T. Nguyen, Lee M. Yeoh, Scott A. Chisholm & Michael F. Duffy (2019): Developments in drug design strategies for bromodomain protein inhibitors to target *Plasmodium falciparum* parasites, Expert Opinion on Drug Discovery, DOI: 10.1080/17460441.2020.1704251

To link to this article: https://doi.org/10.1080/17460441.2020.1704251

The vast majority of global malaria mortality is caused by the apicomplexan parasite *Plasmodium falciparum*. The emerging resistance of *Plasmodium* to antimalarials is driving efforts to identify new drugs. *Plasmodium* parasites tightly regulate dynamic transcription of most of their genes both throughout their asexual, intra-erythrocytic cell-cycle (Bozdech et al., 2003; Reid et al., 2018) and during development into other differentiated forms (Gural et al., 2018; Lopez-Barragan et al., 2011; Reid et al., 2018; Vivax Sporozoite, 2019; Yeoh et al., 2017). *P. falciparum* maintains an unusually high proportion of its remarkably AT-rich genome as euchromatin, regardless of whether genes are transcribed (Salcedo-Amaya et al., 2009). However, the euchromatin displays dynamic patterns of histone post-translational modifications (PTMs), some of which are unique to Apicomplexa (Ay et al., 2015; Cui and Miao, 2010; Duffy et al., 2012, 2014; Gupta and Bozdech, 2017; Talbert et al., 2012). Many

of the histone PTMs are associated with alterations in gene transcription presumably due to altered chromatin structure or due to the proteins that bind the histone modifications, which recruit effector complexes.

The maintenance of histone-acetylation homeostasis is critical for *Plasmodium* survival (Darkin-Rattray et al., 1996) and gene regulation (Duraisingh et al., 2005). Histone acetylation is regulated by the antagonistic activity of lysine acetyltransferases (KATs) and histone deacetylases (HDACs). Many potent inhibitors of different classes of HDACs have been described for *P. falciparum* and other human-infecting parasites including *Toxoplasma gondii*, *Trypanosoma brucei* and *Schistosoma mansoni* (Andrews et al., 2000; Bougdour et al., 2009; Chen et al., 2008; Darkin-Rattray et al., 1996; Patil et al., 2010; Strobl et al., 2007), making lysine acetylation an attractive drug target.

Bromodomains (BRDs) bind acetylated lysines on histone tails or other proteins (Dhalluin et al., 1999). The structure of the BRD consists of a left-handed bundle of four alpha-helices, and a hydrophobic pocket where acetylated lysine interaction occurs (figure 1.3). The hydrophobic pocket is formed by the inter-helical BC and ZA loops that are highly variable in length and sequence. Specificity for an acetylated lysine and its surrounding environment is determined by the polymorphisms within the hydrophobic pocket (Dhalluin et al., 1999; Filippakopoulos et al., 2012). BRDs have a wide range of affinities for the diverse array of histone lysine acetylations. Many BRDs can bind more than one acetylation, and some can bind multiple acetylations simultaneously (Filippakopoulos et al., 2012). Consequently, BRD inhibitors often have some level of activity on more than one BRD (Andrieu et al., 2016). BRD-containing proteins tend to be scaffolding proteins (Denis, 2001) for downstream signalling pathways, but some also contain other functional domains such as histone acetylases or methyltransferases (Dhalluin et al., 1999; Filippakopoulos et al., 2010).

The Bromo- and Extra-terminal domain (BET) family is a well-studied example of a BRD family in humans. Dysfunction of these BRD proteins has been linked to various types of cancer, inflammation, neurological disorder, and cardiovascular disease (Chung et al., 2012; Ferri et al., 2016; Jung et al., 2015). The interaction pocket can be drugged (Runcie et al., 2018)and several classes of small molecule inhibitors of BRD proteins are currently being developed and tested in various clinical trials as cancer therapies (Andrieu et al., 2016; Boi et al., 2015). Possibly the unique or divergent *P. falciparum* bromodomain proteins could also be targeted by new antimalarial therapeutics. This review discusses the *P. falciparum*

bromodomain proteins (PfBDPs), and strategies and challenges for PfBDP-targeted drug discovery including the importance of specificity assays for this process.

1.4.1. Bromodomain proteins of *P. falciparum*

P. falciparum has at least eight putative PfBDPs (Table 1.1). Jeffers et al. named two of these as PfBDP3 (Pf3D7_0110500) and PfBDP4 (Pf3D7_1475600) (Jeffers et al., 2017), consistent with the *T. gondii* orthologues' nomenclature (TgBDP3 and TgBDP4). However, contemporaneous publications used the inverse of this nomenclature (Hui D, 2016; Toenhake et al., 2018). We will follow the Jeffers' nomenclature for this review. PfBDPs are transcribed in asexual and sexual blood-stage parasites, liver-stage hypnozoites and mosquito stage parasites (Lopez-Barragan et al., 2011) (Table 1.1), but functional information is only available for asexual blood stage parasites.

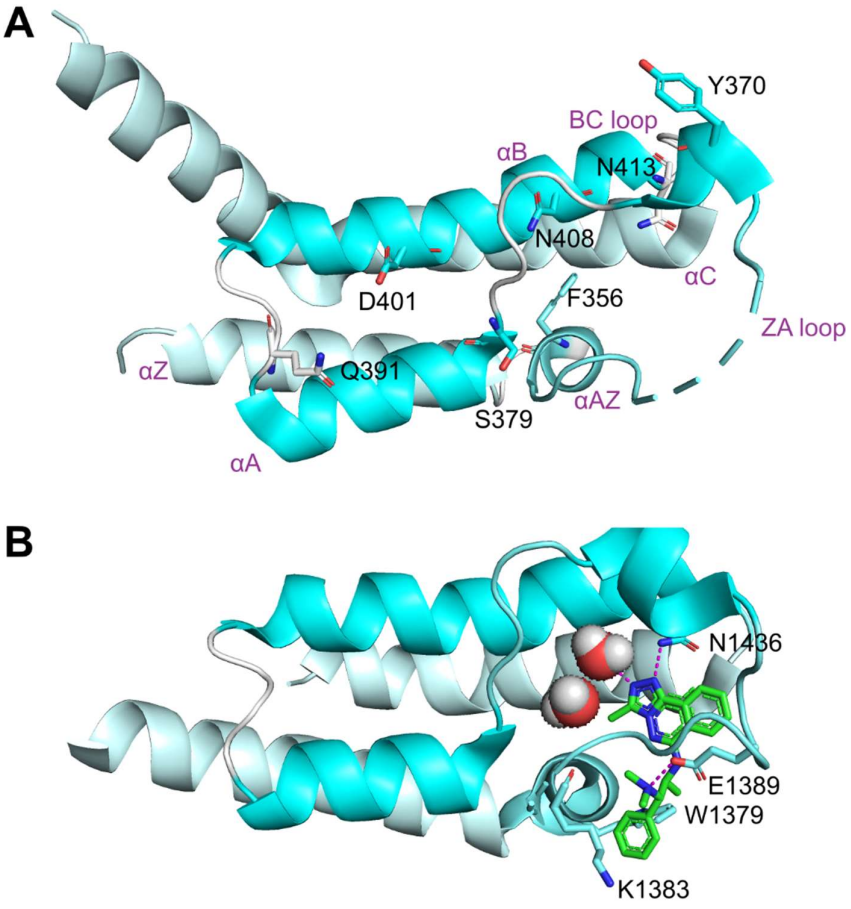

Figure 1.3 Representative crystal structures of bromodomain in *P. falciparum*

A) Image of PfBDP1 structure PDB ID: 3FKM(Wernimont et al.), adapted from Wernimont et al. (Wernimont and Edwards, 2009) under the Creative Commons Attribution 4.0 International Public License (https://creativecommons.org/licenses/by/4.0/legalcode) using PyMOL(Schrodinger, 2015) from RCSB PDB(Burley et al., 2019). Conserved interaction residues and the BC and ZA-loops are highlighted. The dotted line signifies missing density in the ZA-loop.

B) Image of L-45 bound to PfGCN5 PDB ID: 5TPX, adapted from Moustakim et al. (Moustakim et al., 2017), under the Creative Commons Attribution 4.0 International Public License (https://creativecommons.org/licenses/by/4.0/legalcode) using PyMOL(Schrodinger, 2015). Conserved interaction residues are highlighted. L-45 (green sticks) binds in the acetyl-lysine binding pocket of PfGCN5 and makes hydrogen bonds (magenta) to N1436 and a water molecule. A salt bridge (magenta) is also formed between L-45 and E1389.

PfGCN5 is an orthologue of the GCN5 protein in *S. cerevisiae*. PfGCN5 is the only *P. falciparum* BRD with a human ortholog, however, they are divergent (figure 1.4). Both *S. cerevisiae* and *P. falciparum* GCN5 proteins possess a lysine acetyltransferase (KAT) domain. PfGCN5 preferentially acetylates lysine residues on the histone H3 tail, including H3K9 and H3K14 (Fan et al., 2004). In a recent study, PfGCN5 was localised upstream of the open-reading frame of a gene, which resulted in activation of the epigenetically-silenced gene via increased local H3 acetylation (Xiao et al., 2019). Treatment with curcumin kills *P. falciparum,* inhibits KAT activity of recombinant PfGCN5 and decreases *P. falciparum* H3 acetylation (Cui et al., 2007a) *in vitro*. However curcumin treatment also generates harmful reactive oxygen species in the parasite (Cui et al., 2007a), and inhibits many other proteins in mammalian cells (Banerjee et al., 2018; Ravish and Raghav, 2014; Yin et al., 2018) so its effects on *P. falciparum* could be unrelated to PfGCN5 inhibition. The function of the bromodomain (BRD) in PfGCN5 has not been characterised.

The essential bromodomain protein 1 (PfBDP1) interacts with PfBDP2 and is required for expression of many genes including the coordinated expression of erythrocyte-invasion genes (Josling et al., 2015). PfBDP1 is recruited to a subset of these invasion genes by the transcription factor ApiAP2-I (Santos et al., 2017). Little is known about the functions of the remaining PfBDPs; PfSET1 contains a predicted SET (Su(var), enhancer of zeste, trithorax) histone methyltransferase domain, and interference with PfSET1 transcription during the

asexual blood stage leads to down-regulation of many genes (Xiao et al., 2019). PfBDP5/TAF1 is a putative homologue of the TFIID (transcription factor II D) complex member TAF1 (TATA-binding protein associated factor 1) based on predicted tertiary structure (Callebaut et al., 2005). The BRD of PfTAF2 (PF3D7_0724700) is the *P. falciparum* orthologue of the predicted *T. gondii* TFIID complex member TAF2 (figure 1.4).

The BRDs of these PfBDPs have no clear orthologues outside Apicomplexa (Figure 1.4). The relatively short length of the BRD produces poor bootstraps, making it difficult to elucidate broad relationships between the major clades. In general, the *P. falciparum* BDPs have one-to-one orthology with *T. gondii* BDPs, with the possible exception of BDP4. *T. gondii* BDPs are essential during the tachyzoite's replicative stage, except for TgBDP5 and TgGCN5A, the latter is one of the two GCN5 KAT proteins (Sidik et al., 2016). In the murine malaria parasite *P. berghei*, PbBDP1, PbGCN5 and PbSET1 are essential while disruption of PbBDP2 slows parasite growth (Schwach et al., 2015). A recent *piggyBac* transposon forward-genetic screen in *P. falciparum* found four out of eight PfBDPs (PfBDP1, PfBDP2, PfTAF2 and PfGCN5) were devoid of insertions (Figure 1.5) suggesting they were essential (Zhang et al., 2018). PfBDP3 had multiple insertions with one site upstream of the BRD, and PfBDP5/TAF1 and PfSET1 both had one insertion site upstream of the BRDs. This suggests that the PfBDP3, PfTAF1 and PfSET1 BRDs are not essential for blood stage parasite survival, although mutation of both PfBDP3 and PfSET1 affected parasite growth rates. However, functional studies suggested that mislocalisation of PfBDP5/TAF1 led to growth defect in the parasites (Hoeijmakers et al., 2019). PfBDP4 had a single insertion site downstream of the BRD, so any impact on the function of this domain cannot be inferred (Zhang et al., 2018).

Table 1.1. Bromodomain proteins in *Plasmodium falciparum*

Gene ID	Annotation	Protein name	PDB ID(Burley et al., 2019)	Transcriptional level (Gural et al., 2018; Lopez-Barragan et al., 2011) (FPKM)							
				Ring	Early Troph	Late Troph	Schizont	Gametocyte II	Gametocyte V	Ookinete	*P. vivax* Hypnozoite
PF3D7_1033700	Bromdomain protein 1	PfBDP1	3FKM(Wernimont et al.)	159.14	135.54	145.66	63.31	17.76	106.51	258.53	29.37
PF3D7_1212900	Bromdomain protein 2	PfBDP2		100.53	166.74	152.79	36.58	70.16	92.38	137.03	395.78
PF3D7_0110500	Bromdomain protein 3	PfBDP3	4PY6(Fonseca et al.)	13.85	49.01	23.37	5.69	35.73	44.92	48.36	6.36
PF3D7_1475600	Bromdomain protein 4	PfBDP4	4NXJ, 5VS7	44.07	39.03	32.22	11.03	8.52	22.98	14.94	93.78
PF3D7_1234100	Bromodomain protein, putative	PfTAF1		45.17	43.93	20.8	9.59	11.65	45.8	36.64	8.71
PF3D7_0724700	Bromodomain protein, putative	PfTAF2		29.18	31.53	19.85	9.23	16.88	28.14	14.63	5.48

PF3D7_0823300	Histone acetyltransferase GCN5	PfGCN5	4QNS(Fonseca et al.), 5TPX(Moustakim et al., 2017)	107.4	339.01	150.96	59.27	34.02	37.29	30.77	39.34
PF3D7_0629700	SET domain protein, putative	PfSET1		30.06	49.36	45.02	15.28	12.42	33.75	44.78	47.01

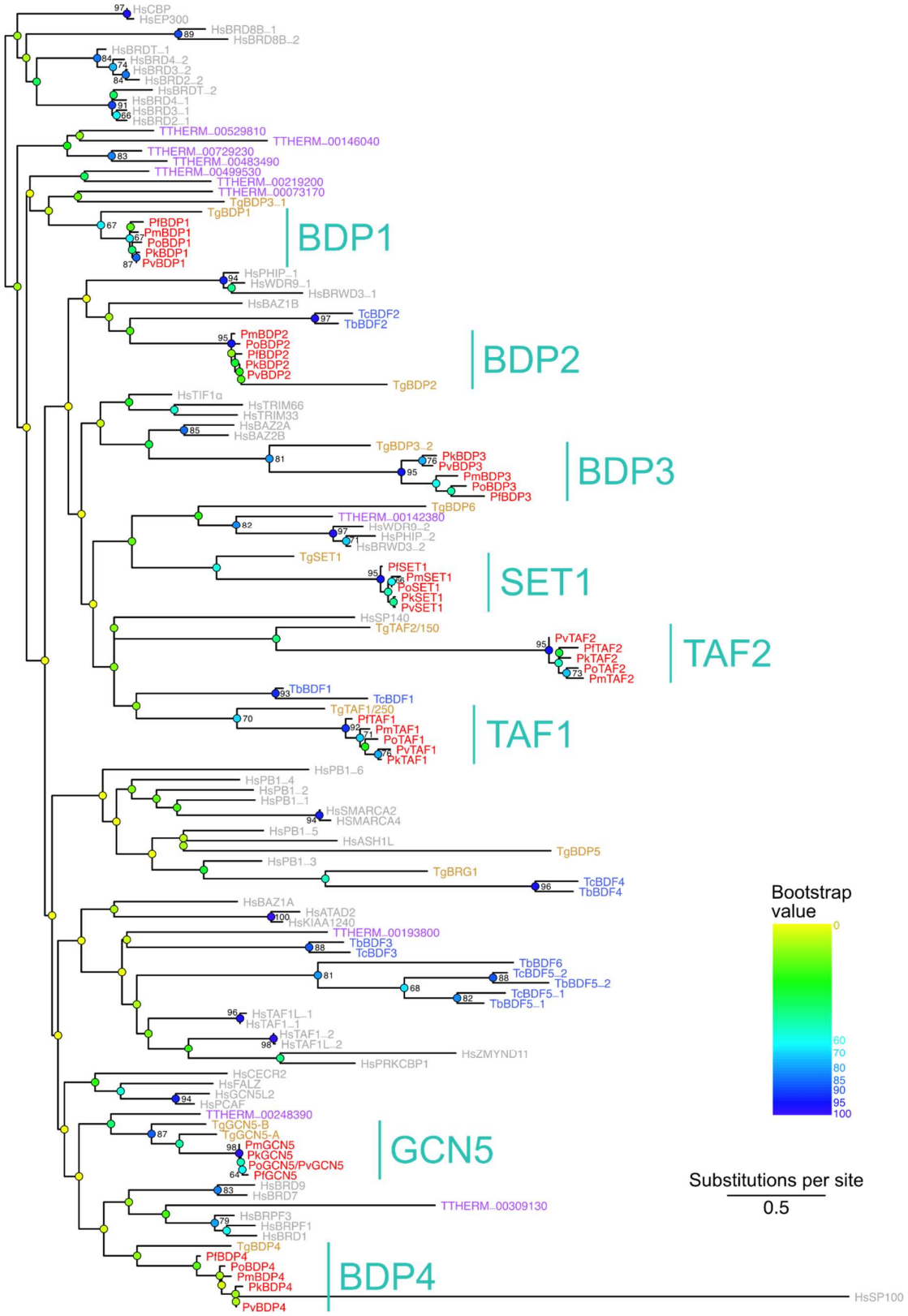

Figure 1.4 Phylogeny of bromodomains from *Plasmodium falciparum* (Pf), *P. knowlesi* (Pk), *P. malariae* (Pm), *P. ovale* (Po), *P. vivax* (Pv), *Toxoplasma gondii* (Tg), *Tetrahymena*

***thermophila* (TTHERM), *Trypanosoma brucei* (Tb), *Trypanosoma cruzi* (Tc), and *Homo sapiens* (Hs).** Nodes are coloured according to bootstraps, as per the legend, with bootstraps of 60 and over explicitly quantified. Parasites gene names are derived from Jeffers et al. (Jeffers et al., 2017), with gene IDs used for novel proteins. Other *Plasmodium spp.* Gene names are derived from the syntenic *P. falciparum* gene. Gene names are appended with an underscore (e.g. TgBDP3_2) when multiple bromodomains were identified in the same protein; lower numbers in the suffix indicate higher E values for that protein. Apicomplexan bromodomain clades are labelled with teal text to the right. This figure was created by collating putative bromodomain proteins using a combination of annotated-domain searches, orthologous group identification (Chen et al., 2006), and sequence similarity searches (Aurrecoechea et al., 2008). BRDs were then identified with HMMer 3 and 2 (Eddy, 1998), aligned with Clustal Omega (Sievers et al., 2011), curated in Jalview (Waterhouse et al., 2009) , the maximum-likelihood phylogeny generated with PhyML(Guindon et al., 2010), unrooted tree generated with FigTree(Rambaut), and further manipulated in Inkscape (InkscapeTeam).

1.4.2. Drug discovery approaches in *P. falciparum*

The ideal antimalarial therapeutic compounds will kill asexual replicating parasites and sexual-stage gametocytes to prevent disease and transmission. Furthermore, they should kill rapidly, preferably be long-lasting, and affect multiple *Plasmodium* species. They will also prevent relapse from dormant liver-resident forms of *P. vivax* and *P. ovale* and offer chemoprophylactic protection (Katsuno et al., 2015). Checkpoint criteria have been established for hit and lead compounds (Katsuno et al., 2015). Hit compounds should have an EC_{50} less than 1 μM, and selectivity greater than ten-fold for *P. falciparum* over mammalian cell lines. Lead compounds should have an EC_{50} less than 100 nM, selectivity of greater than 100-fold and *in vivo* efficacy of 90% parasite clearance at less than 50 mg/kg in a severe combined immunodeficiency mouse model. These stringent criteria allow rapid triage of phenotypic hits.

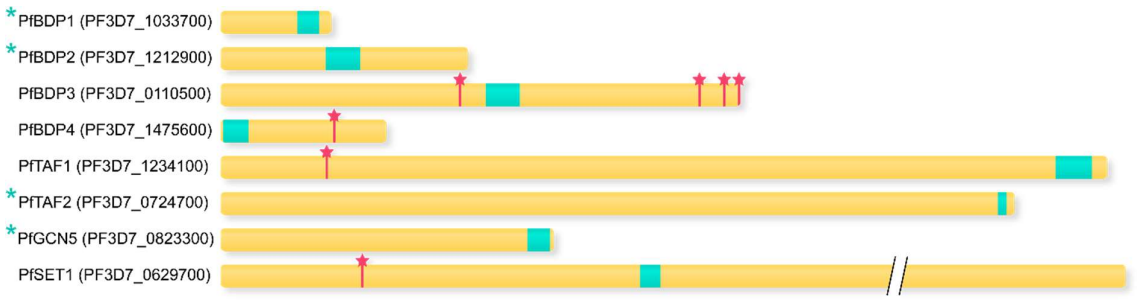

Figure 1.5 Models of Plasmodium falciparum bromodomain protein genes. Bromodomains were identified by HMMer 3 and 2(Eddy, 1998), and are marked in teal on the gene model. Red starred lines represent *piggyBac* transposon insertion sites as identified by mutagenesis screens(Zhang et al., 2018) and reported by PlasmoDB(Aurrecoechea et al., 2008). Teal asterisks indicate genes that were not perturbed in the screen.

Phylogenetic analysis revealed that the BRDs of *P. falciparum* are conserved in the other *Plasmodium* species that infect humans (*P. vivax, P. malariae, P. knowlesi* and *P. ovale*) (Figure 1.4), but no structural analysis has yet been published for the BRDs from these other *Plasmodium* species. *Plasmodium* BDPs are expressed both in the intermediate host's blood and in the mosquito stages of the parasite's life cycle (Bozdech et al., 2003; Gural et al., 2018; Lopez-Barragan et al., 2011; Reid et al., 2018; Vivax Sporozoite, 2019; Yeoh et al., 2017) (Table 1.1). BRD proteins are also transcribed in the quiescent liver-phase hypnozoites in *P. vivax* (Gural et al., 2018) although little is known about their function during the liver stage and whether they play a role in epigenetic regulation of *P. vivax* hypnozoites (Table 1.1). This suggests that they could make promising cross-species and multi-stage drug targets. The unique sequence of the *P. falciparum* BRDs compared to human BRDs suggests scope for inhibitor selectivity (figure 1.3). Also, the rapid development of inhibitors for human BRDs suggests that compounds that meet the criteria above and inhibit the *P. falciparum* BRDs may be readily found.

High-throughput phenotypic screens using malaria parasite whole-cell growth assays have identified many hit compounds. For example, the 400 hit compounds screened by GlaxoSmithKline (Gamo et al., 2010), Novartis (Guiguemde et al., 2010) and St. Jude Children's Research Hospital (Meister et al., 2011) that were selected for inclusion in the Medicines for Malaria Venture's Malaria box and distributed to the malaria research community (Spangenberg et al., 2013). Mutations in the genes encoding the targets of these hit compounds are selected for by prolonged exposure to sublethal concentrations of the compounds (Cowell et al., 2017). These mutations are then identified by genome sequencing of resistant parasites, this approach could also be applied to targeted screens of putative BRD inhibitors.

1.4.3. Target-based drug discovery and development for bromodomain proteins in *P. falciparum*

In contrast to phenotypic screens, target-based approaches identify 'hits' against an essential target that is unique to the parasite. The aim is to design or identify small molecules that occupy the acetylation binding pocket and interrupt the binding of BRD proteins to acetylated lysine residues. In an example of a parasite target-based study two inhibitors of human BRDs, JQ-1 and I-BET151, were shown to interact with recombinant bromodomain factor 3 (BDF3) from the *Trypanosoma cruzi* parasite that causes Chagas disease. Overexpression of BDF3 rescued *T. cruzi* from inhibitory effects of these compounds, suggesting specificity for this target (Alonso et al., 2016). The IC_{50} of these compounds for wildtype insect infective, *T. cruzi* epimastigotes were both less than 10 μM (Alonso et al., 2016). This meets the criteria for *T. cruzi* inhibitor hits (Katsuno et al., 2015), and together with evidence of specificity for BDF3 from target-based drug discovery, suggests further medicinal-chemistry may be warranted to improve these compounds potency and selectivity for *T. cruzi*.

Four of the eight *P. falciparum* BRDs have been expressed as recombinant proteins in BL2(DE3) *E. coli*. These were used to solve crystal structures for the *P. falciparum* BRDs (Table 1.1, figure 1.3). At least one of these recombinant *P. falciparum* BRDs can bind compounds (figure 1.3 and see section 1.4.3.2 below). Thus, the recombinant *P. falciparum* BRDs can be used to develop assays to screen compound libraries for inhibitors specific for PfBDPs.

Differential Scanning Fluorimetry (DSF) allows screening of compounds against a target protein by measuring the stability of a protein under thermal stress (Niesen et al., 2007).

Compounds that bind with high affinity stabilise the target protein and therefore protect it from thermal stress. DSF does not require knowledge of the native ligand but only provides an indication of probable binding (Koshland, 1958). DSF can also be used to determine the selectivity of compounds (Galdeano and Ciulli, 2016), for example, selectivity of the compound LP99 for BRD7/BRD9 bromodomains was demonstrated by a DSF screen of LP99 against a target panel that included 48 other human BRD proteins (Clark et al., 2015). Isothermal titration calorimetry (ITC) can be used to measure transfer of energy during binding of candidate compounds to recombinant BRDs and thus determine binding affinity (K_D). Both DSF and ITC are used extensively and are complementary to other methods in fragment-based drug discovery and design of chemical probes against human BRDs (Bamborough and Chung, 2015; Dutra et al., 2017; Jiang et al., 2019).

Alternatively, amplified luminescent proximity homogeneous assays (AlphaScreen) or time-resolved fluorescence resonance energy transfer (TR-FRET) assays can be developed to screen compounds for competitive inhibition of recombinant BRD binding to acetylated histone N-terminal tail peptides (Jung et al., 2014; Yasgar et al., 2016). Both AlphaScreen and TR-FRET assays can be used for high-throughput screens and to generate K_D values, but they require the knowledge of the native acetylated histone ligand of the BRD. These methods have been successful in identifying compounds targeting BRDs in human studies, such as the discovery of the BET bromodomain inhibitor JQ-1 (Filippakopoulos et al., 2010; Wu et al., 2019; Zou et al., 2019), and can be applied to PfBDPs.

Crystallography and NMR spectroscopy are commonly used in drug discovery to determine protein structures. Crystallography facilitates fragment-based drug discovery by providing three-dimensional structures of target proteins with bound ligands. Crystal structures inform virtual docking studies (Sun et al., 2017) and hits from such studies, or from high-throughput drug screens such as AlphaScreen (Lolli and Caflisch, 2016), can be confirmed by further crystallography with bound receptor.

Fragment-based drug discovery using NMR spectroscopy could allow detection of compounds with weaker binding (Harner et al., 2013; Hoffer et al., 2011) to the *P. falciparum* BRDs. Through identifying ligand binding sites and modes of binding (Harner et al., 2013; Jennings et al., 2014) NMR can help establish the structure activity relationships of lead compounds to determine the 'active' chemical groups (Harner et al., 2013) responsible for the inhibitory effect. Protein-observed fluorine NMR (PrOF NMR) assay quantifies ligand binding affinities through detecting perturbation of fluorine resonances (Kirberger et al., 2019). PrOF NMR was

used to identify a small molecule called rac-1 which caused chemical shifts of the tryptophan residue located in the BRD hydrophobic pocket (also known as the WPF shelf (Jennings et al., 2014) of PfGCN5 and human BPTF (Kirberger et al., 2019). Interestingly, both proteins also have similar binding affinity for acetylated peptides (Perell et al., 2017). This chemical shift was absent (BRD4 and BRDT), or slight (PCAF) in other human BRDs suggesting that the rac-1 interaction with PfGCN5 and human BPTF was selective (Kirberger et al., 2019). Furthermore, rac-1, also known as GSK1379725A, can inhibit *P. falciparum* whole-parasite growth in a phenotypic screen (Gamo et al., 2010) and was included in the Malaria Box (Spangenberg et al., 2013). It will be useful to confirm whether rac-1 kills *P. falciparum* parasites via inhibition of bromodomain proteins.

1.4.3.1. In silico modelling and virtual docking studies

High-throughput in silico screening has become increasingly attractive due to the demand for a cost-effective drug discovery and development pipeline. Pharmacophore modelling allows prediction of protein-ligand interactions by either ligand-based or structure-based modelling. While very efficient, the false-positive rate for the approach is high because it can only consider a few chemical features of the BRD acetylation binding site as query input, leading to an incomplete picture of the steric restrictions of the site (Yang, 2010). A structure-based pharmacophore modelling screen requires a 3D crystal structure in complex with an inhibiting compound. A pharmacophore model was generated for the PfBDP3 crystal structure (PDB ID 4PY6) (Fonseca et al.) in complex with the BI-2536 compound and used to screen a commercial library generating 38 hit compounds (Chua et al., 2018). Subsequently, the hit compounds together with four known inhibitors of human BRDs (bromosporine, CPI-203, PFI-4 and SGC-CBP30) were analysed in docking studies with the essential PfGCN5 (PDB ID 4QNS) (Fonseca et al.) and PfBDP1 (PDB ID 3FKM) (Wernimont et al.) and also tested for *in vitro* growth inhibition. The three hits from the 42 compounds tested in the parasite growth inhibition assay all failed the *P. falciparum* hit criteria (Katsuno et al., 2015) as they all had an IC50 greater than 3 μM after a 72-h incubation with parasites (Chua et al., 2018) (Table 1.2). Of these three, only SGC-CBP30 was a validated BRD inhibitor that preferentially binds to the bromodomain of human CREBBP/CBP and p300 proteins, and interferes with their regulatory function in inflammatory cytokine production (Hammitzsch et al., 2015). While SGC-CBP30 inhibits parasite growth with an IC50 of 10 μM after a 48-h incubation, the selectivity ratio between human and *P. falciparum* is low (Chua et al., 2018). Although not a promising hit, SGC-CBP30 warrants further investigation for specificity of binding to *P. falciparum* BRDs using the

biochemical assays described in section 4 above and the parasite cell biology assays described in the expert opinion below. The other three human BRD inhibitors tested had IC50s higher than 26 μM and probably do not warrant further investigation. The future release of additional 3D structures of essential PfBDPs complexed with inhibitors could allow for the *in silico* discovery of other, novel PfBDP inhibitor scaffolds for further medicinal chemistry development.

1.4.3.2. Repurposing human BRD inhibitors to target bromodomain proteins in *P. falciparum*

Selective binding of compounds to BRDs can be optimised by medicinal chemistry using a promiscuous inhibiting scaffold. Bromosporine (Picaud et al., 2016) and [1,2,4]triazolo[4,3-*a*]phthalazines (Fedorov et al., 2014) are potent pan-BRD inhibitors that target a wide range of BET and non-BET BRDs in human. Their derivatives can be specifically customised to the acetylation binding site of the BRD of the protein of interest, to make novel inhibitors or chemical probes. L-45 is a triazolophthalazine derivative compound which has high binding affinity to human PCAF (ITC K_D=126 nM) and PfGCN5 (ITC K_D=280 nM)(Moustakim et al., 2017). A crystal structure showed that L-45 made key interactions with residues in the PfGCN5 BRD (PDB ID 5TPX) binding pocket (figure 1.3B) that are conserved between PfGCN5 and human PCAF (Moustakim et al., 2017). Further design of PfBDP-selective compounds may be possible via targeting the substitution of E750 in human PCAF for K1383 in PfGCN5 located at the outer edge of the acetyl-lysine binding pocket (Moustakim et al., 2017). Although L-45 is not selective for PfGCN5, it has no cytotoxicity for peripheral blood mononuclear cells treated with 10 μM L-45 for 24 hours (Moustakim et al., 2017). The use of L-45 for *in vitro* studies of *P. falciparum* will help validate PfGCN5 as a drug target and determine the biological consequences of PfGCN5 inhibition. Although no pan-BRD inhibitors are currently available for *P. falciparum*, the example of L-45 demonstrates the potential for medicinal-chemistry optimisation of PfBDP inhibitor design.

Table 1.2. Summary of key compounds in current PfBDPs studies from Chua et al.(Chua et al., 2018) and Moustakim et al.(Moustakim et al., 2017).

Compound	Structure	Predicted target	*In vitro* IC50 (μM)		Cytotoxicity
			48-hr assay	72-hr assay	
SGC-CBP30	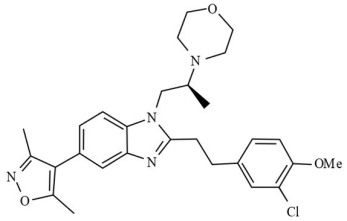	PfBDP1, PfGCN5	10.03 (±0.32)	3.16 (±1.94)	SI* ~ 2-7 fold
OSSK_842646	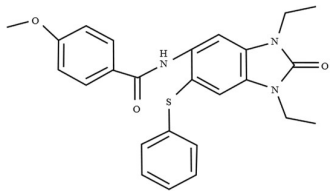	PfGCN5	11.28 (±2.00)	6.35 (±2.45)	SI* > 4**

OSSL_258906	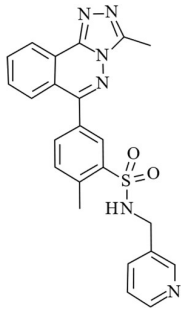	PfGCN5	11.80 (±3.06)	5.96 (±1.19)	SI* > 4**
L-45 (L-Moses)	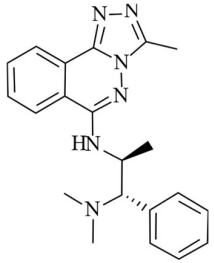	PfGCN5	n/a		Not observed in PBMC after 24 h at 10 µM

*Selectivity index as ratio between IC50 of *in vitro* parasite culture and IC50 of HEK 293 cells

** IC50 value of HEK 293 was not obtainable

1.5. Functional studies of PfBDPs

Recently, PfBDPs were detected in pulldowns of acetylated peptides of histone N-terminal tails and thus, confirming that PfBDPs can recognise histone acetylation (Hoeijmakers et al., 2019). PfBDP1 and PfBDP2 showed the lowest selectivity towards histone acetylation as they interacted with essentially all the acetylated peptide included in this study, except for H3K9ac and selected acetylated H2B.Z peptides. Interestingly, while they could interact with H2B.Z K3/K8/K13/K14/K18ac peptide, PfBDP1 and PfBDP2 were not detected when H2B.Z was either only acetylated at K3/K8 or K13/K14/K18 (Hoeijmakers et al., 2019). This phenomenon has been previously reported in which interaction of human BRD proteins to acetylated lysine sites depends on neighbouring histone modifications (Filippakopoulos et al., 2012). On the other hand, PfGCN5 and PfBDP4 bindings were more selective. PfGCN5 interacted mainly with the active histone mark H3K4me3 and, to a lesser extent, H4 acetylations while PfBDP4 was pulled down together with H2B.Z and H4 acetylation (Hoeijmakers et al., 2019). Finally, the interaction with acetylated peptide was most limited for PfBDP5/TAF1 and PfBDP3 (Hoeijmakers et al., 2019).

The connectivity between PfBDPs and other chromatin-associated proteins was also assessed using immunoprecipitation mass spectrometry (Hoeijmakers et al., 2019). Previously, we showed that PfBDP1 is important for the coordinated regulation of invasion genes and interacts with PfBDP2 the STF AP2-I(Josling et al., 2015; Santos et al., 2017). The PfBDP1-PfBDP2 complex was confirmed in Hoeijmakers et al. and they showed wide connectivity to other chromatin-associated proteins suggesting their possible role in assisting regulatory complexes to interact with histone acetylation (Hoeijmakers et al., 2019). PfBDP4 interacted with the STF AP2-I (Santos et al., 2017) as well as SWIB (chromatin-remodelling), HMGB (DNA-binding) and CHD1 (chromodomain helicase DNA binding) (Hoeijmakers et al., 2019) and thus, implying that PfBDP4 and binding partners are likely to be involved in the regulation of gene expression. PfBDP5/TAF1, as expected, formed complex with other *P. falciparum* TAF proteins (Hoeijmakers et al., 2019) as PfBDP5/TAF1 is a component of the pre-initiation complex (Callebaut et al., 2005). PfGCN5 and its coactivator ADA2 were predicted to either form a complex with PHD-finger protein 1 (PHD1) or with PHD-finger protein 2 (PHD2) and PfNAPS (Hoeijmakers et al., 2019) which is responsible for nucleosome assembly (Chandra et al., 2005; Gill et al., 2010; Navadgi et al., 2006). Lastly, IP pulldown of PfBDP4 was not performed in this study although PfBDP4 was found as binding partner of PfBDP5/TAF1 and PF3D7_1451200 of which is associated HP1 (Hoeijmakers et al., 2019).

Overall, PfBDPs are promising cross-species and multi-stage drug targets. They can recognise histone acetylation and likely play key roles in the regulation of gene regulation via interaction with transcription factors and other chromatin-associated proteins. Target-based drug discovery strategies including high-throughput screens, *in silico* modelling, and chemical biology have identified a small number of compounds that can interact with PfBDPs. Future studies can further dissect the functional roles of PfBDPs as well as using growth inhibition assays and other *in vitro* bioassays to understand the consequences of parasite treatment with these hit compounds.

2. Hypotheses and Aims

The hypothesis of this work is that *Plasmodium falciparum* bromodomain proteins play an important role in the regulation of gene expression and that they can be targeted by inhibitors.

The aims of this study are:

1) To determine the importance of the PfBDP3 and PfBDP4 during the asexual, blood stage
2) To identify genomic enrichment of PfBDP3 and PfBDP4
3) To test hit compounds against the BRDs of PfBDPs in an *in vitro* assay to determine their effect on parasite growth

3. Materials and Methods

3.1. General cell biology methods of *P. falciparum*

3.1.1. *P. falciparum* parasite culture

P. falciparum parasites were cultured in Petri dishes as previously described (Trager and Jenson, 1978). The culture was fed with RPMI-HEPES (Gibco) containing 50:50 ratio of AlbuMAX™ (Gibco) to heat-inactivated human serum, 0.2% sodium bicarbonate and 4% human O+ red blood cells (Australian Red Cross Blood Service). Parasite cultures were incubated at 37ºC in air-tight containers containing 1% O_2, 5% CO_2 and 94% N_2. Parasite smears were stained with Giemsa and counted using a light microscope to maintain 0.5%-12% parasitaemia. Genetically modified parasite lines expressing recombinant proteins included introduced genes encoding drug resistance and so were grown with appropriate drug, either 2.5 nM WR99210 (Walter Reed Army Institute of Research) or 1µg/mL blasticidin (Sigma).

3.1.2. Synchronisation

Ring stage parasites were synchronised using sorbitol (Lambros and Vanderberg, 1979). The culture was spun to pellet RBCs which were resuspended in ten pellet volumes of 5% sorbitol. The suspension was incubated in a 37ºC water bath for 5 minutes. Then, it was centrifuged at 2000*g* for 5 minutes and the supernatant was removed. The blood pellet was returned to culture with fresh media. To obtain highly synchronous culture, double sorbitol synchronization was performed 10-12 hours apart, which created a 4 to 6-hour window of parasite developmental stages.

3.1.3. Freezing and thawing

For freezing *P. falciparum* culture at approximately 5% parasitemia and 4% haematocrit was centrifuged at 2000*g* for 5 minutes and the supernatant discarded. The packed RBC pellet was resuspended in a total of 2 pellet volumes of glycerolyte 57 (Fenwal) in two steps. The first 1/3 of a pellet volume of glycerolyte 57 was added dropwise to the packed RBC pellet with gentle mixing by swirling the tube. The mixture was then left undisturbed for 5 minutes at room temperature (RT). Next, the remaining volume of glycerolyte 57 was added dropwise with gentle mixing by swirling the tube. Aliquots of 300 µL to 1mL were stored in cryovials placed in isopropanol at -80°C for 1 day. Cryopreserved cultures were stored either at -80°C or in liquid nitrogen.

For thawing, NaCl thawing solutions were pre-warmed to 37°C. Cryopreserved *P. falciparum*-infected RBCs were rapidly thawed in a 37°C water bath for 1-2 minutes. The content of the cryovial was transferred to a 10 ml tube and 1/10th volume of sterile 12% NaCl solution was added dropwise with gentle mixing by swirling the tube. The tube was left undisturbed for 5 minutes at RT before adding 10 volumes of sterile 1.6% NaCl solution to the tube. The sample was centrifuged at 1500 rpm for 5 minutes at RT and the supernatant was removed. The pellet was resuspended in pre-warmed RPMI-HEPES media supplemented with 0.25% Albumax (Invitrogen), 5% heat-inactivated human serum (Australian Red Cross Blood Service) and fresh RBC for culturing.

3.1.4. Transfection

P. falciparum transfection was as previously described (Deitsch et al., 2001a) with modifications. Linearised donor plasmid and circular pUF1-Cas9 plasmid were co-transfected into ring-stage parasites. 100 µg of the donor plasmid was linearised by restriction enzyme digestion with PvuI overnight at 37°C according to the manufacturer's instructions (NEBiolabs). The next morning additional PvuI were added and the sample was incubated at 37°C for another 2 hours. Approx 4 µL of the reaction was tested by agarose electrophoresis to confirm complete plasmid linearisation. The linearised donor plasmid was then ethanol precipitated with 1/10 volume of 3M sodium acetate (pH 5.2) and 2.5 volumes of 100% ethanol at -20°C for a minimum of 30 minutes. 100 µg of the circular pUF1-Cas9G plasmid was also ethanol precipitated as described above. The precipitated plasmids were pelleted by centrifugation at 8000 *g* for 15 minutes at 4°C and washed once with sterile 70% ethanol. After air-drying, the DNA pellets were dissolved in 15 µL pre-warmed 37°C TE buffer (10 mM Tris pH 8.0, 1 mM EDTA) and combined. Pre-warmed cytomix was then added (120 mM KCl, 0.15 mM $CaCl_2$, 2 mM EGTA, 5 mM $MgCl_2$, 10 mM K_2HPO_4/KH_2PO_4 pH 7.6, 25 mM Hepes pH 7.6) to a total volume of 400 µL.

5mL of *P. falciparum* 3D7 clone with a parasitemia of 4-6% synchronised rings and a haematocrit of 3% was pelleted (150 µL packed blood), washed with cytomix and mixed with the DNA solution. The suspension was electroporated with the Bio-Rad Gene Pulser Xcell Electroporation Systems in a 0.2cm cuvette at 0.31 kV, 950 µF and infinite resistance. Immediately afterwards, electroporated cells were suspended in 10 mL pre-warmed medium and 150 µL fresh RBC (approximately 3% haematocrit) and returned to a 37°C incubator. 2.5 nM WR99210 (Walter Reed Army Institute of Research) was added to the culture

approximately 24 hours after the transfection and was maintained in culture until parasites were recovered.

3.1.5. Cloning by limiting dilution

To obtain clones of a parasite line, synchronised trophozoites were diluted so that one well of a 96-well plate (100 µL culture/well, 3% haematocrit) contained either 10 parasites/well (10 wells) or 1 parasite/well (20 wells) or 0.3 parasites/well (30 wells). Wells were fed with fresh medium and 2.5 nM WR99210 (Walter Reed Army Institute of Research) routinely every 4 days. The wells with 10 parasites/well were used to confirm that cultures were growing although these were not used to obtain clones. When parasites were detectable by Giemsa-stained blood smears (after approximately 15 days) in the wells containing 1 parasite/well and 0.3 parasites/well, these cultures were expanded to obtain sufficient genomic DNA for genotyping by diagnostic PCR.

3.1.6. Lysate harvest and cellular fractionation

To release parasites from RBCs, parasite culture was spun down, and the pellet was washed with PBS before adding ice-cold Saponin to a final concentration of 0.075% and incubated on ice for 5 minutes. Saponin-lysed cells were pelleted by centrifugation at 2500*g* for 5 minutes and washed twice with 10 ml of ice-cold PBS. To harvest total protein lysate, the pellet was suspended in 30-100 µL 2x Laemmli buffer and boiled at 95°C for 10 minutes. After centrifugation at 2500*g* for 10 minutes at RT, the supernatant containing the total protein lysate was transferred to a new tube.

For cellular fraction, the saponin-lysed cells were incubated on ice with 500 µL lysis buffer (20mM Hepes, pH 7.8, 10mM KCl, 1mM EDTA, 1mM DTT, 1x Protease inhibitors (Roche, cat no. 4693159001)) for 15 minutes. After swelling the cells, parasite cell membranes were selectively lysed by addition of IGEPAL 630 (Sigma, cat no. I8896) to 0.65% v/v and incubation on ice for 1 minute. The nuclei were spun at 2500g for 10 minutes at 4ºC. Cytoplasmic proteins solubilised in the supernatant were stored at -80ºC (C-Fraction). The insoluble, nuclear pellet was washed with lysis buffer and then vigorously agitated in extraction buffer (20mM Hepes, pH 7.8, 800mM KCl, 1mM EDTA, 1mM DTT, 1x Protease Inhibitors) for 30 minutes at 4ºC. The resulting suspension was centrifuged at 2500*g* for 30 minutes and the supernatant, containing soluble nuclear proteins, was collected (Ns-Fraction). The pellet was dissolved by boiling in 2x Laemmli buffer and then spun 8000*g* for 10 minutes and then the supernatant, that contained histones and proteins tightly associated with chromatin, was

diluted in dilution buffer (20 mM HEPES, 1 mM DTT, 1 mM EDTA and 30% glycerol) and stored at -80ºC (Ni-Fraction). All fractions were analysed by Western Blot.

3.2. Molecular biology methods

3.2.1. DNA amplification by polymerase chain reaction (PCR)

To assemble components of the donor plasmid, the PCR amplification of the 3D7 genome was performed using 0.2 µL Q5 high fidelity DNA polymerase (NEBiolabs, M0491), 2 µL Q5 reaction buffer, 0.25 mM dNTPs, 1 µM of each primer (Appendix, table 9.1) and between 2.5 to 15 ng template DNA in a 20 µL reaction. The PCR conditions were 94°C for 2 minutes for the initial denaturation and 30 cycles of 94°C for 30 seconds for denaturation, and 56.1°C for 30 seconds for annealing and 68°C for 2 minutes for extension, followed by a final extension at 68°C for 5 minutes. PCR products were purified using the QIAquick PCR purification kit (Qiagen) according to the manufacturer's instructions. Purified PCR products were quantified by agarose gel electrophoresis.

To screen bacterial colonies or genotype integrated parasites, PCR amplification was performed using 0.25 µL Taq polymerase (NEBiolabs, M0267), 5 µL Thermopol buffer, 0.2 mM dNTPs, 0.2 µM of each primer (Appendix, table 9.1) and less than 1 µg of DNA in a 50 µL reaction. The PCR conditions were 95°C for 30 seconds for the initial denaturation and 30 cycles of 95°C for 30 seconds for denaturation, and 45°C for 30 seconds for annealing and 64°C for 2 minutes for extension, followed by a final extension at 68°C for 5 minutes. PCR products were analysed by agarose gel electrophoresis to confirm the presence of the product at the correct size.

3.2.2. Restriction enzyme digestion and ligation

Restriction enzyme digestion was performed with conditions as recommended by NEBiolabs. Generally, 1 to 5 µg of DNA were digested in a 50 µL reaction consisted of 1X buffer and restriction enzymes of interest. The total amount of restriction enzyme added did not exceed 10% of the total reaction volume (5 µL) to prevent star activity leading to non-specific digestion. The reaction was incubated at 37°C for 1 hour and inactivated at 65°C for 20 minutes unless indicated otherwise by NEBiolabs. Afterwards, an aliquot of the reaction was loaded on agarose gel electrophoresis to confirm complete digestion of the reaction. Digested products were ligated using T4 DNA ligase (NEBiolabs, M0202) according to the manufacturer's instructions.

3.2.3. Bacterial transformation

The *E. coli* XL10-Gold ultracompetent cells (50 µL aliquots) were thawed on ice before 2 µL of the assembled product from the previous step was added to the cells. The content was gently mixed by flicking the tube 5 times and was placed on ice for 30 minutes. The mixture of cells and DNA were heat-shocked at 42°C for 30 seconds and then immediately placed on ice for 2 minutes. 600 µL of super optimal broth (SOC – 2% w/v Tryptone, 0.5% w/v yeast extract, 0.05% w/v NaCl, 2.5 mM KCl, 10 mM $MgCl_2$ and 20 mM glucose, pH 7.0) was added to the mixture and incubated at 37°C for 60 minutes with constant agitation (approximately 250 rpm). After incubation, 20-100 µL of the cell mixture was spread on LB agar plates (1% w/v tryptone, 0.5% w/v yeast extract, 0.5% w/v NaCl and 2% w/v bacteriological grade agar) with 100 µg/mL Ampicillin or 50 µg/mL Kanamycin, depending on the antibiotic resistance gene of the plasmid. The plate was incubated overnight at 37°C. Once the correct plasmid was confirmed by diagnostic PCR, a bacterial colony was grown in LB media (1% w/v tryptone, 0.5% w/v yeast extract and 0.5% w/v NaCl) to obtain more copies of the plasmid. Plasmids were extracted with QIAprep ® kits (QIAGEN) as per the manufacturer's instructions.

3.2.4. Generating constructs for BDP3*glmS*

The PTEX150 plasmid described in Elsworth et al. (Elsworth et al., 2014), which contains three HA tags and *glmS*, was used as the backbone construct to generate the donor construct for BDP3*glmS*. The 3' homology arm of PfBDP3 was amplified by Q5 PCR using HN47 and HN48 primers (Appendix, table 9.1) of which restriction sites for KasI and BstAPI restriction enzymes, respectively, were incorporated into the primers. The PTEX150 plasmid and 3' homology arm PCR products were digested with KasI (NEBiolabs) and BstAPI (NEBiolabs) in CutSmart ® buffer and ligated as described in chapter 3.2.2. The ligated plasmid, named PfBDP3-3prime, was transformed into XL10-Gold ultracompetent cells and propagated as described in chapter 3.2.3 and checked by Sanger sequencing for correct ligation.

The 5' homology arm of PfBDP3 was amplified by Q5 PCR using HN52 and HN53 primers (Appendix, table 9.1) of which restriction sites for BglII and PstI restriction enzymes, respectively, were incorporated into the primers. The PfBDP3-3prime plasmid and 5' homology arm PCR products were digested with BglII (NEBiolabs) and PstI (NEBiolabs) in CutSmart ® buffer and ligated as described in chapter 3.2.2. The ligated plasmid, named PfBDP3*glmS*, was transformed as described above.

The pUF1-Cas9G was previously described in Wilde et al. (Wilde et al., 2019) and was used in this study. The guide RNA was designed in an online tool called Benchling. The pUF1-Cas9G was digested with BtgZI (NEBiolabs). Double-stranded guide RNA sequence was assembled by annealing two complementary oligos (Appendix, table 9.1) with overhangs which can be ligated to the BtgZI-digested pUF1-Cas9G. The ligated plasmid was transformed and propagated as described above.

3.2.5. Western blot

Proteins were separated by SDS-PAGE through either NuPAGE™ Novex™ 3-8% Tris Acetate or 4-12% Bis-Tris polyacrylamide gels at 120 V for 90 minutes. Proteins in the gel were transferred to a nitrocellulose membrane in transfer buffer (190 mM Glycine, 25 mMTris, 0.1% SDS and 20% Methanol) at 400mA for 1 hour. Protein transfer was verified by Ponceau staining (0.1% Ponceau Red and 5% Acetic acid) for 30 seconds followed by rinsing with H_2O. The membrane was blocked with TBS-T/5% non-fat milk (500 mM Tris, 1.50 M NaCl, pH 7.5 and 0.05% Tween) at RT for 30 minutes followed by incubation with primary antibody (Appendix, table 9.2) in TBS-T/5% non-fat milk overnight at 4^{o}C. On the next day, the membrane was washed three times with TBS-T and blocked with TBS-T/5% non-fat milk before incubation with HRP-conjugated secondary antibody (Appendix, table 9.2) at RT for 2 hours. The membrane was washed three times with TBS-T. Finally, substrates from the Pierce Super Pico kit (Thermo Scientific, cat no. 35065) was added to the membrane and signal was captured using a Bio-rad ChemiDoc ™ Touch Gel Imaging system.

3.2.6. Immunofluorescence assay

Blood smears of parasite cultures on glass microscope slides were air-dried overnight and fixed in 10% Methanol/ 90% Acetone. A silicon pen (DakoCytomation) was used to separate the fields on the slide. After rehydrating the fixed material in PBS, the mouse primary antibody against Ty1-epitope tag (diluted 1 in 5000 or 1 in 10000 in PBS/1%BSA) was added to the field and incubated for 2 hours at room temperature. The fields were washed three times with sufficient PBS to cover the whole field (minimum 50 µL PBS per wash) prior to the 2-hour incubation with secondary antibody mouse AlexaFluor 488 (Invitrogen, A11001) (diluted 1 in 1000) and Hoechst 33342 dye. The fields were washed with PBS as above and then the slides were mounted with anti-fading mounting medium (Invitrogen ProLongAntifade) and a coverslip. The mounted slides were cured overnight and analysed using a 100x Oil Objective light microscope.

3.2.7. DNA extraction from *P. falciparum* culture

Genomic DNA of *P. falciparum* culture was harvested using the QIAamp DNA blood mini kit (QIAGEN) according to the instructions of the manufacturer. Up to 200 µL packed RBC of around 2-5% parasitemia was used for each extraction column. The genomic DNA was eluted in 50 µL distilled water at RT.

3.3. Determination of *P. falciparum* growth rate or PfBDP knockdown/knockdown

To measure the effect that induction of PfBDP knockout or knockdown has on parasite growth, 3D7-PfBDP3-*loxP-glmS* and the parental control 3D7 DiCre cultures with 0.2% parasitemia and 2% hematocrit were incubated with 100 µM rapamycin and/or 2.5 mM GlcN or vehicle controls for 5 days in a 96-well plate. Each well contained 100 µL of culture and each condition was tested in four technical replicates. Uninfected (RBC only) samples were included to establish a baseline for the raw readout. The plate was placed in an air-tight container at 37°C. After 5 days, the plate was analysed using a SYBR Green I assay. 100 µL of lysis buffer (20 mM Tris-HCl, pH 7.5, 5mM EDTA, pH 8.0, 0.008% w/v Saponin, 0.08% v/v Triton X-100 and 0.1 µL/mL SYBR green I (Invitrogen)) was added to each well and was resuspended by pipetting up and down until the solution became clear. The plate was incubated in the dark for at least 1 hour before measuring the fluorescence using a FLUOstar ® Omega plate reader. The fluorescence of uninfected RBCs was subtracted from the fluorescence of *P. falciparum* iRBCs samples.

3.4. Materials to determination of PfBDP knockout and knockdown

To test the inducible knockout and knockdown systems Petri dishes with 24 mL of the 3D7-PfBDP4-*loxP-glmS* parasite line with <1% parasitemia, 3% haematocrit were cultured with 100 µM rapamycin and/or 2.5 mM glucosamine (GlcN) or an equivalent amount of DMSO and/or water in vehicle only-control cultures. The BDP3*glmS* parasite line was tested similarly but with 2.5 mM GlcN or vehicle only. After 24 hours, 20 mL of each culture was harvested and genomic DNA and total protein lysate extracted for quantitative PCR (chapter 3.5) and western blot analysis, respectively. western blot was performed as described in chapter 3.2.4 with rat anti-HA (Roche, 11867423001) primary antibody and goat anti-rat (Abcam, ab97057) secondary antibody (Appendix, table 9.2).

The remaining 4 mL culture was centrifuged, and the blood pellet was washed with pre-warmed media and then subcultured at a 1 in 6 dilution by adding fresh media, fresh blood and rapamycin/glucosamine/vehicle as previously up to a final volume of 24 mL at 3% haematocrit. Cultures were harvested using the protocol described above every cycle (48 hours) for genomic DNA and total protein lysate after the first harvest on day 24.

3.5. Determination of PfBDP knockout by quantitative PCR

qPCR was performed in 384-well reaction plates using previously published conditions in Petter et al. (Petter et al., 2011) and was performed on a Biorad CFX96 touch RT-PCR machine (Biorad). Each 10-µL reaction contained 5 µL SYBR Green PCR master mix (Applied Biosystems), 1.5 µL of 2 µM primer stock of each primer and 2 µL diluted DNA. qPCR reactions were prepared in duplicates and the primers used are listed in Appendix Table 9.1.

For excision quantification in chapter 4, the intact PfBDP4 locus was expressed as a percentage in relative to skeleton-binding protein (SBP) ($2^{-\Delta Ct}$ x 100%) which acts as a house-keeping gene where $\Delta Ct = Ct_{PfBDP4\_intact} - Ct_{SBP}$. For ChIP-qPCR in chapter 5, the enrichment of DNA was expressed as a percentage input ($2^{-\Delta Ct}$ x 100%) where $\Delta Ct = Ct_{BDPTy\_TY\_ChIP} - Ct_{BDPTy\_input}$. To normalised ChIP enrichment for non-specific signal, delta delta Ct was calculated by this formula $\Delta\Delta Ct = (Ct_{BDPTy\_TY\_ChIP} - Ct_{BDPTy\_input}) - (Ct_{3D7\_TY\_ChIP} - Ct_{3D7\_input})$ and fold enrichment was expressed as $2^{-\Delta\Delta Ct}$.

3.6. Materials for ChIP-seq

3.6.1. Nuclei harvest for crosslink-chromatin immunoprecipitation (X-linked ChIP)

Cultures were harvested for X-linked ChIP so that there were approximately 10^8 IE for each ChIP. 122 mL of a synchronous schizont culture with 8-10% parasitemia and 3% haematocrit were harvested. Matched RNA samples were harvested by spinning down 10 mL of the same culture, dissolving the RBC pellet in 6 mL of Trizol and incubating the Trizol solution at 37°C for 5 minutes before storing it at -80°C. 7 mL of 16% w/v formaldehyde (Pierce ™) was added to 112 mL of the remaining culture to make a final concentration of 1% w/v formaldehyde. Cells were crosslinked at 37°C for 10 minutes. Then, the reaction was quenched by the addition of glycine to a final concentration of 125 mM and incubation on ice for 5 minutes. Cells were pelleted by centrifugation at 1500 rpm at 4°C for 5 minutes and the supernatant was removed. The pellet was resuspended in 10 times the pellet volume of ice-cold PBS and 0.075% saponin

and incubated on ice for 5 minutes to lyse the RBCs. The suspension was subjected to centrifugation at 2000*g* for 10 minutes and the supernatant containing the lysed RBC contents was removed. The parasite pellet was washed twice with cold PBS and incubated on ice with lysis buffer (10 mM Hepes, pH 7.9, 10 mM KCl, 0.1 mM EDTA, 0.1 mM EGTA, 1 mM DTT, 1x Protease inhibitors) for 10 minutes before adding IGEPAL 630 to a final concentration of 0.25% v/v. The parasite was lysed in a glass 1.5mL Dounce homogeniser with 100 strokes for every 10^9 iRBC. Nuclei were spun down at 14000 rpm for 10 minutes and washed twice with the lysis buffer.

The samples were resuspended in SDS lysis buffer (1% SDS, 10 mM EDTA, 50 mM Tris-HCl, pH 8.1) or Shearing buffer (0.1% SDS, 1 mM EDTA, 10 mM Tris-HCl, pH 7.6) for sonication with the Diagenode Bioruptor or the Covaris S220 system, respectively. The conditions for each system are discussed in more details in chapter 5.2.2.1. The size distribution of DNA fragments was confirmed by agarose gel electrophoresis while the integrity of the TY-epitope tag was checked by western blot analysis.

3.6.2. Nuclei harvest for native ChIP

Cultures were harvested for native ChIP so that there were approximately 10^8 IE for each ChIP. For native ChIP, 135 mL of a synchronous schizont culture with 8-10% parasitemia and 3% haematocrit were harvested. Matched RNA samples were harvested by spinning down 10 mL of the same culture, resuspending the RBC pellet in 6 mL of Trizol and incubating the Trizol mix at 37°C for 5 minutes before storing it at -80°C. The remaining 125 mL of the culture was centrifuged, and the supernatant was removed to collect the packed RBC pellet. Then, the pellet was resuspended in 10 times the pellet volume of ice-cold PBS and 0.075% cold saponin and incubated on ice for 5 minutes. It was centrifuged at 2500 rpm for 10 minutes and the supernatant containing the lysed RBC contents was removed. The parasite pellet was washed twice with cold PBS. To swell and release the parasite nuclei, 500 µL of cold swelling buffer (SB) (10 mM HEPES, pH 7.9, 10 mM KCl, 0.1 mM EDTA, 0.1 mM EGTA, 1 mM DTT, 1X protease inhibitor without EDTA and 10 mM sodium butyrate) for each 10^9 iRBC was added to the parasite pellet and the mixture was placed on ice for 10 minutes. IGEPAL 630 was then added to make a final concentration of 0.65%. After a 1-minute incubation on ice, parasite nuclei were collected by centrifugation at 8000*g* for 10 minutes at 4°C. The pellet was washed once with 500 µL of SB for each 10^9 iRBC. The pellet containing parasite nuclei was resuspended in 250 µL of chromatin digestion (CD) buffer (50 mM Tris, pH 7.4, 4 mM $MgCl_2$, 1 mM $CaCl_2$, 1X protease inhibitor without EDTA and 5 mM sodium butyrate) for each 10^9

iRBC and was digested with 20 KU of Mnase at 37°C for 15 minutes. EDTA was then added to a final concentration of 10 mM to stop the digestion followed by centrifugation at 14000 rpm for 5 minutes at 4°C. The supernatant which contained the digested mono- and poly-nucleosomes was transferred to a new tube.

3.7. ChIP assay

For schizont nuclei, an estimated 10^8 parasites were used for each ChIP. Prior to the ChIP assay, protein G agarose beads were washed and blocked in ChIP dilution buffer (0.01% SDS, 1.1% Triton-X100, 1.2 mM EDTA, 16.7 mM Tris-HCl, pH 8.1, 150 mM NaCl) with 0.1% BSA. Washed beads were made into a 50% slurry for ChIP-seq. Sonicated samples were diluted 1 in 10 with ChIP dilution buffer and were pre-cleared with 50 µL of 50% bead slurry at 4°C for 1 hour on a rotator. An aliquot of 50 uL was kept separately as input material for ChIP-qPCR and ChIP-seq normalisation. For each ChIP, 30uL of the protein G bead slurry, 5 µg of mouse monoclonal anti-TY antibody (Sigma, SAB4800032) or 2 µg of rabbit polyclonal anti-TY antibody (GenScript, A01004) and a volume of precleared, sonicated nuclei equivalent to 10^8 parasites were incubated together overnight at 4°C with rotation. On the next day, the beads were pelleted and washed once with low salt buffer (0.1% SDS, 1% Triton X-100, 2 mM EDTA, 20 mM Tris-HCl, pH 8.1, 150 mM NaCl), once with high salt buffer (0.1% SDS, 1% Triton X-100, 2 mM EDTA, 20 mM Tris-HCl, pH 8.1, 500 mM NaCl), once with LiCl immune complex buffer (250 mM LiCl, 1% IGEPAL 630, 1 mM EDTA, 10 mM Tris-HCl, pH 8.1) at 4°C and twice with TE buffer (10 mM Tris-HCl, pH 8.0, 1 mM EDTA, pH 8.0) at RT with rotation. Finally, complexes that bound to the beads, as well as input samples, were eluted twice, each time with 100uL of elution buffer (1% SDS, 0.1M $NaHCO_3$) at RT with rotation. Eluted samples were reverse cross-linked in 500mM of NaCl overnight at 45°C. On the next day, the eluted DNA was extracted using the Qiagen MinElute column following the manufacturer's instructions. ChIP-DNA was eluted sequentially twice from columns with 25uL of MiliQ per elution.

ChIP DNA was analysed by qPCR as described in chapter 5. qPCR was performed using the same conditions as for the quantitation of intact PfBDP4 locus described above. The enrichment of DNA was expressed as a percentage input (($2^{-\Delta Ct}$ x 100)%) where $\Delta Ct = Ct_{BDPTy\_TY\_ChIP} - Ct_{BDPTy\_input}$. To normalise ChIP enrichment for non-specific signal, the input normalised ChIP was further transformed to fold enrichment over non-specific ChIP of wildtype 3D7 parasites using $2^{-\Delta\Delta Ct}$ where $\Delta\Delta Ct = (Ct_{BDPTy\_TY\_ChIP} - Ct_{BDPTy\_input}) - (Ct_{3D7\_TY\_ChIP} - Ct_{3D7\_input})$.

3.7.1. ChIP library preparation

ChIP-seq libraries were prepared using the NEBNext DNA kit as per the manufacturer's instructions with the following modifications. ChIP-seq libraries were not size selected. USER excision was performed to cut the Uracil in the loop adapter after adaptor ligation. 3 µL of USER enzyme was added to ligated materials and incubated at 37°C for 15 minutes. USER excised DNA was purified with 1X AMPure XP beads (Beckman Coulter) and 23 µL of purified DNA was enriched by PCR amplification in 10µL of 5x KAPA HiFi buffer, 1.5µL of 10 mM dNTP, 2.5 µL Universal primers, 2.5 µL index primers, 1 µL KAPA HiFi (1U/uL) and 9.5 µL of H_2O. The PCR protocol was initial denaturation at 98°C 2 minutes, 15 cycles of denaturation at 98°C 15 seconds, annealing/extension at 65°C 2 minutes and a final extension at 65°C 5 minutes. Finally, samples were purified using 0.9X AMPure XP beads to minimise adapter contamination while maximising the recovery of the library. ChIP-seq libraries were subjected to QC for library fragment distribution on a BioAnalyzer or Tapestation before being sequenced on a Novaseq 6000 Next-generation sequencing machine.

3.8. RNA extraction and purification

Frozen, Trizol (Invitrogen) solubilised, iRBCs were thawed rapidly at 37°C. All steps of RNA extraction and purification used RNase-free tubes and solutions to avoid RNA degradation. $1/5^{th}$ total Trizol volume of Chloroform (Sigma) was added to the sample and mixed well by vortexing for 15 seconds. The sample was incubated at RT for 3 minutes before spinning it at 9000-12000g at 4°C for 30 minutes. The aqueous supernatant containing nucleic acids was aspirated to a new tube and an equal volume of 70% ethanol was added. The total volume was then applied to an RNeasy mini column (Qiagen) according to the manufacturer's instructions and the RNA was eluted in DEPC water. Contaminating DNA in the eluted material was degraded by incubating it at RT for 10 minutes with DNase I (Qiagen) according to the manufacturer's instructions. A second RNeasy mini column (Qiagen) was used to purify the post-DNase treated RNA. The RNA was eluted using RNase-free water. The level of DNA contamination in the eluted RNA sample was determined by qPCR.

3.8.1. RNA library preparation

RNA-seq libraries were prepared using the NEBNext Ultra directional RNAseq kit as per the manufacturer's instructions with modifications as below. Size selection for optimal library size (between 200 bp to 600 bp) performed using 0.5X followed by 0.3X volumes of AMPure XP beads. The final library amplification step was performed using the KAPA HiFi kit with the

following condition: 10µL of 5x KAPA HiFi buffer, 1.5µL of 10 mM dNTP, 2.5 µL Universal primers, 2.5 µL index primers, 1 µL KAPA HiFi (1U/uL), 23 µL of purified DNA and 9.5 µL of H2O. Amplification was performed at 37°C 15 minutes for USER excision, then 98°C for 1 minute for initial denaturation, then 12 cycles of denaturation at 98°C for 10 seconds and annealing/extension at 65°C for 1 minute and a final extension at 65°C for 5 minutes. Finally, samples were purified with 0.8X volume of AMPure XP beads to remove adapters that may interfere with the sequencing run. RNA-seq libraries were subjected to QC for library fragment size distribution on a BioAnalyzer or Tapestation before being sequenced on a Novaseq 6000 Next-generation sequencing machine.

3.9. Bioinformatics analyses

ChIP-seq data analyses

```
# Quality control of raw sequencing data using fastqc which was
# developed by the Babraham Bioinformatics group

fastqc ~/path/ChIP_TY_R1.fastq.gz

fastqc ~/path/ChIP_TY_R2.fastq.gz


# Trim adapters and clean raw sequencing using fastp (Chen et al., 2018)

fastp \
--dont_overwrite \
--overrepresentation_analysis \
--thread 4 \
--html ~/path/fastp_report_ChIP_TY.html \
--json ~/path/fastp_report_ChIP_TY.json \
--in1 ~/path/ChIP_TY_R1.fastq.gz \
--in2~/path/ChIP_TY_R1.fastq.gz \
--out1 ~/path/ChIP_TY_R1.fastp_trimmed.fastq.gz \
--out2 ~/path/ChIP_TY_R2.fastp_trimmed.fastq.gz


# BWA alignment to 3D7 genome (Li, 2013)

bwa mem -t 5 ~/path/PlasmoDB-44_Pfalciparum3D7_Genome.fasta \
ChIP_TY_R1.fastp_trimmed.fastq.gz  ChIP_TY_R2.fastp_trimmed.fastq.gz > ChIP_TY_mapped.sam


# Convert sam, sort and index BAM file using Samtools (Li et al., 2009)

samtools sort ChIP_TY_mapped.sam -o ChIP_TY_mapped_sorted.bam && samtools index
ChIP_TY_mapped_sorted.bam ChIP_TY_mapped_sorted.bai
```

```
# ChIP peak calling using macs (Zhang et al., 2008)

macs2 callpeak -t ChIP_TY_mapped_sorted.bam -c ChIP_input_mapped_sorted.bam -f BAMPE -g
23E06 -n BDP3ty_Sz_rep3 -q0.01


# Convert to bedgraph file for visualisation in Integrative Genomics Viewer
# or IGV (Robinson et al., 2011) using BEDTools (Quinlan and Hall, 2010)

bedtools genomecov -ibam ChIP_TY_mapped_sorted.bam -bga -trackline >
ChIP_TY_mapped_sorted.bedgraph


# Deeptools (Ramírez et al., 2014): calculate correlation between replicates

multiBamSummary bins -b ChIP_TY_rep1_mapped_sorted.bam
ChIP_input_rep1_mapped_sorted.bam ChIP_TY_rep2_mapped_sorted.bam
ChIP_input_rep2_mapped_sorted.bam -out ChIP_ multibam_sum.npz

plotCorrelation -in ChIP_ multibam_sum.npz -o ChIP_correlation_heatmap.png -l ChIP_TY_rep1
ChIP_input_rep1 ChIP_TY_rep2 ChIP_input_rep2 -c pearson -p heatmap --plotNumbers --colorMap
RdYlBu

# Deeptools (Ramírez et al., 2014): plot the profile of BDP4ty ChIP-seq across the CDS of closest genes

computeMatrix scale-regions -p 5 -S ~/output/BDP3ty_Sz_rep1_log2ratio.bw\
 -R BDP4ty_Sz_rep1_closest_genes_2fold_sorted.bed \
 --beforeRegionStartLength 2000 --regionBodyLength 2500 --afterRegionStartLength 2000 \
 -out ~/output/BDP4ty_Sz_matrix_closest.gz\
--outFileNameMatrix ~/output/BDP4ty_Sz_matrix_closest.tab --startLabel 5'end --endLabel 3'end --
samplesLabel BDP4ty_Sz_rep1_ChIP


plotProfile -m ~/output/BDP4ty_Sz_matrix_closest.gz -out
~/output/Profile_BDP3ty_Sz_matrix_closest.pdf --plotFileFormat pdf --yAxisLabel "log2(ChIP_input)" -
-legendLocation upper-right --yMin -0.5 --yMax 2 --startLabel 5'end --endLabel 3'end


# Deeptools (Ramírez et al., 2014): plot the profile of BDP4ty, BDP1 and AP2-I ChIP-seq across
# ATAC-seq and AP2-I intersecting regions

computeMatrix reference-point -S  output/hannah/AP2I_ChIP_merge.bam_input_log2.bw
output/hannah/cat_S_H3_input_log2.bw output/hannah/BDP3ty_Sz_rep4_log2ratio.bw
output/hannah/allBDP1SzCHiP_sorted.bam_input_log2.bw \

      -R output/hannah/ATACset40_closest_to_AP2I_summits_stranded.bed -out
output/hannah/BDP3_AP2I_H3_BDP1.gz --outFileNameMatrix
output/hannah/BDP3_AP2I_H3_BDP1.tab --samplesLabel AP2-I H3 BDP4ty_Sz BDP1_Sz -p 5 --
beforeRegionStartLength 2000 --afterRegionStartLength 2000
```

plotProfile -m output/hannah/BDP3_AP2I_H3_BDP1.gz -out output/hannah/ProfileBDP3_AP2I_H3_BDP1.pdf --outFileNameData Profile_BDP34_AP2I_new --plotType lines --refPointLabel ATAC_summit --samplesLabel AP2I H3 BDP4 BDP1 --yAxisLabel "log2 ratio over input" --legendLocation upper-right --plotFileFormat pdf --yMin -1.5 --yMax 2 --plotWidth 9

RNA-seq data analyses

Quality control of raw sequencing data using fastqc which was developed by the Babraham
Bioinformatics group
fastqc ~/path/RNA_BDP4ty_Sz_rep1_R1.fastq.gz
fastqc ~/path/RNA_BDP4ty_Sz_rep1_R2.fastq.gz

Quality and adaptor trimming of sequencing data using trim galore which was developed by the
Babraham Bioinformatics group

trim_galore --phred33 --paired RNA_BDP4ty_Sz_rep1_R1.fastq RNA_BDP4ty_Sz_rep1_R2.fastq

Make index files for genome for STAR RNA-seq mapper (Dobin et al., 2012)

STAR --runMode genomeGenerate --runThreadN 2 --genomeDir /home/hanahng/db/ 3D7_v42_STAR_index --genomeFastaFiles PlasmoDB-42_Pfalciparum3D7_Genome.fasta --sjdbGTFfile PlasmoDB-42_Pfalciparum3D7.exons_only_for_star.gff --sjdbOverhang 150 --genomeSAindexNbases 11

Map sequences to indexed 3D7 genome using STAR RNA-seq mapper (Dobin et al., 2012)

STAR --genomeDir /home/hanahng/db/ 3D7_v42_STAR_index --runThreadN 2 --alignIntronMin 5 --alignIntronMax 5000 --outSAMattrIHstart 0 --outSAMtype BAM Unsorted --quantMode TranscriptomeSAM GeneCounts --readFilesIn RNA_BDP4ty_Sz_rep1_R1_val_1.fq RNA_BDP4ty_Sz_rep1_R1_val_2.fq – outFileNamePrefix BDP4ty_Sz_rep1_star_mapped

Sort and index BAM file using Samtools (Li et al., 2009)

samtools sort BDP4ty_Sz_star_mappedAligned.out.bam -o BDP4ty_Sz_rep1_star_mappedAligned_ sorted.out.bam
samtools index BDP4ty_Sz_rep1_star_mappedAligned_sorted.out.bam
BDP4ty_Sz_rep1_star_mappedAligned_
sorted.out.bai

Reads Per Kilobase of transcript, per Million mapped reads (RPKM) was determined using the R
packages Rsubread (Liao et al., 2019), limma (Ritchie et al., 2015) and edgeR (Robinson et al., 2009)
distributed by the Bioconductor project (Gentleman et al., 2004) which openly distributes and
promotes development of R software packages for bioinformatics analysis.

Load libraries

----

library(Rsubread)
library(limma)
library(edgeR)

Define paths

Define bam_list, which is a tab-delimited file specifying the paths to the bam files as follows:
CellType BamFile
BDP4ty BDP4ty_Sz_rep1_star_mappedAligned_sorted.out.bam

gff_file="PlasmoDB-42_Pfalciparum3D7.exons_only_for_star.gff"
all_bam_list="bam_list"

Import bam data into R

----

all_targets <- readTargets(file=all_bam_list)
all_celltype <- factor(all_targets$CellType)
all_design <- model.matrix(~all_celltype)

all_fcounts <-
featureCounts(files=all_targets$BamFile,annot.ext=gff_file,nthreads=8,isPairedEnd=TRUE,strandSpecific=2)
#all_fcounts <-
featureCounts(files=all_targets$BamFile,annot.ext=gff_file,nthreads=8,isPairedEnd=TRUE,strandSpecific=1)
#all_fcounts <-
featureCounts(files=all_targets$BamFile,annot.ext=gff_file,nthreads=8,isPairedEnd=TRUE,strandSpecific=0)

x <- DGEList(counts=all_fcounts$counts, genes=all_fcounts$annotation[,c("GeneID","Length")])
x_rpkm <- rpkm(x,x$genes$Length)

write.csv(x_rpkm,file="all_rpkm")

3.10. Determination of inhibitory activity of compounds

3.10.1. Growth inhibition assay

The growth inhibition assay was adapted from (Wilson et al., 2010). 150 µL of approximately 1% parasitaemia ring stage culture was grown per well in a 96-well plate in a range of concentrations of compounds and vehicle control (DMSO). Each condition was tested in four technical replicates. After 72 hours, the culture was diluted 1 in 3 and washed in PBS once, before the parasites were stained in 10 µg/mL Ethidium Bromide in PBS for 30 minutes. The stained cells were washed three times in PBS and fixed for 2 hours in 2% paraformaldehyde before they were analysed by flow cytometry.

3.10.2. Flow cytometry and determining the half-maximal inhibitory concentration (IC_{50})

A HyperCyt® Autosampler (IntelliCyt, NM, USA) plate reader attached to a CyAnADP analyser (Beckman Coulter) was used for flow cytometry. The flow cytometer was calibrated with beads purchased from the manufacturer to assure accuracy in acquisition. CS2-GFP population gating was performed as previously described (Wilson et al., 2010) while for non-GFP parasite lines such as K1, late-stage parasites were identified as EtBr-positive events. Samples were analysed with Hyperview® analysis software. Parasitaemia was the percentage of the late-stage parasite count to total RBC count for each condition. Parasite relative growth was calculated as the percentage of parasitaemia in drug-treated compared to parasitaemia in DMSO negative controls. Subsequent IC_{50} determination and statistical analysis were performed in GraphPad Prism.

4. Determining the essentiality of PfBDPs during the parasite asexual life cycle

4.1. Introduction

BRDs recognise acetylated lysines in histone tails allowing BRD proteins to "read" the histone modifications and interact with chromatin. In humans, BRD proteins are involved in a wide range of functions in gene regulation (Andrieu et al., 2016; Denis, 2001). Dysfunctions of these BRD proteins have been linked to various type of diseases such as cancer (Ferri et al., 2016; Filippakopoulos et al., 2010; Jung et al., 2015). The *P. falciparum* bromodomain protein 1 (PfBDP1) is essential for the coordinated regulation of parasite invasion of erythrocytes (Josling et al., 2015). Therefore, we hypothesise that other PfBDPs are also transcriptional regulators for the parasite.

A recent forward genetic screen used transposon mutagenesis to determine the essentiality of *P. falciparum* genes for the asexual, blood-stage by determining mutability and the cost of fitness (Zhang et al., 2018). Four out of eight PfBDPs were devoid of insertions in this screen suggesting that they were essential for the parasite (PfBDP1, PfBDP2, PfBDP6 and PfGCN5) (Zhang et al., 2018) (figure 1.5, Chapter 1). PfBDP4 is among the 'mutable' BDPs (Zhang et al., 2018). One piggyBac transposon site was found in the coding sequence of BDP4, and the mutated parasite did not display a growth defect (Zhang et al., 2018). However, the insertion site was downstream of the BRD. Therefore, the essentiality of the BRD of PfBDP4 cannot be inferred from this screen as the domain may still be intact in these parasites. This screen also found four transposon sites in the CDS of PfBDP3 including one site upstream of the BRD of PfBDP3, indicating that PfBDP3 is not required for parasite survival during the asexual life cycle (Zhang et al., 2018). This chapter aims to determine the importance of the BRDs of PfBDP4 and PfBDP3 and the essentiality of these proteins by generating an inducible knockout and/or knockdown system to delete their BRDs.

Gene deletion is commonly used to determine the function of a protein of interest (POI). However, as the deletion of essential genes is lethal to parasites, essentiality is typically inferred through the inability to recover knockout parasites from the rare recombination events that give rise to classical knockouts. Thus, the phenotypes that contribute to death cannot be studied. This project employs conditional gene knockout and tuneable, gene expression knockdown systems. These systems create a window of time to study the change in phenotypes after the expression of the POI is interrupted before the parasite dies.

Conditional knockout (KO) and knockdown systems were used to target the loci of PfBDPs or their expression at mRNA levels, respectively. The conditional KO system used here was the Cre-lox recombination system. Targeted recombination occurs when Cre recombinase recognises and recombines two *loxP* loci leading to the deletion of the DNA sequence between these two sites. To allow inducible control over the activity of the Cre recombinase, the protein is split into two parts in which each component is fused to either an FK506-binding protein (FKBP12) or the rapamycin domain of FKBP12-rapamycin-associated protein (FRB). Upon addition of a ligand called rapamycin, the activity of the Cre recombinase is activated as the two components heterodimerise via the FKBP12 and FRB binding to rapamycin (Jullien et al., 2007; Jullien et al., 2003; O'Neill et al., 2011). In *P. falciparum*, dimerisable Cre (DiCre) was successfully expressed and integrated to the 3D7 parasite genome and has been used previously to disrupt *P. falciparum* genes (Collins et al., 2013a; Tibúrcio et al., 2019; Wilde et al., 2019; Yap et al., 2014).

In order to generate PfBDP conditional knockdowns, a self-cleaving glucosamine-6-phosphate activated ribozyme (*glmS*) and a 3' untranslated region of the *P. berghei* DHFR were introduced to the 3' end of the CDS of PfBDPs. The ribozyme is activated by the addition of the inducer glucosamine-6-phosphate leading to the cleavage of the 3' untranslated region and mRNA degradation (Prommana et al., 2013). In addition, the amount of glucosamine-6-phosphate can be titrated to fine-tune the preferred amount of protein expression for different growth assays. Inclusion of DiCRe inducible KO and *glmS* mRNA knockdown in a single parasite allows these systems to work independently or synergistically so that any parasites that escape knockout can undergo PfBDP mRNA knockdown to maximise reduction of PfBDPs expression in the parasite (Wilde et al., 2019).

4.2. Results

4.2.1. PfBDP4 is essential for *P. falciparum* parasite during the asexual life cycle

4.2.1.1. Generating transgenic parasites with inducible PfBDP4 knockout and mRNA knockdown using CRISPR-Cas9

A dual conditional knockout and knockdown PfBDP4 parasite line (3D7-PfBDP4-*loxP-glmS*) was kindly provided by a member of our laboratory, Dr. Lee Yeoh, for the functional studies reported in this chapter. 3D7-PfBDP4-*loxP-glmS* was generated from the 3D7 DiCre parental parasite line which was gifted to our laboratory from the Cowman laboratory (Wilde et al., 2019). Donor constructs were adapted from Wilde et al. 2019 for *P. falciparum* BDPs by Dr. Yeoh and the CRISPR gene-editing technology was utilised to rapidly obtain transgenic parasites (figure 4.1). A copy of the human *dhfr* gene was integrated into the genome downstream of the modified *Pfbdp4* locus to select for transgenic parasites using WR99210 drug (Fidock and Wellems, 1997). The modified *Pfbdp4* locus includes three hemagglutinin (HA) tags at the 3' of the gene for detection by Western blot. Two *loxP* sites flank the BRD and the HA tags. The addition of rapamycin induces the dimerization of the Cre recombinase which leads to the recombination of the two *loxP* sites. As a result, the locus between the *loxP* sites is excised from the parasite genome to generate a knockout (figure 4.1). The *glmS* downstream of the second *loxP* site cleaves mRNA when glucosamine is added to the culture leading to degradation of the mRNA.

The donor plasmids were linearised by restriction enzymes and co-transfected with a pUF1-Cas9G plasmid (figure 4.1) into the 3D7 DiCre parasite line. WR99210-resistant parasites were recovered 3 to 4 weeks after transfection. Excitingly, only the recombinant *Pfbdp4* locus with the integrated cassette was detected by diagnostic PCR (figure 4.2) indicating that the CRISPR gene-editing technology was highly efficient.

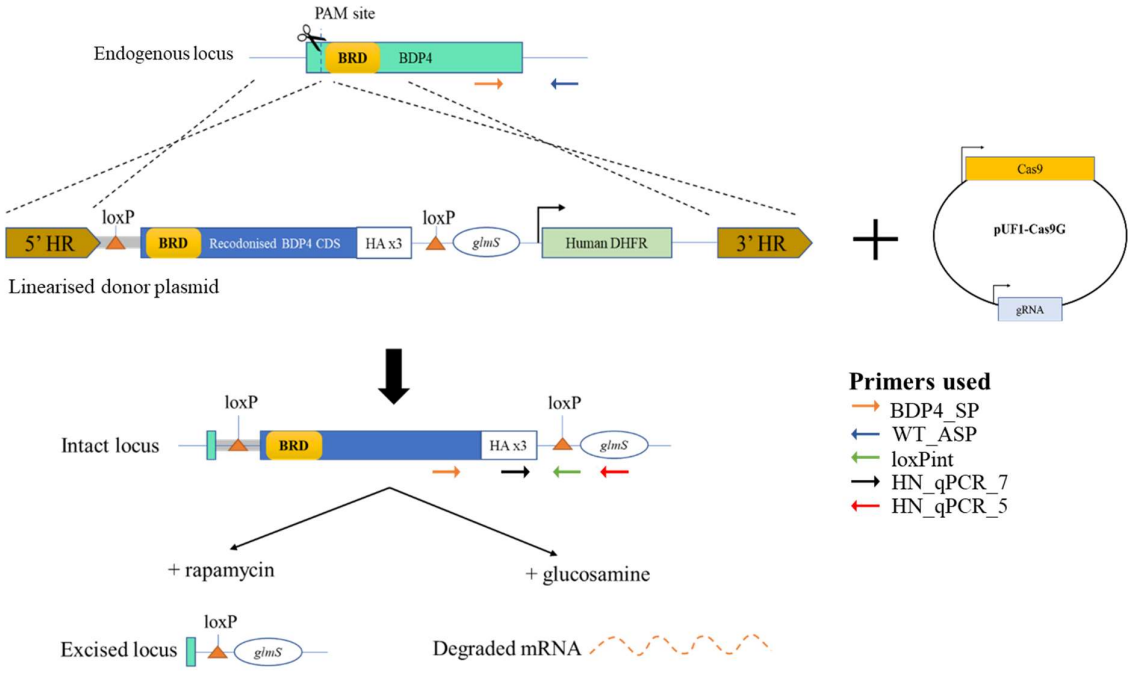

Figure 4.1 The design of 3D7-PfBDP4-*loxP-glmS* parasite line with a dual inducible knockout and knockdown system targeting the *Pfbdp4* locus introduced by CRISPR gene-editing. Linearised donor plasmid was co-transfected with a pUF1-Cas9G plasmid which contained the Cas9 and the guide RNA to induce a DNA double-stranded break at the protospacer adjacent motif (PAM) site of interest. Three HA tags were introduced at the 3-prime end of the CDS. The first *loxP* site was part of a synthetic intron (shaded grey) and the second *loxP* site is located downstream of the HA tags followed by the ribozyme riboswitch *GlmS*. Knockout is induced by the addition of rapamycin while mRNA knockdown is induced by the addition of glucosamine (GlcN). The chosen PAM site was mutated in the donor sequence to prevent repetitive cutting induced by Cas9 after integration. Primer BDP4_SP and WT_ASP were used to detect wildtype *Pfbdp4* locus, primer BDP4_SP and *loxP*int were used to detect integrated BDP4 locus. Primers HN_qPCR_7 and HN_qPCR_5 were used to quantify the intact BDP4 locus discussed in chapter 4.2.1.4 (Appendix, table 9.1).

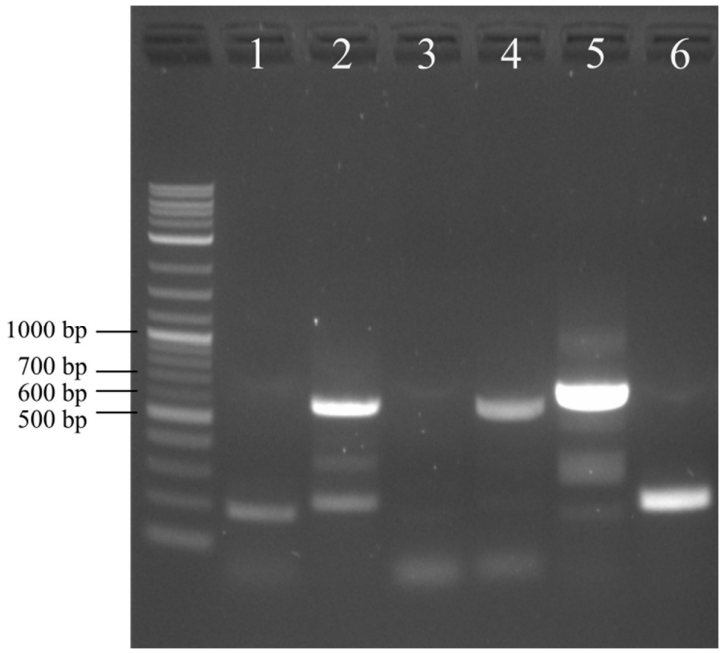

Figure 4.2 Diagnostic PCR of 3D7-PfBDP4-*loxP-glmS* parasite line. PCR products amplified from the genomic DNA of 3D7-PfBDP4-*loxP-glmS* parasite line was harvested in 2 replicates (Rep 1: lane 1 and 2, rep 2: lane 3 and 4) and the genomic DNA of the parental parasite line 3D7 DiCre that was used as a control (lane 5 and 6). Samples were tested for the *Pfbdp4* wildtype locus (primer BDP4_SP and WT_ASP) in lane 1, 3 and 5 and for the *Pfbdp4* integrated locus (primer BDP4_Sp and *loxP*int) in lane 2, 4 and 6. PCR primer positions are indicated in figure 4.1. Expected PCR amplicon sizes for the wildtype and integrated locus are 677 bp and 605 bp, respectively.

4.2.1.2. Determining depletion of PfBDP4 by Western blot

Disruption of PfBDP4 expression by inducible knockout and knockdown was analysed by Western blot. To maximise the effect, inducers of both knockout and knockdown (rapamycin and glucosamine, respectively) were used in this experiment. 3D7-PfBDP4-*loxP-glmS* parasites were synchronised with sorbitol and separated into 2 cultures which **(1)** received 100 µM rapamycin and 2.5 mM glucosamine (GlcN), or **(2)** were treated with vehicle control. Parasite total lysate was harvested and resuspended in SDS loading buffer on day 1 post-induction and every cycle (48 hours) afterwards (figure 4.3).

On day 1 post-induction, there was little difference observed between the control and induced culture. However, less PfBDP4 was detected in the induced culture than in the control after 5 days of induction (figure 4.3). This showed that the conditional knockout/knockdown systems successfully reduced the total amount of PfBDP4 after 5 days of induction.

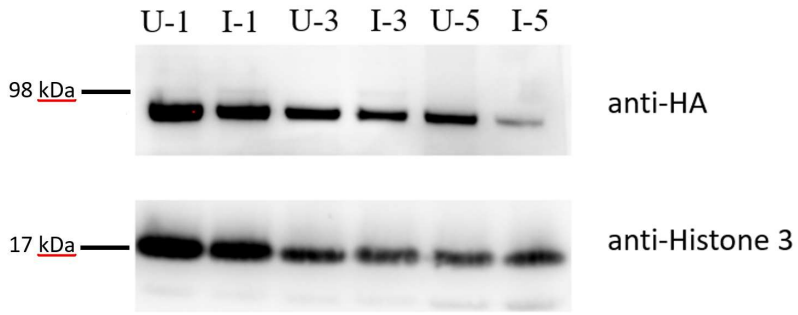

Figure 4.3 Western blot analysis of the induced and uninduced culture of unclone 3D7-PfBDP4-*loxP-glmS* parasite line. Lanes were labelled with the condition (U – uninduced/vehicle control, I – induced with rapamycin and glucosamine) followed by the day of which the total protein lysate was harvested (day 1, 3 or 5). The membrane was probed with rat anti-HA for PfBDP4 detection, followed by HRP-conjugated goat anti-rat; and rabbit anti-histone 3 as a loading control, followed by HRP-conjugated goat anti-rabbit. Expected sizes of PfBDP4 and histone 3 are 90 kDa and 18 kDa, respectively.

4.2.1.3. Measuring parasite growth when PfBDP4 is disrupted

3D7-PfBDP4-*loxP-glmS* was cloned by limiting dilution and clones were screened by diagnostic PCR to confirm *Pfbdp4* integration (figure 4.4). Next, the effect of loss of PfBDP4 on parasite growth was tested. For the growth assay, a synchronised culture of 3D7-PfBDP4-*loxP-glmS* (clone F4) was cultured in media with either **(1)** 100 μM rapamycin or **(2)** 2.5 mM GlcN or **(3)** 100 μM rapamycin and 2.5 mM GlcN or **(4)** vehicle control. A similar experiment was also performed on the parental parasite line 3D7 DiCre to control for non-specific effects caused by the inducers. Total DNA was measured with SYBR Green I assay as an indication of growth on day 5 post-induction (figure 4.5). Fluorometer raw output readings were normalised to vehicle control to yield percentage growth and growth of the test line 3D7-PfBDP4-*loxP-glmS* was compared to the control, parental line, 3D7 DiCre (Mann-Whitney U test) (figure 4.5). Each growth assay condition was tested in four technical replicates and the experiment was performed in three biological replicates. Genomic DNA from this experiment was also harvested for the analysis discussed in chapter 4.2.1.4.

The SYBR growth assay revealed that incubating 3D7-PfBDP4-*loxP-glmS* parasites with rapamycin led to a significant decrease in parasite growth in comparison to the control parental line 3D7 DiCre which showed no change in growth (30% growth decrease, $p < 0.0001$) (figure 4.5). However, when induction with GlcN was tested growth of the 3D7-PfBDP4-*loxP-glmS* parasite line was not decreased compared to the 3D7 DiCre ($p = 0.2145$) (figure 4.5) although both appeared to be inhibited compared to the vehicle control. This indicates that rapamycin is not toxic for the parasites and the growth defect is specific to the deletion of *Pfbdp4* locus, whereas GlcN affects parasite growth in both the 3D7 DiCre control as well as the 3D7-PfBDP4-*loxP-glmS* parasite line. Using both inducers inhibited growth more than induction with only rapamycin ($p = 0.0001$), possibly due to the cumulative effect of the growth defect from the rapamycin induction and the non-specific toxicity of GlcN (figure 4.5). Consequently, only rapamycin-induced knockout was used for subsequent experiments.

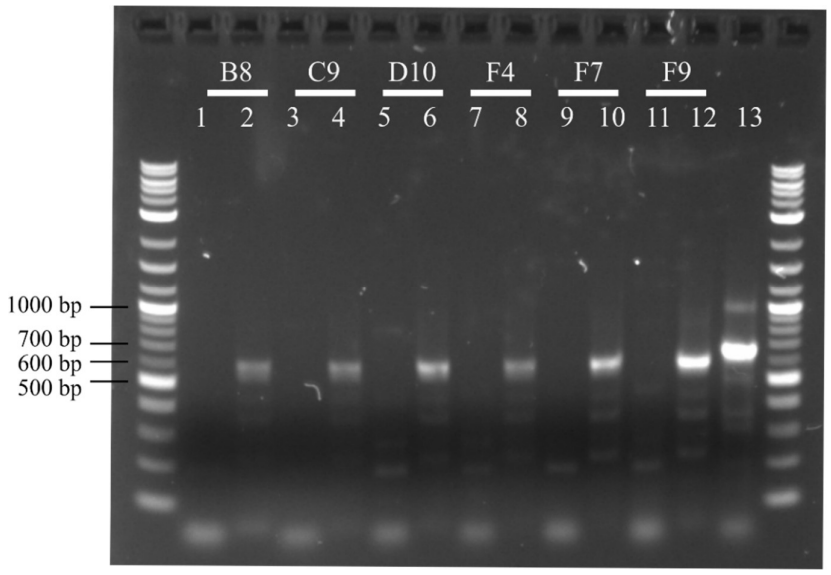

Figure 4.4 Diagnostic PCR of 3D7-PfBDP4-*loxP-glmS* parasite clones. Clone names (B8, C9, D10, F4. F7 and F9) are displayed on top of the gel. Clones were tested for the *Pfbdp4* wildtype locus (primer BDP4_SP and WT_ASP as per figure 4.1) in odd-numbered lanes – lane 1 to 11 and clones were tested for the *Pfbdp4* integrated locus (primer BDP4_Sp and *loxP*int as per figure 4.1) in even-numbered lanes – lane 2 to 12. Lane 13 was a positive control containing the wildtype *Pfbdp4* locus. Expected PCR amplicon sizes for the wildtype and integrated locus are 677 bp and 605 bp, respectively.

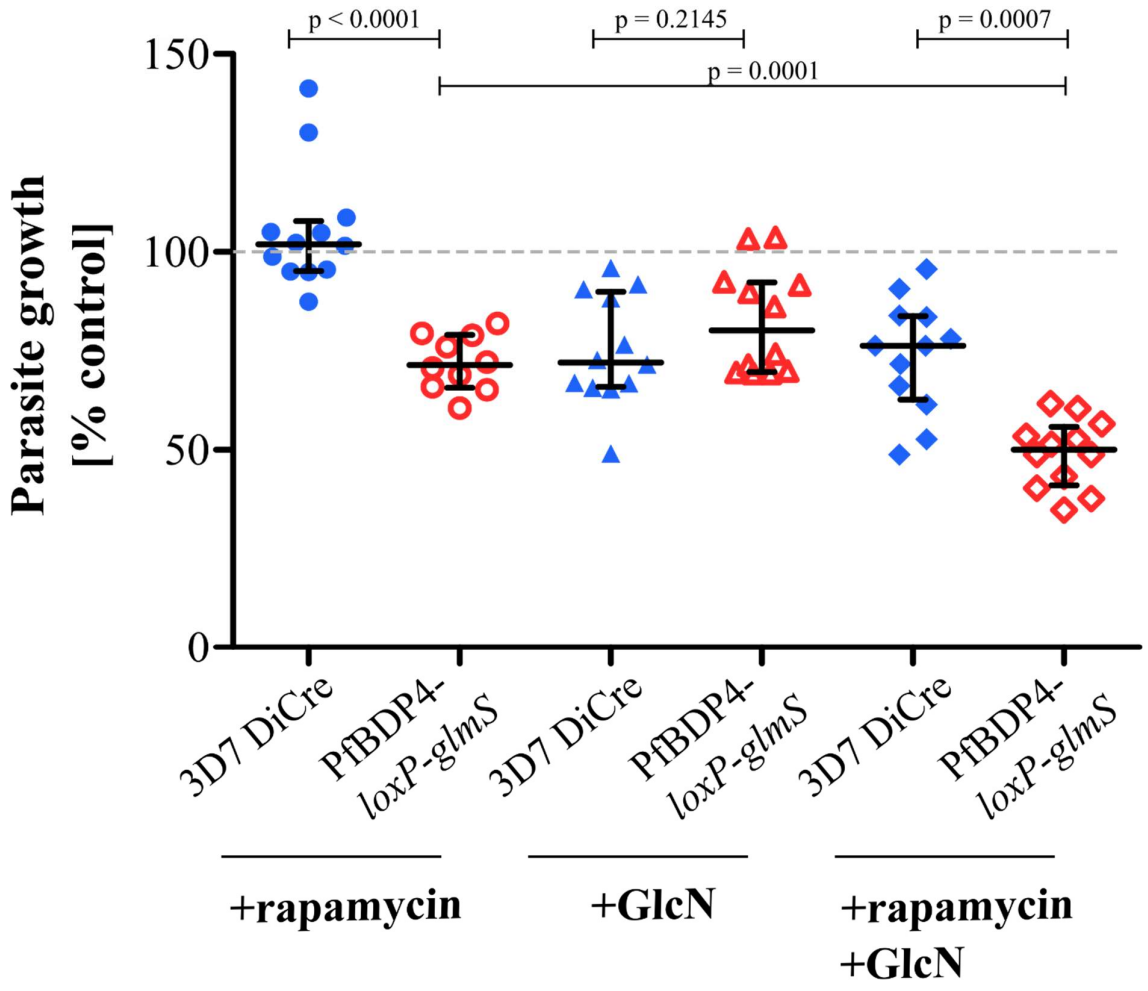

Figure 4.5 Five-day SYBR Green I growth assay of 3D7-PfBDP4-*loxP-glmS* and 3D7 DiCre parasites. 3D7 DiCre (filled, blue) and 3D7-PfBDP4-*loxP-glmS* (unfilled, red) parasites were cultured with 100 μM rapamycin and/or 2.5 mM GlcN (x-axis). Their growth was measured and expressed as a percentage relative to vehicle control (y-axis). The median and interquartile range are displayed for each condition. P-values were obtained by the Mann-Whitney U test.

4.2.1.4. Quantifying loss of PfBDP4 by quantitative PCR

In order to determine the efficiency of the inducible knockout system used in 3D7-PfBDP4-*loxP-glmS*, it is important to determine the proportion of parasites that were excised. qPCR was used to quantify proportions throughout growth. The design of primers that are specific to the excised locus has been particularly challenging due to the low complexity of the region after excision occurred. Consequently, only primers that target the intact locus were successfully used for qPCR (Appendix, table 9.1).

The rapamycin-induced excision of PfBDP4 was quantitated in single replicates of two clones of 3D7-PfBDP4-*loxP-glmS* to confirm similar excision efficiency between clones. Cultures were continuously grown in media with 100 μM rapamycin. Genomic DNA was harvested 24 hours after induction and every 48 hours afterwards until day 9. The signal of the intact locus was normalised to the skeleton binding protein 1 (SBP-1) gene (Appendix, table 9.1). Detection of the intact, recombinant PfBDP4 locus was similar between clone F4 and D10 on days 1, 3 and 5 (figure 4.6). However, these clones responded differently after day 5 when the levels of intact PfBDP4 started to increase in clone D10. This suggests that there is some variability in the rates of PfBDP4 deletion between clones, especially during long-term culturing. As a result, the clone F4 of the 3D7-PfBDP4-*loxP-glmS* was selected for subsequent experiments.

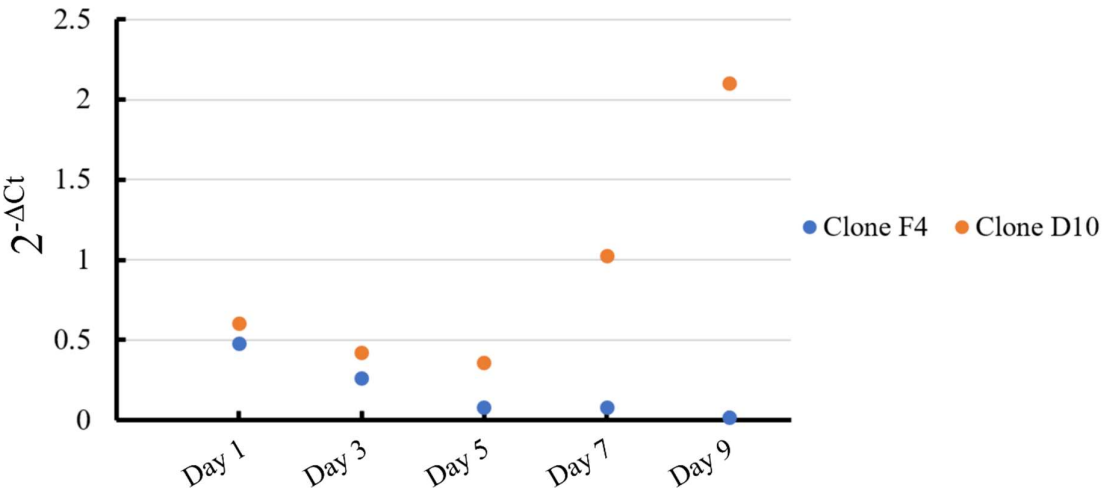

Figure 4.6 Quantification of PfBDP4 excision induced by treating two clones of 3D7-PfBDP4-*loxP-glmS* parasites with rapamycin. The intact PfBDP4 locus was quantified by qPCR. The signal was normalised to the skeleton-binding protein 1 (SBP-1) ($2^{-\Delta Ct}$) (y-axis).

To further assess growth in the presence of continual rapamycin-induced Di-Cre excision the 3D7-PfBDP4-*loxP-glmS* was synchronised and continuously cultured with 100 µM rapamycin. Genomic DNA was harvested at 24 hours after induction (day 1) and every 48 hours afterwards until day 9. The experiment was performed in three biological replicates. The genomic DNA of parasites treated with the vehicle control (DMSO) was harvested on day 1 for all replicates as well as also on day 3, 5 and day 7 for replicate 2 and 3. The intact locus was quantified and normalised to vehicle control (DMSO) samples which contained 100% intact *Pfbdp4* locus (figure 4.7). The loss of *Pfbdp4* on day 1 (50% of intact *Pfbdp4*) and day 3 (37% of intact *Pfbdp4*) was statistically significant in comparison to the vehicle control with p-values of 0.0395 and 0.0177, respectively. However, excision was not significantly different from vehicle controls on day 5 of induction (t-test p = 0.1467). Longer induction led to less efficient excision by the DiCre recombinase and a highly variable excision rate between biological replicates (figure 4.7). The inducible knockout system could achieve a maximum knockout rate of between 40 to 60 percent, which is consistent with the growth inhibition of 3D7-PfBDP4-*loxP-glmS* that was induced by rapamycin.

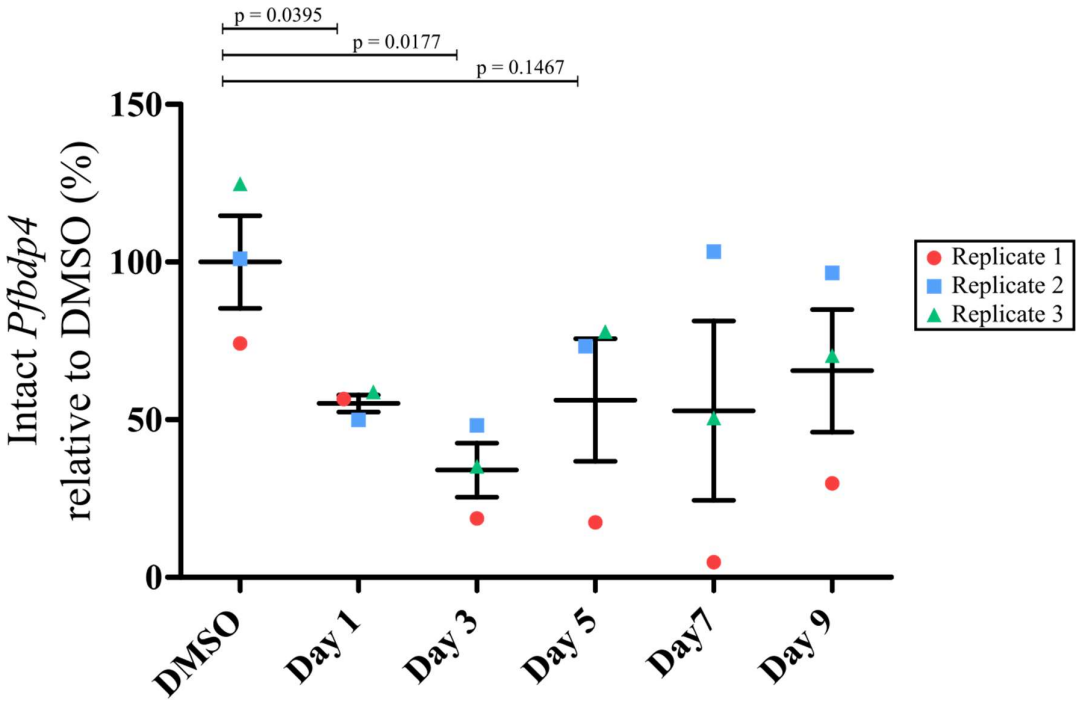

Figure 4.7 Quantification of PfBDP4 excision induced by treating 3D7-PfBDP4-*loxP-glmS* parasites (clone F4) with rapamycin. The intact PfBDP4 locus was quantified by qPCR and normalised to the vehicle control (DMSO) for three biological replicates. P-values were obtained using a two-tailed t-test. The mean and standard error of the mean (SEM) of three biological replicates is indicated for each harvest time point.

The preceding data showed that parasites with the intact PfBDP4 locus can outgrow the knockout despite continuous induction of knockout. This suggests that the parasites become refractory to induction of knockout. In addition, continual induction could result in an unknown proportion of new knockouts induced in each cycle. Thus, freshly induced KO parasites in the cycle examined may die but are replaced by KO parasites induced in the subsequent cycles leading to a persistent proportion of KO parasites. This would prevent inferring non-essentiality from the detection of the KO locus. To more accurately assess the lethality of knockout, the growth rates of parasites with either an intact or a knockout *bdp4* locus were compared. 3D7-PfBDP4-*loxP-glmS* clone F4 was synchronised with sorbitol and incubated with either 100 µM rapamycin or DMSO vehicle control for 24 hours. Genomic DNA was harvested before all cultures were washed and fed with fresh RPMI-HEPES. Parasites were incubated at 37°C and monitored by qPCR every 48 hours from the time of the wash. The experiment was performed in three biological replicates. The genomic DNA of parasites treated with the vehicle control

(DMSO) was harvested on day 1 for all replicates as well as also on day 3, 5 and day 7 for replicate 2 and 3.

On day 1 when rapamycin was removed from the culture, the ratio of intact to knockout *bdp4* locus was approximately 1:1 as 50% of the culture had the unexcised *bdp4* locus (t-test p = 0.0043) (figure 4.8). On day 3, 48 hours after rapamycin was removed, the population of parasites carrying the intact locus persisted at 50% of the population (t-test p = 0.0283) in comparison to DMSO control parasites. After day 3, parasites with intact *Pfbdp4* expanded and there was a trend to increasing percentage of the unexcised locus. The data point for replicate 3 on day 7 is a probable technical outlier (2.5 x 100% intact control) but was included in the presented data as it did not change the conclusion of the experiment. This experiment confirmed that parasites with the intact PfBDP4 locus can outgrow the knockout.

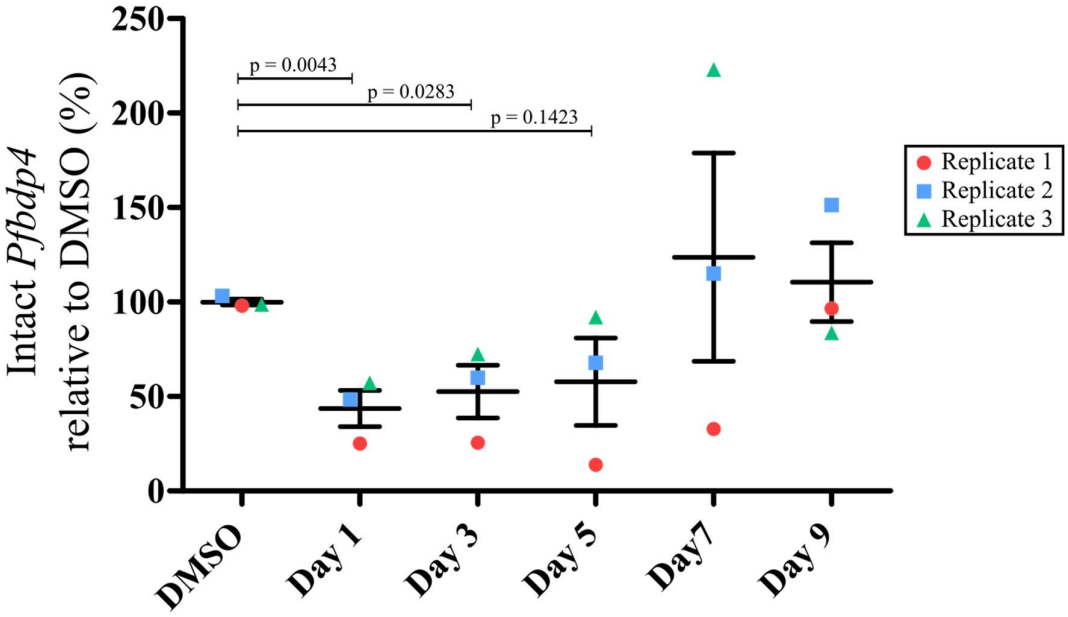

Figure 4.8 Quantitative PCR showed a trend that parasites with intact PfBDP4 expanded faster than PfBDP4 knockout parasites in a mixed culture. Parasites were induced with rapamycin for 24 hours to achieve approx. 50% of unexcised locus before rapamycin was removed from the culture. Parasites were cultured with standard supplemented RPMI-HEPES media and genomic DNA was harvested every 48 hours (x-axis). The intact PfBDP4 locus was quantified by qPCR and normalised to the average of vehicle controls (DMSO) (y-axis). P-values were obtained using a two-tailed t-test. The mean and standard error of the mean (SEM) of three biological replicates are indicated for each harvest time point.

To assess whether the knockout (KO) induced growth inhibition was lethal, we attempted to clone KO parasites. As maximum excision occurred on day 3 post-induction, these cultures were used for limiting dilution cloning in attempts to recover clones of PfBDP4 knockout parasites. Three limiting dilution cloning experiments were performed. From qPCR, 70% of the PfBDP4 loci were intact at the time of cloning. Therefore, if the KO was not lethal, we expected to recover 24 KO clones and 56 wildtype clones from the 80 plated clones. However, after limiting dilution cloning, no KO clones and 24 wildtype clones were recovered. This demonstrated that disruption of PfBDP4 was statistically associated with lack of parasite growth (Fishers exact test $p<0.0001$) (Table 4.1). Thus, these experiments strongly suggest that PfBDP4 is essential for blood-stage, asexual growth of *P. falciparum*.

Table 4.1 Number of parasites with KO and wildtype *Pfbdp4* that were recovered after limiting dilution cloning. Fischer's exact test $p < 0.0001$.

	Did not grow	Grew
Knockout *Pfbdp4* clones	24	0
Wildtype *Pfbdp4* clones	32	24

4.2.2. Generating PfBDP3 inducible knockdown system

CRISPR-Cas9 gene-editing technology was used to generate a conditional knockdown of the PfBDP3 parasite line (BDP3*GlmS*) to assess PfBDP3 essentiality (figure 4.9). This was a critical step for validating PfBDP3 as the putative target of the bromodomain inhibitor BI2536 (Chapter 6). The donor construct sequence was determined by Sanger sequencing before transfection to ensure the HA tags were in the correct reading frame (Appendix, figure 9.1). Integrated parasites were selected by WR99210 and recovered within 4 weeks post-transfection. Clones of BDP3*GlmS* were obtained by limiting dilution cloning and diagnostic PCR confirmed these clones had the modified *bdp3* locus (figure 4.10). The construct was confirmed by Sanger sequencing (Appendix, figure 9.1) confirming that the HA tag is in-frame and no STOP codon was introduced between the end of the PfBDP3 and the HA tag. However, the tagged PfBDP3 could not be detected by either rat or mouse anti-HA so western blot could not be used to determine the knockdown of PfBDP3 (figure 4.11).

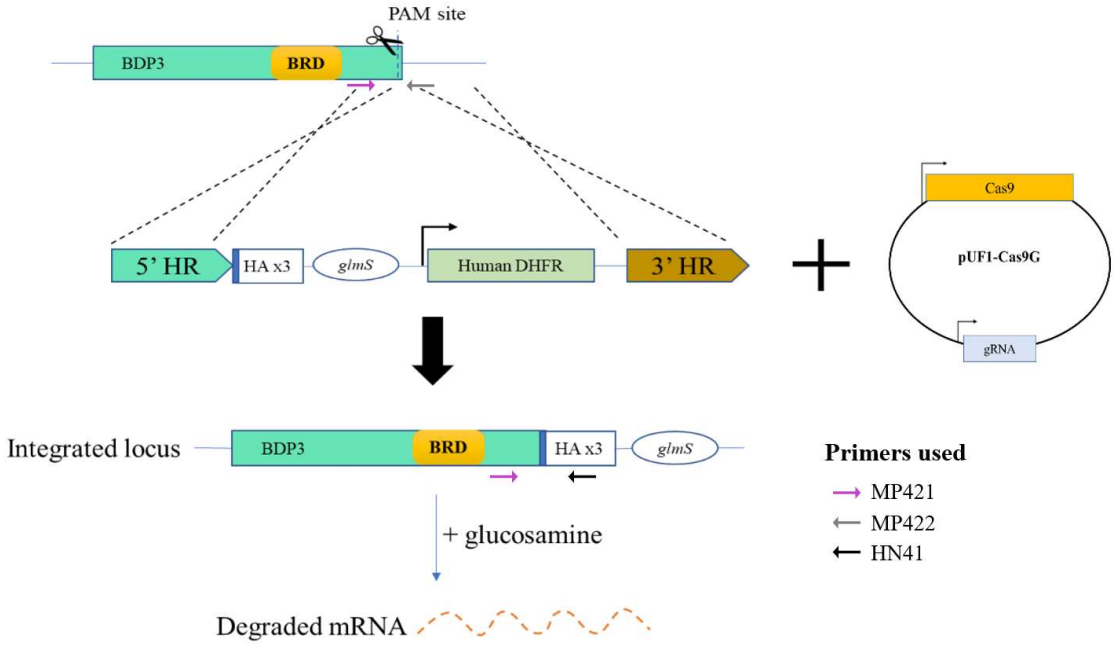

Figure 4.9 The BDP3*glmS* parasite line with inducible mRNA knockdown targeting the *Pf*bdp3 locus introduced by CRISPR gene-editing. Linearised donor plasmid was co-transfected with the PUF1-Cas9G plasmid which contains the Cas9 and the guide RNA sequence to induce a DNA double-stranded break at the PAM site of interest at the 3 prime end of *Pfbdp3*. Three HA tags were introduced at the 3 prime of the CDS followed by the ribozyme riboswitch *glmS*. The chosen PAM site was mutated in the donor sequence to prevent repetitive

cutting induced by Cas9 after integration. Primer MP421 and MP422 (1424 bp) were used to detect wildtype *Pfbdp3*, and primer MP421 and HN41 (1184 bp) were used to detect integrated *Pfbdp3* (Appendix, table 9.1).

To observe whether GlcN induction leads to any changes in BDP3*glmS* growth, parasites were synchronised and cultured with GlcN. Parasite growth was determined by counting smears every cycle (48 hours) post-induction. By smear, no difference in growth was observed between vehicle control and GlcN treated cells (figure 4.12). Overall, it remains unclear whether expression of PfBDP3 could be knocked down using the *glmS* ribozyme riboswitch system.

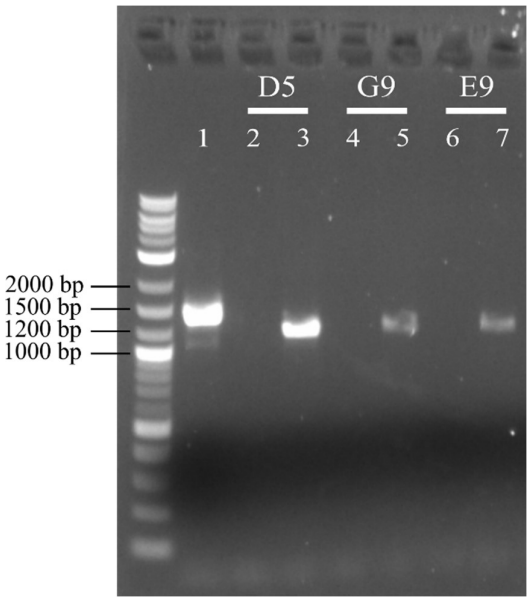

Figure 4.10 Diagnostic PCR of BDP3*glmS* clones. Clone names (D5, G9 and E9) are displayed on top of the gel. Lane 1 was the positive control of the wildtype locus (primer MP421 and MP422). Lane 2, 4 and 6 were genomic DNA of BDP3*glmS* clones tested for the *Pfbdp3* wildtype locus (primer MP421 and MP422, as per figure 4.9) while lane 3, 5 and 7 were tested for the *Pfbdp3* integrated locus (primer MP421 and HN41, as per figure 4.9) Expected PCR amplicon sizes for the wildtype and integrated locus are 1424 bp and 1184 bp, respectively.

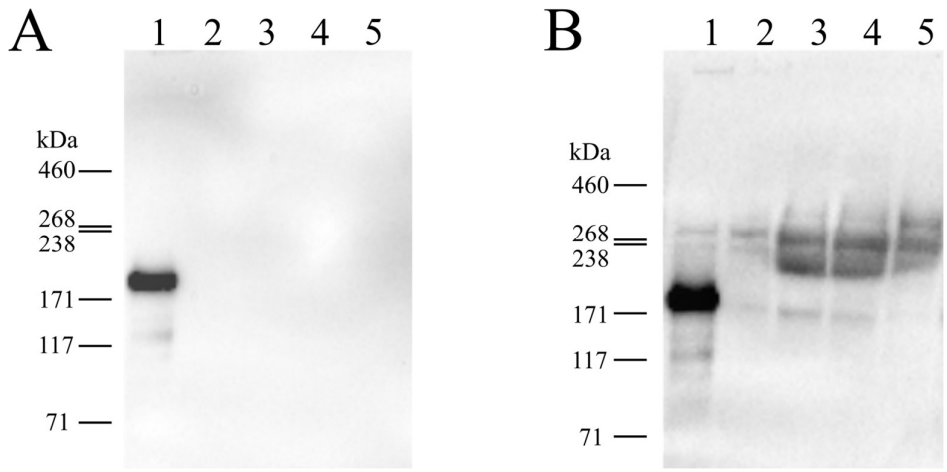

Figure 4.11 Western blot analysis of BDP3*glmS* parasite line. A protein that was tagged with HA was used as a positive control (lane 1) as well as four replicates of BDP3*glmS* (lane 2-5). Total cell lysates of saponin-lysed cultures were harvested and probed with (A) rat anti-HA antibody and (B) mouse anti-HA antibody. The expected size of the positive control and tagged PfBDP3 are 170 kDa and 270 kDa, respectively.

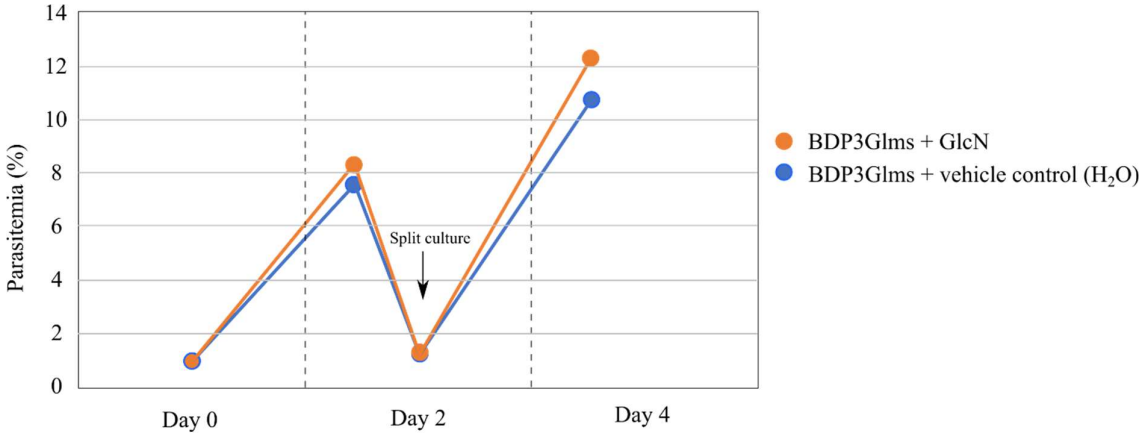

Figure 4.12 Parasite growth of BDP3*glmS* culture that was induced with GlcN or grown with vehicle control. Parasite growth was monitored by smear every 48 hours after induction and cultures were split on day 2 to prevent the parasite from overgrowing. Parasitemia is the percentage of infected cells in the blood smear (100 x #infected cells / #total RBC x 100).

4.3. Discussion

This chapter aimed to demonstrate the functions of PfBDPs in *P. falciparum*. The CRISPR Cas9 gene-editing technology was pivotal to the functional studies of PfBDPs. The technique allowed high-efficiency integration of constructs into the locus of interest and transgenic parasites were recovered quickly, some within 2 weeks post-transfection. A significant advantage of CRISPR-Cas9 directed double-stranded breaks is that the increased efficiency of integration allowed approaches that increased stringency, thus reducing background and laborious screening. In particular, transfecting intraerythrocytic parasites with linear donor constructs prevented the propagation of the donor plasmid in transgenic parasites. Consequently, there was no need to employ negative selection or enrich for integrated parasites by multiple rounds of WR99210 cycling.

Rapamycin-induced DiCre deletion of PfBDP4 inhibits parasite growth. This was demonstrated by parasites carrying the wildtype PfBDP4 locus outcompeting the PfBDP4 knockout parasites over time. Differential gene expression analysis using RNA-seq as well as phenotypic assays will further reveal pathways that were affected by disrupting PfBDP4. However, this has proved to be challenging with the current 3D7-PfBDP4-*loxP*-*glmS* parasite line due to the incomplete excision induced by rapamycin. In theory, the parasites should continue to excise the locus between the *loxP* sites when rapamycin is available in the culture. Excision of the PfBDP4 locus was detected after a 24-hour induction with rapamycin but was insufficient to significantly alter the growth of the induced culture compared to the uninduced control (figure 4.7). Maximum excision of PfBDP4 was 50% of the population of parasites after 72 hours of incubation with rapamycin (figure 4.7). Surprisingly, the parasites then seemed to become desensitised to rapamycin and the excision rate diminished after 72 hours induction despite continuing exposure to rapamycin. The delay in maximum excision requires that rapamycin induction should be started days before commencing assays. Even then, the inconsistent rate of excision could impact the reproducibility of these experiments.

It is possible that the DiCre expression was not consistent between different 3D7-PfBDP4-*loxP*-*glmS* parasite clones. The DiCre genes and the blasticidin S deaminase gene were integrated into the 3D7 parasite genome at the *rh3* gene locus (Wilde et al., 2019), and integrants were selected by blasticidin resistance. *Rh3* encodes the reticulocyte binding protein homologue 3 which is non-essential during the blood stage (Zhang et al., 2018). Previous

studies also showed that *rh3* locus is highly enriched with the repressive histone mark H3K9me3 as well as heterochromatin protein 1 (HP1) (Flueck et al., 2009; Fraschka et al., 2018; Jiang et al., 2013; Lopez-Rubio et al., 2009). As a result, it is possible that the region of *rh3* locus is subject to epigenetic silencing during the blood stage, and hence, potentially loss of DiCre expression in these parasites. For future experiments, these parasites could be selected on blasticidin to enhance the expression of DiCre and quantitative reverse transcriptase (qRT-PCR) should be used to monitor the level of DiCre expression and PfBDP4 locus excision.

The NF54 parasite line also had the DiCre cassette integrated, but into the locus of the *P. falciparum s47* gene (Tibúrcio et al., 2019). This gene plays important roles in mosquito immune evasion and malaria transmission (Canepa et al., 2016; Canepa et al., 2018; Molina-Cruz et al., 2017; Molina-Cruz et al., 2013). Compared to *rh3*, *s47* is found in euchromatic regions of the parasite genome and disruption of *s47* did not affect parasite growth during the asexual stage (Tibúrcio et al., 2019). To investigate whether the partial KO we observed was a phenotype specific to the 3D7 line, our collaborator Dr. Michaela Petter from Erlangen University, Germany subsequently transfected the same PfBDP4-*loxP-glmS* and pUF1-Cas9G constructs into the NF54 DiCre parental parasite line and the transfectant was named NF54-PfBDP4-*loxP-glmS* to distinguish it from the 3D7-PfBDP4-*loxP-glmS* line discussed in the results above. Preliminary western blot results from our collaborator's laboratory showed that more than 90% of PfBDP4 was knocked out after 24-hour induction with rapamycin. This further suggests that the incomplete excision observed in the 3D7-PfBDP4-*loxP-glmS* was likely due to the inconsistent level of DiCre expression. NF54-PfBDP4-*loxP-glmS* will be a useful tool to further dissect pathways that are responsible for the growth defect observed when PfBDP4 was knocked out.

Previous proteomic studies showed that PfBDP4 interacts with two *trans* factors AP2-I and PfBDP1 that regulate the transcription of invasion genes (Hoeijmakers et al., 2019; Santos et al., 2017). This suggests that PfBDP4 may also regulate invasion genes and it is predicted that knocking out PfBDP4 will impact parasite invasion. To assess this possibility future work will monitor schizonts of the induced PfBDP4 knockout in NF54-PfBDP4-*loxP-glmS* for any change in egress and merozoite invasion phenotypes using live-cell imaging as done previously for PfBDP1 (Josling et al., 2015).

In addition, PfBDP4 was also pulled down together with other chromatin-associated proteins such as HMGB3, CHD1 and SWIB (Hoeijmakers et al., 2019). HMGB3 has a helix-to-helix motif that can bind to DNA and CHD1 has two putative histone methyllysine-binding

chromodomains. SWIB is a subunit of the SWI/SNF chromatin remodelling complex and disruption of SWIB led to impaired development of *Plasmodium* parasites (Wang and Zhang, 2020). These findings further implicate PfBDP4 in chromatin structure and gene regulation. Near homogeneous excision of PfBDP4 in the NF54-PfBDP4-*loxP-glmS* parasites will allow RNA-seq transcriptional profiles of induced and uninduced parasites across the IDC to be compared and to identify genes that are differentially expressed in KO parasites.

One of the reasons PfBDPs are promising drug targets is their transcription in multiple stages of the parasite lifecycle (Katsuno et al., 2015). An advantage of the NF54 parasite line is its ability to produce higher numbers of gametocytes compared to the 3D7 line. By inducing PfBDP4 knockout in NF54-PfBDP4-*loxP-glmS* before and after commitment to gametocytogenesis, it is possible to investigate the effect PfBDP4 knockout has on gametocytogenesis and gametocyte development. This system also allows induction of PfBDP4 knockout in sexual blood stages and during liver-stage development to assess PfBDP4 function outside of the IDC (Tibúrcio et al., 2019).

While the Cre-lox system achieved some KO of PfBDP4 and inhibited parasite growth, attempts to use the *glmS* ribozyme to conditionally knockdown PfBDP4 did not significantly alter parasite growth. Previous reports indicated that 5 mM GlcN is toxic for *P. falciparum* and hampered trophozoite development and cell invasion (Howard et al., 1982; Naik et al., 2003). GlcN also exerted cytotoxic effects on human cancer cells that varied from DNA synthesis inhibition to cell death (Chesnokov et al., 2009). Induction with 2.5 mM GlcN for up to 72 hours does not harm parasites (Prommana et al., 2013) but the 3D7-PfBDP4-*loxP-glmS* parasite line did not show any change in growth at 72h induction, so induction with GlcN was continued for a further 48h. A mild growth defect was observed in the 3D7-PfBDP4-*loxP-glmS* after 120h induction although this growth inhibition was also observed in the parental 3D7 DiCre line. The variable levels of GlcN cytotoxicity to different parasite lines mitigated against its further optimisation for these experiments. A greater and significant growth reduction of 3D7-PfBDP4-*loxP-glmS* was observed when both GlcN and rapamycin was used in comparison to rapamycin treatment alone. It is challenging to determine whether GlcN induced PfBDP KD is working synergistically with rapamycin induction or, whether the additional growth inhibition is due to GlcN toxicity. However, it is evident that the conditional knockdown did not contribute to the majority of the growth defect and protein knockdown.

The latter part of this chapter discusses the methods used to disrupt expression of PfBDP3 in the parasite and the challenges in generating a conditional knockdown PfBDP3 parasite line.

While integration at the PfBDP3 locus was confirmed by PCR (figure 4.10), the HA-epitope tagged PfBDP3 was not detectable by western blots. PfBDP3-3xHA could also not be detected in another, independently made, 3D7-PfBDP3-*loxP-glmS* parasite line. These results were unexpected because a BDP3-Ty epitope-tagged recombinant parasites can be detected by western blot as discussed in Chapter 5. Possibly the presence of the HA tag altered the stability of the C-terminal of the protein which led to degradation of the HA epitope tag. Future work could introduce a C-terminal Ty1 epitope tag to PfBDP3, as it has been successfully used in this study (Chapter 5). Quantitative reverse transcriptase PCR (qRT-PCR) could have been used to compare the amount of PfBDP3 mRNA between induced PfBDP3 mRNA knockdown and uninduced cultures. However, other members of the lab subsequently, stably deleted the BRD of PfBDP3 and saw no growth defect. This was consistent with the *piggyBac* transposon mutagenesis screen in *P. falciparum* showing that PfBDP3 is non-essential during the asexual stage (Zhang et al., 2018). Therefore, further investigation of PfBDP3 essentiality using this BDP3*GlmS* parasite line will not be pursued.

While the function of PfBDP3 remains unknown, PfBDP3 was pulled down together with PfBDP5/TAF1, which is important for gene transcription and parasite growth, and another protein PF3D7_1451200, which interacts with the HP1 protein (Hoeijmakers et al., 2019). In addition to PfBDP3 and HP1, PF3D7_1451200 also interacts with MYST, which is responsible for the acetylation of H4 and belongs to the histone acetyltransferase NuA4 complex (Miao et al., 2010). In *Trypanosoma brucei* parasite which causes sleeping sickness, a component of the MYST family called HAT-1 is a histone acetyltransferase that modulates telomeric silencing (Kawahara et al., 2008) and in yeast, two HATs of the MYST-family are also involved in telomeric silencing (Clarke et al., 2006; Reifsnyder et al., 1996). This may explain why MYST and one other component of the histone acetyltransferase NuA4 complex were indirectly associated with HP1 via PF3D7_1451200.

Previously, one BRD was predicted for PfBDP3 and reported in the UniProt database and reviewed in Jeffers et al. (Jeffers et al., 2017). Our collaborators at the Structural Genomics Consortium discovered and solved the crystal structure of a second BRD in PfBDP3 (confidential unpublished data). Therefore, the existing BRD will be referred to as PfBDP3.1 and the newly discovered BRD as PfBDP3.2. As PfBDP3 has two BRDs, it is possible that PfBDP3 is a scaffold that is associated with both gene activation (PfBDP5/TAF1) and gene silencing. In chapter 4, our preliminary results suggested that PfBDP3 is enriched in the heterochromatin. Therefore, PfBDP3 remains an interesting target to study because many

virulence genes, such as the *var* multi-gene family, as well as genes that are critical for stage transition, such as the transcription factor AP2-G, are silenced in the heterochromatic regions of *P. falciparum*. Future experiments should aim to determine whether disruption of PfBDP3 affects the silencing of these genes or the parasite capability to activate silenced genes. In the lab, a PfBDP3 knockout parasite line was obtained. RNA-seq can be performed on this BDP3KO line to investigate any differential expression of silenced genes and the gametocyte conversion rate can also be compared between wildtype and knockout parasite lines. In addition, the integrity of heterochromatic regions can be assessed by ChIP-seq of HP1 or the histone repressive mark H3K9me3. Moving forward, it will be interesting to determine whether heterochromatin and gene silencing is disrupted when PfBDP3 is deleted.

In conclusion, this chapter describes the first evidence that intact PfBDP4 is required for normal growth of *P. falciparum* parasites. Our results provide exciting leads to further utilise our transgenic parasite line to determine pathways that are dysregulated when PfBDP4 is disrupted. Also, understanding the phenotype of BDP4 knockout parasite will greatly help future efforts to discover drugs that target PfBDP4.

5. Identifying genomic enrichment of PfBDP4 and PfBDP3 using chromatin immunoprecipitation sequencing (ChIP-seq)

5.1. Introduction

Currently, there is little direct evidence indicating that PfBDPs other than PfBDP1 and PfBDP2 are associated with chromatin. In the previous chapter, we showed that disruption of PfBDP4 caused a growth defect in the parasite. Our collaborator at the Structural Genomics Consortium (SGC) successfully obtained a crystal structure of PfBDP4 in complex with acetylated H4K5 peptide (PDB ID: 5VS7) (Hou et al.) which implied PfBDP4 functions in reading histone acetylation and possibly in gene regulation. In addition, PfBDP4 is a member of an epigenetic reader complex that contains the transcription factor AP2-I (Hoeijmakers et al., 2019); and PfBDP4 was also precipitated together with PfBDP1, PfBDP2 and several AP2 STFs from nuclear extract by an immobilised oligonucleotide containing a predicted STF binding DNA motif from *P. falciparum* (Toenhake et al., 2018). Therefore, PfBDP4 is predicted to be involved in the regulation of gene expression.

The investigation of PfBDP3 is also of interest because the SGC obtained a crystal structure of PfBDP3 in complex with a small molecule called BI-2536 in its acetylation binding pocket (PDB ID: 4PY6) (Fonseca et al.). This is the first clue indicating that PfBDPs can be developed into novel targets for antimalarial therapy. Therefore, understanding the function of PfBDP3 and its association with the parasite genome will be invaluable for determining its value as a drug target and help the design of assays to assess whether a compound is on-target.

Chromatin immunoprecipitation in combination with high-throughput sequencing (ChIP-seq) is a method that can be used to determine the genomic localisation of PfBDPs. This chapter aims to use ChIP-seq to understand the potential roles of PfBDP4 and PfBDP3 in *P. falciparum* by determining the genomic localisation of PfBDP4 and PfBDP3 and to utilise bioinformatic analyses to identify genes and pathways that they might be regulating.

5.2. Results

5.2.1. PfBDPs are nuclear proteins

To investigate the PfBDPs at the molecular level, parasite lines expressing PfBDPs fused with 3' Ty1-epitope tags were generated in the laboratory by single-crossover homologous recombination (figure 5.1) and summarised in table 5.1. Ty-tagged parasite lines could be analysed using a commercially available Ty-1 antibody thus avoiding the need for time-consuming and costly generation of antibodies that are specific to individual PfBDPs. However, it is worth noting that the use of epitope tag can occasionally interfere with the protein function. Ty1 is a small tag that has been successfully used to tag histone H2A and other proteins in *P. falciparum* previously (Bártfai et al., 2010; Kuang et al., 2017; Neveu et al., 2018; Vembar et al., 2015).

To investigate the subcellular localization of the PfBDPs, cellular fractionation was performed on the tagged lines across the asexual life cycle (figure 5.2). The cytoplasmic fractions (C) represent proteins that were found outside of the nucleus. The nuclei were extracted with high salt buffer under reducing conditions to obtain the soluble nuclear fractions (Ns), while the remaining insoluble nuclear pellet (Ni) was extracted with SDS under reducing conditions and consists of histones and other proteins that were integral to chromatin. In general, the abundance of PfBDP4 in the nucleus was highest in schizonts whereas the peak expression of PfBDP3 was observed in trophozoites (figure 5.2). The western blot analysis revealed that PfBDP4 was found at equal levels in both nuclear fractions across the asexual life cycle indicating that a portion of PfBDP4 was tightly associated with chromatin. A small amount of PfBDP4 was also detected in the cytoplasmic fraction during the ring stage. PfBDP3 was detected mainly in the Ns fraction, although it was still clearly associated with the nuclear insoluble material in trophozoites. Interestingly, we observed a strong band of a smaller size than expected for full-length PfBDP3 in the cytoplasmic fraction (C) in schizonts, indicating that PfBDP3 may be processed in the cytoplasm at this stage. By immunofluorescent assay (IFA), the Ty1 tagged PfBDP3 and PfBDP4 proteins colocalised with the DNA stain DAPI (figure 5.3).

Table 5.1 Summary of the PfBDPs that were included in this study.

Name	Accession	Cellular fractionation	Immunofluorescence assay (IFA)	ChIP-seq
PfBDP3	PF3D7_0110500	Nuclear fractions	Colocalise with DNA	Trophozoite
PfBDP4	PF3D7_1475600	Nuclear and cytoplasmic fractions	Colocalise with DNA	Schizont

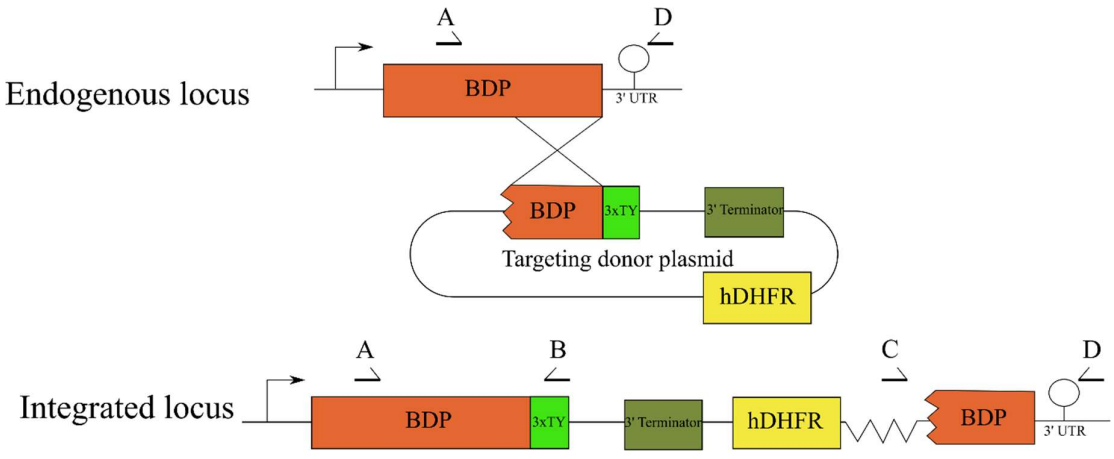

Figure 5.1 Generating parasites expressing Ty1-epitope tagged PfBDPs in *P. falciparum*. The diagram shows the endogenous PfBDP gene, targeting plasmid and integration after homologous recombination. The targeting plasmid included three Ty1 tags fused to the C-terminus of the homologous region of the PfBDP of interest. The human dihydrofolate reductase (hDHFR) gene was used to generate parasites resistant to WR99210 selection. Oligonucleotide binding sites for diagnostic PCRs are shown in the diagram. Primer A and B were used to confirm 5' integration, primer C and D were used to confirm 3' integration, primer A and D were used to detect wildtype locus.

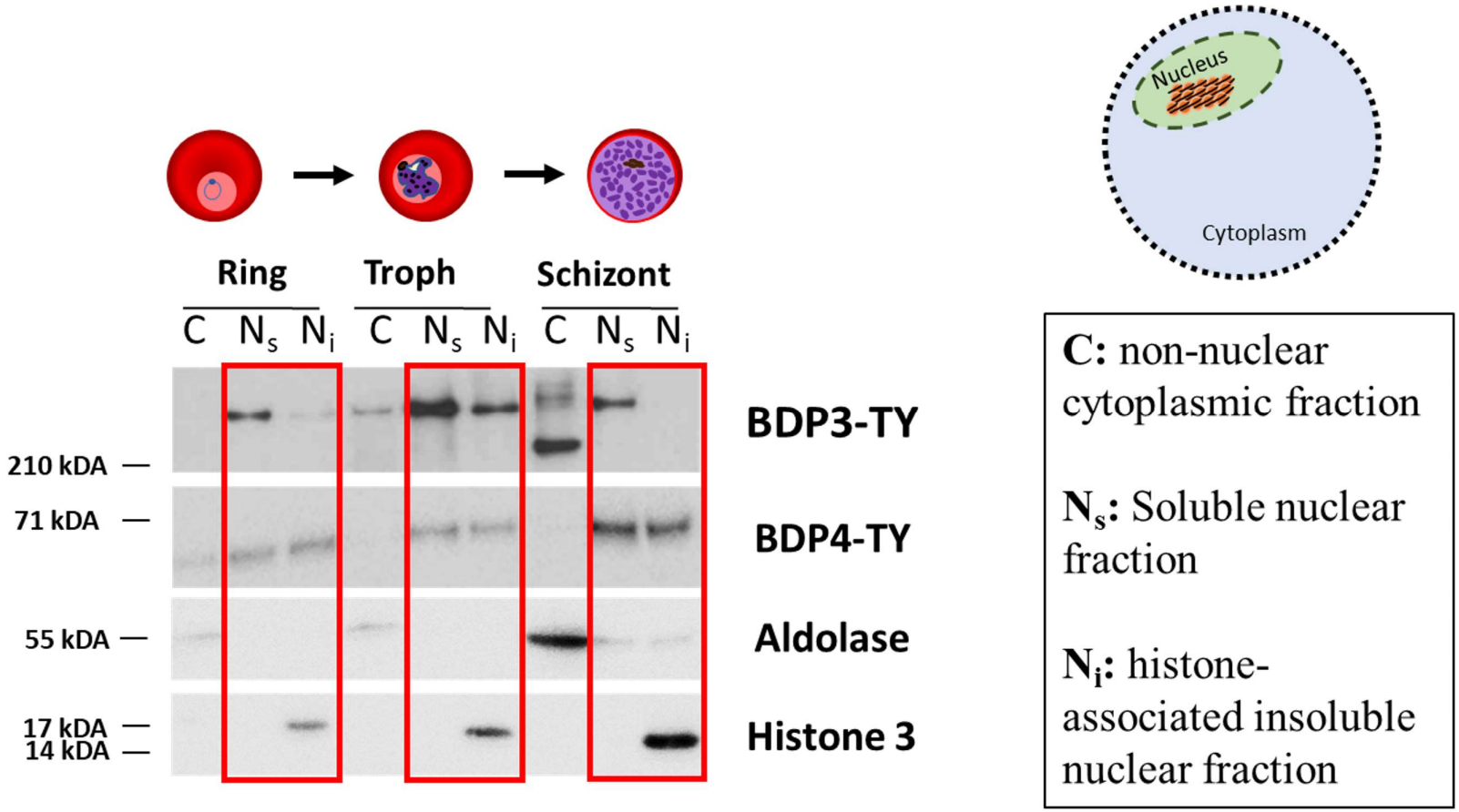

Figure 5.2 Cellular localisation of PfBDPs by cellular fractionation. Western blot analysis of parasites expressing Ty1-tagged parasite lines (PfBDP3 and PfBDP4 tagged lines). Fraction C contains proteins that are found in the cytoplasm which is outside of the nucleus. Fraction Ns contains proteins that can be solubilised by high salt and reducing buffer while Ni contains histones and proteins which are insoluble in a high salt buffer. Aldolase and histone 3 were used as a loading control for fraction C and fraction Ni, respectively.

In humans, BRD proteins are essential for coordinated gene regulation. For example, several functions of hsBRD4 include acting as a scaffold for transcription factors and other chromatin-associated protein (Wu et al., 2006), maintaining chromatin structure via its C-terminal domain (Wang et al., 2012) as well as regulating the cell cycle via interaction with the signal-induced proliferation-associated protein 1 (Farina et al., 2004). PfBDP3 and 4 are found in the nucleus of *P. falciparum* suggesting that they have nuclear functions and may be involved in the regulation of gene expression.

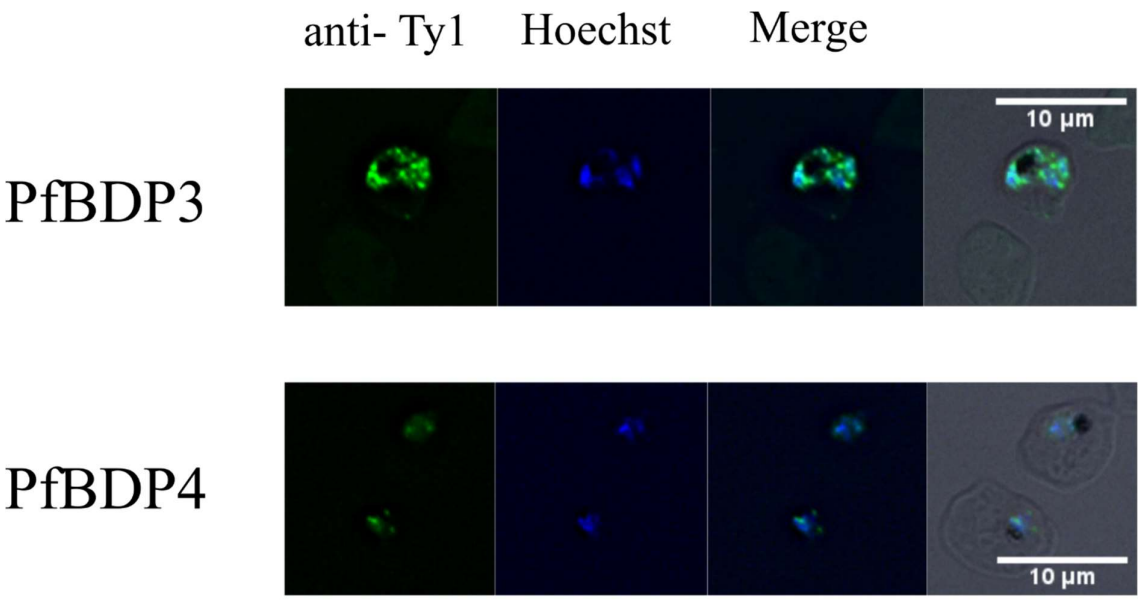

Figure 5.3. Immunofluorescence assay of PfBDP3 and PfBDP4. Parasites were crosslinked with 100% methanol on a slide. Monoclonal mouse anti-Ty1 and Hoechst were used to visualise the localisation of the tagged protein and the DNA, respectively.

5.2.2. ChIP-seq protocol optimisation for PfBDPs

Two common methods of ChIP are crosslinked and native ChIP. In crosslinked (X-linked) ChIP, formaldehyde reacts with primary amines to form reactive Schiff bases that can then form covalent bonds with amino groups on amino acids or nucleic acids that are in close proximity (Hoffman et al., 2015). The crosslinked nuclei are then sonicated and sheared into smaller fragments. A key advantage of X-linked ChIP is the ability to capture genomic interaction sites of proteins other than histones that may have weaker interactions with chromatin. Therefore, crosslinking can preserve the chromatin-associated complex better than native ChIP. However, there is a risk of over-crosslinking and false signals from proteins that are not specifically interacting with the chromatin.

Native ChIP does not require crosslinking and the genome is digested into fragments by micrococcal nuclease (MNase). As a result, native ChIP can increase sensitivity and resolution due to reduced epitope masking, although it may not be suitable for non-histone proteins. Many studies have successfully used both methods in ChIP-seq for *P. falciparum*. Here, as ChIP-seq for PfBDP has not been performed previously with the exception of PfBDP1 (Josling et al., 2015), we aimed to compare X-linked and native ChIP for the Ty1-tagged PfBDP parasite lines to determine the most suitable method.

5.2.2.1. Optimisation of X-linked ChIP-seq

To determine the genome-wide localization of the PfBDPs by ChIP-seq, the optimal conditions for fixation and chromatin shearing were established. After the parasites were crosslinked by paraformaldehyde (PFA) and the nuclei were harvested, chromatin was sonicated. Effective sonication needs to successfully shear DNA into fragments with appropriate length for the subsequent sequencing step on the Next Generation Sequencing Illumina platform while maintaining the integrity of protein complexes and the epitope tag on the PfBDPs which is critical for the immunoprecipitation procedure.

Here, X-linked PfBDP4ty nuclei were sonicated under different conditions using two sonicators: a Diagenode Bioruptor and a Covaris s220, which were both successfully used for *Plasmodium* samples previously (Bunnik et al., 2018; Duffy et al., 2017). Sonicated samples were analysed for the size of DNA fragments by DNA gel electrophoresis as well as for the integrity of the PfBDP4Ty fusion protein by western blot (figure 5.4).

Little difference was observed when the nuclei were sonicated with the Bioruptor for 16 or 28 cycles, as the DNA fragments from both samples range from 100 bp to 600 bp (figure 5.4A) and PfBDP4ty was detected by western blot (figure 5.4B). The Covaris performed significantly better than the Bioruptor in fragmenting the DNA with 13 Watts for 15-20 minutes yielding the best result with fragments smaller than 300 bp in size (figure 5.4A). However, detection of PfBDP4ty was almost abolished after sonication in the Covaris for 5 minutes at 13 Watts (figure 5.4B). While the PfBDP4ty was detectable when materials were sonicated in the Covaris at 24 Watts for 3 minutes, the Bioruptor was a more consistent system. Therefore, we concluded that the Covaris sonication was too harsh for maintaining the integrity of the epitope tag and may compromise the ChIP experiment. While the Bioruptor yielded slightly larger DNA fragments in comparison to the Covaris, they were well within the recommended size range for Illumina sequencing and the Ty1 tag remained intact. Consequently, the Bioruptor was used for sonication of the PfBDP ChIP-seq protocol.

5.2.2.2. Validation of antibodies for ChIP

Mouse monoclonal and a rabbit polyclonal anti-Ty1 antibodies were tested to optimise signal to background noise ratios for the immunoprecipitation. X-linked chromatin from PfBDP3ty and negative control 3D7 parasites were harvested and precipitated with either 5 µg mouse anti-Ty1 or 2 µg rabbit anti-Ty1. To compare the DNA enrichment between these samples, the 5' untranslated regions and the coding sequences (CDS) of ten genes with variable expression patterns were amplified by qPCR (figure 5.5) (Appendix, table 9.1).

The qPCR signal was normalised to the total genomic starting material (input). A similar proportion of signal was observed with both mouse and rabbit Ty1 antibodies (figure 5.5A) suggesting that chromatin can be precipitated using either of these antibodies. To assess the non-specific signal from each antibody, the qPCR signal of each region was further normalised to the signal from material immunoprecipitated from wildtype, 3D7 negative control samples (figure 5.5B). The fold enrichment relative to negative control was consistently higher with the mouse antibody than with the rabbit antibody. This indicates that the rabbit antibody precipitated more non-specific DNA from the 3D7 negative control. Therefore, 5 µg mouse monoclonal anti-Ty1 antibody was used for all the ChIP-seq experiments described in this chapter.

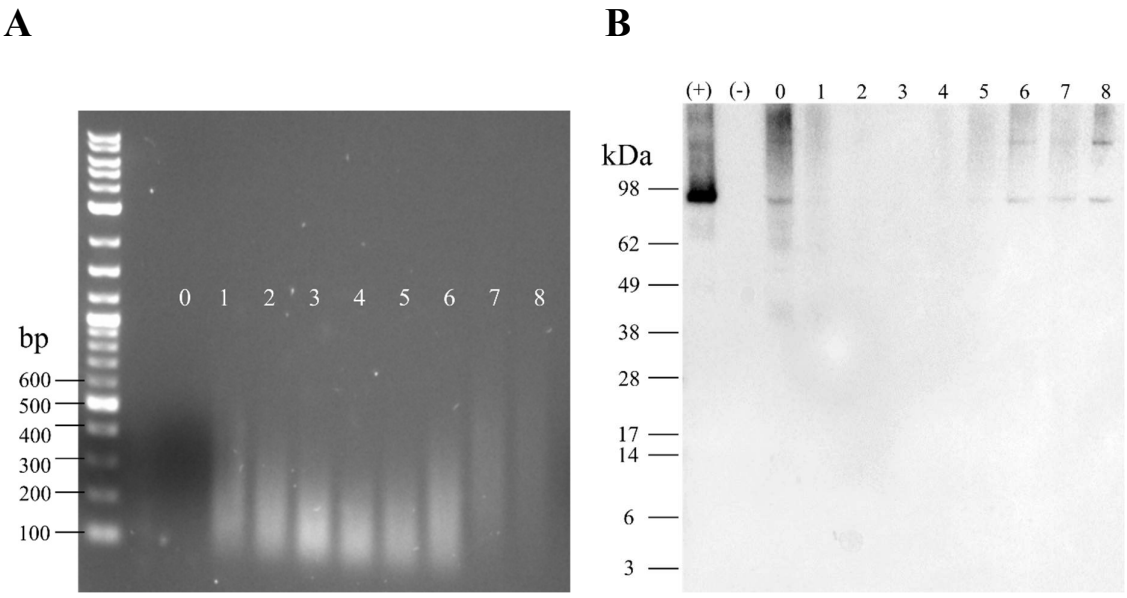

Figure 5.4 Comparison of chromatin shearing using Covaris and Bioruptor sonicators. Loading order: (+) positive, (-) negative control, lane (0)-unsonicated, Covaris: lane (1)-13 Watts/5 min, (2)-13 Watts/10 min, (3)-13 Watts/15 min, (4)-13 Watts/20 min, (5)-15 Watts/8 min, (6)-24 Watts/3 min, Bioruptor: lane (7)-16 cycles, (8)-28 cycles. **(A)** DNA gel electrophoresis of sonicated samples. **(B)** Western blot analyses of sonicated samples; expected PfBDP4 size is 86 kDa.

A

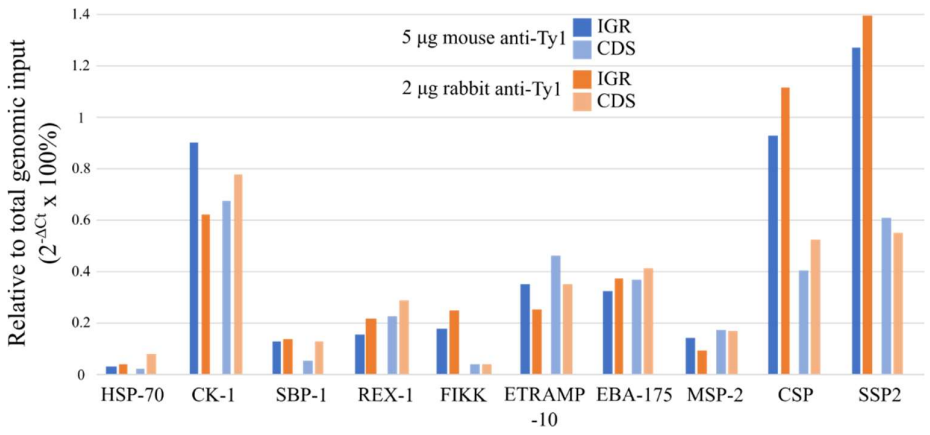

B

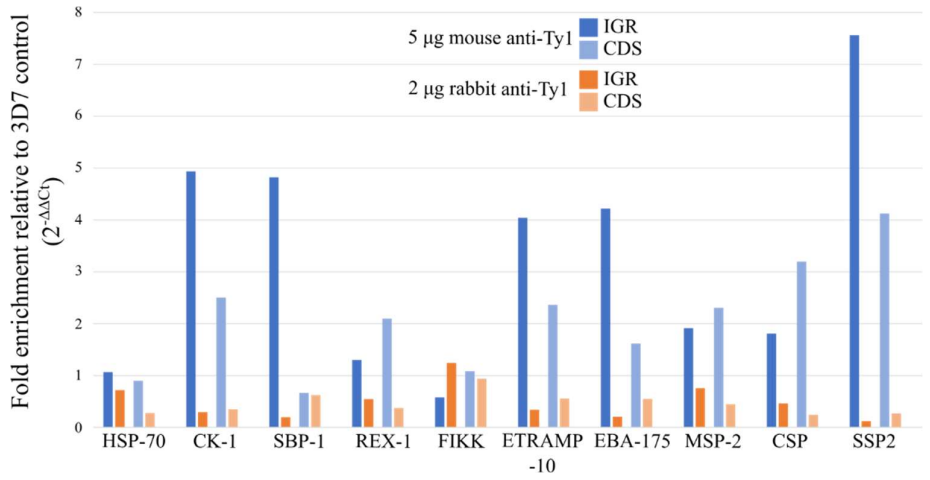

Figure 5.5 Validation of antibodies for ChIP. ChIP-qPCR from chromatin samples tested with either 5 µg mouse anti-Ty1 (blue) or 2 µg rabbit anti-Ty1 (orange). For each gene, primers were designed to target the 5' untranslated intergenic region (IGR) in dark colours as well as the coding sequence (CDS) in light colours. **(A)** The signal was normalised to the total genomic input ($2^{-\Delta Ct}$) and expressed as a percentage of input (y-axis). **(B)** The signal was further normalised to the 3D7 no-tag control and expressed as fold enrichment ($2^{-\Delta\Delta Ct}$) (y-axis).

5.2.2.3. Comparison of X-linked and native ChIP

X-linked and native ChIPs were performed for the PfBDP4ty parasite line during the schizont stage with 10^8 infected cells per schizont ChIP. The native ChIP protocol was previously optimised by other members in the lab. When cells were crosslinked with PFA, a band of around 86 kDa consistent with the size of PfBDP4ty was detected in the elution post-ChIP and was absent from the unbound fraction confirming that the method can successfully pulldown PfBDP4ty protein (figure 5.6). In the X-linked samples, a band of around 198 kDa was detected which might be a complex of PfBDP4 and other nuclear proteins that were crosslinked together. However, in native ChIP, tagged protein was observed pre-ChIP but was not successfully immunoprecipitated (figure 5.6). It is possible that the washing conditions used for the native ChIP protocol were too stringent and the tagged protein complex was washed off the beads. In summary, it was decided that the optimal conditions for PfBDP ChIPs were X-linked nuclei sonicated with the Bioruptor and ChIP'ed with 5 µg mouse antibody.

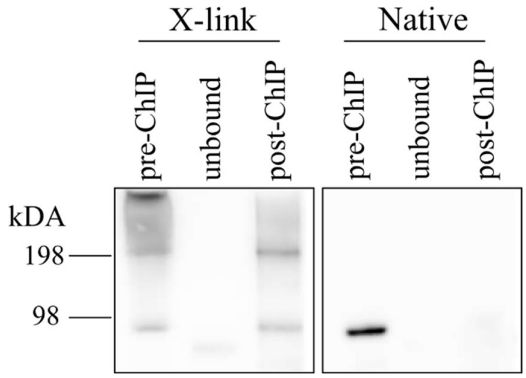

Figure 5.6 Western blot analysis comparing X-linked and native ChIP of BDP4ty. The molecular weight of PfBDP4ty was 86 kDa. Samples before the ChIP experiment (pre-ChIP), supernatant after ChIP (unbound) and elution of the ChIP experiment (post-ChIP) were collected for western blot analysis.

5.2.3. PfBDP4 is enriched upstream of invasion genes and highly expressed genes in schizonts

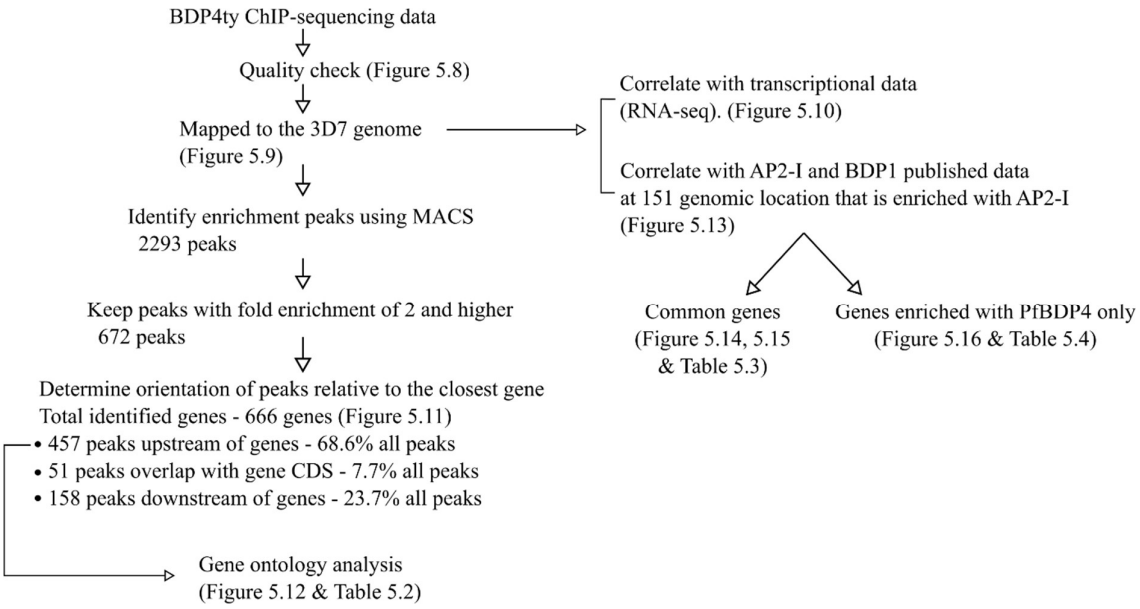

Figure 5.7 Summary of analyses performed for PfBDP4 ChIP-sequencing data. Detailed bioinformatics commands for each analysis are included in Chapter 3.

X-linked ChIP followed by Illumina sequencing was performed for tightly synchronised PfBDP4ty schizonts using the mouse anti-Ty1 antibody to identify PfBDP4 enrichment in the *P. falciparum* genome (PfBDP4ty_TY). The pre-ChIP material (input) was also sequenced and used to normalise the PfBDP4ty_TY reads in subsequent analyses. The sequencing data of two biological replicates were mapped to the 3D7 genome (PlasmoDB, version 44 (Aurrecoechea et al., 2008)) to generate BAM files. All analyses performed for the ChIP-seq data were summarised in a flowchart in figure 5.7

Principal Component Analysis (PCA) (deeptools (Ramírez et al., 2014)) showed input samples (Replicate 1_input and 2_input) clustered together (figure 5.8A). The anti-Ty immunoprecipitated replicates (Replicate 1_TY and 2_TY) can be distinguished from the input samples in principal component 2 (PC2) (figure 5.8A). Furthermore, Pearson correlation coefficients confirmed that the PfBDP4ty_TY biological replicates strongly correlated with each other and clustered together ($r = 0.79$) while the input samples formed a separate cluster indicating that the ChIP was reproducible (figure 5.8B). Correlation coefficients between

PfBDP4ty_TY and input samples were low (figure 5.8B) suggesting that the read coverages of the anti-TY immunoprecipitated samples were different from their controls. Only replicate 1 data are reported for this chapter because replicate 2 sequences were only obtained very recently. However, the strong correlation between the two replicates underpins the validity of our results. All concatenated replicates will be analysed for future publication.

When the sequencing coverage of Replicate 1_TY was inspected by the IGV genome browser, clear peaks were observed (figure 5.9) indicating these DNA sequences were precipitated together with PfBDP4ty during the ChIP experiment. The Model-based Analysis of ChIP-Seq (MACS) version 2.1.2 (Zhang et al., 2008) identified 2293 sites where PfBDP4 is enriched in the *P. falciparum* genome compared to the input signal (figure 5.7). To investigate the relationship between PfBDP4 enrichment and gene expression, the transcriptional profile of schizonts from the same parasite line was determined by RNA-seq and was correlated with the PfBDP4 enrichment profile (figure 5.10). This analysis revealed that PfBDP4 was highly enriched upstream of the coding sequence of genes highly expressed in Schizonts. Therefore, it is likely that PfBDP4 is part of a complex that regulates gene expression in *P. falciparum*, consistent with its identification in complex with AP2-I (Hoeijmakers et al., 2019).

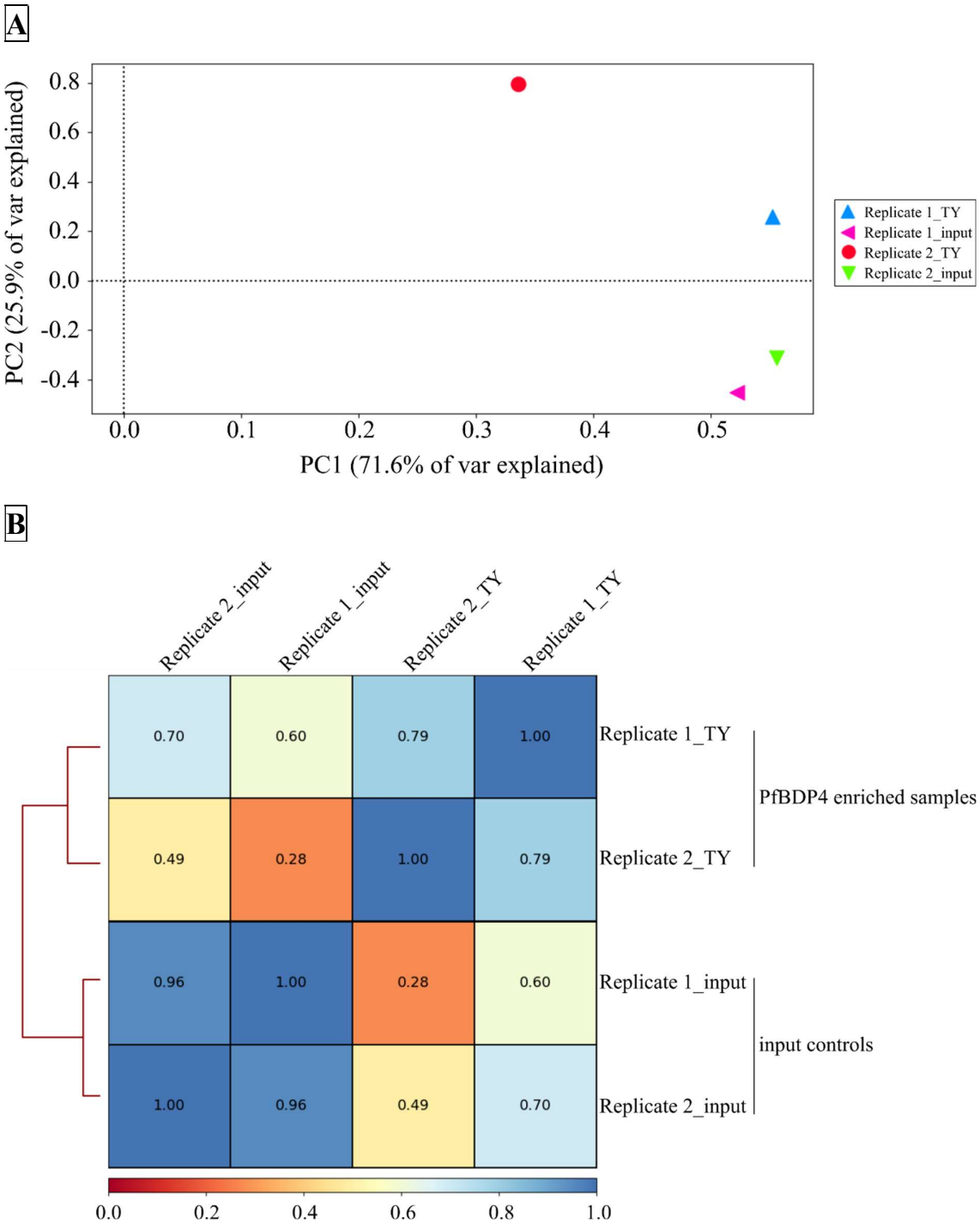

Figure 5.8 BDP4Ty ChIP replicates strongly correlated with each other and formed a cluster separate from the inputs in (A) PCA plot and (B) Pearson correlation heatmap. PCA plot and Pearson correlation coefficients between two biological PfBDP4ty_TY replicates

(Replicate 1_TY and 2_TY) and their inputs (Replicate 1_input and 2_input) were determined using the deepTools suite (Ramírez et al., 2014) to compare the read coverage of the BAM files across the genome. The correlation coefficients (displayed in boxes) of two PfBDP4 enriched replicates and their matched, control input samples are presented as a heatmap with hierarchical clustering performed as a feature of the plotCorrelation tool (Ramírez et al., 2014).

To ensure that the enrichment signals were biologically relevant, only 672 peaks with at least 2-fold enrichment in PfBDP4 relative to input samples (figure 5.7) were kept for subsequent analyses. Genes that were associated with PfBDP4 were defined as genes that were closest to a peak summit using BEDtools (Quinlan and Hall, 2010). A peak summit was defined as the nucleotide position where the enrichment peak was the highest. As an example, *msp-1* and *ron-3* were selected as they were the genes closest to the peaks shown in (figure 5.9A and B). Occasionally, two peak summits were associated with the same gene. In the example in figure 5.9C, two peaks were considered the closest to PF3D7_1013200, although the more distal peak could be marking the promoter of the divergent transcribed, adjacent gene PF3D7_1013100.1. In this case, only the gene that was reported as closest (eg. PF3D7_1013200) was included in the final gene list of 666 genes (figure 5.7). From this, the average enrichment profile of PfBDP4 was plotted for the PfBDP4-associated genes (figure 5.11) and similarly to the observation in figure 5.10, PfBDP4 was most enriched in the promoter region upstream of the gene CDS (figure 5.11). Next, the location of each PfBDP4 peak relative to its closest gene was determined by BEDtools (Quinlan and Hall, 2010). 457 (68.6%) peaks were upstream of the genes' CDSs (Appendix, table 9.3), 158 (23.7%) peaks were downstream and 51 (7.7%) peaks were inside the gene CDS.

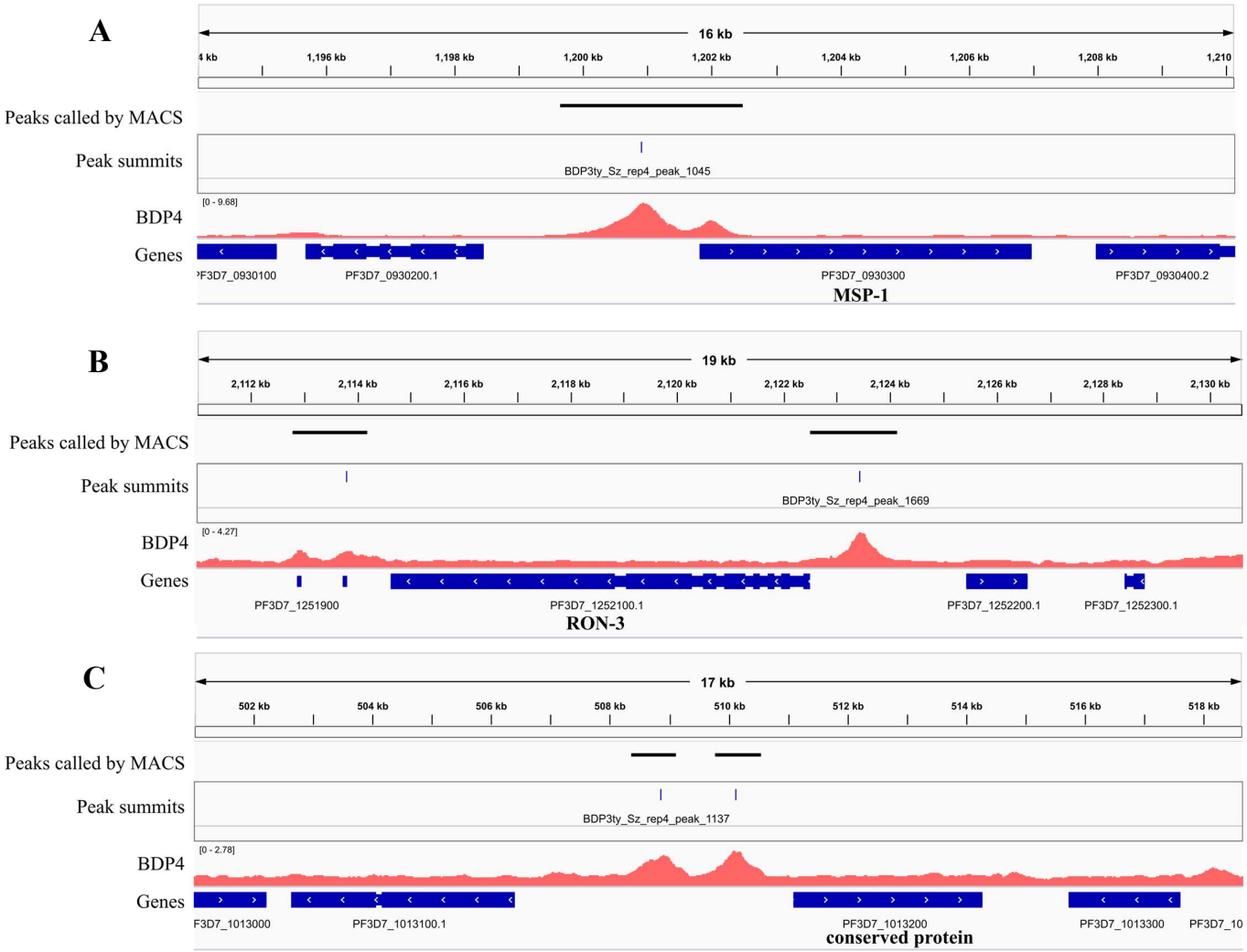

Figure 5.9 Representative snapshots from the IGV genome browser showing PfBDP4 enrichment normalised to input (log2(ChIP/input) - red). The peaks and peak summits identified by MACS (Zhang et al., 2008) are indicated above the ChIP-seq tracks and the 3D7 gene annotations (blue) are included below, arrows on gene annotations indicate direction of transcription. One PfBDP4 enrichment peak was identified upstream of (A) *msp-1* and (B) *ron-3* while two PfBDP4 peaks were identified upstream of PF3D7_1013200.

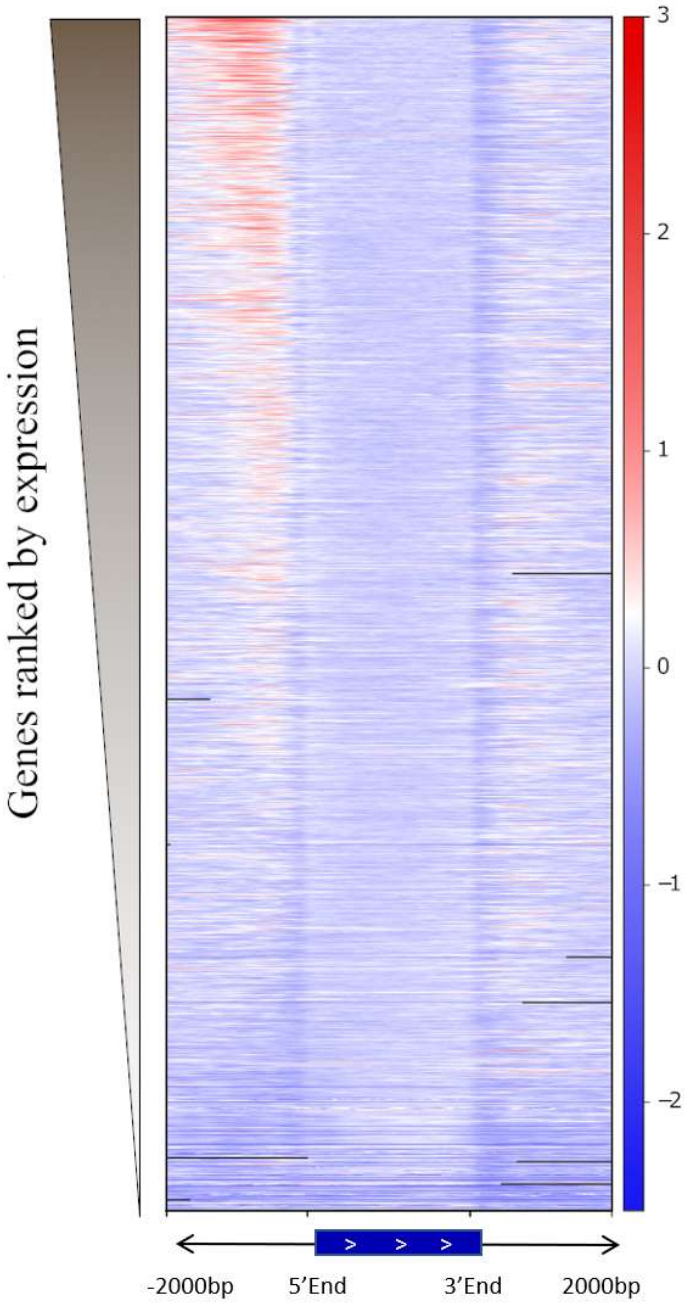

Figure 5.10 BDP4 enrichment correlates with gene transcription. Gene transcripts during the schizont stage were ranked by RPKM with the most highly expressed genes located on the top of the heatmap (y-axis). Regions of 2000 bp upstream and downstream of the CDS for all 3D7 *P. falciparum* genes are depicted on the x-axis. The heatmap was generated by deepTools (Ramírez et al., 2014).

To determine the biological processes that PfBDP4 may regulate, the 457 genes, which had PfBDP4 enriched at putative promoters upstream of their CDS were selected for subsequent gene ontology (GO) analysis using the PlasmoDB website (Aurrecoechea et al., 2008). The pathways were summarised and visualised by REVIGO (Supek et al., 2011) (figure 5.12) (Table 5.2). 'Entry into host cell' was the most significant GO term with 19 genes belonging to this term (Table 5.2). Among these 19 genes, many of them are members of the *msp*, *ron* and *rhopH* gene families which encodes proteins found on the surface of the merozoites, in the rhoptry neck, the rhoptry bulb and the glideosome. Also, 'chromatin assembly or disassembly' was identified which includes histone 3 (H3), H4, H2A.Z and H2B.Z (Table 5.2). While they were not part of this GO term, H2B and CenH3 were also present in the initial gene list of 457 genes indicating that PfBDP4 was enriched upstream of many histone proteins in *P. falciparum*. Notably, PfBDP4 was also enriched upstream of SERA4, -5, -6 and -7 as well as four members of the ApiAP2 family (AP2-I, AP2-exp, PF3D7_1456000 and PF3D7_0613800).

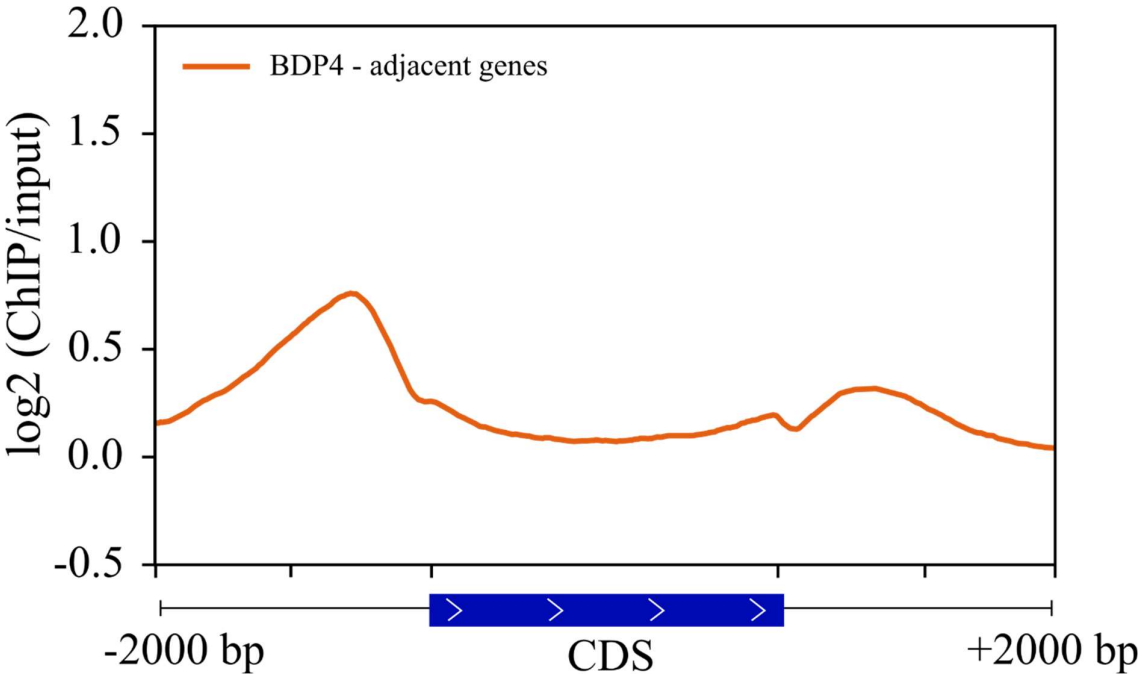

Figure 5.11 ChIPseq analysis of BDP4Ty. Average enrichment profile (deepTools (Ramírez et al., 2014)) of PfBDP4 (orange) for 666 genes that were closest to PfBDP4 ChIPseq peaks (MACS (Zhang et al., 2008)). 2000 bp upstream of the start codon and 2000 bp downstream of the stop codon were plotted each side of the length normalised CDS.

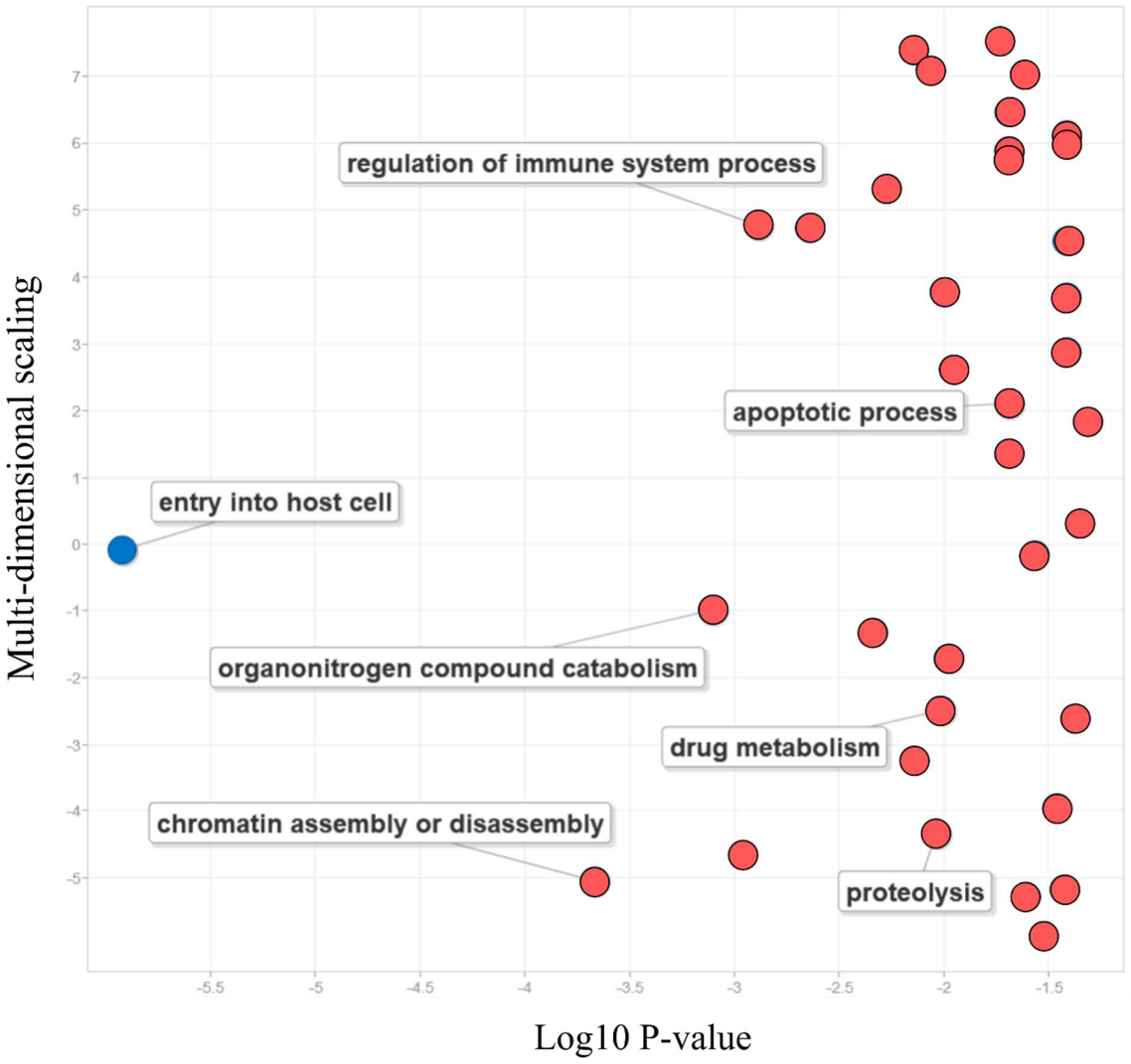

Figure 5.12. Graphical representation by REVIGO of the gene ontology pathways identified for peaks upstream of PfBDP4. GO terms were identified using the analysis tool from PlasmoDB (Aurrecoechea et al., 2008). REVIGO uses multi-dimensional scaling to reduce the dimensionality of the matrix (Supek et al., 2011). The blue dot signifies GO terms with Bonferroni adjusted p-value less than 0.05 while the red dots are GO terms with adjusted p-value higher than 0.05. The names of some pathways were highlighted, and the rest of the GO terms can be found in table 5.2.

Table 5.2 Gene ontology analysis for genes that were enriched with PfBDP4 in their promoters.

GO term ID	Description	Bckgd count	Result count	log_{10} p-value	Bonferroni adjusted P-value
GO:0030260	entry into host cell	66	19	-5.9198	0.0008778
GO:0006333	chromatin assembly or disassembly	12	6	-3.6671	0.1606
GO:1901565	organonitrogen compound catabolic process	102	19	-3.1043	0.5867
GO:0030163	protein catabolic process	89	17	-2.959	0.8199
GO:0002682	regulation of immune system process	11	5	-2.8869	0.9679
GO:0032507	maintenance of protein location in cell	4	3	-2.6413	1.0
GO:0009056	catabolic process	153	23	-2.3364	1.0
GO:0051235	maintenance of location	5	3	-2.2716	1.0
GO:0006359	regulation of transcription from RNA polymerase III promoter	2	2	-2.1423	1.0
GO:0007052	mitotic spindle organization	2	2	-2.1423	1.0
GO:0048583	regulation of response to stimulus	16	5	-2.0661	1.0
GO:0006508	proteolysis	171	24	-2.0383	1.0
GO:0017144	drug metabolic process	75	13	-2.017	1.0
GO:0006119	oxidative phosphorylation	6	3	-1.9987	1.0
GO:0002376	immune system process	11	4	-1.9802	1.0

GO:0015672	monovalent inorganic cation transport	30	7	-1.9556	1.0
GO:0055114	oxidation-reduction process	90	14	-1.732	1.0
GO:0006915	apoptotic process	3	2	-1.6904	1.0
GO:0008219	cell death	3	2	-1.6904	1.0
GO:0006275	regulation of DNA replication	3	2	-1.6904	1.0
GO:0006490	oligosaccharide-lipid intermediate biosynthetic process	3	2	-1.6904	1.0
GO:0006488	dolichol-linked oligosaccharide biosynthetic process	3	2	-1.6904	1.0
GO:0008610	lipid biosynthetic process	67	11	-1.6158	1.0
GO:0051259	protein oligomerization	8	3	-1.6075	1.0
GO:0006796	phosphate-containing compound metabolic process	267	32	-1.5656	1.0
GO:0006793	phosphorus metabolic process	269	32	-1.5249	1.0
GO:0006464	cellular protein modification process	252	30	-1.462	1.0
GO:0006325	chromatin organization	30	6	-1.4274	1.0
GO:0006544	glycine metabolic process	4	2	-1.4143	1.0
GO:0042133	neurotransmitter metabolic process	4	2	-1.4143	1.0
GO:0001505	regulation of neurotransmitter levels	4	2	-1.4143	1.0
GO:0046470	phosphatidylcholine metabolic process	4	2	-1.4143	1.0
GO:0042775	mitochondrial ATP synthesis coupled electron transport	4	2	-1.4143	1.0

GO:0006091	generation of precursor metabolites and energy	47	8	-1.3751	1.0
GO:1901135	carbohydrate derivative metabolic process	129	17	-1.3535	1.0
GO:0007017	microtubule-based process	40	7	-1.3111	1.0

5.2.4. PfBDP4 genomic enrichment correlates with AP2-I and PfBDP1 enrichment upstream of invasion genes

As PfBDP4 was enriched in the promoter of invasion genes, it was of interest to determine whether PfBDP4 is associated with other *trans* factors that regulate the invasion genes. Therefore, the PfBDP4 ChIP-seq dataset was correlated with the published sequencing data of the transcription factor AP2-I and the BRD protein PfBDP1 which are critical for the coordinated regulation of invasion (Josling et al., 2015; Santos et al., 2017) (figure 5.13).

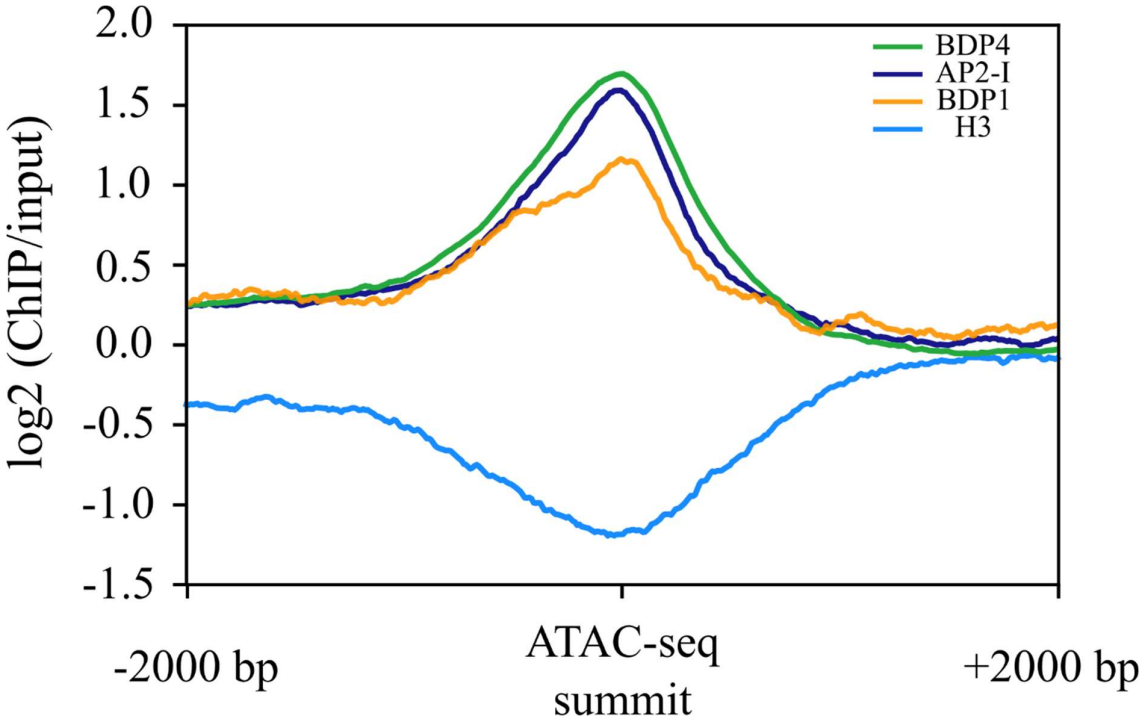

Figure 5.13 Enrichment profile of AP2-I, PfBDP1, PfBDP4 and H3 at ATACseq summits. Averaged profile plot showing log2(ChIP/input) of PfBDP4 (green), AP2-I (navy), PfBDP1 (orange) and histone 3 (blue) across 2000 bp upstream to 2000 bp downstream of the 151 ATAC-seq peak summits found upstream of genes that also had upstream AP2-I peaks in schizont stages. The peaks have been orientated in the same direction as the adjacent, downstream genes. The plot was generated by deepTools (Ramírez et al., 2014) using published datasets (Josling et al., 2015; Santos et al., 2017; Toenhake et al., 2018).

Recently, an ATAC-seq study in *P. falciparum* determined chromatin accessibility during the parasite asexual life cycle (Toenhake et al., 2018) and Santos et al. identified 157 genes that were enriched with AP2-I in their promoters (data obtained from AP2-I merged peaks (Santos et al., 2017)). We intersected these two datasets to obtained 151 ATAC-seq regions, that were also enriched with AP2-I, For these 151 loci, we plotted the enrichment profiles of AP2-I (Santos et al., 2017), PfBDP1 (Josling et al., 2015) and PfBDP4 normalised to input and centred on the ATAC-seq summit (figure 5.13). Histone 3 ChIP data were also included in the analyses and confirmed ATACseq results, indicating that these nucleosome depleted regions allow TF and regulatory complex binding (figure 5.13).

Interestingly, PfBDP4 and PfBDP1 were both enriched at exposed, putative regulatory and AP2-I enriched regions and the AP2-I profile at these ATACseq peaks was very similar to the PfBDP4 profile and overlaid the PfBDP1 enrichment (figure 5.13). This finding is consistent with previous observations from proteomic studies showing that these three proteins interact with each other (Hoeijmakers et al., 2019; Santos et al., 2017).

29 genes had upstream intersecting peaks of AP2-I (157 genes), PfBDP1 (119 genes, filtered from genes published in Josling et. al) and PfBDP4 (457 genes) (figure 5.14) (Appendix, table 9.3) (Josling et al., 2015; Santos et al., 2017). Predictably, the most significant GO term was entry into host cell (figure 5.15).

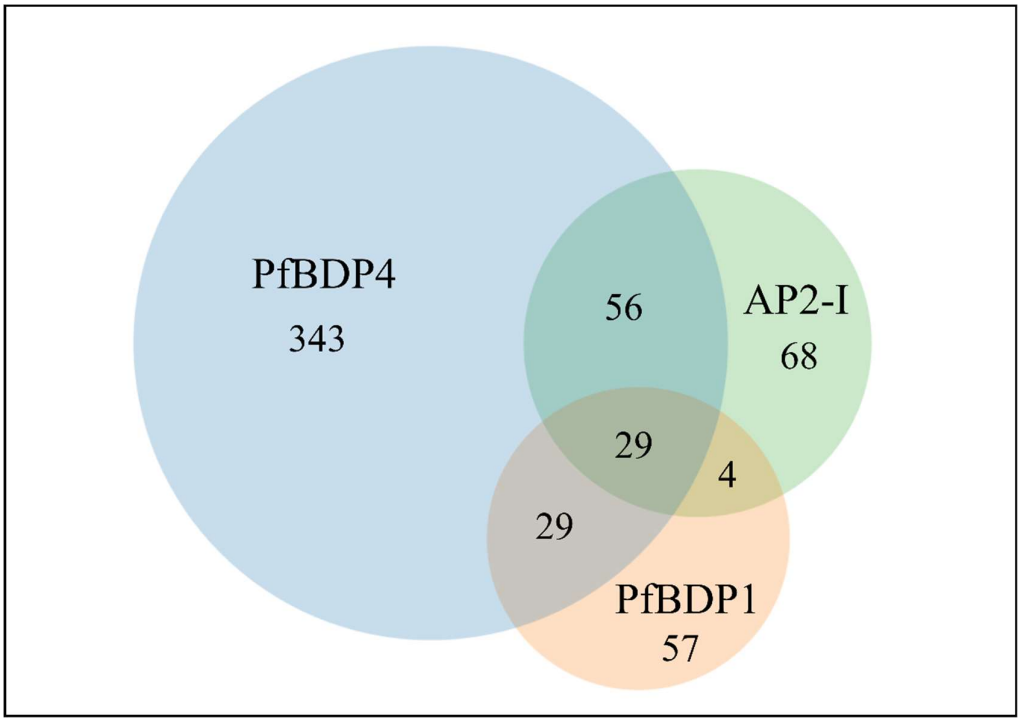

Figure 5.14 Venn diagram of the number of genes downstream of peaks of AP2-I, PfBDP1 and PfBDP4. PfBDP1, orange, AP2-I, green and PfBDP4, blue.

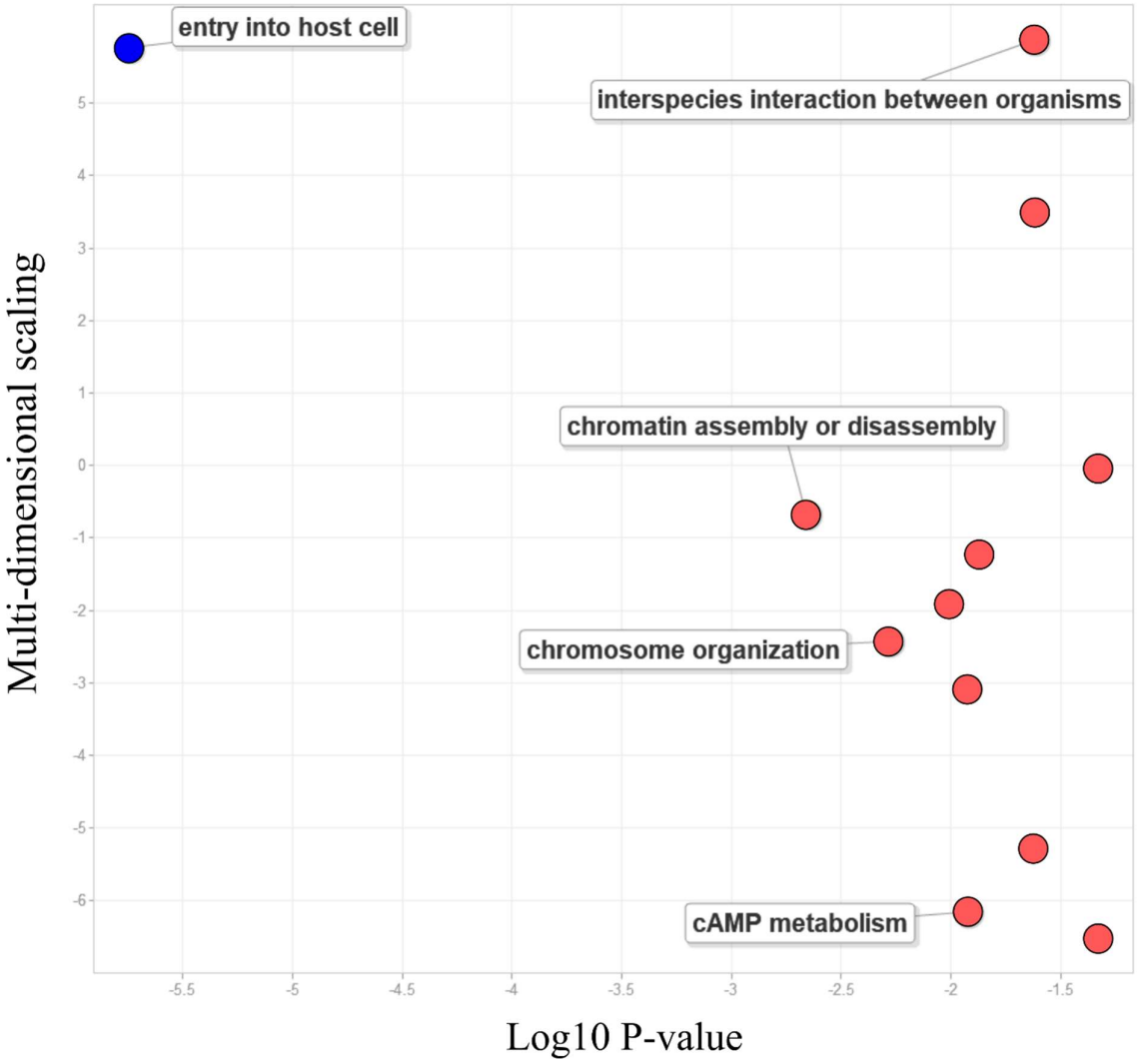

Figure 5.15 Graphical representation by REVIGO of the gene ontology pathways identified for 29 genes shared between AP2-I, PfBDP1 and PfBDP4. The X-axis shows the $\log_{10}$ of the P-value. REVIGO used multi-dimensional scaling to reduce the dimensionality of the matrix and the scale is shown on the y-axis (Supek et al., 2011). The blue dot signifies GO terms with Bonferroni adjusted p-value less than 0.05 while the red dots are GO terms with adjusted p-value higher than 0.05. The names of some pathways were highlighted, and the rest of the GO terms can be found in table 5.3.

Table 5.3 Gene ontology analysis for genes that were enriched with AP2-I, PfBDP1 and PfBDP4 in their promoters.

GO term ID	Description	Bckgd count	Result count	log10 p-value	Bonferroni adjusted P-value
GO:0030260	entry into host cell	66	6	-5.7457	0.0002083
GO:0006333	chromatin assembly and disassembly	12	2	-2.66	0.2538
GO:0051704	multi-organism process	388	6	-1.6164	1
GO:0046058	cAMP metabolic process	2	1	-1.9238	1
GO:0097164	ammonium ion metabolic process	8	1	-1.3292	1
GO:0046470	phosphatidylcholine metabolic process	4	1	-1.6253	1
GO:0051276	chromosome organization	60	3	-2.2846	1
GO:0009187	cyclic nucleotide metabolic process	8	1	-1.3292	1
GO:0007052	mitotic spindle organization	2	1	-1.9238	1
GO:0006325	chromatin organization	30	2	-1.8697	1
GO:0006996	organelle organization	144	4	-2.0081	1
GO:0044419	interspecies interaction between organisms	387	6	-1.6214	1

5.2.5. PfBDP4 also has binding sites unique from AP2-I and PfBDP1

A large proportion of the identified genes did not overlap with either PfBDP1 or AP2-I (figure 5.14). GO analysis showed that many of these genes are involved in different pathways of metabolic processing (figure 5.16, table 5.4). Enriched GO terms included 'organonitrogen compound catabolism, drug metabolism, proteolysis, oxidation-reduction process' and two proliferation cell nuclear antigens from 'regulation of DNA replication'. 19 genes belong to the most significant GO term – organonitrogen compound catabolism in which five proteasome subunits, as well as three putative ubiquitin-conjugating enzyme E2, were identified suggesting that PfBDP4 may regulate genes that are involved in proteolysis. In addition, PfBDP4 was also enriched upstream of several protein kinases including *P. falciparum* casein kinase 1 which belonged to the phosphorus metabolism GO term.

Overall, we showed that while PfBDP4 shares some target sites in the genome with PfBDP1 and AP2-I and they presumably regulate invasion genes together, it also has unique enrichment sites that are upstream of genes involved in proteolysis and phosphorylation among other pathways.

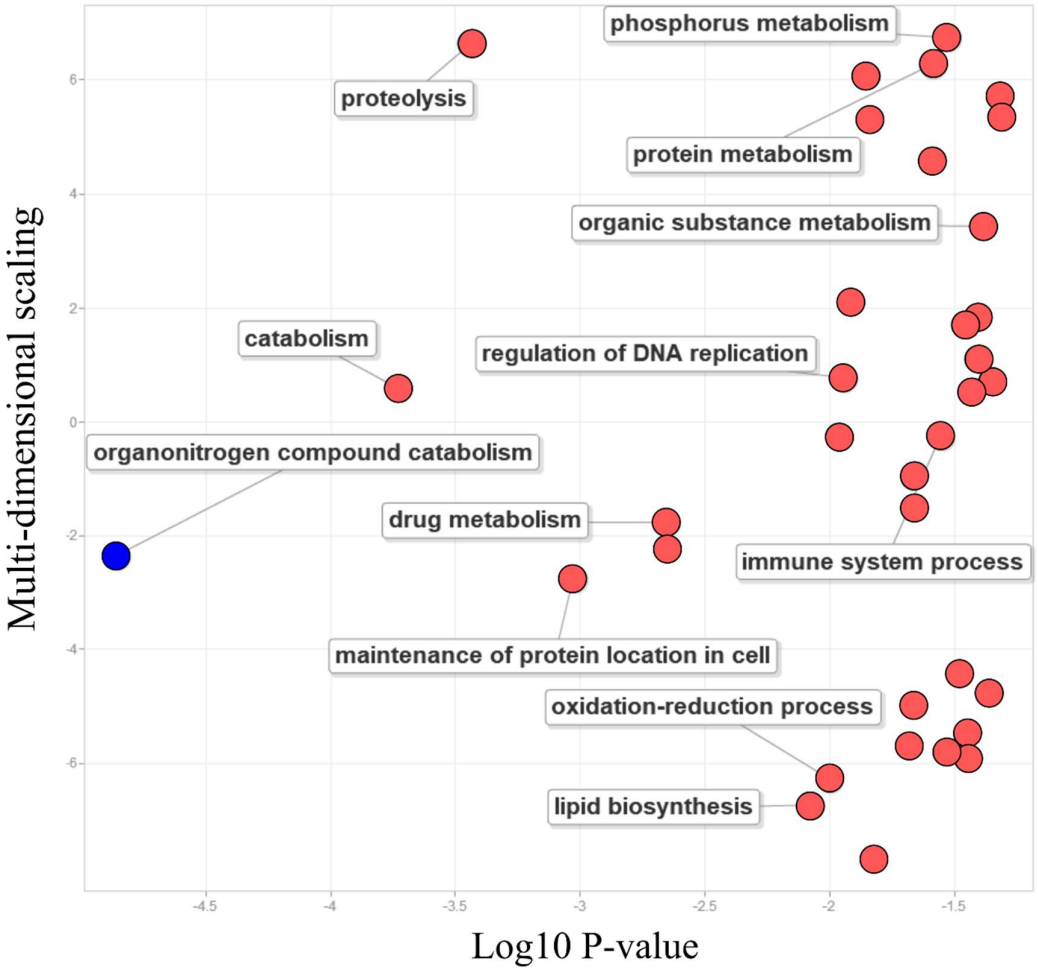

Figure 5.16. Graphical representation by REVIGO of the gene ontology pathways identified for 343 genes that were only enriched with PfBDP4. The X-axis shows the $\log_{10}$ of the P-value. REVIGO used multi-dimensional scaling to reduce the dimensionality of the matrix and the scale is shown on the y-axis (Supek et al., 2011). The blue dot signifies GO terms with Bonferroni adjusted p-value less than 0.05 while the red dots are GO terms with adjusted p-value higher than 0.05. The names of some pathways were highlighted, the remaining GO terms can be found in Table 5.4

Table 5.4 Gene ontology analysis for genes that were enriched with only PfBDP4 and were not overlapped with AP2-I and PfBDP1 in their promoter regions.

GO term ID	Description	Bckgd count	Result count	log10 p-value	Bonferroni adjusted P-value
GO:1901565	organonitrogen compound catabolic process	102	19	-4.8589	0.009744
GO:0009056	catabolic process	153	22	-3.7306	0.1309
GO:0006508	proteolysis	171	23	-3.4387	0.2563
GO:0032507	maintenance of protein location in cell	4	3	-3.0279	0.6602
GO:0017144	drug metabolic process	75	12	-2.6564	1
GO:0051235	maintenance of location	5	3	-2.6507	1
GO:0008610	lipid biosynthetic process	67	10	-2.0788	1
GO:0055114	oxidation-reduction process	90	12	-2.0021	1
GO:0002440	production of molecular mediator of immune response	8	3	-1.9641	1
GO:0006275	regulation of DNA replication	3	2	-1.946	1
GO:1901564	organonitrogen compound metabolic process	841	68	-1.9133	1
GO:0006464	cellular protein modification process	252	25	-1.8492	1
GO:1901135	carbohydrate derivative metabolic process	129	15	-1.839	1

GO:1901137	carbohydrate derivative biosynthetic process	95	12	-1.8235	1
GO:0006629	lipid metabolic process	111	13	-1.6799	1
GO:0006544	glycine metabolic process	4	2	-1.6634	1
GO:0042133	neurotransmitter metabolic process	4	2	-1.6634	1
GO:0001505	regulation of neurotransmitter levels	4	2	-1.6634	1
GO:0019538	protein metabolic process	682	55	-1.5879	1
GO:0006091	generation of precursor metabolites and energy	47	7	-1.5864	1
GO:0002376	immune system process	11	3	-1.5559	1
GO:0008152	metabolic process	1478	108	-1.5331	1
GO:0006793	phosphorus metabolic process	269	25	-1.5305	1
GO:0009205	purine ribonucleoside triphosphate metabolic process	39	6	-1.4812	1
GO:0051052	regulation of DNA metabolic process	5	2	-1.4598	1
GO:0015988	energy coupled proton transmembrane transport, against electrochemical gradient	12	3	-1.4512	1
GO:0090662	ATP hydrolysis coupled transmembrane transport	12	3	-1.4512	1
GO:0048519	negative regulation of biological process	30	5	-1.4323	1

GO:0010243	response to organonitrogen compound	21	4	-1.4073	1
GO:0034976	response to endoplasmic reticulum stress	21	4	-1.4073	1
GO:0071704	organic substance metabolic process	1389	101	-1.3861	1
GO:0070085	glycosylation	13	3	-1.3574	1
GO:0050794	regulation of cellular process	280	25	-1.3495	1
GO:0044260	cellular macromolecule metabolic process	810	62	-1.3205	1
GO:0044237	cellular metabolic process	1322	96	-1.3123	1

5.2.6. PfBDP3 is enriched in the heterochromatin of *P. falciparum*

Our collaborator at the SGC, who obtained the crystal structure of PfBDP3.2, showed that the recombinant PfBDP3.2 interacted with an H4 peptide that had four acetylated lysine residues (confidential unpublished data). Because the peak expression of PfBDP3 (figure 5.2) and H4ac were most abundant in trophozoites (Gupta et al., 2013), we performed X-link ChIP-seq of PfBDP3ty on trophozoites and preliminary results from one replicate are presented. The sequencing data were analysed as described for PfBDP4ty and the IGV genome browser was used to visualise the normalised PfBDP3ty sequencing coverage (figure 5.17). Interestingly, the pattern of enrichment of PfBDP3ty was limited to specific regions of the chromosomes especially near the ends of the chromosomes where HP1 and H3K9me3 are particularly abundant (figure 5.17) (Flueck et al., 2009; Fraschka et al., 2018; Jiang et al., 2013; Lopez-Rubio et al., 2009). PfBDP3 is also enriched in the CDS of genes which are normally epigenetically silenced during the asexual stage such as the master regulator AP2-G (figure 5.17C), which is responsible for differentiating the parasite into sexual and transmissible forms (Kafsack et al., 2014).

As previously mentioned, PfBDP3 can be mutated at multiple points N terminal of the bromodomains using the *piggyBac* mutagenesis system (figure 1.5), and mutants can grow normally *in vitro* suggesting that PfBDP3 is dispensable during the asexual life cycle (Zhang et al., 2018). This is not inconsistent with PfBDP3 having an important function in facultative heterochromatin which is enriched in contingency genes that are typically not required for survival *in vitro* of asexual parasites. Overall, this is interesting, counter-intuitive evidence of an acetyl-lysine binding bromodomain protein associated with deacetylated heterochromatin.

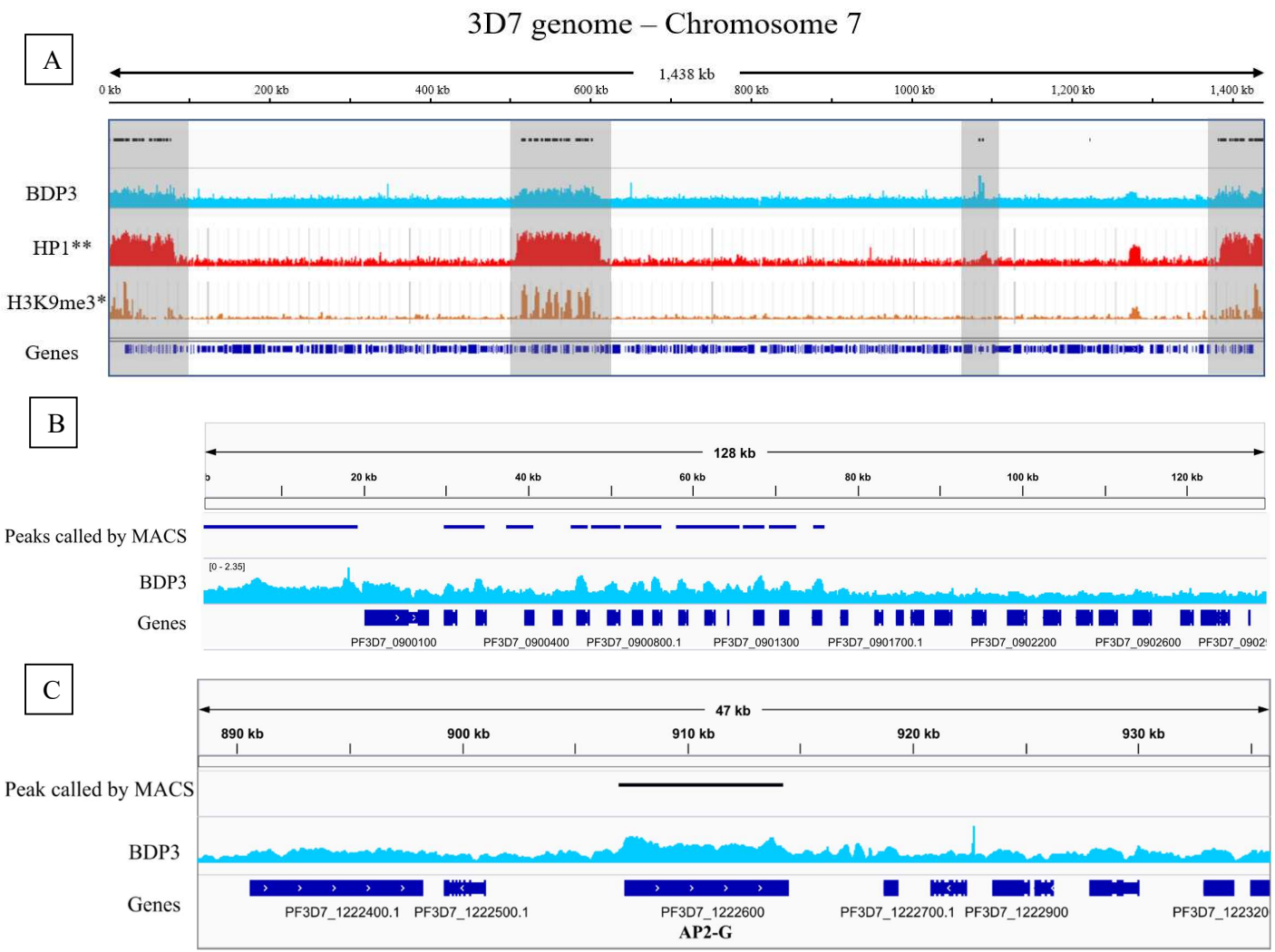

Figure 5.17 Representative profiles of PfBDP3 enrichment (log2(ChIP/input) (aqua). (A) Snapshot of chromosome 7 of the 3D7 genome with PfBDP3 (blue), heterochromatic regions (shaded grey), HP1 (red) (Fraschka et al., 2018) and H3K9me3 (orange) (Jiang et al., 2013). (B) Snapshot of PfBDP3 enrichment at the end of chromosome 9. (C) Snapshot of chromosome 12 taken from the IGV genome browser showing that PfBDP3 is enriched in the CDS of the gametocyte master regulator AP2-G.

5.3. Discussion

This chapter showed that PfBDPs are nuclear proteins. PfBDP4 was most abundant in schizonts while PfBDP3 protein expression peaked in trophozoite and schizonts. A processed form of PfBDP3 was also found in the cytoplasm of schizonts. In addition, all of the tested PfBDPs localised to the nucleus of the parasite, similar to a previous report (Oehring et al., 2012) and indicating that tagged proteins have not mis-localised. Using an optimised protocol, ChIP-sequencing for PfBDP4 and PfBDP3 was successfully performed for schizont and trophozoite stage parasites, respectively. Bioinformatic analyses of these sequencing data revealed key, novel insights into these PfBDPs' potential functions as gene regulators during the asexual stage of *P. falciparum*.

5.3.1. PfBDP4

Our ChIP-seq data showed that PfPfBDP4 was mostly enriched upstream of highly expressed genes during the schizont stage. This indicates that PfBDP4 enrichment correlates with gene expression. In addition, 92% of PfBDP4 enrichment was found in the intergenic regions of *P. falciparum*, with 68.6% of these peaks upstream of the closest gene. Interestingly, PfBDP4 was most enriched in the regions between 250 bp to 1000 bp 5' upstream of the CDS of which contain transcription factor binding sites such as AP2-I. Histone PTMs, such as H3K9ac, H3K56ac, H4K8ac, H4K16ac and H4ac4, are abundant in the 5' untranslated promoter regions of genes (Bártfai et al., 2010; Gupta et al., 2013; Karmodiya et al., 2015; Lopez-Rubio et al., 2009; Salcedo-Amaya et al., 2009). Among those, many previous studies showed that the enrichment of H3K9ac in the promoters correlates with gene transcription during the schizont stage (Bártfai et al., 2010; Gupta et al., 2013; Karmodiya et al., 2015; Salcedo-Amaya et al., 2009) and some studies suggest that the presence of acetylated H4, H3K14ac, H3K56ac, H3K18ac and H3K27ac also associates with active gene transcription (Duffy et al., 2017; Gupta et al., 2013). As PfBDP4 displayed selective binding towards H2B.Z and H4 acetylation (Hoeijmakers et al., 2019), the presence of PfBDP4 is consistent with the enrichment of acetylation in these regions. Therefore, PfBDP4 is likely to be a part of a complex that binds to the regulatory regions 5' upstream genes where it may contribute to gene activation. A smaller proportion of these peaks were downstream of the closest gene. However, almost all of the downstream peaks (146 out of 158 peaks) were found in the intergenic region between two tail-to-head orientated genes indicating that PfBDP4 is upstream and may be associated

with the neighbouring genes. Therefore, it is also possible that these PfBDP4 peaks are involved in regulating the neighbouring genes.

There were 457 genes with PfBDP4 enriched upstream of their start codon. Gene ontology analysis of these genes revealed that entry to host was the most significant GO term with 19 genes belonging to this term. These genes encoded for proteins that are found on the surface of the merozoite eg. MSPs, and various proteins found in the rhoptry neck, the rhoptry bulb and the glideosome. Notably, PfBDP4 is highly enriched at the 5' upstream as well as at the ATG of MSP-1. Much evidence in the literature demonstrates that MSP-1 is important for erythrocyte invasion and parasite egress (Blackman et al., 1990; Das et al., 2015). In particular, MSP-1 forms complexes with other MSPs to mediate an interaction with RBCs (Baldwin et al., 2015; Lin et al., 2016a). Antibodies against MSP-1 have been associated with parasite inhibition *in vitro* (Blackman et al., 1990; Woehlbier et al., 2006) and naturally acquired protection in patients (al-Yaman et al., 1996; Conway et al., 2000; Egan et al., 1996; Jäschke et al., 2017); and several clinical trials have used MSP-1 as a vaccine candidate (Blank et al., 2020; Ogutu et al., 2009; Sheehy et al., 2012). In addition to genes linked to invasion, PfBDP4 was enriched upstream of SERA5 and SERA6 which play a critical role during IDC egress (Collins et al., 2017; Ruecker et al., 2012). Disruption of both of these genes led to a growth defect as parasites cannot properly egress (Collins et al., 2017; Ruecker et al., 2012). In the future, it will be interesting to determine whether PfBDP4 regulates the expression of SERA5 and SERA6 and whether interruption of PfBDP4 could lead to defect in egress.

PfBDP1 and the transcription factor AP2-I are the only known *trans* factors currently known to play a role in regulating invasion genes (Josling et al., 2015; Santos et al., 2017). Over half of the AP2-I or PfBDP1 ChIPseq peaks (Josling et al., 2015; Santos et al., 2017) intersected PfBDP4 ChIPseq peaks and the 29 genes downstream of all 3 intersecting peaks were strongly associated with invasion. This is consistent with the finding that PfBDP4, PfBDP1 and AP2-I interact and possibly form a complex as observed in a recent proteomic study (Hoeijmakers et al., 2019). AP2-I can bind its target DNA motifs in the absence of PfBDP1 (Santos et al., 2017). In the future, it will be interesting to see whether the presence of PfBDP4 is required for the binding of AP2-I at the promoter of invasion genes and how PfBDP4 is interacting with PfBDP1 and AP2-I. This can be done using the approach of Santos et al. 2018 by modifying our NF54-PfBDP4-*LoxP-glmS* parasite line described in Chapter 4 to express AP2-I fused with 3' GFP. The enrichment of AP2-I can then be monitored after the PfBDP4 gene is ablated. In addition to the invasion genes, the promoter regions of the histones H2A, H4, as well as the

apicomplexan-specific histone variant H2B.Z, were enriched with all three *trans* factors. These histones are core components for chromatin assembly.

While AP2-I is most transcribed in trophozoites (Lopez-Barragan et al., 2011), (Lopez-Barragan et al., 2011), the transcription of PfBDP4 peaks in rings, indicating that PfBDP4 likely has additional functions to the regulation of invasion. Indeed, 344 of the genes with PfBDP4 enriched upstream of their CDS had no overlap with PfBDP1 or AP2-I (figure 5.14). Many of the GO terms identified for these genes were related to the metabolism of proteins. This study showed that PfBDP4 was enriched upstream of five beta-type subunits and one alpha-type subunit of the 20S core complex out of the seven alpha and beta-type subunits of the 20S catalytic core complex of the proteasome in *P. falciparum*(Aminake et al., 2012). In addition, three putative E2 ubiquitin-conjugating proteins were also enriched with PfBDP4 in their promoters. In general, protein degradation involves ubiquitination that tags the proteins which are destined for degradation by the proteasome or recycling. The proteasome is a major complex that controls the degradation of proteins to maintain proteostasis in the cell (Aminake et al., 2012; Ponts et al., 2008). Inhibitors targeting the proteasome have been proposed as candidates for anti-cancer as well as antimalarial therapy (Czesny et al., 2009; Gantt et al., 1998; Kreidenweiss et al., 2008; Prasad et al., 2013). Therefore, this suggests that PfBDP4 regulates genes that are involved in proteolysis and protein metabolism. Future experiments can investigate whether PfBDP4 regulates metabolic pathways by analysing the metabolomic profile of the conditional knockout parasite line discussed in Chapter 4 and compare it to the profile of wildtype parasites.

Overall, this part of the project provided a novel understanding of PfBDP4 functions in the regulation of invasion genes and other pathways. This data will help to design phenotype assays using the PfBDP4 conditional knockout parasite line that will probe the role of PfBDP4 in the biological pathways implicated by the ChIP-seq analysis.

5.3.2. PfBDP3

In contrast to PfBDP4, PfBDP3 was enriched across gene bodies and was mainly found in heterochromatin. Notably, PfBDP3 was enriched in the CDS of the transcription factor AP2-G, which is responsible for the regulation of sexual differentiation (Kafsack et al., 2014), and the multigene families of *P. falciparum*. Heterochromatin in *P. falciparum* is mainly limited to the sub-telomeric regions and a few intra-chromosome islands (Flueck et al., 2009; Lopez-Rubio et al., 2009). The hallmark of heterochromatin includes enrichment of the HP1 and the histone repressive mark H3K9me3 (Flueck et al., 2009; Fraschka et al., 2018; Jiang et al., 2013;

Lopez-Rubio et al., 2009). Heterochromatin has been well-studied in *P. falciparum* because of its function in epigenetic silencing of the *var* family of virulence genes. The *var* genes encode PfEMP1s that are expressed on the iRBC surface where they mediate antigenic variation and cytoadhesion (Lavstsen et al., 2003; Montgomery et al., 2007; Salanti et al., 2003). Only one *var* gene is active at a given time during the asexual stage (Biggs et al., 1991; Dzikowski et al., 2006; Scherf et al., 1998; Voss et al., 2006) and the ability to switch from one PfEMP1 variant to another one allows the parasite to evade the host's immune system and to establish chronic infection (Dzikowski et al., 2006; Scherf et al., 1998; Voss et al., 2006). It was unexpected to find PfBDP3 enrichment in the heterochromatin environment where acetylation is generally depleted.

PfBDP3 could bind other acetylated trans factors to play a role in maintaining the compaction of heterochromatic DNA, or PfBDP3 could transiently interact with euchromatic islands within heterochromatin to recruit appropriate TFs when the chromatin becomes relaxed. In a quantitative proteomic study, PfBDP3 was pulled down together with a conserved Plasmodium protein (PF3D7_1451200) which interacts with HP1 as well as two acetyltransferase MYST and NuA4 (Hoeijmakers et al., 2019). HP1 or heterochromatin protein 1 is central for the formation of heterochromatin as well as control of clonally variant genes (Brancucci et al., 2014; Flueck et al., 2009). Interestingly, the acetyltransferase MYST has previously been associated with var regulation (Miao et al., 2010). PfBDP3 was also detected in the pulldown of the PfBDP5/TAF1 complex which is orthologous to the TAF1 general transcription factor (Callebaut et al., 2005) as well as displaying some weak interactions with the epigenetic PfBDP1 complex and the PfBDP4 complex (Hoeijmakers et al., 2019). PfBDP5/TAF1, PF3D7_1451200, HP1 and MYST proteins are all acetylated (Cobbold et al., 2016) so PfBDP3 could bind these proteins' acetylations and potentially act as a scaffold to connect proteins in a complex or between complexes. The association with heterochromatin explains why PfBDP3 was dispensable during the *in vitro* asexual life cycle because heterochromatin is the site for contingency gene families that are largely not essential for survival *in vitro* of asexual blood stage parasites.

Replicates of the ChIP-seq experiment need to be performed to confirm the association with heterochromatin and complementary functional studies should be performed to investigate whether deletion of PfBDP3 leads to deregulation of virulence genes and/or gametocyte induction in *P. falciparum*.

Furthermore, PfBDP3 may also have other functions in the parasite cytoplasm as a proportion of PfBDP3, especially a smaller and processed form of PfBDP3, was also detected in the cytoplasm (figure 5.2). In the BDP3ty construct (figure 5.1), the TY epitope tag was integrated into the 3-prime of the PfBDP3 coding sequence. Hence, detection of the TY tag indicates that the C-terminus of PfBDP3 was intact. The calculated molecular weight of the portion of PfBDP3 with intact BRDs and C-terminus is approximately 130 kDa which is smaller than the observed processed form of PfBDP3 at around 210kDa (figure 5.2). Therefore, if the proteolytic activity only happened at the N-terminus, the processed form of PfBDP3 likely retained the BRDs. In the future, the sub-cellular localisation of PfBDP3 can be further investigated using high-resolution microscopy; and immunoprecipitation-mass spectrometry can be used to determine proteins which interact with PfBDP3 in the parasite's nucleus and cytoplasm.

Overall, the preliminary ChIP-seq results showed that PfBDP3 is associated with heterochromatin in trophozoites. This data sets a foundation to further investigate the role of PfBDP3 in regulating epigenetically silenced gene and its other functions in the parasite's cytoplasm during the parasite asexual, blood stage life cycle.

6. Determining parasite growth inhibition when treated by putative BRD inhibitors

6.1. Introduction

In recent years, a growing number of BRD protein inhibitors have been identified and investigated as novel therapies for various types of cancer, inflammation, neurological disorder, and cardiovascular disease (Chung et al., 2012; Ferri et al., 2016; Jung et al., 2015) and some have progressed to preclinical or clinical trials (Alqahtani et al., 2019; Andrieu et al., 2016; Chung et al., 2012; Lewin et al., 2018; Perez-Salvia and Esteller, 2017). Many of these compounds target members of the Bromodomain and Extra-Terminal motif (BET) protein family, such as the bromodomain inhibitor JQ-1 (Filippakopoulos et al., 2010; Wu et al., 2019; Zou et al., 2019). *P. falciparum* harbours unique bromodomain proteins which are present in both the human host's blood and in the mosquito stages of the parasite's life cycle (Bozdech et al., 2003; Gural et al., 2018; Lopez-Barragan et al., 2011; Yeoh et al., 2017). Hence, these proteins are promising candidates for novel antimalarial therapies.

Our collaborators at the SGC performed screens against a large panel of compounds to identify existing and novel compounds that target the BRD of PfBDPs. They did this by performing differential scanning fluorimetry (DSF) to compare PfBDP stability in the presence or absence of tested compound under thermal stress (Tm) (Niesen et al., 2007) and a thermal shift indicates an interaction between the tested compound and the PfBDP. AlphaScreen (Yasgar et al., 2016) was also performed to determine if these compounds can disrupt the interaction between PfBDPs and acetyl-lysines in histone N-terminal tail peptides. This part of the project aims to further investigate the effect of novel hit compounds and their half-maximal growth inhibition concentration (IC_{50}) against *P. falciparum*.

6.2. Results

In order to test the effect of putative *P. falciparum* BRD inhibitors on parasite culture, a 96-well, micro-plate growth inhibition assay was adapted from Wilson et. al. (Wilson et al., 2010). The CS2-GFP parasite line maintains the pHGBrHrBl-1/2 plasmid to express GFP (Wilson et al., 2010) and was a kind gift to us from Dr Danny Wilson. For each compound, CS2-GFP parasites were incubated in a range of concentrations for 72 hours. Then, the cells were stained with ethidium bromide and were analysed by flow cytometry. The GFP and EtBr-positive population was counted and normalised to the count of the total red blood cell population. A minimum of 2 biological replicates was performed for each compound included in this chapter. Information and IC_{50} values for all compounds tested in this chapter are summarised in Table 6.1.

6.2.1. BI-2536 and BI-6727

6.2.1.1. BI-2536 and BI-6727 kills *in vitro P. falciparum* parasite culture

Our collaborators at the SGC solved the structure of PfBDP3.2 which co-crystallised with BI-2536 (PDB ID: 4PY6) (Fonseca et al.) and showed by DSF, AlphaScreen and calorimetry that BI-2536 strongly binds *P. falciparum* PfBDP3.2 (confidential unpublished data). Therefore, we investigated the effect of BI-2536 on *P. falciparum*.

Growth assays showed that BI-2536 is a potent compound, which inhibits *in vitro* asexual *P. falciparum* growth with an IC_{50} of 52.48 nM (95%CI = 48.67 nM to 56.59 nM) (figure 6.1A). This is around 2-fold higher than the AlphaScreen IC_{50} of 25 nM calculated when BI-2536 was tested with the human BRD4 (Ember et al., 2014). To assess BI-2536 cross-reactivity with antimalarials known to elicit resistance, the activity of BI-2536 was tested against the multidrug-resistant parasite line K1 that has known chloroquine and pyrimethamine resistance-associated mutations (Ding et al., 2012; Kayser et al., 2001; Ponnudurai et al., 1981). A similar IC_{50} of 57.08 nM (95%CI = 45.99 nM to 70.85 nM) was observed when BI-2536 was tested against K1 parasite line (figure 6.1A) suggesting that BI-2536 is not targeting the proteins conferring chloroquine and pyrimethamine resistance on K1.

BI-6727 is a derivative from BI-2536 and has similar targets in humans including Plk1 and BRD4 (Rudolph et al., 2009). Our collaborators at the SGC showed that BI-6727, like BI-2536, interacts with the recombinant bromodomain of PfBDP3.2 by DSF and AlphaScreen. BI-6727

inhibited in vitro *P. falciparum* growth with an IC50 of 107.7 nM (95%CI = 92.96 nM to 124.7 nM) (figure 6.1.B), which is approximately 3.4-fold higher than the BI-2536 IC50.

A

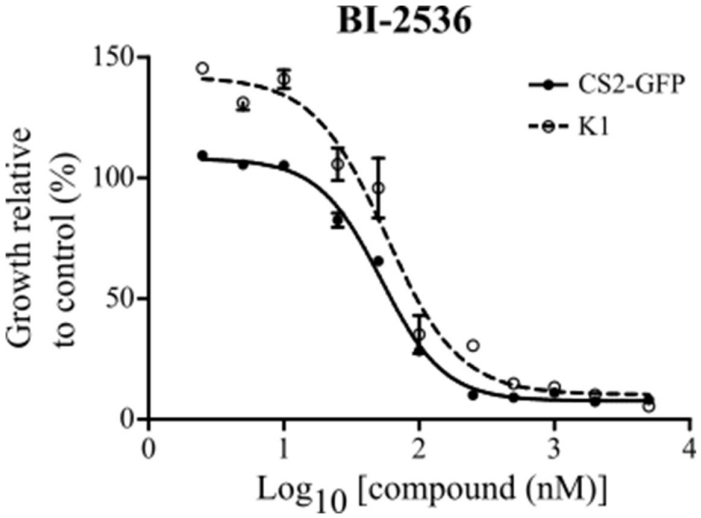

B

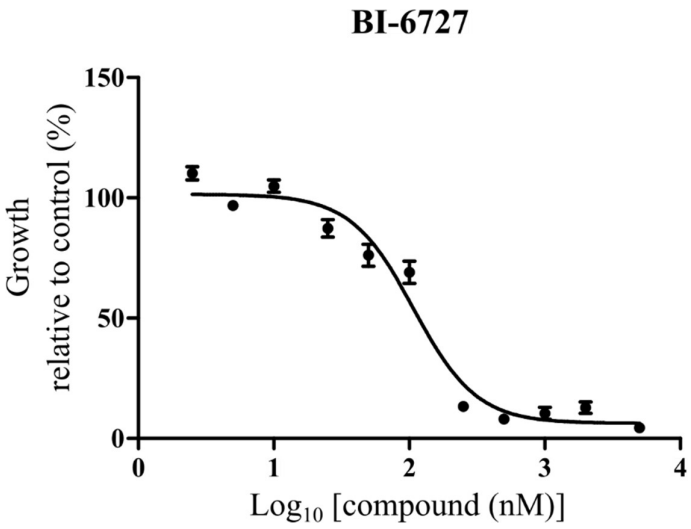

Figure 6.1. Parasite growth curves of CS2-GFP parasites (continuous line) and multi-resistant K1 parasites (dotted line) grown in the presence of (A) BI-2536 and (B) BI-6727. Parasite lines were incubated with a range of compound concentrations (x-axis) for 72 hours and parasite growth was measure by flow cytometry and normalised to vehicle control (y-axis). The mean and standard error of the mean (SEM) was used to plot the growth curve. The data were fitted to a four-parameter dose-response curve to determine IC_{50} values.

6.2.1.2. BI-2536 is a fast-acting compound that affects parasite development during the asexual life cycle

Previously, our lab observed that parasites could not progress in their life cycle regardless of when BI-2536 was added (unpublished data). In order to investigate the time of action of BI-2536 during the parasite asexual life cycle in more detail, we added 484 nM (>IC_{90}) of BI-2536 to tightly synchronised parasites. Two time points were selected for the start of drug treatment: ring (8-10 hpi) and schizont stage (38-40 hpi). After 6 hours of incubation, the drug was removed and the cells were washed before returning to culture for another 24 hours. Then, samples were collected for flow cytometry analyses at 40 hpi and 16 hpi (+1 cycle), respectively. Infected cells were counted and normalised to total red blood cells for both controls and treated conditions. Three technical replicates were performed for each time point, and an unpaired t-test with Welch's correction was used to compare between control and treated conditions.

After exposure to BI-2536, significantly fewer ring-treated parasites could develop into schizonts (figure 6.2). The cultures were also monitored for 24 hours after the harvest time point by Giemsa staining and eventually died. Similarly, while some treated schizonts successfully reinvaded to continue the next cycle, there was a statistically significant decrease in the number of infected cells detected after 24 hours (16 hpi +1 cycle) (figure 6.2). These data suggest that BI-2536 is a fast-acting compound, with the short exposure to BI-2536 during the ring stage being sufficient to disrupt the parasite cycle. The treatment also influences parasite growth but to lesser effect when used at a later stage.

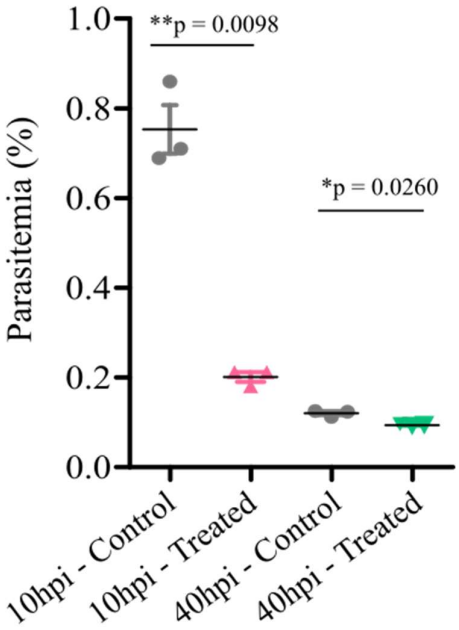

Figure 6.2. BI-2536 inhibits parasite growth after a short 6-hour incubation. BI-2536 significantly disrupted ring-treated (pink) parasites from developing into schizonts. The growth of schizonts treated in the next cycle (green) was also significantly affected but to a lesser effect. For each condition, technical replicate readings are displayed as dot points with the condition mean (black line) and error bars (SEM). P-values were calculated using the unpaired t-test with Welch's correction.

6.2.2. L-45 and its analogs

L-45 was derived from the scaffold of the pan-BRD inhibitor [1,2,4]triazolo[4,3-*a*]phthalazines (Fedorov et al., 2014; Moustakim et al., 2017). The compound has key interactions with conserved residues of human PCAF and PfGCN5 and was co-crystallised with PfGCN5 (PDB 5TPX) by our collaborators at the SGC (Moustakim et al., 2017). L-45 inhibited parasite growth *in vitro* with an IC_{50} of 713.5 nM (95%CI = 612.9 nM to 830.5 nM) (figure 6.3, table 6.1).

In addition, we also received compounds that are derived from or related to L-45 (MM-compound series, figure 6.4). The IC_{50} values of these compounds were determined using our growth inhibition assay and summarised in table 6.1. Seven compounds from the series of L-

45 analogues (MM4353, 4357, 4397, 4441, 4442, 444 and 4445) displayed slightly improved activity (less than 800 nM) in comparison to L-45, while the IC_{50} from the remaining L-45 analogues were either similar to or higher than L-45 (figure 6.4, table 6.1).

6.2.3. Inhibitory activity of other hit compounds

Eight commercially available hit compounds that had a thermal shift (delta Tm) of at least 2°C by DSF and reactivity by AlphaScreen (table 6.1) were selected for further investigation in our growth assay.

All eight lead compounds exhibited poor inhibitory efficacy against *in vitro* parasite culture. The IC_{50} values were only determined for four compounds (7951010, 59941420, PP242 and NI-57) although the curves for PP242 and NI-57 did not plateau at high concentration (figure 6.5, table 6.1).

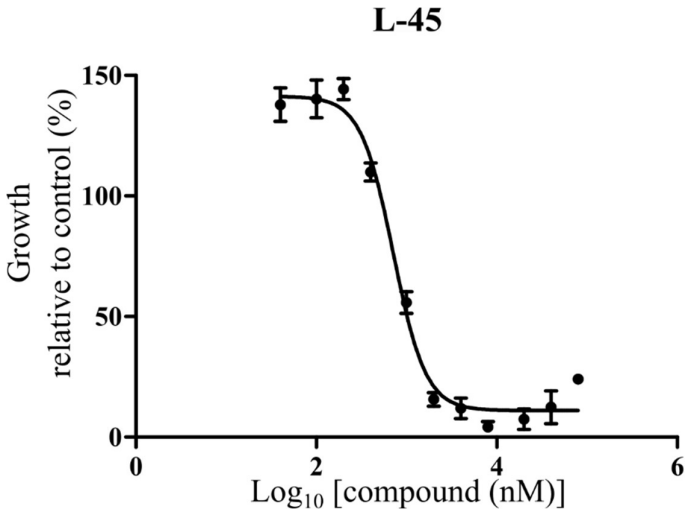

Figure 6.3 Parasite growth curves in the presence of L-45/L-Moses. Parasite lines were incubated with a range of compound concentrations of L-45/L-Moses (x-axis) for 72 hours and parasite growth was measure by flow cytometry and normalised to vehicle control (y-axis). The mean and standard error of the mean (SEM) was used to plot the growth curve. The data was fitted to a four-parameter dose-response curve to determine the IC_{50} value for L-45/L-Moses.

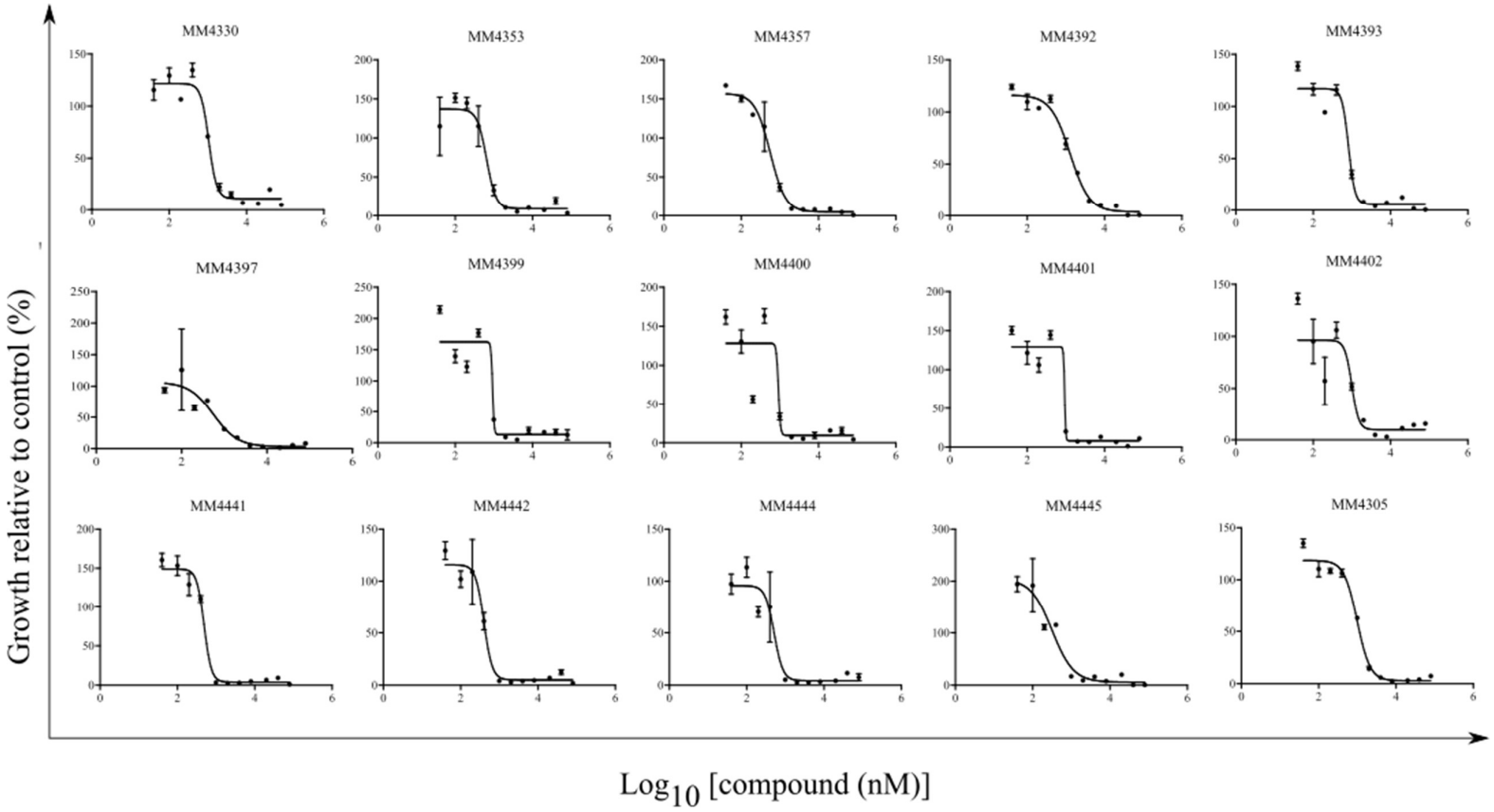

Figure 6.4. Parasite growth curves for a panel of chemical analogs of L-45. The range of compound concentrations used are shown on the x-axes and normalised parasite growth is shown on the y-axes. The IC_{50} of each compound was determined using a four-parameter dose-response curve model and was summarised in table 6.1.

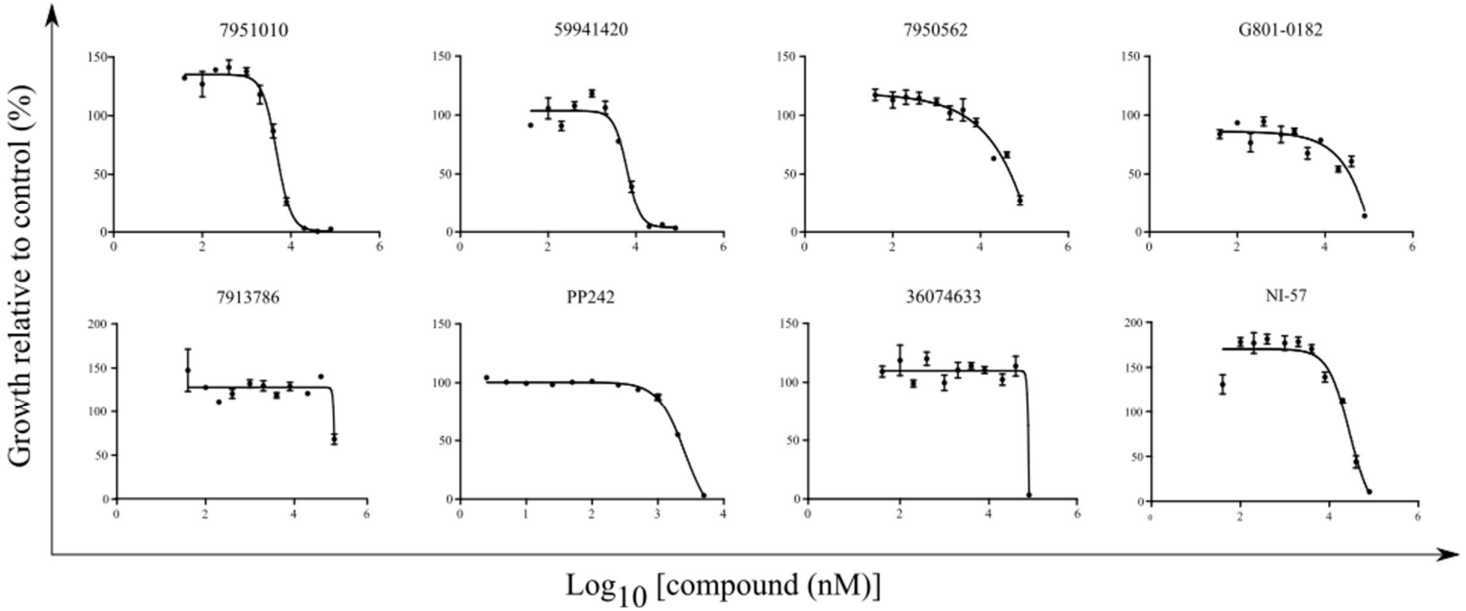

Figure 6.5. A panel of parasite growth curves for hit compounds previously identified in biochemical assays. Putative PfBDP inhibitors were identified by our collaborators at the SGC by DSF and ALPHAscreen. The range of compound concentrations used are shown on the x-axes and normalised parasite growth is shown on the y-axes. The IC_{50} of each compound was determined using a four-parameter dose-response curve model and was summarised in table 6.1.

Table 6.1. Summary of compounds screened against *in vitro* parasite culture

Name	Structure	IC_{50} (nM) – [95% CI]	Putative target in *P. falciparum* (determined by assay)	Target in human
BI-2536	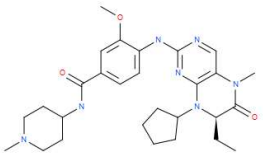	52.48 [48.67 – 56.59]	PfBDP3.2 (DSF, AlphaScreen and crystal structure PDB ID: 4PY6 (Fonseca et al.))	HsPlk-1 (Lénárt et al., 2007; Steegmaier et al., 2007) HsBRDs (Chen et al., 2015; Ember et al., 2014)
BI-6727	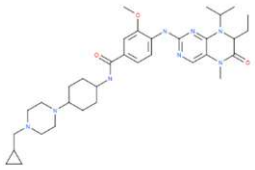	107.7 [92.96 – 124.7]	PfBDP3.2 (DSF and AlphaScreen)	HsPlk-1 (Rudolph et al., 2009) HsBRDs (Ciceri et al., 2014)
L-45	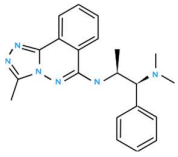	713.5 [612.9 – 830.5]	PfGCN5 (DSF and crystal structure PDB ID: 5TPX (Moustakim et al., 2017))	HsPCAF (Moustakim et al., 2017)
7951010	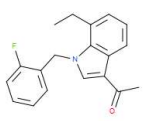	4813 [4292 – 5398]	PfBDP1 (DSF)	

59941420	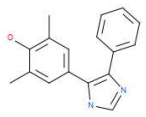	6267 [5357 – 7333]	PfGCN5 (DSF)	
7950562	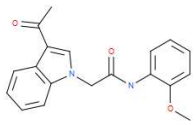	Undetermined	PfBDP1 (DSF)	
G801-0182	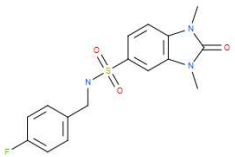	Undetermined	PfGCN5 (DSF) and PfBDP4 (AlphaScreen)	
7913786	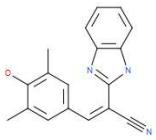	Undetermined	PfBDP3.2 (DSF)	
PP242	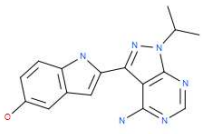	2585 [2143 – 3118]	PfBDP4 (DSF and AlphaScreen)	Human mTORC kinase (Gordeev et al., 2015; Xing et al., 2014) HsBRDs (Ciceri et al., 2014)
36074633	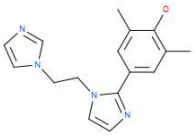	Undetermined	PfGCN5 (DSF)	
NI-57	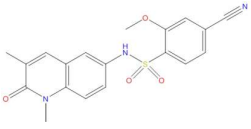	28384 [17586 – 45811]	PfBDP4 (DSF)	HsBRPF (Igoe et al., 2017)
MM4330	N/A	1058 [945.4 – 1183]		

MM4353		650.4 [451.7 – 936.5]	PfGCN5 (confidential unpublished data)	
MM4357		567.1 [420.7 – 764.5]		
MM4392		1288 [1102 – 1507]		
MM4393		819.5 [642.4 – 1045]		
MM4397		553.2 [195.9 – 1562]		
MM4399		926.6 [Very wide]		
MM4400		920.4 [Very wide]		
MM4401		930.6 [Very wide]		
MM4402		999.2 [798.1 – 1251]		
MM4441		490.6 [415.1 – 579.7]		
MM4442		400.0 [328.1 – 478.6]		
MM4444		512.7 [338.1 – 777.5]		
MM4445		316.7 [193.7 – 517.7]		
MM4305		983.3 [865.7 – 1117]		

6.3. Discussion

In this chapter, growth inhibition assays were performed for hit compounds identified using biochemical assays and medicinal chemistry (Moustakim et al., 2017) by our collaborators at the SGC. BI-2536 and its derivative BI-6727 had the highest *in vitro* activity against blood stage parasites of all the hit compounds. BI-2536 was first discovered as a highly potent inhibitor against human Polo-like kinase 1 (Plk1) with an IC50 of 0.83 nM against HeLa cells (Lénárt et al., 2007; Steegmaier et al., 2007) and has been used in clinical trials for cancer treatments for its activity against Plk1 (Gandhi et al., 2009; Mross et al., 2012; Mross et al., 2008; Schöffski et al., 2010; Sebastian et al., 2010). It also inhibits the function of human BRDs including BRD 2, 3 and 4 (Chen et al., 2015; Ember et al., 2014). However, Plk1 was not reported in the red blood cell proteome (Pasini et al., 2006) and *P. falciparum* lacks a Plk1 orthologue leading us to believe that the target of BI-2536 in *P. falciparum* may be a bromodomain protein. The killing effect of BI-2536 in asexual blood stage parasites was rapid, especially against young parasites, and showed no observable cross-resistance with previously known chloroquine and pyrimethamine resistance-associated mutations (Ding et al., 2012; Kayser et al., 2001; Ponnudurai et al., 1981).

However, it is likely that BI-2536 is not killing the parasite by targeting its putative target PfBDP3.2. A recent forward genetic screen used the piggyBac transposon system to determine the essentiality of all genes in *P. falciparum* (Zhang et al., 2018). In this screen recovery of parasite clones, which have inserted DNA segments called transposons into the CDS of genes - thus leading to stop codons and frameshifts - indicates that these genes are mutable and may thus not be essential for parasite survival (Zhang et al., 2018). In this study, three transposon sites were identified in the CDS of PfBDP3 and one site was found 5' upstream of the BRD of PfBDP3. The insertion of the transposon changed the sequence of PfBDP3 from the site, which suggests that the BRDs of PfBDP3 is dispensable during the asexual blood stage (Zhang et al., 2018) (chapter 1.4, figure 1.5 –(Nguyen et al., 2020)). Consistent with this data, others in our lab successfully knocked out the BRD of PfBDP3 in our lab and observed no changes in parasite growth (unpublished data). In addition, as discussed in chapter 5, preliminary ChIP-seq data for PfBDP3 during trophozoite stage showed that PfBDP3 was enriched in heterochromatin and genes found in these regions are typically not critical for the survival of *in vitro* parasites. Consequently, while BI-2536 may have an affinity for the BRD binding pocket of PfBDP3, the severe growth inhibition observed when cultures were treated with BI-2536 was most likely not due to inhibition of PfBDP3. Furthermore, our laboratory has

recovered BI-2536 resistant parasites, confirming that BI-2536 has a parasite-specific target and preliminary single nucleotide polymorphism (SNP) analysis showed that there was no mutation in the CDS of any PfBDPs (Yeoh et al., unpublished). In humans, BI-2536 can target both Plk1 and BRD4 although its potency against Plk1 exceeds its potency against BRD4 by more than 25 times (Ember et al., 2014; Lénárt et al., 2007; Steegmaier et al., 2007). It is possible that BI-2536 also has a kinase target in *P. falciparum* and inhibition of this kinase is lethal for the parasite. Further SNP analysis of the BI-2536 resistant parasites may reveal targets and pathways of BI-2536 during the asexual life cycle.

While BI-2536 has potent antimalarial activity against *in vitro* culture, the use of BI-2536 might be limited to in vitro application due to its potential adverse effects on the human targets. Plk1 is a mitotic kinase that is present in proliferating cells. BI-2536 killed cardiac proliferating cells in a rat model at an IC_{50} comparable to the IC_{50} reported for P. falciparum (Table 6.1) (Lu et al., 2010). At 100 nM, it also causes aneuploidy in terminally differentiated cells (Lu et al., 2010). Another human target for BI-2536 is BRD4 which has many different important roles including suppressing the transcription of HIV type 1 (HIV-1) in latent reservoir cells. BRD4 induces autophosphorylation of cyclin-dependent kinase 9 (CDK9) and inhibits CDK9 kinase activity to phosphorylate RNAPII (Zhou et al., 2009). Both BRD4 and the phosphorylated form of CDK9 are enriched at the long terminal repeat (LTR) promoter of HIV-1 in latent reservoir cells. Treatment with BI-2536 interferes with BRD4 localisation to the HIV-1 LTR promoter and leads to reactivation of latent HIV-1 (Gohda et al., 2018). It was proposed that BI-2536 could be used in combination with another anti-viral treatment to eliminate HIV reservoirs (Gohda et al., 2018). As a result, careful consideration and further optimisation for BI-2536 is required, especially when the prevalence of HIV and malaria co-infection is high in malaria-epidemic regions (reviewed in (Kwenti, 2018)).

Our collaborators at the SGC screened recombinant *P. falciparum* BRDs of PfBDP1, PfBDP3.2 (unpublished data), PfBDP4 and PfGCN5 against a large panel of BRD inhibitors using DSF and AlphaScreen platforms. Hit compounds tested in this study were shortlisted if they stabilised the recombinant BRDs with a thermal shift (delta Tm) of at least 2°C by DSF and/or interfered with the interaction between the recombinant BRDs and acetylated peptides by AlphaScreen. In this study, we showed that some of these hit compounds can inhibit *P. falciparum* growth with an IC_{50} in the micromolar range. The putative targets for 7951010 and 59941420 are PfBDP1 and PfGCN5, respectively (table 6.1). Both proteins are indispensable during the parasite asexual life cycle (Zhang et al., 2018) and PfBDP1 is essential for the

coordinated regulation of invasion genes (Josling et al., 2015). However, these compounds exhibited poor activity in *in vitro* parasite culture, which may be due to poor interaction with the target within the parasites or unfavourable pharmacokinetic properties.

The putative target for PP242 and NI-57 is PfBDP4, which was identified as an essential protein in Chapter 4. PP242 targets the mammalian target of rapamycin (mTOR) kinase and there is no mTOR homolog in *P. falciparum*. It inhibits proliferation in rodent tumour cells at 1500 nM (Gordeev et al., 2015) as well as in *in vitro* human cell lines of gastric cancer and endothelial cells at IC_{50} between 50 and 500 nM (Xing et al., 2014). PP242 also showed some affinity towards human BRD proteins (Ciceri et al., 2014) although it was not as potent as against its mTOR kinase target. NI-57 is a product of target-based drug discovery and was described as a promiscuous chemical probe for bromodomain and PHD finger (BRPF) proteins with K_d values for recombinant BRPF proteins ranging from 31 to 410 nM (Igoe et al., 2017). While PP242 and NI-57 showed some inhibitory activity, their IC_{50} were too high to be considered as lead compounds for antimalarials (MMV criteria is IC_{50} less than 1 μM criteria) (Katsuno et al., 2015). However, their structures could be valuable as scaffolds if their on-target specificity against PfBDP4 is confirmed.

We showed that L-45 can inhibit *P. falciparum* growth in the sub-micromolar range. In addition, Moustakim et al. showed that L-45 had no observable cytotoxicity on peripheral blood mononuclear cells at 10 μM after 24 hours although an IC_{50} was not reported in this study (Moustakim et al., 2017). Selectivity assay can be designed to determine the cytotoxicity against human cells such as the cytotoxicity assay previously described in drug discovery pipelines for *P. falciparum* BDPs and HDACs (Chua et al., 2018; Engel et al., 2015). For example, L-45 and other hit compounds can be tested to determine IC_{50} values against human cell lines and a ratio of $IC_{50\text{-human}}$ to $IC_{50\text{-}P.\ falciparum}$ is calculated to determine the selectivity index. L-45 will also be a useful chemical probe to study the biological consequences of PfGCN5 inhibition. In addition, we also tested different derivatives of L-45 (MM-series, table 5.1) with PfGCN5 as their presumed target and observed a range of IC_{50}'s against *in vitro* culture. Although none of the compounds from this series showed reliably increased efficacy, a few compounds exhibited slightly improved IC_{50} compared to L-45. Correlation between the IC_{50} of these compounds and their structure will provide key insights into the activity of different functional groups of L-45. It is also worth noting that while doing this may improve the potency of the compounds, it may not improve the specificity of L-45 against PfGCN5. Therefore, future experiments need to include specificity assays against PfGCN5 and other

PfBDPs to validate the targets of these compounds. The example of L-45 demonstrates the potential for designing novel specific inhibitors to BDP targets. In the case of PfGCN5, future compound design can potentially leverage critical amino sequence differences between human PCAF and PfGCN5 (Moustakim et al., 2017).

In order to further explore the use of these compounds, it is of utmost importance to develop *in vitro* parasite assays to determine whether the inhibitory effect is on-target. Unfortunately, up to the current date, there is no known *P. falciparum* on-target chemical probe or inhibitor as a standard for the development of these assays. One possible method is to test novel compounds against parasites expressing altered levels of BDPs such as wildtype, BDP knockdown or BDP overexpressing parasite lines. The expectation is to observe a shift in susceptibility when a drug inhibitory effect is specific to the BDP target. For example, the effect of an on-target drug should be more severe when the target BDP is knocked down and less severe when the target BDP is over-expressed. This technique was successfully applied to *Trypanosoma cruzi* parasites and specificity of JQ-1 and I-BET151 for *T. cruzi* bromodomain factor 3 was confirmed (Alonso et al., 2016). A PfBDP1 overexpressing line has been described previously (Josling et al., 2020) and this strategy can be used to generate other PfBDPs overexpressing lines. Another method to validate specificity is to generate resistant parasites by exposing them to sublethal concentrations of compound over a prolonged period. The genomes of compound-resistant parasites are sequenced to identify polymorphisms that are associated with resistance (Ariey et al., 2014; Xie et al., 2018) although the arise of polymorphisms from unrelated or off-target genes can compensate for the effect of compounds.

Overall, this chapter demonstrated the parasite growth inhibitory effect of putative *P. falciparum* BRD inhibitors and discussed some potential *in vitro* assays to validate compound specificity. The rate of discovery and development of BRD inhibitors has been remarkable in the past decade. PfBDPs are enticing drug targets for novel antimalarials because some do, or may, play important roles in gene regulation and some of them are essential for the parasite. Moving forward, as many of these compounds originally came from studies in humans or have been screened against known human BRD proteins, it is critical to design specificity assays to ensure that lead compounds are targeting *P. falciparum* pathways.

7. Conclusions and future outlooks

The malaria parasite *P. falciparum* relies on the interaction between *trans* factors and the dynamic chromatin landscape, including extensive histone PTMs, to regulate its gene expression. Histone acetylation is particularly abundant in *P. falciparum* with sites of lysine acetylation that are unique to *P. falciparum* (Miao et al., 2006; Trelle et al., 2009). Recently, the study of *P. falciparum* bromodomain proteins, which can interact with histone acetylation, has provided new insights into how histone acetylation and *trans* factors contribute to the regulation of gene transcription. Given the paucity of identified STFs in *P. falciparum*, the combinatorial interaction between PfBDPs and STFs as well as other chromatin-associated proteins (Hoeijmakers et al., 2019) can help explain the tight temporal regulation of gene expression.

Histone acetylation could be an important therapeutic target as highlighted by the expanding discovery of drugs that disturb the balance of acetylation and parasite growth by inhibiting proteins that can write (HAT) and erase (HDAC) acetylation (Andrews et al., 2009; Bougdour et al., 2009; Chen et al., 2008; Coetzee et al., 2020; Kumar et al., 2017; Patil et al., 2010; Strobl et al., 2007). Most of the PfBDPs are unique to Apicomplexa and are expressed in multiple stages across the *P. falciparum* life cycle (Bozdech et al., 2003; Gural et al., 2018; Lopez-Barragan et al., 2011; Yeoh et al., 2017) making them potential drug targets. Currently, several classes of BRD inhibitors against Bromo- and Extra-Terminal domain (BET) proteins are in clinical trials as novel cancer therapies (Alqahtani et al., 2019; Chung et al., 2012; Lewin et al., 2018; Perez-Salvia and Esteller, 2017). Commercially available compound libraries of BRD modulators and inhibitors could be leveraged to develop a drug discovery pipeline for *P. falciparum*. Therefore, this study aimed to understand the biology of PfBDPs and to explore the possibility of identifying inhibitors against PfBDPs.

Previously, we showed that PfBDP1 is essential for parasite survival and regulates the expression of genes that are involved in invasion (Josling et al., 2015). In the *piggyBac* transposon forward-genetic screen, the CDS of PfBDP1 was devoid of insertion confirming its importance for the parasite (Zhang et al., 2018). This study also showed that PfBDP2, PfTAF2 and PfGCN5 were also essential whereas the BRDs of PfBDP3, PfSET1 and PfBDP5/TAF1 were dispensable for the asexual, blood stage parasites as these proteins had one insertion site upstream of their BRDs (Zhang et al., 2018). Incorrect and cytoplasmic localisation of PfBDP5/TAF1 is lethal for the parasite (Hoeijmakers et al., 2019) but this may be a consequence of its inappropriate accumulation in the cytoplasm. The essentiality of the BRD

of PfBDP4 has not yet been assessed as the insertion in the CDS of PfBDP4 was downstream of its BRD (Zhang et al., 2018). In the work presented here, PfBDP4 and PfBDP3 were assessed for their essentiality using reverse genetics. The functions of the two proteins were also inferred by determining their localisation within the genome of *P. falciparum* and identifying pathways associated with the genes that PfBDPs likely regulated.

Previously, PfBDP4 was pulled down together with acetylated H2B.Z and H4 peptides (Hoeijmakers et al., 2019) and it was co-crystallised with a H4K5ac peptide (PDB ID: 5VS7) (Hou et al.) which demonstrates that PfBDP4 can bind acetyl-lysines on histone N-terminal tails. Furthermore, PfBDP4 was also detected in a DNA pulldown with an immobilised, predicted regulatory DNA motif using proteomic approaches (Toenhake et al., 2018). These observations pointed to a function of PfBDP4 in the regulation of gene expression. This study presents the first direct evidence demonstrating that PfBDP4 interacts with the genome of *P. falciparum* and was enriched in the promoters of highly expressed genes in schizonts, especially genes that are involved in erythrocyte egress and invasion processes. Histone acetylations including H3K9ac and H4ac are enriched in intergenic and promoter regions (Bártfai et al., 2010; Gupta et al., 2013; Karmodiya et al., 2015; Salcedo-Amaya et al., 2009) so the enrichment of PfBDP4 in these regions was consistent with its BRD binding histone acetylation. Overall, these data strongly supported the hypothesis that PfBDP4 can bind histone acetylations and is involved in the regulation of gene expression.

Disruption of the BRD of PfBDP4 led to a parasite growth defect. As mentioned above this is not inconsistent with the disruption of PfBDP4 downstream of the BRD by the integration of a transposon (Zhang et al., 2018) because the parasites might still have expressed a truncated version of PfBDP4 with a functional BRD. By directly deleting the BRD of PfBDP4, the study presented in this thesis revealed that the BRD of PfBDP4 is important for the survival of *P. falciparum* and implicates its ability to interact with acetylated histones as an essential function.

ChIP-sequencing and bioinformatic analyses revealed that the 457 genes with upstream PfBDP4 peaks included a significant enrichment of genes involved in parasite invasion. These genes are also regulated by the transcription factor AP2-I and the bromodomain protein PfBDP1 (Josling et al., 2015; Santos et al., 2017). The interaction between these three proteins has been shown in other proteomic studies (Hoeijmakers et al., 2019; Santos et al., 2017) and our study further confirmed that they share similar genomic localisation in the promoters of invasion-associated genes. Together, this shows that the chromatin environment upstream of these invasion-associated genes, which is enriched with the AP2-binding motif and histone

acetylation, allows specific recruitment of AP2-I, PfBDP1 and PfBDP4 to properly coordinate the regulation of these genes. This also shows that the function of PfBDP1 (Josling et al., 2015) and PfBDP4 are not redundant as disruption of either protein was lethal for the parasite.

PfBDP4 probably also regulates biological pathways other than invasion that are independent from AP2-I and PfBDP1 as the majority of the PfBDP4 enrichment sites did not overlap with these other two proteins. These unique sites of PfBDP4 enrichment included sites upstream of genes that are components of the 20S catalytic core complex of the proteasome, E2 ubiquitin-conjugating proteins as well as other metabolic and signalling processes such as lipid metabolism and phosphorylation. The function of PfBDP4 in regulating invasion, proteostasis and other metabolic processes can be validated in the future using the NF54-PfBDP4-*loxP*-*glmS* parasite line generated in our laboratory. RNA-seq will determine transcriptional changes in genes that are dysregulated when PfBDP4 is disrupted and determine whether these genes are directly regulated by PfBDP4 by correlating the transcriptomes with our ChIP-seq data. In addition, metabolomics can be utilised to determine whether knocking out PfBDP4 leads to a change in the parasite's metabolic profile, especially changes in small peptides, lipids or amino acids and metabolites. This comparative metabolomic approach has been successfully used for *P. falciparum* (Counihan et al., 2017) and will help narrow down specific metabolic pathways that are regulated by PfBDP4. Phenotypic assays such as invasion assay, which monitors parasite using time-lapse imaging and microscopy, and gametocytogenesis assay can also be performed to validate pathways that are affected by the deletion of PfBDP4.

PfBDP3 was predicted to be dispensable for the *in vitro* survival of parasites during the asexual life cycle (Zhang et al., 2018) and showed little interaction with acetyl-lysines on histone N-terminal peptides (Hoeijmakers et al., 2019). While PfBDP3 knockdown of the BDP3*glmS* parasite generated in this study needs to be confirmed by qRT-PCR, other members in the lab have successfully deleted the BRD of PfBDP3 using a different approach and observed no growth defect in the parasite, confirming PfBDP3 is a dispensable gene. Interestingly, ChIP-seq results showed that PfBDP3 was enriched in trophozoite heterochromatin, where genes are epigenetically silenced. These genes include variant surface antigen multigene families and the master regulator of gametocytogenesis, AP2-G (Kafsack et al., 2014). In other organisms, there is evidence that bromodomain-containing proteins can contribute to silencing gene expression. An example is the human BRD4, which binds H4K16ac at autophagy gene promoters (Sakamaki et al., 2017). BRD4 then interacts with the human G9a methyltransferase which silences autophagy genes by methylating H3K9 (Casciello et al., 2015; Sakamaki et al., 2017).

Another example is the human TIP5 or BAZ2A protein, which possesses a plant homeodomain (PHD) finger – BRD domain. TIP5 is a component of the nucleolar remodelling complex (NoRC) that mediates the repression of ribosomal DNA transcription by altering a nucleosome position in the rDNA promoters (Strohner et al., 2004; Tallant et al., 2015).

Human BRD proteins can also recognise non-histone acetylation (Huang et al., 2009; Narita et al., 2019; Sanchez and Zhou, 2009). In *P. falciparum*, Cobbold et al. identified non-histone acetylation using mass spectrometry and showed that acetylation of lysines in the transcription factor AP2-I was important for its DNA binding activity (Cobbold et al., 2016). PfBDP3 was co-immunoprecipitated with PF3D7_1451200 and PfBDP5/TAF1 (Hoeijmakers et al., 2019) which both possess lysine residues that can be acetylated (Cobbold et al., 2016). The function of PF3D7_1451200 has not been determined although it has been co-immunoprecipitated with HP1 and gametocyte development 1 (GDV1) (Filarsky et al., 2018; Hoeijmakers et al., 2019). It is possible that PfBDP3 can read non-histone acetylation and was enriched in heterochromatin via the interaction with PF3D7_1451200.

Further functional studies should be performed to determine whether PfBDP3 is involved in heterochromatic silencing of genes that are important for the evasion of the host immune system and for the sexual differentiation that allows transmission of malaria. Another possible function of PfBDP3 is to act as a scaffold to recruit complexes for gene activation when the heterochromatin becomes relaxed. A role for PfBDP3 in gene activation was suggested by the coIP of PfBDP3 with PfBDP5/TAF1, which is a subunit of the TFIID of the pre-initiation complex and is essential for parasite growth (Callebaut et al., 2005; Hoeijmakers et al., 2019).

Another goal of this project was to test putative PfBDP inhibitors using *in vitro* assays to determine their IC_{50} against *P. falciparum*. A previous study utilised *in silico* modelling and virtual docking to identify lead compounds against PfBDPs and tested them using an *in vitro* growth inhibition assay (Chua et al., 2018). Another study used medicinal chemistry to specifically design a compound called L-45 that has a high binding affinity to PfGCN5 and human PCAF (Moustakim et al., 2017). Our collaborators at the SGC used recombinant BRD of PfBDP1, PfBDP3 (second BRD), PfBDP4 and PfGCN5 in biochemical assays such as AlphaScreen and differential scanning fluorimetry (DSF) for drug screening and identified candidate hit compounds as well as their predicted PfBDP target. For this study, I tested all hit compounds that were commercially available from the SGC screens as well as L-45 and its analogues in an *in vitro* growth inhibition assay.

Among these, BI-2536 and its derivative BI-6727 were the most potent compounds. The crystal structure of the PfBDP3.2 was obtained with BI-2536 in its binding pocket (PDB ID: 4PY6)(Fonseca et al.) and the compound was predicted to inhibit PfBDP3.2 in the recombinant PfBDP3.2 drug screens. BI-2536 rapidly inhibited the development of the parasite with an IC_{50} of approximately 53 nM in a 72-hour assay. However, as we now know that disruption of PfBDP3 does not lead to parasite death, we concluded that the growth defect observed in these assays with BI-2536 was not due to inhibition of PfBDP3. In humans, the targets of BI-2536 are the kinase Plk-1 and some members of the Bromo- and Extra-Terminal domain (BET) such as BRD4 (Chen et al., 2015). Although no orthologue of Plk-1 was identified in the parasite, it is possible that BI-2536 was inhibiting a different kinase in the parasite. Furthermore, BI-2536 is only suitable for *in vitro* studies of the parasite as it is also very potent against human targets and has been shown to have adverse effects such as re-activation of HIV-1 transcription in latent reservoirs (Gohda et al., 2018). Finally, this study also demonstrated that the L-45 compound can inhibit parasite growth with an IC_{50} of less than 1 μM and the series of derivative compounds of L-45 further suggests the possibility to improve L-45 potency using medicinal chemistry.

To take these or future hit compounds forward and to expand on this work, it is important to develop *in vitro* parasite specificity assays for target validation. Also, as many of these compounds originate from human studies or have been screened against human targets, it is critical to incorporate selectivity assays into the workflow to ensure that the compounds selectively inhibit *P. falciparum* PfBDPs and do not adversely affect human cells.

In summary, the work presented in this thesis showed that the bromodomain of PfBDP4 is essential and that PfBDP4 is associated with active promoters of genes involved in selected processes that are critical for parasite survival. In contrast, PfBDP3 is non-essential during the parasite asexual life cycle and is enriched in heterochromatin implying it has a role in gene silencing. The assays for testing BRD inhibitors in *P. falciparum* that were developed in this study demonstrated the feasibility of this approach. Furthermore, these assays confirmed the anti-parasitic activity of a chemical series predicted from structural studies. Future work can exploit these assays and knowledge of PfBDP essentiality and function to develop rational approaches to PfBDP inhibitor design in the quest to develop novel antimalarials.

8. Bibliography

Adjalley, S.H., Chabbert, C.D., Klaus, B., Pelechano, V., and Steinmetz, L.M. (2016). Landscape and Dynamics of Transcription Initiation in the Malaria Parasite *Plasmodium falciparum*. Cell reports *14*, 2463-2475.

Agarwal, S., Singh, M.K., Garg, S., Chitnis, C.E., and Singh, S. (2013). Ca2+-mediated exocytosis of subtilisin-like protease 1: a key step in egress of *Plasmodium falciparum* merozoites. Cellular Microbiology *15*, 910-921.

al-Yaman, F., Genton, B., Kramer, K.J., Chang, S.P., Hui, G.S., Baisor, M., and Alpers, M.P. (1996). Assessment of the role of naturally acquired antibody levels to *Plasmodium falciparum* merozoite surface protein-1 in protecting Papua New Guinean children from malaria morbidity. The American journal of tropical medicine and hygiene *54*, 443-448.

Alexander, D.L., Arastu-Kapur, S., Dubremetz, J.-F., and Boothroyd, J.C. (2006). *Plasmodium falciparum* AMA1 Binds a Rhoptry Neck Protein Homologous to TgRON4, a Component of the Moving Junction in *Toxoplasma gondii*. Eukaryotic Cell *5*, 1169.

Alonso, Alonso, V., Ritagliati, C., Cribb, P., Cricco, J., and Serra, E.C. (2016). Overexpression of bromodomain factor 3 in *Trypanosoma cruzi* (TcBDF3) affects differentiation of the parasite and protects it against bromodomain inhibitors. FEBS Journal *283*, 2051-2066.

Alqahtani, A., Choucair, K., Ashraf, M., Hammouda, D.M., Alloghbi, A., Khan, T., Senzer, N., and Nemunaitis, J. (2019). Bromodomain and extra-terminal motif inhibitors: a review of preclinical and clinical advances in cancer therapy. Future science OA *5*, Fso372.

Aly, A.S.I., Vaughan, A.M., and Kappe, S.H.I. (2009). Malaria parasite development in the mosquito and infection of the mammalian host. Annual review of microbiology *63*, 195-221.

Aminake, M.N., Arndt, H.-D., and Pradel, G. (2012). The proteasome of malaria parasites: A multi-stage drug target for chemotherapeutic intervention? International Journal for Parasitology: Drugs and Drug Resistance *2*, 1-10.

Amit-Avraham, I., Pozner, G., Eshar, S., Fastman, Y., Kolevzon, N., Yavin, E., and Dzikowski, R. (2015). Antisense long noncoding RNAs regulate var gene activation in the malaria parasite *Plasmodium falciparum*. Proc Natl Acad Sci U S A *112*, E982-991.

Andersson, U., Erlandsson-Harris, H., Yang, H., and Tracey, K.J. (2002). HMGB1 as a DNA-binding cytokine. Journal of leukocyte biology *72*, 1084-1091.

Andersson, U., Wang, H., Palmblad, K., Aveberger, A.C., Bloom, O., Erlandsson-Harris, H., Janson, A., Kokkola, R., Zhang, M., Yang, H.*, et al.* (2000). High mobility group 1 protein (HMG-1) stimulates proinflammatory cytokine synthesis in human monocytes. J Exp Med *192*, 565-570.

Andrews, K.T., Tran, T.N., Wheatley, N.C., and Fairlie, D.P. (2009). Targeting Histone Deacetylase Inhibitors for Anti-Malarial Therapy. Current Topics in Medicinal Chemistry *9*, 292-308.

Andrews, K.T., Walduck, A., Kelso, M.J., Fairlie, D.P., Saul, A., and Parsons, P.G. (2000). Anti-malarial effect of histone deacetylation inhibitors and mammalian tumour cytodifferentiating agents. Int J Parasitol *30*, 761-768.

Andrieu, G., Belkina, A.C., and Denis, G.V. (2016). Clinical trials for BET inhibitors run ahead of the science. Drug Discov Today Technol *19*, 45-50.

Angeletti, D., Kiwuwa, M.S., Byarugaba, J., Kironde, F., and Wahlgren, M. (2013). Elevated levels of high-mobility group box-1 (HMGB1) in patients with severe or uncomplicated *Plasmodium falciparum* malaria. The American journal of tropical medicine and hygiene *88*, 733-735.

Aravind, L., Iyer, L.M., Wellems, T.E., and Miller, L.H. (2003). Plasmodium Biology: Genomic Gleanings. Cell *115*, 771-785.
Ariey, F., Witkowski, B., Amaratunga, C., Beghain, J., Langlois, A.C., Khim, N., Kim, S., Duru, V., Bouchier, C., Ma, L.*, et al.* (2014). A molecular marker of artemisinin-resistant *Plasmodium falciparum* malaria. Nature *505*, 50-55.
Aurrecoechea, C., Brestelli, J., Brunk, B.P., Dommer, J., Fischer, S., Gajria, B., Gao, X., Gingle, A., Grant, G., Harb, O.S.*, et al.* (2008). PlasmoDB: a functional genomic database for malaria parasites. Nucleic Acids Research *37*, D539-D543.
Ay, F., Bunnik, E.M., Varoquaux, N., Vert, J.P., Noble, W.S., and Le Roch, K.G. (2015). Multiple dimensions of epigenetic gene regulation in the malaria parasite *Plasmodium falciparum*: gene regulation via histone modifications, nucleosome positioning and nuclear architecture in *P. falciparum*. Bioessays *37*, 182-194.
Balaji, S., Babu, M.M., Iyer, L.M., and Aravind, L. (2005). Discovery of the principal specific transcription factors of Apicomplexa and their implication for the evolution of the AP2-integrase DNA binding domains. Nucleic Acids Res *33*, 3994-4006.
Baldwin, M.R., Li, X., Hanada, T., Liu, S.C., and Chishti, A.H. (2015). Merozoite surface protein 1 recognition of host glycophorin A mediates malaria parasite invasion of red blood cells. Blood *125*, 2704-2711.
Bamborough, P., and Chung, C.-w. (2015). Fragments in bromodomain drug discovery. MedChemComm *6*, 1587-1604.
Bancells, C., Llora-Batlle, O., Poran, A., Notzel, C., Rovira-Graells, N., Elemento, O., Kafsack, B.F.C., and Cortes, A. (2019). Revisiting the initial steps of sexual development in the malaria parasite *Plasmodium falciparum*. Nature microbiology *4*, 144-154.
Banerjee, S., Ji, C., Mayfield, J.E., Goel, A., Xiao, J., Dixon, J.E., and Guo, X. (2018). Ancient drug curcumin impedes 26S proteasome activity by direct inhibition of dual-specificity tyrosine-regulated kinase 2. Proc Natl Acad Sci U S A *115*, 8155-8160.
Bártfai, R., Hoeijmakers, W.A.M., Salcedo-Amaya, A.M., Smits, A.H., Janssen-Megens, E., Kaan, A., Treeck, M., Gilberger, T.-W., Françoijs, K.-J., and Stunnenberg, H.G. (2010). H2A.Z Demarcates Intergenic Regions of the *Plasmodium falciparum* Epigenome That Are Dynamically Marked by H3K9ac and H3K4me3. PLOS Pathogens *6*, e1001223.
Bartoloni, A., and Zammarchi, L. (2012). Clinical aspects of uncomplicated and severe malaria. Mediterr J Hematol Infect Dis *4*, e2012026-e2012026.
Baruch, D.I., Pasloske, B.L., Singh, H.B., Bi, X., Ma, X.C., Feldman, M., Taraschi, T.F., and Howard, R.J. (1995). Cloning the *P. falciparum* gene encoding PfEMP1, a malarial variant antigen and adherence receptor on the surface of parasitized human erythrocytes. Cell *82*, 77-87.
Beeson, J.G., and Brown, G.V. (2002). Pathogenesis of *Plasmodium falciparum* malaria: the roles of parasite adhesion and antigenic variation. Cellular and Molecular Life Sciences CMLS *59*, 258-271.
Bennink, S., Kiesow, M.J., and Pradel, G. (2016). The development of malaria parasites in the mosquito midgut. Cell Microbiol *18*, 905-918.
Berger, S.L., Kouzarides, T., Shiekhattar, R., and Shilatifard, A. (2009). An operational definition of epigenetics. Genes Dev *23*, 781-783.
Berhane, A., Russom, M., Bahta, I., Hagos, F., Ghirmai, M., and Uqubay, S. (2017). Rapid diagnostic tests failing to detect *Plasmodium falciparum* infections in Eritrea: an investigation of reported false negative RDT results. Malaria Journal *16*, 105.
Besteiro, S., Dubremetz, J.-F., and Lebrun, M. (2011). The moving junction of apicomplexan parasites: a key structure for invasion. Cellular Microbiology *13*, 797-805.
Bhowmick, K., Tehlan, A., Sunita, Sudhakar, R., Kaur, I., Sijwali, P.S., Krishnamachari, A., and Dhar, S.K. (2020). *Plasmodium falciparum* GCN5 acetyltransferase follows a novel

proteolytic processing pathway that is essential for its function. Journal of Cell Science *133*, jcs236489.
Biggs, B.A., Gooze, L., Wycherley, K., Wollish, W., Southwell, B., Leech, J.H., and Brown, G.V. (1991). Antigenic variation in *Plasmodium falciparum*. Proc Natl Acad Sci U S A *88*, 9171-9174.
Bischoff, E., and Vaquero, C. (2010). In silico and biological survey of transcription-associated proteins implicated in the transcriptional machinery during the erythrocytic development of *Plasmodium falciparum*. BMC Genomics *11*, 34.
Blackman, M.J. (2008). Malarial proteases and host cell egress: an 'emerging' cascade. Cellular Microbiology *10*, 1925-1934.
Blackman, M.J., Heidrich, H.G., Donachie, S., McBride, J.S., and Holder, A.A. (1990). A single fragment of a malaria merozoite surface protein remains on the parasite during red cell invasion and is the target of invasion-inhibiting antibodies. Journal of Experimental Medicine *172*, 379-382.
Blank, A., Furle, K., Jaschke, A., Mikus, G., Lehmann, M., Husing, J., Heiss, K., Giese, T., Carter, D., Bohnlein, E.*, et al.* (2020). Immunization with full-length *Plasmodium falciparum* merozoite surface protein 1 is safe and elicits functional cytophilic antibodies in a randomized first-in-human trial. NPJ Vaccines *5*, 10.
Boi, M., Gaudio, E., Bonetti, P., Kwee, I., Bernasconi, E., Tarantelli, C., Rinaldi, A., Testoni, M., Cascione, L., Ponzoni, M.*, et al.* (2015). The BET Bromodomain Inhibitor OTX015 Affects Pathogenetic Pathways in Preclinical B-cell Tumor Models and Synergizes with Targeted Drugs. Clin Cancer Res *21*, 1628-1638.
Boschet, C., Gissot, M., Briquet, S., Hamid, Z., Claudel-Renard, C., and Vaquero, C. (2004). Characterization of PfMyb1 transcription factor during erythrocytic development of 3D7 and F12 *Plasmodium falciparum* clones. Mol Biochem Parasitol *138*, 159-163.
Bougdour, A., Maubon, D., Baldacci, P., Ortet, P., Bastien, O., Bouillon, A., Barale, J.C., Pelloux, H., Menard, R., and Hakimi, M.A. (2009). Drug inhibition of HDAC3 and epigenetic control of differentiation in Apicomplexa parasites. J Exp Med *206*, 953-966.
Boyle, M.J., Reiling, L., Feng, G., Langer, C., Osier, F.H., Aspeling-Jones, H., Cheng, Y.S., Stubbs, J., Tetteh, K.K.A., Conway, D.J.*, et al.* (2015). Human antibodies fix complement to inhibit *Plasmodium falciparum* invasion of erythrocytes and are associated with protection against malaria. Immunity *42*, 580-590.
Bozdech, Z., Llinas, M., Pulliam, B.L., Wong, E.D., Zhu, J., and DeRisi, J.L. (2003). The transcriptome of the intraerythrocytic developmental cycle of *Plasmodium falciparum*. PLoS Biol *1*, E5.
Brancucci, N.M., Goldowitz, I., Buchholz, K., Werling, K., and Marti, M. (2015). An assay to probe *Plasmodium falciparum* growth, transmission stage formation and early gametocyte development. Nat Protoc *10*, 1131-1142.
Brancucci, N.M.B., Bertschi, N.L., Zhu, L., Niederwieser, I., Chin, W.H., Wampfler, R., Freymond, C., Rottmann, M., Felger, I., Bozdech, Z.*, et al.* (2014). Heterochromatin protein 1 secures survival and transmission of malaria parasites. Cell Host Microbe *16*, 165-176.
Brancucci, N.M.B., Gerdt, J.P., Wang, C., De Niz, M., Philip, N., Adapa, S.R., Zhang, M., Hitz, E., Niederwieser, I., Boltryk, S.D.*, et al.* (2017). Lysophosphatidylcholine Regulates Sexual Stage Differentiation in the Human Malaria Parasite *Plasmodium falciparum*. Cell *171*, 1532-1544.e1515.
Brasil, P., Zalis, M.G., de Pina-Costa, A., Siqueira, A.M., Júnior, C.B., Silva, S., Areas, A.L.L., Pelajo-Machado, M., de Alvarenga, D.A.M., da Silva Santelli, A.C.F.*, et al.* (2017). Outbreak of human malaria caused by *Plasmodium simium* in the Atlantic Forest in Rio de Janeiro: a molecular epidemiological investigation. The Lancet Global Health *5*, e1038-e1046.

Brewster, D.R., Kwiatkowski, D., and White, N.J. (1990). Neurological sequelae of cerebral malaria in children. Lancet (London, England) *336*, 1039-1043.
Briquet, S., Boschet, C., Gissot, M., Tissandie, E., Sevilla, E., Franetich, J.F., Thiery, I., Hamid, Z., Bourgouin, C., and Vaquero, C. (2006). High-mobility-group box nuclear factors of *Plasmodium falciparum*. Eukaryot Cell *5*, 672-682.
Briquet, S., Lawson-Hogban, N., Boisson, B., Soares, M.P., Peronet, R., Smith, L., Menard, R., Huerre, M., Mecheri, S., and Vaquero, C. (2015). Disruption of Parasite hmgb2 Gene Attenuates *Plasmodium berghei* ANKA Pathogenicity. Infect Immun *83*, 2771-2784.
Brolin, K.J., Ribacke, U., Nilsson, S., Ankarklev, J., Moll, K., Wahlgren, M., and Chen, Q. (2009). Simultaneous transcription of duplicated var2csa gene copies in individual *Plasmodium falciparum* parasites. Genome Biol *10*, R117.
Bryant, J.M., Regnault, C., Scheidig-Benatar, C., Baumgarten, S., Guizetti, J., and Scherf, A. (2017). CRISPR/Cas9 Genome Editing Reveals That the Intron Is Not Essential for var2csa Gene Activation or Silencing in *Plasmodium falciparum*. mBio *8*.
Bunnik, E.M., Cook, K.B., Varoquaux, N., Batugedara, G., Prudhomme, J., Cort, A., Shi, L., Andolina, C., Ross, L.S., Brady, D.*, et al.* (2018). Changes in genome organization of parasite-specific gene families during the *Plasmodium* transmission stages. Nature Communications *9*, 1910.
Bunnik, E.M., Polishko, A., Prudhomme, J., Ponts, N., Gill, S.S., Lonardi, S., and Le Roch, K.G. (2014). DNA-encoded nucleosome occupancy is associated with transcription levels in the human malaria parasite *Plasmodium falciparum*. BMC genomics *15*, 347-347.
Burley, S.K., Berman, H.M., Bhikadiya, C., Bi, C., Chen, L., Di Costanzo, L., Christie, C., Dalenberg, K., Duarte, J.M., Dutta, S.*, et al.* (2019). RCSB Protein Data Bank: biological macromolecular structures enabling research and education in fundamental biology, biomedicine, biotechnology and energy. Nucleic Acids Res *47*, D464-d474.
Calderwood, M.S., Gannoun-Zaki, L., Wellems, T.E., and Deitsch, K.W. (2003). *Plasmodium falciparum* var genes are regulated by two regions with separate promoters, one upstream of the coding region and a second within the intron. The Journal of biological chemistry *278*, 34125-34132.
Callebaut, I., Prat, K., Meurice, E., Mornon, J.P., and Tomavo, S. (2005). Prediction of the general transcription factors associated with RNA polymerase II in *Plasmodium falciparum*: conserved features and differences relative to other eukaryotes. BMC Genomics *6*, 100.
Campbell, T.L., De Silva, E.K., Olszewski, K.L., Elemento, O., and Llinás, M. (2010). Identification and Genome-Wide Prediction of DNA Binding Specificities for the ApiAP2 Family of Regulators from the Malaria Parasite. PLOS Pathogens *6*, e1001165.
Canepa, G.E., Molina-Cruz, A., and Barillas-Mury, C. (2016). Molecular Analysis of Pfs47-Mediated *Plasmodium* Evasion of Mosquito Immunity. PloS one *11*, e0168279-e0168279.
Canepa, G.E., Molina-Cruz, A., Yenkoidiok-Douti, L., Calvo, E., Williams, A.E., Burkhardt, M., Peng, F., Narum, D., Boulanger, M.J., Valenzuela, J.G.*, et al.* (2018). Antibody targeting of *a specific region of Pfs47 blocks Plasmodium falciparum* malaria transmission. npj Vaccines *3*, 26.
Casciello, F., Windloch, K., Gannon, F., and Lee, J.S. (2015). Functional Role of G9a Histone Methyltransferase in Cancer. Front Immunol *6*, 487-487.
Chan, J.A., Howell, K.B., Reiling, L., Ataide, R., Mackintosh, C.L., Fowkes, F.J., Petter, M., Chesson, J.M., Langer, C., Warimwe, G.M.*, et al.* (2012). Targets of antibodies against *Plasmodium falciparum*-infected erythrocytes in malaria immunity. The Journal of clinical investigation *122*, 3227-3238.
Chandra, B.R., Olivieri, A., Silvestrini, F., Alano, P., and Sharma, A. (2005). Biochemical characterization of the two nucleosome assembly proteins from *Plasmodium falciparum*. Mol Biochem Parasitol *142*, 237-247.

Chen, B.-S., and Hampsey, M. (2002). Transcription Activation: Unveiling the Essential Nature of TFIID. Current Biology *12*, R620-R622.
Chen, F., Mackey, A.J., Stoeckert, C.J., Jr, and Roos, D.S. (2006). OrthoMCL-DB: querying a comprehensive multi-species collection of ortholog groups. Nucleic Acids Research *34*, D363-D368.
Chen, L., Yap, J.L., Yoshioka, M., Lanning, M.E., Fountain, R.N., Raje, M., Scheenstra, J.A., Strovel, J.W., and Fletcher, S. (2015). BRD4 Structure–Activity Relationships of Dual PLK1 Kinase/BRD4 Bromodomain Inhibitor BI-2536. ACS Medicinal Chemistry Letters *6*, 764-769.
Chen, P.B., Ding, S., Zanghì, G., Soulard, V., DiMaggio, P.A., Fuchter, M.J., Mecheri, S., Mazier, D., Scherf, A., and Malmquist, N.A. (2016). *Plasmodium falciparum* PfSET7: enzymatic characterization and cellular localization of a novel protein methyltransferase in sporozoite, liver and erythrocytic stage parasites. Sci Rep *6*, 21802.
Chen, S., Zhou, Y., Chen, Y., and Gu, J. (2018). fastp: an ultra-fast all-in-one FASTQ preprocessor. Bioinformatics (Oxford, England) *34*, i884-i890.
Chen, Y., Lopez-Sanchez, M., Savoy, D.N., Billadeau, D.D., Dow, G.S., and Kozikowski, A.P. (2008). A series of potent and selective, triazolylphenyl-based histone deacetylases inhibitors with activity against pancreatic cancer cells and *Plasmodium falciparum*. J Med Chem *51*, 3437-3448.
Chesnokov, V., Sun, C., and Itakura, K. (2009). Glucosamine suppresses proliferation of human prostate carcinoma DU145 cells through inhibition of STAT3 signaling. Cancer Cell Int *9*, 25-25.
Chua, M.J., Robaa, D., Skinner-Adams, T.S., Sippl, W., and Andrews, K.T. (2018). Activity of bromodomain protein inhibitors/binders against asexual-stage *Plasmodium falciparum* parasites. Int J Parasitol Drugs Drug Resist *8*, 189-193.
Chung, Chung, C.-w., and Tough, D.F. (2012). Bromodomains: a new target class for small molecule drug discovery. Drug discovery today Therapeutic strategies *9*, e111-e120.
Chung, W.Y., Gardiner, D.L., Anderson, K.A., Hyland, C.A., Kemp, D.J., and Trenholme, K.R. (2007). The CLAG/RhopH1 locus on chromosome 3 of *Plasmodium falciparum*: Two genes or two alleles of the same gene? Molecular and Biochemical Parasitology *151*, 229-232.
Ciceri, P., Müller, S., O'Mahony, A., Fedorov, O., Filippakopoulos, P., Hunt, J.P., Lasater, E.A., Pallares, G., Picaud, S., Wells, C.*, et al.* (2014). Dual kinase-bromodomain inhibitors for rationally designed polypharmacology. Nature Chemical Biology *10*, 305-312.
Clark, P.G.K., Vieira, L.C.C., Tallant, C., Fedorov, O., Singleton, D.C., Rogers, C.M., Monteiro, O.P., Bennett, J.M., Baronio, R., Müller, S.*, et al.* (2015). LP99: Discovery and Synthesis of the First Selective BRD7/9 Bromodomain Inhibitor. Angewandte Chemie International Edition *54*, 6217-6221.
Clarke, A.S., Samal, E., and Pillus, L. (2006). Distinct roles for the essential MYST family HAT Esa1p in transcriptional silencing. Molecular biology of the cell *17*, 1744-1757.
Cobbold, S.A., Santos, J.M., Ochoa, A., Perlman, D.H., and Llinás, M. (2016). Proteome-wide analysis reveals widespread lysine acetylation of major protein complexes in the malaria parasite. Sci Rep *6*, 19722.
Coetzee, N., von Grüning, H., Opperman, D., van der Watt, M., Reader, J., and Birkholtz, L.-M. (2020). Epigenetic inhibitors target multiple stages of *Plasmodium falciparum* parasites. Sci Rep *10*, 2355.
Coleman, B.I., Skillman, K.M., Jiang, R.H.Y., Childs, L.M., Altenhofen, L.M., Ganter, M., Leung, Y., Goldowitz, I., Kafsack, B.F.C., Marti, M.*, et al.* (2014). A *Plasmodium falciparum* histone deacetylase regulates antigenic variation and gametocyte conversion. Cell Host Microbe *16*, 177-186.

Collins, C.R., Das, S., Wong, E.H., Andenmatten, N., Stallmach, R., Hackett, F., Herman, J.-P., Müller, S., Meissner, M., and Blackman, M.J. (2013a). Robust inducible Cre recombinase activity in the human malaria parasite *Plasmodium falciparum* enables efficient gene deletion within a single asexual erythrocytic growth cycle. Molecular Microbiology *88*, 687-701.
Collins, C.R., Hackett, F., Atid, J., Tan, M.S.Y., and Blackman, M.J. (2017). The *Plasmodium falciparum* pseudoprotease SERA5 regulates the kinetics and efficiency of malaria parasite egress from host erythrocytes. PLoS pathogens *13*, e1006453-e1006453.
Collins, C.R., Hackett, F., Strath, M., Penzo, M., Withers-Martinez, C., Baker, D.A., and Blackman, M.J. (2013b). Malaria parasite cGMP-dependent protein kinase regulates blood stage merozoite secretory organelle discharge and egress. PLoS pathogens *9*, e1003344-e1003344.
Comeaux, C.A., Coleman, B.I., Bei, A.K., Whitehurst, N., and Duraisingh, M.T. (2011). Functional analysis of epigenetic regulation of tandem RhopH1/clag genes reveals a role in *Plasmodium falciparum* growth. Molecular Microbiology *80*, 378-390.
Conway, D.J., Cavanagh, D.R., Tanabe, K., Roper, C., Mikes, Z.S., Sakihama, N., Bojang, K.A., Oduola, A.M., Kremsner, P.G., Arnot, D.E*., et al.* (2000). A principal target of human immunity to malaria identified by molecular population genetic and immunological analyses. Nature medicine *6*, 689-692.
Cortés, A., Carret, C., Kaneko, O., Yim Lim, B.Y.S., Ivens, A., and Holder, A.A. (2007). Epigenetic silencing of *Plasmodium falciparum* genes linked to erythrocyte invasion. PLoS pathogens *3*, e107-e107.
Coulson, R.M.R., and Ouzounis, C.A. (2003). The phylogenetic diversity of eukaryotic transcription. Nucleic Acids Research *31*, 653-660.
Counihan, N.A., Chisholm, S.A., Bullen, H.E., Srivastava, A., Sanders, P.R., Jonsdottir, T.K., Weiss, G.E., Ghosh, S., Crabb, B.S., Creek, D.J*., et al.* (2017). *Plasmodium falciparum* parasites deploy RhopH2 into the host erythrocyte to obtain nutrients, grow and replicate. eLife *6*, e23217.
Cowell, A.N., Istvan, E.S., Lukens, A.K., Gomez-Lorenzo, M.G., Vanaerschot, M., Sakata-Kato, T., Flannery, E.L., Magistrado, P., Owen, E., Abraham, M*., et al.* (2017). Mapping the malaria parasite druggable genome by using in vitro evolution and chemogenomics. Science (New York, NY) *359*, 191-199.
Cowman, A.F., and Crabb, B.S. (2006). Invasion of red blood cells by malaria parasites. Cell *124*, 755-766.
Cowman, A.F., Tonkin, C.J., Tham, W.H., and Duraisingh, M.T. (2017). The Molecular Basis of Erythrocyte Invasion by Malaria Parasites. Cell Host & Microbe *22*, 232-245.
Crowley, V.M., Rovira-Graells, N., de Pouplana, L.R., and Cortés, A. (2011). Heterochromatin formation in bistable chromatin domains controls the epigenetic repression of clonally variant *Plasmodium falciparum* genes linked to erythrocyte invasion. Molecular Microbiology *80*, 391-406.
Cui, L., Fan, Q., Cui, L., and Miao, J. (2008). Histone lysine methyltransferases and demethylases in *Plasmodium falciparum*. Int J Parasitol *38*, 1083-1097.
Cui, L., and Miao, J. (2010). Chromatin-mediated epigenetic regulation in the malaria parasite *Plasmodium falciparum*. Eukaryot Cell *9*, 1138-1149.
Cui, L., Miao, J., and Cui, L. (2007a). Cytotoxic Effect of Curcumin on Malaria Parasite *Plasmodium falciparum*: Inhibition of Histone Acetylation and Generation of Reactive Oxygen Species. Antimicrobial agents and chemotherapy *51*, 488-494.
Cui, L., Miao, J., Furuya, T., Li, X., Su, X.Z., and Cui, L. (2007b). PfGCN5-mediated histone H3 acetylation plays a key role in gene expression in *Plasmodium falciparum*. Eukaryot Cell *6*, 1219-1227.

Czesny, B., Goshu, S., Cook, J.L., and Williamson, K.C. (2009). The proteasome inhibitor epoxomicin has potent *Plasmodium falciparum* gametocytocidal activity. Antimicrobial agents and chemotherapy *53*, 4080-4085.
Darkin-Rattray, S.J., Gurnett, A.M., Myers, R.W., Dulski, P.M., Crumley, T.M., Allocco, J.J., Cannova, C., Meinke, P.T., Colletti, S.L., Bednarek, M.A*., et al.* (1996). Apicidin: a novel antiprotozoal agent that inhibits parasite histone deacetylase. Proc Natl Acad Sci U S A *93*, 13143-13147.
Das, S., Hertrich, N., Perrin, A.J., Withers-Martinez, C., Collins, C.R., Jones, M.L., Watermeyer, J.M., Fobes, E.T., Martin, S.R., Saibil, H.R*., et al.* (2015). Processing of *Plasmodium falciparum* Merozoite Surface Protein MSP1 Activates a Spectrin-Binding Function Enabling Parasite Egress from RBCs. Cell Host Microbe *18*, 433-444.
Dastidar, E.G., Dzeyk, K., Krijgsveld, J., Malmquist, N.A., Doerig, C., Scherf, A., and Lopez-Rubio, J.J. (2013). Comprehensive histone phosphorylation analysis and identification of Pf14-3-3 protein as a histone H3 phosphorylation reader in malaria parasites. PLoS One *8*, e53179.
de Mendoza, A., Sebé-Pedrós, A., Šestak, M.S., Matejčić, M., Torruella, G., Domazet-Lošo, T., and Ruiz-Trillo, I. (2013). Transcription factor evolution in eukaryotes and the assembly of the regulatory toolkit in multicellular lineages. Proceedings of the National Academy of Sciences of the United States of America *110*, E4858-E4866.
De Silva, E.K., Gehrke, A.R., Olszewski, K., León, I., Chahal, J.S., Bulyk, M.L., and Llinás, M. (2008). Specific DNA-binding by Apicomplexan AP2 transcription factors. Proceedings of the National Academy of Sciences of the United States of America *105*, 8393-8398.
Deitsch, K., Driskill, C., and Wellems, T. (2001a). Transformation of malaria parasites by the spontaneous uptake and expression of DNA from human erythrocytes. Nucleic acids research *29*, 850-853.
Deitsch, K.W., Calderwood, M.S., and Wellems, T.E. (2001b). Malaria. Cooperative silencing elements in var genes. Nature *412*, 875-876.
Denis, G.V. (2001). Bromodomain motifs and "scaffolding"? Front Biosci *6*, D1065-1068.
DeSimone, T.M., Bei, A.K., Jennings, C.V., and Duraisingh, M.T. (2009). Genetic analysis of the cytoplasmic domain of the PfRh2b merozoite invasion protein of *Plasmodium falciparum*. International journal for parasitology *39*, 399-405.
Dhalluin, C., Carlson, J.E., Zeng, L., He, C., Aggarwal, A.K., and Zhou, M.M. (1999). Structure and ligand of a histone acetyltransferase bromodomain. Nature *399*, 491-496.
Ding, X.C., Ubben, D., and Wells, T.N.C. (2012). A framework for assessing the risk of resistance for anti-malarials in development. Malaria Journal *11*, 292.
Dobin, A., Davis, C.A., Schlesinger, F., Drenkow, J., Zaleski, C., Jha, S., Batut, P., Chaisson, M., and Gingeras, T.R. (2012). STAR: ultrafast universal RNA-seq aligner. Bioinformatics (Oxford, England) *29*, 15-21.
Duffy, M.F., Selvarajah, S.A., Josling, G.A., and Petter, M. (2012). The role of chromatin in *Plasmodium* gene expression. Cell Microbiol *14*, 819-828.
Duffy, M.F., Selvarajah, S.A., Josling, G.A., and Petter, M. (2014). Epigenetic regulation of the *Plasmodium falciparum* genome. Brief Funct Genomics *13*, 203-216.
Duffy, M.F., Tang, J., Sumardy, F., Nguyen, H.H.T., Selvarajah, S.A., Josling, G.A., Day, K.P., Petter, M., and Brown, G.V. (2017). Activation and clustering of a *Plasmodium falciparum* var gene are affected by subtelomeric sequences. The FEBS Journal *284*, 237-257.
Duraisingh, M.T., Maier, A.G., Triglia, T., and Cowman, A.F. (2003). Erythrocyte-binding antigen 175 mediates invasion in *Plasmodium falciparum* utilizing sialic acid-dependent and -independent pathways. Proc Natl Acad Sci U S A *100*, 4796-4801.

Duraisingh, M.T., Voss, T.S., Marty, A.J., Duffy, M.F., Good, R.T., Thompson, J.K., Freitas-Junior, L.H., Scherf, A., Crabb, B.S., and Cowman, A.F. (2005). Heterochromatin silencing and locus repositioning linked to regulation of virulence genes in *Plasmodium falciparum*. Cell *121*, 13-24.
Dutra, L.A., Heidenreich, D., Silva, G.D.B.d., Man Chin, C., Knapp, S., and Santos, J.L.D. (2017). Dietary Compound Resveratrol Is a Pan-BET Bromodomain Inhibitor. Nutrients *9*, 1172.
Dzikowski, R., Frank, M., and Deitsch, K. (2006). Mutually Exclusive Expression of Virulence Genes by Malaria Parasites Is Regulated Independently of Antigen Production. PLOS Pathogens *2*, e22.
Dzikowski, R., Li, F., Amulic, B., Eisberg, A., Frank, M., Patel, S., Wellems, T.E., and Deitsch, K.W. (2007). Mechanisms underlying mutually exclusive expression of virulence genes by malaria parasites. EMBO Rep *8*, 959-965.
Eddy, S.R. (1998). Profile hidden Markov models. Bioinformatics (Oxford, England) *14*, 755-763.
Egan, A.F., Morris, J., Barnish, G., Allen, S., Greenwood, B.M., Kaslow, D.C., Holder, A.A., and Riley, E.M. (1996). Clinical immunity to *Plasmodium falciparum* malaria is associated with serum antibodies to the 19-kDa C-terminal fragment of the merozoite surface antigen, PfMSP-1. The Journal of infectious diseases *173*, 765-769.
Elsworth, B., Matthews, K., Nie, C.Q., Kalanon, M., Charnaud, S.C., Sanders, P.R., Chisholm, S.A., Counihan, N.A., Shaw, P.J., Pino, P.*, et al.* (2014). PTEX is an essential nexus for protein export in malaria parasites. Nature *511*, 587-591.
Ember, S.W.J., Zhu, J.-Y., Olesen, S.H., Martin, M.P., Becker, A., Berndt, N., Georg, G.I., and Schönbrunn, E. (2014). Acetyl-lysine binding site of bromodomain-containing protein 4 (BRD4) interacts with diverse kinase inhibitors. ACS chemical biology *9*, 1160-1171.
Engel, J.A., Jones, A.J., Avery, V.M., Sumanadasa, S.D.M., Ng, S.S., Fairlie, D.P., Skinner-Adams, T., and Andrews, K.T. (2015). Profiling the anti-protozoal activity of anti-cancer HDAC inhibitors against *Plasmodium* and *Trypanosoma* parasites. International journal for parasitology Drugs and drug resistance *5*, 117-126.
Essien, K., Hannenhalli, S., and Stoeckert, C.J., Jr. (2008). Computational analysis of constraints on noncoding regions, coding regions and gene expression in relation to *Plasmodium* phenotypic diversity. PloS one *3*, e3122-e3122.
Faast, R., Thonglairoam, V., Schulz, T.C., Beall, J., Wells, J.R.E., Taylor, H., Matthaei, K., Rathjen, P.D., Tremethick, D.J., and Lyons, I. (2001). Histone variant H2A.Z is required for early mammalian development. Current Biology *11*, 1183-1187.
Fan, Q., An, L., and Cui, L. (2004). *Plasmodium falciparum* histone acetyltransferase, a yeast GCN5 homologue involved in chromatin remodeling. Eukaryot Cell *3*, 264-276.
Fan, Q., Miao, J., Cui, L., and Cui, L. (2009). Characterization of PRMT1 from *Plasmodium falciparum*. Biochem J *421*, 107-118.
Farina, A., Hattori, M., Qin, J., Nakatani, Y., Minato, N., and Ozato, K. (2004). Bromodomain protein Brd4 binds to GTPase-activating SPA-1, modulating its activity and subcellular localization. Mol Cell Biol *24*, 9059-9069.
Farrow, R.E., Green, J., Katsimitsoulia, Z., Taylor, W.R., Holder, A.A., and Molloy, J.E. (2011). The mechanism of erythrocyte invasion by the malarial parasite, *Plasmodium falciparum*. Seminars in cell & developmental biology *22*, 953-960.
Fedorov, O., Lingard, H., Wells, C., Monteiro, O.P., Picaud, S., Keates, T., Yapp, C., Philpott, M., Martin, S.J., Felletar, I.*, et al.* (2014). [1,2,4]triazolo[4,3-a]phthalazines: inhibitors of diverse bromodomains. J Med Chem *57*, 462-476.
Ferri, E., Petosa, C., and McKenna, C.E. (2016). Bromodomains: Structure, function and pharmacology of inhibition. Biochem Pharmacol *106*, 1-18.

Fidock, D.A., and Wellems, T.E. (1997). Transformation with human dihydrofolate reductase renders malaria parasites insensitive to WR99210 but does not affect the intrinsic activity of proguanil. Proceedings of the National Academy of Sciences of the United States of America *94*, 10931-10936.
Filarsky, M., Fraschka, S.A., Niederwieser, I., Brancucci, N.M.B., Carrington, E., Carrió, E., Moes, S., Jenoe, P., Bártfai, R., and Voss, T.S. (2018). GDV1 induces sexual commitment of malaria parasites by antagonizing HP1-dependent gene silencing. Science *359*, 1259.
Filippakopoulos, P., Picaud, S., Mangos, M., Keates, T., Lambert, J.P., Barsyte-Lovejoy, D., Felletar, I., Volkmer, R., Muller, S., Pawson, T.*, et al.* (2012). Histone recognition and large-scale structural analysis of the human bromodomain family. Cell *149*, 214-231.
Filippakopoulos, P., Qi, J., Picaud, S., Shen, Y., Smith, W.B., Fedorov, O., Morse, E.M., Keates, T., Hickman, T.T., Felletar, I.*, et al.* (2010). Selective inhibition of BET bromodomains. Nature *468*, 1067-1073.
Flaus, A., Rencurel, C., Ferreira, H., Wiechens, N., and Owen-Hughes, T. (2004). Sin mutations alter inherent nucleosome mobility. EMBO J *23*, 343-353.
Flueck, C., Bartfai, R., Niederwieser, I., Witmer, K., Alako, B.T.F., Moes, S., Bozdech, Z., Jenoe, P., Stunnenberg, H.G., and Voss, T.S. (2010). A major role for the *Plasmodium falciparum* ApiAP2 protein PfSIP2 in chromosome end biology. PLoS pathogens *6*, e1000784-e1000784.
Flueck, C., Bartfai, R., Volz, J., Niederwieser, I., Salcedo-Amaya, A.M., Alako, B.T.F., Ehlgen, F., Ralph, S.A., Cowman, A.F., Bozdech, Z.*, et al.* (2009). *Plasmodium falciparum* heterochromatin protein 1 marks genomic loci linked to phenotypic variation of exported virulence factors. PLoS pathogens *5*, e1000569-e1000569.
Fonseca, M., Tallant, C., Hutchinson, A., Savitsky, P., Krojer, T., Filippakopoulos, P., Loppnau, P., Brennan, P.E., von Delft, F., Dong, A.*, et al.* Crystal Structure of bromodomain of PFA0510w from *Plasmodium falciparum*.
Fonseca, M., Tallant, C., Knapp, S., Loppnau, P., von Delft, F., Wernimont, A.K., Arrowsmith, C.H., Edwards, A.M., Bountra, C., Hui, R.*, et al.* Crystal structure of bromodomain from *Plasmodium faciparum* GCN5, PF3D7_0823300.
Fox, B.A., Li, W.-B., Tanaka, M., Inselburg, J., and Bzik, D.J. (1993). Molecular characterization of the largest subunit of *Plasmodium falciparum* RNA polymerase I. Molecular and Biochemical Parasitology *61*, 37-48.
Fraschka, S.A., Filarsky, M., Hoo, R., Niederwieser, I., Yam, X.Y., Brancucci, N.M.B., Mohring, F., Mushunje, A.T., Huang, X., Christensen, P.R.*, et al.* (2018). Comparative Heterochromatin Profiling Reveals Conserved and Unique Epigenome Signatures Linked to Adaptation and Development of Malaria Parasites. Cell Host Microbe *23*, 407-420.e408.
Fraschka, S.A., Henderson, R.W., and Bartfai, R. (2016). H3.3 demarcates GC-rich coding and subtelomeric regions and serves as potential memory mark for virulence gene expression in *Plasmodium falciparum*. Sci Rep *6*, 31965.
Freitas-Junior, L.H., Hernandez-Rivas, R., Ralph, S.A., Montiel-Condado, D., Ruvalcaba-Salazar, O.K., Rojas-Meza, A.P., Mancio-Silva, L., Leal-Silvestre, R.J., Gontijo, A.M., Shorte, S.*, et al.* (2005). Telomeric heterochromatin propagation and histone acetylation control mutually exclusive expression of antigenic variation genes in malaria parasites. Cell *121*, 25-36.
French, J.B., Cen, Y., and Sauve, A.A. (2008). *Plasmodium falciparum* Sir2 is an NAD+-dependent deacetylase and an acetyllysine-dependent and acetyllysine-independent NAD+ glycohydrolase. Biochemistry *47*, 10227-10239.
Fu, J., Hou, J., Liu, L., Chen, L., Wang, M., Shen, Y., Zhang, Z., and Bao, X. (2013). Interplay between BDF1 and BDF2 and their roles in regulating the yeast salt stress response. The FEBS Journal *280*, 1991-2001.

Galdeano, C., and Ciulli, A. (2016). Selectivity on-target of bromodomain chemical probes by structure-guided medicinal chemistry and chemical biology. Future medicinal chemistry *8*, 1655-1680.
Gamo, Gamo, F.-J., Sanz, L., Vidal, J., de Cozar, C., Alvarez, E., Lavandera, J.-L., Vanderwall, D., Green, D.V.S., Kumar, V*., et al.* (2010). Thousands of chemical starting points for antimalarial lead identification. Nature *465*, 305-310.
Gandhi, L., Chu, Q.S., Stephenson, J., Johnson, B.E., Govindan, R., Bonomi, P., Eaton, K., Fritsch, H., Munzert, G., and Socinski, M. (2009). An open label phase II trial of the Plk1 inhibitor BI 2536, in patients with sensitive relapse small cell lung cancer (SCLC). Journal of Clinical Oncology *27*, 8108-8108.
Gannoun-Zaki, L., Jost, A., Mu, J., Deitsch, K.W., and Wellems, T.E. (2005). A silenced *Plasmodium falciparum* var promoter can be activated in vivo through spontaneous deletion of a silencing element in the intron. Eukaryot Cell *4*, 490-492.
Gantt, S.M., Myung, J.M., Briones, M.R., Li, W.D., Corey, E.J., Omura, S., Nussenzweig, V., and Sinnis, P. (1998). Proteasome inhibitors block development of *Plasmodium* spp. Antimicrobial agents and chemotherapy *42*, 2731-2738.
Gao, X., Gunalan, K., Yap, S.S.L., and Preiser, P.R. (2013). Triggers of key calcium signals during erythrocyte invasion by *Plasmodium falciparum*. Nature Communications *4*, 2862.
García-Oliver, E., Ramus, C., Perot, J., Arlotto, M., Champleboux, M., Mietton, F., Battail, C., Boland, A., Deleuze, J.-F., Ferro, M*., et al.* (2017). Bdf1 Bromodomains Are Essential for Meiosis and the Expression of Meiotic-Specific Genes. PLOS Genetics *13*, e1006541.
Gardner, M.J., Hall, N., Fung, E., White, O., Berriman, M., Hyman, R.W., Carlton, J.M., Pain, A., Nelson, K.E., Bowman, S*., et al.* (2002). Genome sequence of the human malaria parasite *Plasmodium falciparum*. Nature *419*, 498-511.
Gentleman, R.C., Carey, V.J., Bates, D.M., Bolstad, B., Dettling, M., Dudoit, S., Ellis, B., Gautier, L., Ge, Y., Gentry, J*., et al.* (2004). Bioconductor: open software development for computational biology and bioinformatics. Genome Biology *5*, R80.
Ghosh, A.K., and Jacobs-Lorena, M. (2009). Plasmodium sporozoite invasion of the mosquito salivary gland. Current opinion in microbiology *12*, 394-400.
Gill, J., Kumar, A., Yogavel, M., Belrhali, H., Jain, S.K., Rug, M., Brown, M., Maier, A.G., and Sharma, A. (2010). Structure, localization and histone binding properties of nuclear-associated nucleosome assembly protein from *Plasmodium falciparum*. Malaria journal *9*, 90-90.
Gill, J., Yogavel, M., Kumar, A., Belrhali, H., Jain, S.K., Rug, M., Brown, M., Maier, A.G., and Sharma, A. (2009). Crystal structure of malaria parasite nucleosome assembly protein: distinct modes of protein localization and histone recognition. The Journal of biological chemistry *284*, 10076-10087.
Gissot, M., Briquet, S., Refour, P., Boschet, C., and Vaquero, C. (2005). PfMyb1, a *Plasmodium falciparum* transcription factor, is required for intra-erythrocytic growth and controls key genes for cell cycle regulation. Journal of molecular biology *346*, 29-42.
Gissot, M., Ting, L.M., Daly, T.M., Bergman, L.W., Sinnis, P., and Kim, K. (2008). High mobility group protein HMGB2 is a critical regulator of *plasmodium* oocyst development. The Journal of biological chemistry *283*, 17030-17038.
Goel, V.K., Li, X., Chen, H., Liu, S.C., Chishti, A.H., and Oh, S.S. (2003). Band 3 is a host receptor binding merozoite surface protein 1 during the *Plasmodium falciparum* invasion of erythrocytes. Proc Natl Acad Sci U S A *100*, 5164-5169.
Gohda, J., Suzuki, K., Liu, K., Xie, X., Takeuchi, H., Inoue, J.-I., Kawaguchi, Y., and Ishida, T. (2018). BI-2536 and BI-6727, dual Polo-like kinase/bromodomain inhibitors, effectively reactivate latent HIV-1. Sci Rep *8*, 3521-3521.

Gopalakrishnan, A.M., Nyindodo, L.A., Ross Fergus, M., and López-Estraño, C. (2009). *Plasmodium falciparum*: Preinitiation complex occupancy of active and inactive promoters during erythrocytic stage. Experimental Parasitology *121*, 46-54.
Gordeev, S.A., Bykova, T.V., Zubova, S.G., Bystrova, O.A., Martynova, M.G., Pospelov, V.A., and Pospelova, T.V. (2015). mTOR kinase inhibitor pp242 causes mitophagy terminated by apoptotic cell death in E1A-Ras transformed cells. Oncotarget *6*, 44905-44926.
Guiguemde, Guiguemde, W.A., Shelat, A., Bouck, D., Duffy, S., Crowther, G., Davis, P., Smithson, D., Connelly, M., Clark, J.*, et al.* (2010). Chemical genetics of *Plasmodium falciparum*. Nature *465*, 311-315.
Guillemette, B., Bataille, A.R., Gevry, N., Adam, M., Blanchette, M., Robert, F., and Gaudreau, L. (2005). Variant histone H2A.Z is globally localized to the promoters of inactive yeast genes and regulates nucleosome positioning. PLoS Biol *3*, e384.
Guindon, S., Dufayard, J.-F., Lefort, V., Anisimova, M., Hordijk, W., and Gascuel, O. (2010). New Algorithms and Methods to Estimate Maximum-Likelihood Phylogenies: Assessing the Performance of PhyML 3.0. Systematic Biology *59*, 307-321.
Gupta, A.P., and Bozdech, Z. (2017). Epigenetic landscapes underlining global patterns of gene expression in the human malaria parasite, *Plasmodium falciparum*. Int J Parasitol *47*, 399-407.
Gupta, A.P., Chin, W.H., Zhu, L., Mok, S., Luah, Y.H., Lim, E.H., and Bozdech, Z. (2013). Dynamic epigenetic regulation of gene expression during the life cycle of malaria parasite *Plasmodium falciparum*. PLoS Pathog *9*, e1003170.
Gural, N., Mancio-Silva, L., Miller, A.B., Galstian, A., Butty, V.L., Levine, S.S., Patrapuvich, R., Desai, S.P., Mikolajczak, S.A., Kappe, S.H.I.*, et al.* (2018). In Vitro Culture, Drug Sensitivity, and Transcriptome of *Plasmodium Vivax* Hypnozoites. Cell Host Microbe *23*, 395-406 e394.
Hammitzsch, A., Tallant, C., Fedorov, O., O'Mahony, A., Brennan, P.E., Hay, D.A., Martinez, F.O., Al-Mossawi, M.H., de Wit, J., Vecellio, M.*, et al.* (2015). CBP30, a selective CBP/p300 bromodomain inhibitor, suppresses human Th17 responses. Proc Natl Acad Sci U S A *112*, 10768-10773.
Han, Y.S., Thompson, J., Kafatos, F.C., and Barillas-Mury, C. (2000). Molecular interactions between *Anopheles stephensi* midgut cells and *Plasmodium berghei*: the time bomb theory of ookinete invasion of mosquitoes. EMBO J *19*, 6030-6040.
Harner, M.J., Frank, A.O., and Fesik, S.W. (2013). Fragment-based drug discovery using NMR spectroscopy. J Biomol NMR *56*, 65-75.
Harris, P.K., Yeoh, S., Dluzewski, A.R., O'Donnell, R.A., Withers-Martinez, C., Hackett, F., Bannister, L.H., Mitchell, G.H., and Blackman, M.J. (2005). Molecular identification of a malaria merozoite surface sheddase. PLoS Pathog *1*, 241-251.
Hashimoto, H., Zhang, X., Vertino, P.M., and Cheng, X. (2015). The Mechanisms of Generation, Recognition, and Erasure of DNA 5-Methylcytosine and Thymine Oxidations. The Journal of biological chemistry *290*, 20723-20733.
Hedges, S.B. (2002). The origin and evolution of model organisms. Nature reviews Genetics *3*, 838-849.
Higgins, S.J., Xing, K., Kim, H., Kain, D.C., Wang, F., Dhabangi, A., Musoke, C., Cserti-Gazdewich, C.M., Tracey, K.J., Kain, K.C.*, et al.* (2013). Systemic release of high mobility group box 1 (HMGB1) protein is associated with severe and fatal *Plasmodium falciparum* malaria. Malar J *12*, 105.
Hoch, D.A., Stratton, J.J., and Gloss, L.M. (2007). Protein-protein Forster resonance energy transfer analysis of nucleosome core particles containing H2A and H2A.Z. Journal of molecular biology *371*, 971-988.

Hoeijmakers, W.A., Salcedo-Amaya, A.M., Smits, A.H., Francoijs, K.J., Treeck, M., Gilberger, T.W., Stunnenberg, H.G., and Bartfai, R. (2013). H2A.Z/H2B.Z double-variant nucleosomes inhabit the AT-rich promoter regions of the *Plasmodium falciparum* genome. Mol Microbiol *87*, 1061-1073.
Hoeijmakers, Wieteke Anna M., Miao, J., Schmidt, S., Toenhake, C.G., Shrestha, S., Venhuizen, J., Henderson, R., Birnbaum, J., Ghidelli-Disse, S., Drewes, G.*, et al.* (2019). Epigenetic reader complexes of the human malaria parasite, *Plasmodium falciparum*. Nucleic Acids Research *47*, 11574-11588.
Hoffer, L., Renaud, J.P., and Horvath, D. (2011). Fragment-based drug design: computational & experimental state of the art. Combinatorial chemistry & high throughput screening *14*, 500-520.
Hoffman, E.A., Frey, B.L., Smith, L.M., and Auble, D.T. (2015). Formaldehyde Crosslinking: A Tool for the Study of Chromatin Complexes. Journal of Biological Chemistry *290*, 26404-26411.
Hou, C.F.D., Loppnau, P., Dong, A., Bountra, C., Edwards, A.M., Arrowsmith, C.H., Hui, R., Walker, J.R., and (SGC), S.G.C. Bromodomain of PF3D7_1475600 from *Plasmodium falciparum* complexed with peptide H4K5ac.
Howard, R.J., Haynes, J.D., McGinniss, M.H., and Miller, L.H. (1982). Studies on the role of red blood cell glycoproteins as receptors for invasion by *Plasmodium falciparum* merozoites. Molecular and Biochemical Parasitology *6*, 303-315.
Huang, B., Yang, X.D., Zhou, M.M., Ozato, K., and Chen, L.F. (2009). Brd4 coactivates transcriptional activation of NF-kappaB via specific binding to acetylated RelA. Mol Cell Biol *29*, 1375-1387.
Hui D, F.M., Josling G, Tallant C, Wernimont A, Fedorov O, Hutchinson A, Loppnau P, Duffy M, Knapp S, Hui Raymond (2016). *Plasmodium* bromodomain PfBDP4. In A Target Enabling Package (TEP).
Idro, R., Carter, J.A., Fegan, G., Neville, B.G., and Newton, C.R. (2006). Risk factors for persisting neurological and cognitive impairments following cerebral malaria. Archives of disease in childhood *91*, 142-148.
Idro, R., Marsh, K., John, C.C., and Newton, C.R.J. (2010). Cerebral malaria: mechanisms of brain injury and strategies for improved neurocognitive outcome. Pediatr Res *68*, 267-274.
Igoe, N., Bayle, E.D., Tallant, C., Fedorov, O., Meier, J.C., Savitsky, P., Rogers, C., Morias, Y., Scholze, S., Boyd, H.*, et al.* (2017). Design of a Chemical Probe for the Bromodomain and Plant Homeodomain Finger-Containing (BRPF) Family of Proteins. Journal of Medicinal Chemistry *60*, 6998-7011.
InkscapeTeam, T. (2004). Inkscape, version 0.92.4 (website: http://www.inkscape.org).
Ishibashi, T., Dryhurst, D., Rose, K.L., Shabanowitz, J., Hunt, D.F., and Ausio, J. (2009). Acetylation of vertebrate H2A.Z and its effect on the structure of the nucleosome. Biochemistry *48*, 5007-5017.
Issar, N., Roux, E., Mattei, D., and Scherf, A. (2008). Identification of a novel post-translational modification in *Plasmodium falciparum*: protein sumoylation in different cellular compartments. Cell Microbiol *10*, 1999-2011.
Iwanaga, S., Kaneko, I., Kato, T., and Yuda, M. (2012). Identification of an AP2-family protein that is critical for malaria liver stage development. PLoS One *7*, e47557.
Iyer, L.M., Anantharaman, V., Wolf, M.Y., and Aravind, L. (2008). Comparative genomics of transcription factors and chromatin proteins in parasitic protists and other eukaryotes. International Journal for Parasitology *38*, 1-31.
Jacobson, R.H., Ladurner, A.G., King, D.S., and Tjian, R. (2000). Structure and function of a human TAFII250 double bromodomain module. Science *288*, 1422-1425.

Jäschke, A., Coulibaly, B., Remarque, E.J., Bujard, H., and Epp, C. (2017). Merozoite Surface Protein 1 from *Plasmodium falciparum* is a Major Target of Opsonizing Antibodies in Individuals with Acquired Immunity against Malaria. Clinical and Vaccine Immunology *24*, e00155-00117.
Jeffers, V., Yang, C., Huang, S., and Sullivan, W.J. (2017). Bromodomains in Protozoan Parasites: Evolution, Function, and Opportunities for Drug Development. Microbiology and Molecular Biology Reviews *81*, e00047-00016.
Jennings, L.E., Measures, A.R., Wilson, B.G., and Conway, S.J. (2014). Phenotypic screening and fragment-based approaches to the discovery of small-molecule bromodomain ligands. Future medicinal chemistry *6*, 179-204.
Jiang, F., Wei, Q., Li, H., Li, H., Cui, Y., Ma, Y., Chen, H., Cao, P., Lu, T., and Chen, Y. (2019). Discovery of novel small molecule induced selective degradation of the bromodomain and extra-terminal (BET) bromodomain protein BRD4 and BRD2 with cellular potencies. Bioorganic & Medicinal Chemistry, 115181.
Jiang, L., Mu, J., Zhang, Q., Ni, T., Srinivasan, P., Rayavara, K., Yang, W., Turner, L., Lavstsen, T., Theander, T.G.*, et al.* (2013). PfSETvs methylation of histone H3K36 represses virulence genes in *Plasmodium falciparum*. Nature *499*, 223-227.
Jin, Y., Kebaier, C., and Vanderberg, J. (2007). Direct Microscopic Quantification of Dynamics of *Plasmodium berghei* Sporozoite Transmission from Mosquitoes to Mice. Infection and Immunity *75*, 5532.
Jing, Q., Cao, L., Zhang, L., Cheng, X., Gilbert, N., Dai, X., Sun, M., Liang, S., and Jiang, L. (2018). *Plasmodium falciparum* var Gene Is Activated by Its Antisense Long Noncoding RNA. Frontiers in microbiology *9*, 3117.
Joshi, M.B., Lin, D.T., Chiang, P.H., Goldman, N.D., Fujioka, H., Aikawa, M., and Syin, C. (1999). Molecular cloning and nuclear localization of a histone deacetylase homologue in *Plasmodium falciparum*. Mol Biochem Parasitol *99*, 11-19.
Josling, G.A., Petter, M., Oehring, S.C., Gupta, A.P., Dietz, O., Wilson, D.W., Schubert, T., Langst, G., Gilson, P.R., Crabb, B.S.*, et al.* (2015). A *Plasmodium falciparum* Bromodomain Protein Regulates Invasion Gene Expression. Cell Host Microbe *17*, 741-751.
Josling, G.A., Russell, T.J., Venezia, J., Orchard, L., van Biljon, R., Painter, H.J., and Llinás, M. (2020). Dissecting the role of PfAP2-G in malaria gametocytogenesis. Nature Communications *11*, 1503.
Jullien, N., Goddard, I., Selmi-Ruby, S., Fina, J.-L., Cremer, H., and Herman, J.-P. (2007). Conditional transgenesis using Dimerizable Cre (DiCre). PloS one *2*, e1355-e1355.
Jullien, N., Sampieri, F., Enjalbert, A., and Herman, J.P. (2003). Regulation of Cre recombinase by ligand-induced complementation of inactive fragments. Nucleic Acids Res *31*, e131.
Jung, M., Gelato, K.A., Fernandez-Montalvan, A., Siegel, S., and Haendler, B. (2015). Targeting BET bromodomains for cancer treatment. Epigenomics *7*, 487-501.
Jung, M., Philpott, M., Müller, S., Schulze, J., Badock, V., Eberspächer, U., Moosmayer, D., Bader, B., Schmees, N., Fernández-Montalván, A.*, et al.* (2014). Affinity Map of Bromodomain Protein 4 (BRD4) Interactions with the Histone H4 Tail and the Small Molecule Inhibitor JQ1. Journal of Biological Chemistry *289*, 9304-9319.
Kafsack, B.F., Rovira-Graells, N., Clark, T.G., Bancells, C., Crowley, V.M., Campino, S.G., Williams, A.E., Drought, L.G., Kwiatkowski, D.P., Baker, D.A.*, et al.* (2014). A transcriptional switch underlies commitment to sexual development in malaria parasites. Nature *507*, 248-252.
Kaneko, I., Iwanaga, S., Kato, T., Kobayashi, I., and Yuda, M. (2015). Genome-Wide Identification of the Target Genes of AP2-O, a *Plasmodium* AP2-Family Transcription Factor. PLOS Pathogens *11*, e1004905.

Kappe, S.H., Vaughan, A.M., Boddey, J.A., and Cowman, A.F. (2010). That was then but this is now: malaria research in the time of an eradication agenda. Science *328*, 862-866.
Karmodiya, K., Pradhan, S.J., Joshi, B., Jangid, R., Reddy, P.C., and Galande, S. (2015). A comprehensive epigenome map of *Plasmodium falciparum* reveals unique mechanisms of transcriptional regulation and identifies H3K36me2 as a global mark of gene suppression. Epigenetics & chromatin *8*, 32-32.
Katsuno, Katsuno, K., Burrows, J., Duncan, K., van Huijsduijnen, R., Kaneko, T., Kita, K., Mowbray, C., Schmatz, D., Warner, P.*, et al.* (2015). Hit and lead criteria in drug discovery for infectious diseases of the developing world. Nature Reviews Drug Discovery *14*, 751-758.
Kauth, C.W., Woehlbier, U., Kern, M., Mekonnen, Z., Lutz, R., Mücke, N., Langowski, J., and Bujard, H. (2006). Interactions between Merozoite Surface Proteins 1, 6, and 7 of the Malaria Parasite *Plasmodium falciparum*. Journal of Biological Chemistry *281*, 31517-31527.
Kawahara, T., Siegel, T.N., Ingram, A.K., Alsford, S., Cross, G.A.M., and Horn, D. (2008). Two essential MYST-family proteins display distinct roles in histone H4K10 acetylation and telomeric silencing in trypanosomes. Molecular microbiology *69*, 1054-1068.
Kayser, O., Kiderlen, A.F., and Brun, R. (2001). In Vitro Activity of Aurones against *Plasmodium falciparum* Strains K1 and NF54. Planta Med *67*, 718-721.
Keeley, A., and Soldati, D. (2004). The glideosome: a molecular machine powering motility and host-cell invasion by Apicomplexa. Trends in cell biology *14*, 528-532.
Kensche, P.R., Hoeijmakers, W.A.M., Toenhake, C.G., Bras, M., Chappell, L., Berriman, M., and Bártfai, R. (2016). The nucleosome landscape of *Plasmodium falciparum* reveals chromatin architecture and dynamics of regulatory sequences. Nucleic acids research *44*, 2110-2124.
Kirberger, S.E., Ycas, P.D., Johnson, J.A., Chen, C., Ciccone, M.F., Woo, R.W.L., Urick, A.K., Zahid, H., Shi, K., Aihara, H.*, et al.* (2019). Selectivity, ligand deconstruction, and cellular activity analysis of a BPTF bromodomain inhibitor. Organic & Biomolecular Chemistry *17*, 2020-2027.
Koita, O.A., Doumbo, O.K., Ouattara, A., Tall, L.K., Konare, A., Diakite, M., Diallo, M., Sagara, I., Masinde, G.L., Doumbo, S.N.*, et al.* (2012). False-negative rapid diagnostic tests for malaria and deletion of the histidine-rich repeat region of the hrp2 gene. The American journal of tropical medicine and hygiene *86*, 194-198.
Koshland, D.E. (1958). Application of a Theory of Enzyme Specificity to Protein Synthesis. Proceedings of the National Academy of Sciences of the United States of America *44*, 98-104.
Koussis, K., Withers-Martinez, C., Yeoh, S., Child, M., Hackett, F., Knuepfer, E., Juliano, L., Woehlbier, U., Bujard, H., and Blackman, M.J. (2009). A multifunctional serine protease primes the malaria parasite for red blood cell invasion. EMBO J *28*, 725-735.
Kraemer, S.M., and Smith, J.D. (2003). Evidence for the importance of genetic structuring to the structural and functional specialization of the *Plasmodium falciparum* var gene family. Mol Microbiol *50*, 1527-1538.
Kreidenweiss, A., Kremsner, P.G., and Mordmuller, B. (2008). Comprehensive study of proteasome inhibitors against *Plasmodium falciparum* laboratory strains and field isolates from Gabon. Malar J *7*, 187.
Kuang, D., Qiao, J., Li, Z., Wang, W., Xia, H., Jiang, L., Dai, J., Fang, Q., and Dai, X. (2017). Tagging to endogenous genes of *Plasmodium falciparum* using CRISPR/Cas9. Parasit Vectors *10*, 595-595.
Kulis, M., and Esteller, M. (2010). DNA methylation and cancer. Advances in genetics *70*, 27-56.

Kumar, A., Bhowmick, K., Vikramdeo, K.S., Mondal, N., Subbarao, N., and Dhar, S.K. (2017). Designing novel inhibitors against histone acetyltransferase (HAT: GCN5) of *Plasmodium falciparum*. European Journal of Medicinal Chemistry *138*, 26-37.
Kumar, K., Singal, A., Rizvi, M.M., and Chauhan, V.S. (2008). High mobility group box (HMGB) proteins of *Plasmodium falciparum*: DNA binding proteins with pro-inflammatory activity. Parasitology international *57*, 150-157.
Kumar, S.V., and Wigge, P.A. (2010). H2A.Z-Containing Nucleosomes Mediate the Thermosensory Response in Arabidopsis. Cell *140*, 136-147.
Kwenti, T.E. (2018). Malaria and HIV coinfection in sub-Saharan Africa: prevalence, impact, and treatment strategies. Res Rep Trop Med *9*, 123-136.
Lambros, C., and Vanderberg, J.P. (1979). Synchronization of *Plasmodium falciparum* erythrocytic stages in culture. J Parasitol *65*, 418-420.
Lanzer, M., de Bruin, D., and Ravetch, J.V. (1992). Transcription mapping of a 100 kb locus of *Plasmodium falciparum* identifies an intergenic region in which transcription terminates and reinitiates. EMBO J *11*, 1949-1955.
Lavstsen, T., Salanti, A., Jensen, A.T.R., Arnot, D.E., and Theander, T.G. (2003). Sub-grouping of Plasmodium falciparum 3D7 var genes based on sequence analysis of coding and non-coding regions. Malaria journal *2*, 27-27.
Le Roch, K.G., Zhou, Y., Blair, P.L., Grainger, M., Moch, J.K., Haynes, J.D., De La Vega, P., Holder, A.A., Batalov, S., Carucci, D.J.*, et al.* (2003). Discovery of gene function by expression profiling of the malaria parasite life cycle. Science *301*, 1503-1508.
Lemieux, J.E., Kyes, S.A., Otto, T.D., Feller, A.I., Eastman, R.T., Pinches, R.A., Berriman, M., Su, X.-Z., and Newbold, C.I. (2013). Genome-wide profiling of chromosome interactions in *Plasmodium falciparum* characterizes nuclear architecture and reconfigurations associated with antigenic variation. Molecular microbiology *90*, 519-537.
Lénárt, P., Petronczki, M., Steegmaier, M., Di Fiore, B., Lipp, J.J., Hoffmann, M., Rettig, W.J., Kraut, N., and Peters, J.-M. (2007). The Small-Molecule Inhibitor BI 2536 Reveals Novel Insights into Mitotic Roles of Polo-like Kinase 1. Current Biology *17*, 304-315.
Lespinet, O., Wolf, Y.I., Koonin, E.V., and Aravind, L. (2002). The role of lineage-specific gene family expansion in the evolution of eukaryotes. Genome Res *12*, 1048-1059.
Lewin, J., Soria, J.C., Stathis, A., Delord, J.P., Peters, S., Awada, A., Aftimos, P.G., Bekradda, M., Rezai, K., Zeng, Z.*, et al.* (2018). Phase Ib Trial With Birabresib, a Small-Molecule Inhibitor of Bromodomain and Extraterminal Proteins, in Patients With Selected Advanced Solid Tumors. Journal of clinical oncology : official journal of the American Society of Clinical Oncology *36*, 3007-3014.
Li, H. (2013). Aligning sequence reads, clone sequences and assembly contigs with BWA-MEM. arXiv preprint
Li, H., Handsaker, B., Wysoker, A., Fennell, T., Ruan, J., Homer, N., Marth, G., Abecasis, G., Durbin, R., and Genome Project Data Processing, S. (2009). The Sequence Alignment/Map format and SAMtools. Bioinformatics (Oxford, England) *25*, 2078-2079.
Li, J., Kokkola, R., Tabibzadeh, S., Yang, R., Ochani, M., Qiang, X., Harris, H.E., Czura, C.J., Wang, H., Ulloa, L.*, et al.* (2003). Structural basis for the proinflammatory cytokine activity of high mobility group box 1. Molecular medicine (Cambridge, Mass) *9*, 37-45.
Li, W.-B., Bzik, D.J., Gu, H., Tanaka, M., Fox, B.A., and Inselburg, J. (1989). An enlarged largest subunit or *Plasmodium falciparum* RNA polymerase II defines conserved and variable RNA polymerase domains. Nucleic Acids Research *17*, 9621-9636.
Li, W.-B., Bzik, D.J., Tanaka, M., Gu, H., Fox, B.A., and Inselburg, J. (1991). Characterization of the gene encoding the largest subunit of *Plasmodium falciparum* RNA polymerase III. Molecular and Biochemical Parasitology *46*, 229-239.

Liao, Y., Smyth, G.K., and Shi, W. (2019). The R package Rsubread is easier, faster, cheaper and better for alignment and quantification of RNA sequencing reads. Nucleic Acids Research *47*, e47-e47.
Lin, C.S., Uboldi, A.D., Epp, C., Bujard, H., Tsuboi, T., Czabotar, P.E., and Cowman, A.F. (2016a). Multiple *P. falciparum* Merozoite Surface Protein 1 Complexes Mediate Merozoite Binding to Human Erythrocytes. Journal of Biological Chemistry.
Lin, C.S., Uboldi, A.D., Epp, C., Bujard, H., Tsuboi, T., Czabotar, P.E., and Cowman, A.F. (2016b). Multiple *Plasmodium falciparum* Merozoite Surface Protein 1 Complexes Mediate Merozoite Binding to Human Erythrocytes. Journal of Biological Chemistry *291*, 7703-7715.
Lin, C.S., Uboldi, A.D., Marapana, D., Czabotar, P.E., Epp, C., Bujard, H., Taylor, N.L., Perugini, M.A., Hodder, A.N., and Cowman, A.F. (2014). The Merozoite Surface Protein 1 Complex Is a Platform for Binding to Human Erythrocytes by *Plasmodium falciparum*. Journal of Biological Chemistry *289*, 25655-25669.
Ling, I.T., Florens, L., Dluzewski, A.R., Kaneko, O., Grainger, M., Yim Lim, B.Y.S., Tsuboi, T., Hopkins, J.M., Johnson, J.R., Torii, M.*, et al.* (2004). The *Plasmodium falciparum clag9* gene encodes a rhoptry protein that is transferred to the host erythrocyte upon invasion. Molecular Microbiology *52*, 107-118.
Liu, X., Zhang, X., Wang, C., Liu, L., Lei, M., and Bao, X. (2007). Genetic and Comparative Transcriptome Analysis of Bromodomain Factor 1 in the Salt Stress Response of *Saccharomyces cerevisiae*. Current Microbiology *54*, 325-330.
Lolli, G., and Caflisch, A. (2016). High-Throughput Fragment Docking into the BAZ2B Bromodomain: Efficient in Silico Screening for X-Ray Crystallography. ACS Chem Biol *11*, 800-807.
Lopaticki, S., Maier, A.G., Thompson, J., Wilson, D.W., Tham, W.H., Triglia, T., Gout, A., Speed, T.P., Beeson, J.G., Healer, J.*, et al.* (2011). Reticulocyte and erythrocyte binding-like proteins function cooperatively in invasion of human erythrocytes by malaria parasites. Infect Immun *79*, 1107-1117.
Lopez-Barragan, M.J., Lemieux, J., Quinones, M., Williamson, K.C., Molina-Cruz, A., Cui, K., Barillas-Mury, C., Zhao, K., and Su, X.Z. (2011). Directional gene expression and antisense transcripts in sexual and asexual stages of *Plasmodium falciparum*. BMC Genomics *12*, 587.
Lopez-Rubio, J.J., Gontijo, A.M., Nunes, M.C., Issar, N., Hernandez Rivas, R., and Scherf, A. (2007). 5' flanking region of var genes nucleate histone modification patterns linked to phenotypic inheritance of virulence traits in malaria parasites. Mol Microbiol *66*, 1296-1305.
Lopez-Rubio, J.J., Mancio-Silva, L., and Scherf, A. (2009). Genome-wide analysis of heterochromatin associates clonally variant gene regulation with perinuclear repressive centers in malaria parasites. Cell Host Microbe *5*, 179-190.
Lu, B., Mahmud, H., Maass, A.H., Yu, B., van Gilst, W.H., de Boer, R.A., and Silljé, H.H.W. (2010). The Plk1 Inhibitor BI 2536 Temporarily Arrests Primary Cardiac Fibroblasts in Mitosis and Generates Aneuploidy In Vitro. PLOS ONE *5*, e12963.
Mancio-Silva, L., Lopez-Rubio, J.J., Claes, A., and Scherf, A. (2013). Sir2a regulates rDNA transcription and multiplication rate in the human malaria parasite *Plasmodium falciparum*. Nature Communications *4*, 1530.
Martins, R.M., Macpherson, C.R., Claes, A., Scheidig-Benatar, C., Sakamoto, H., Yam, X.Y., Preiser, P., Goel, S., Wahlgren, M., Sismeiro, O.*, et al.* (2017). An ApiAP2 member regulates expression of clonally variant genes of the human malaria parasite *Plasmodium falciparum*. Sci Rep *7*, 14042.
Marty, A.J., Thompson, J.K., Duffy, M.F., Voss, T.S., Cowman, A.F., and Crabb, B.S. (2006). Evidence that *Plasmodium falciparum* chromosome end clusters are cross-linked by

protein and are the sites of both virulence gene silencing and activation. Molecular Microbiology *62*, 72-83.
Matangkasombut, O., Buratowski, R.M., Swilling, N.W., and Buratowski, S. (2000). Bromodomain factor 1 corresponds to a missing piece of yeast TFIID. Genes & Development *14*, 951-962.
McInroy, G.R., Beraldi, D., Raiber, E.A., Modrzynska, K., van Delft, P., Billker, O., and Balasubramanian, S. (2016). Enhanced Methylation Analysis by Recovery of Unsequenceable Fragments. PLoS One *11*, e0152322.
Meister, S., Plouffe, D., Kuhen, K., Bonamy, G.M.C., Wu, T., Barnes, S.W., Bopp, S., Borboa, R., Bright, A.T., Che, J.*, et al.* (2011). Imaging of *Plasmodium* liver stages to drive next-generation antimalarial drug discovery. Science *334*, 1372-1377.
Merrick, C.J., Dzikowski, R., Imamura, H., Chuang, J., Deitsch, K., and Duraisingh, M.T. (2010). The effect of *Plasmodium falciparum* Sir2a histone deacetylase on clonal and longitudinal variation in expression of the var family of virulence genes. Int J Parasitol *40*, 35-43.
Merrick, C.J., Jiang, R.H.Y., Skillman, K.M., Samarakoon, U., Moore, R.M., Dzikowski, R., Ferdig, M.T., and Duraisingh, M.T. (2015). Functional Analysis of Sirtuin Genes in Multiple *Plasmodium falciparum* Strains. PLOS ONE *10*, e0118865.
Miao, J., Fan, Q., Cui, L., Li, J., Li, J., and Cui, L. (2006). The malaria parasite *Plasmodium falciparum* histones: Organization, expression, and acetylation. Gene *369*, 53-65.
Miao, J., Fan, Q., Cui, L., Li, X., Wang, H., Ning, G., Reese, J.C., and Cui, L. (2010). The MYST family histone acetyltransferase regulates gene expression and cell cycle in malaria parasite *Plasmodium falciparum*. Molecular Microbiology *78*, 883-902.
Miller, L.H., Ackerman, H.C., Su, X.-z., and Wellems, T.E. (2013). Malaria biology and disease pathogenesis: insights for new treatments. Nature medicine *19*, 156-167.
Mira-Martínez, S., Rovira-Graells, N., Crowley, V.M., Altenhofen, L.M., Llinás, M., and Cortés, A. (2013). Epigenetic switches in clag3 genes mediate blasticidin S resistance in malaria parasites. Cellular Microbiology *15*, 1913-1923.
Modrzynska, K., Pfander, C., Chappell, L., Yu, L., Suarez, C., Dundas, K., Gomes, A.R., Goulding, D., Rayner, J.C., Choudhary, J.*, et al.* (2017). A Knockout Screen of ApiAP2 Genes Reveals Networks of Interacting Transcriptional Regulators Controlling the *Plasmodium* Life Cycle. Cell host & microbe *21*, 11-22.
Mok, B.W., Ribacke, U., Rasti, N., Kironde, F., Chen, Q., Nilsson, P., and Wahlgren, M. (2008). Default Pathway of var2csa switching and translational repression in *Plasmodium falciparum*. PloS one *3*, e1982-e1982.
Molina-Cruz, A., Canepa, G.E., and Barillas-Mury, C. (2017). *Plasmodium* P47: a key gene for malaria transmission by mosquito vectors. Current Opinion in Microbiology *40*, 168-174.
Molina-Cruz, A., Garver, L.S., Alabaster, A., Bangiolo, L., Haile, A., Winikor, J., Ortega, C., van Schaijk, B.C.L., Sauerwein, R.W., Taylor-Salmon, E.*, et al.* (2013). The Human Malaria Parasite *Pfs* Gene Mediates Evasion of the Mosquito Immune System. Science *340*, 984.
Montgomery, J., Mphande, F.A., Berriman, M., Pain, A., Rogerson, S.J., Taylor, T.E., Molyneux, M.E., and Craig, A. (2007). Differential var gene expression in the organs of patients dying of *falciparum* malaria. Molecular Microbiology *65*, 959-967.
Moustakim, M., Clark, P.G., Trulli, L., Fuentes de Arriba, A.L., Ehebauer, M.T., Chaikuad, A., Murphy, E.J., Mendez-Johnson, J., Daniels, D., Hou, C.D.*, et al.* (2017). Discovery of a PCAF Bromodomain Chemical Probe. Angew Chem Int Ed Engl *56*, 827-831.
Mross, K., Dittrich, C., Aulitzky, W.E., Strumberg, D., Schutte, J., Schmid, R.M., Hollerbach, S., Merger, M., Munzert, G., Fleischer, F.*, et al.* (2012). A randomised phase II trial of the Polo-like kinase inhibitor BI 2536 in chemo-naïve patients with unresectable exocrine adenocarcinoma of the pancreas – a study within the Central European Society

Anticancer Drug Research (CESAR) collaborative network. British Journal of Cancer *107*, 280-286.
Mross, K., Frost, A., Steinbild, S., Hedbom, S., Rentschler, J., Kaiser, R., Rouyrre, N., Trommeshauser, D., Hoesl, C.E., and Munzert, G. (2008). Phase I Dose Escalation and Pharmacokinetic Study of BI 2536, a Novel Polo-Like Kinase 1 Inhibitor, in Patients With Advanced Solid Tumors. Journal of Clinical Oncology *26*, 5511-5517.
Naik, R.S., Krishnegowda, G., and Gowda, D.C. (2003). Glucosamine inhibits inositol acylation of the glycosylphosphatidylinositol anchors in intraerythrocytic *Plasmodium falciparum*. The Journal of biological chemistry *278*, 2036-2042.
Narita, T., Weinert, B.T., and Choudhary, C. (2019). Functions and mechanisms of non-histone protein acetylation. Nature Reviews Molecular Cell Biology *20*, 156-174.
Navadgi, V.M., Chandra, B.R., Mishra, P.C., and Sharma, A. (2006). The two *Plasmodium falciparum* nucleosome assembly proteins play distinct roles in histone transport and chromatin assembly. The Journal of biological chemistry *281*, 16978-16984.
Neveu, G., Dupuy, F., Ladli, M., Barbieri, D., Naissant, B., Richard, C., Martins, R.M., Lopez-Rubio, J.-J., Bachmann, A., Verdier, F*., et al.* (2018). *Plasmodium falciparum* gametocyte-infected erythrocytes do not adhere to human primary erythroblasts. Sci Rep *8*, 17886-17886.
Newton, C.R., and Krishna, S. (1998). Severe falciparum malaria in children: current understanding of pathophysiology and supportive treatment. Pharmacology & therapeutics *79*, 1-53.
Newton, C.R.J.C., Warn, P.A., Winstanley, P.A., Peshu, N., Snow, R.W., Pasvol, G., and Marsh, K. (1997). Severe anaemia in children living in a malaria endemic area of Kenya. Tropical Medicine & International Health *2*, 165-178.
Nguitragool, W., Bokhari, Abdullah A.B., Pillai, Ajay D., Rayavara, K., Sharma, P., Turpin, B., Aravind, L., and Desai, Sanjay A. (2011). Malaria Parasite clag3 Genes Determine Channel-Mediated Nutrient Uptake by Infected Red Blood Cells. Cell *145*, 665-677.
Nguyen, H.H.T., Yeoh, L.M., Chisholm, S.A., and Duffy, M.F. (2020). Developments in drug design strategies for bromodomain protein inhibitors to target *Plasmodium falciparum* parasites. Expert Opinion on Drug Discovery *15*, 415-425.
Niesen, F.H., Berglund, H., and Vedadi, M. (2007). The use of differential scanning fluorimetry to detect ligand interactions that promote protein stability. Nat Protoc *2*, 2212-2221.
Nowick, K., and Stubbs, L. (2010). Lineage-specific transcription factors and the evolution of gene regulatory networks. Briefings in functional genomics *9*, 65-78.
O'Neill, M.T., Phuong, T., Healer, J., Richard, D., and Cowman, A.F. (2011). Gene deletion from *Plasmodium falciparum* using FLP and Cre recombinases: implications for applied site-specific recombination. Int J Parasitol *41*, 117-123.
Oehring, S.C., Woodcroft, B.J., Moes, S., Wetzel, J., Dietz, O., Pulfer, A., Dekiwadia, C., Maeser, P., Flueck, C., Witmer, K*., et al.* (2012). Organellar proteomics reveals hundreds of novel nuclear proteins in the malaria parasite *Plasmodium falciparum*. Genome Biol *13*, R108.
Ogutu, B.R., Apollo, O.J., McKinney, D., Okoth, W., Siangla, J., Dubovsky, F., Tucker, K., Waitumbi, J.N., Diggs, C., Wittes, J*., et al.* (2009). Blood stage malaria vaccine eliciting high antigen-specific antibody concentrations confers no protection to young children in Western Kenya. PLoS One *4*, e4708.
Otto, T.D., Wilinski, D., Assefa, S., Keane, T.M., Sarry, L.R., Bohme, U., Lemieux, J., Barrell, B., Pain, A., Berriman, M*., et al.* (2010). New insights into the blood-stage transcriptome of *Plasmodium falciparum* using RNA-Seq. Mol Microbiol *76*, 12-24.

Pachebat, J.A., Ling, I.T., Grainger, M., Trucco, C., Howell, S., Fernandez-Reyes, D., Gunaratne, R., and Holder, A.A. (2001). The 22 kDa component of the protein complex on the surface of *Plasmodium falciparum* merozoites is derived from a larger precursor, merozoite surface protein 7. Molecular and Biochemical Parasitology *117*, 83-89.
Park, Y.J., Dyer, P.N., Tremethick, D.J., and Luger, K. (2004). A new fluorescence resonance energy transfer approach demonstrates that the histone variant H2AZ stabilizes the histone octamer within the nucleosome. The Journal of biological chemistry *279*, 24274-24282.
Pasini, E.M., Kirkegaard, M., Mortensen, P., Lutz, H.U., Thomas, A.W., and Mann, M. (2006). In-depth analysis of the membrane and cytosolic proteome of red blood cells. Blood *108*, 791-801.
Patil, V., Guerrant, W., Chen, P.C., Gryder, B., Benicewicz, D.B., Khan, S.I., Tekwani, B.L., and Oyelere, A.K. (2010). Antimalarial and antileishmanial activities of histone deacetylase inhibitors with triazole-linked cap group. Bioorg Med Chem *18*, 415-425.
Perell, G.T., Mishra, N.K., Sudhamalla, B., Ycas, P.D., Islam, K., and Pomerantz, W.C.K. (2017). Specific Acetylation Patterns of H2A.Z Form Transient Interactions with the BPTF Bromodomain. Biochemistry *56*, 4607-4615.
Perez-Salvia, M., and Esteller, M. (2017). Bromodomain inhibitors and cancer therapy: From structures to applications. Epigenetics *12*, 323-339.
Perez-Toledo, K., Rojas-Meza, A.P., Mancio-Silva, L., Hernandez-Cuevas, N.A., Delgadillo, D.M., Vargas, M., Martinez-Calvillo, S., Scherf, A., and Hernandez-Rivas, R. (2009). *Plasmodium falciparum* heterochromatin protein 1 binds to tri-methylated histone 3 lysine 9 and is linked to mutually exclusive expression of var genes. Nucleic Acids Res *37*, 2596-2606.
Petter, M., Lee, C.C., Byrne, T.J., Boysen, K.E., Volz, J., Ralph, S.A., Cowman, A.F., Brown, G.V., and Duffy, M.F. (2011). Expression of *P. falciparum* var genes involves exchange of the histone variant H2A.Z at the promoter. PLoS pathogens *7*, e1001292-e1001292.
Petter, M., Selvarajah, S.A., Lee, C.C., Chin, W.H., Gupta, A.P., Bozdech, Z., Brown, G.V., and Duffy, M.F. (2013). H2A.Z and H2B.Z double-variant nucleosomes define intergenic regions and dynamically occupy var gene promoters in the malaria parasite *Plasmodium falciparum*. Molecular Microbiology *87*, 1167-1182.
Phillips, M.A., Burrows, J.N., Manyando, C., van Huijsduijnen, R.H., Van Voorhis, W.C., and Wells, T.N.C. (2017). Malaria. Nature Reviews Disease Primers *3*, 17050.
Picaud, S., Leonards, K., Lambert, J.P., Dovey, O., Wells, C., Fedorov, O., Monteiro, O., Fujisawa, T., Wang, C.Y., Lingard, H.*, et al.* (2016). Promiscuous targeting of bromodomains by bromosporine identifies BET proteins as master regulators of primary transcription response in leukemia. Sci Adv *2*, e1600760.
Pillai, A.D., Nguitragool, W., Lyko, B., Dolinta, K., Butler, M.M., Nguyen, S.T., Peet, N.P., Bowlin, T.L., and Desai, S.A. (2012). Solute restriction reveals an essential role for clag3-associated channels in malaria parasite nutrient acquisition. Molecular pharmacology *82*, 1104-1114.
Ponnudurai, T., Leeuwenberg, A.D., and Meuwissen, J.H. (1981). Chloroquine sensitivity of isolates of *Plasmodium falciparum* adapted to in vitro culture. Tropical and geographical medicine *33*, 50-54.
Ponts, N., Fu, L., Harris, E.Y., Zhang, J., Chung, D.W., Cervantes, M.C., Prudhomme, J., Atanasova-Penichon, V., Zehraoui, E., Bunnik, E.M.*, et al.* (2013). Genome-wide mapping of DNA methylation in the human malaria parasite *Plasmodium falciparum*. Cell Host Microbe *14*, 696-706.

Ponts, N., Harris, E.Y., Prudhomme, J., Wick, I., Eckhardt-Ludka, C., Hicks, G.R., Hardiman, G., Lonardi, S., and Le Roch, K.G. (2010). Nucleosome landscape and control of transcription in the human malaria parasite. Genome Res *20*, 228-238.
Ponts, N., Saraf, A., Chung, D.W., Harris, A., Prudhomme, J., Washburn, M.P., Florens, L., and Le Roch, K.G. (2011). Unraveling the ubiquitome of the human malaria parasite. The Journal of biological chemistry *286*, 40320-40330.
Ponts, N., Yang, J., Chung, D.-W.D., Prudhomme, J., Girke, T., Horrocks, P., and Le Roch, K.G. (2008). Deciphering the ubiquitin-mediated pathway in apicomplexan parasites: a potential strategy to interfere with parasite virulence. PloS one *3*, e2386-e2386.
Poran, A., Notzel, C., Aly, O., Mencia-Trinchant, N., Harris, C.T., Guzman, M.L., Hassane, D.C., Elemento, O., and Kafsack, B.F.C. (2017). Single-cell RNA sequencing reveals a signature of sexual commitment in malaria parasites. Nature *551*, 95-99.
Prasad, R., Atul, Kolla, V.K., Legac, J., Singhal, N., Navale, R., Rosenthal, P.J., and Sijwali, P.S. (2013). Blocking *Plasmodium falciparum* development via dual inhibition of hemoglobin degradation and the ubiquitin proteasome system by MG132. PLoS One *8*, e73530.
Prommana, P., Uthaipibull, C., Wongsombat, C., Kamchonwongpaisan, S., Yuthavong, Y., Knuepfer, E., Holder, A.A., and Shaw, P.J. (2013). Inducible Knockdown of *Plasmodium* Gene Expression Using the glmS Ribozyme. PLOS ONE *8*, e73783.
Quinlan, A.R., and Hall, I.M. (2010). BEDTools: a flexible suite of utilities for comparing genomic features. Bioinformatics (Oxford, England) *26*, 841-842.
Raisner, R.M., Hartley, P.D., Meneghini, M.D., Bao, M.Z., Liu, C.L., Schreiber, S.L., Rando, O.J., and Madhani, H.D. (2005). Histone Variant H2A.Z Marks the 5′ Ends of Both Active and Inactive Genes in Euchromatin. Cell *123*, 233-248.
Raj, D.K., Nixon, C.P., Nixon, C.E., Dvorin, J.D., DiPetrillo, C.G., Pond-Tor, S., Wu, H.-W., Jolly, G., Pischel, L., Lu, A.*, et al.* (2014). Antibodies to PfSEA-1 block parasite egress from RBCs and protect against malaria infection. Science *344*, 871.
Ralph, S.A., Scheidig-Benatar, C., and Scherf, A. (2005). Antigenic variation in *Plasmodium falciparum* is associated with movement of *var* loci between subnuclear locations. Proceedings of the National Academy of Sciences of the United States of America *102*, 5414.
Rambaut, A. (2009). FigTree, version 1.4.3 (website: http://tree.bio.ed.ac.uk/software/figtree/).
Ramírez, F., Dündar, F., Diehl, S., Grüning, B.A., and Manke, T. (2014). deepTools: a flexible platform for exploring deep-sequencing data. Nucleic acids research *42*, W187-W191.
Rask, T.S., Hansen, D.A., Theander, T.G., Gorm Pedersen, A., and Lavstsen, T. (2010). *Plasmodium falciparum* erythrocyte membrane protein 1 diversity in seven genomes--divide and conquer. PLoS Comput Biol *6*, e1000933.
Ravish, I., and Raghav, N. (2014). Curcumin as inhibitor of mammalian Cathepsin B, Cathepsin H, acid phosphatase and alkaline phosphatase: A correlation with pharmacological activities. Medicinal Chemistry Research *23*.
Reid, A.J., Talman, A.M., Bennett, H.M., Gomes, A.R., Sanders, M.J., Illingworth, C.J.R., Billker, O., Berriman, M., and Lawniczak, M.K. (2018). Single-cell RNA-seq reveals hidden transcriptional variation in malaria parasites. Elife *7*.
Reifsnyder, C., Lowell, J., Clarke, A., and Pillus, L. (1996). Yeast SAS silencing genes and human genes associated with AML and HIV-1 Tat interactions are homologous with acetyltransferases. Nature genetics *14*, 42-49.
Ren, Q., and Gorovsky, M.A. (2001). Histone H2A.Z acetylation modulates an essential charge patch. Mol Cell *7*, 1329-1335.

Riglar, D.T., Richard, D., Wilson, D.W., Boyle, M.J., Dekiwadia, C., Turnbull, L., Angrisano, F., Marapana, D.S., Rogers, K.L., Whitchurch, C.B.*, et al.* (2011). Super-Resolution Dissection of Coordinated Events during Malaria Parasite Invasion of the Human Erythrocyte. Cell Host & Microbe *9*, 9-20.
Ritchie, M.E., Phipson, B., Wu, D., Hu, Y., Law, C.W., Shi, W., and Smyth, G.K. (2015). limma powers differential expression analyses for RNA-sequencing and microarray studies. Nucleic Acids Research *43*, e47-e47.
Robinson, J.T., Thorvaldsdóttir, H., Winckler, W., Guttman, M., Lander, E.S., Getz, G., and Mesirov, J.P. (2011). Integrative genomics viewer. Nature Biotechnology *29*, 24-26.
Robinson, M.D., McCarthy, D.J., and Smyth, G.K. (2009). edgeR: a Bioconductor package for differential expression analysis of digital gene expression data. Bioinformatics (Oxford, England) *26*, 139-140.
Rogerson, S.J., Hviid, L., Duffy, P.E., Leke, R.F., and Taylor, D.W. (2007). Malaria in pregnancy: pathogenesis and immunity. The Lancet Infectious diseases *7*, 105-117.
Roper, C., Pearce, R., Nair, S., Sharp, B., Nosten, F., and Anderson, T. (2004). Intercontinental Spread of Pyrimethamine-Resistant Malaria. Science *305*, 1124.
Rovira-Graells, N., Gupta, A.P., Planet, E., Crowley, V.M., Mok, S., Ribas de Pouplana, L., Preiser, P.R., Bozdech, Z., and Cortes, A. (2012). Transcriptional variation in the malaria parasite *Plasmodium falciparum*. Genome Res *22*, 925-938.
Rowe, J.A., Claessens, A., Corrigan, R.A., and Arman, M. (2009). Adhesion of *Plasmodium falciparum*-infected erythrocytes to human cells: molecular mechanisms and therapeutic implications. Expert reviews in molecular medicine *11*, e16.
Rudolph, D., Steegmaier, M., Hoffmann, M., Grauert, M., Baum, A., Quant, J., Haslinger, C., Garin-Chesa, P., and Adolf, G.R. (2009). BI 6727, a Polo-like kinase inhibitor with improved pharmacokinetic profile and broad antitumor activity. Clin Cancer Res *15*, 3094-3102.
Ruecker, A., Shea, M., Hackett, F., Suarez, C., Hirst, E.M.A., Milutinovic, K., Withers-Martinez, C., and Blackman, M.J. (2012). Proteolytic Activation of the Essential Parasitophorous Vacuole Cysteine Protease SERA6 Accompanies Malaria Parasite Egress from Its Host Erythrocyte. Journal of Biological Chemistry *287*, 37949-37963.
Runcie, A.C., Zengerle, M., Chan, K.H., Testa, A., van Beurden, L., Baud, M.G.J., Epemolu, O., Ellis, L.C.J., Read, K.D., Coulthard, V.*, et al.* (2018). Optimization of a "bump-and-hole" approach to allele-selective BET bromodomain inhibition. Chem Sci *9*, 2452-2468.
Sakamaki, J.-i., Wilkinson, S., Hahn, M., Tasdemir, N., O'Prey, J., Clark, W., Hedley, A., Nixon, C., Long, J.S., New, M.*, et al.* (2017). Bromodomain Protein BRD4 Is a Transcriptional Repressor of Autophagy and Lysosomal Function. Molecular Cell *66*, 517-532.e519.
Salanti, A., Staalsoe, T., Lavstsen, T., Jensen, A.T., Sowa, M.P., Arnot, D.E., Hviid, L., and Theander, T.G. (2003). Selective upregulation of a single distinctly structured var gene in chondroitin sulphate A-adhering *Plasmodium falciparum* involved in pregnancy-associated malaria. Mol Microbiol *49*, 179-191.
Salcedo-Amaya, A.M., van Driel, M.A., Alako, B.T., Trelle, M.B., van den Elzen, A.M., Cohen, A.M., Janssen-Megens, E.M., van de Vegte-Bolmer, M., Selzer, R.R., Iniguez, A.L.*, et al.* (2009). Dynamic histone H3 epigenome marking during the intraerythrocytic cycle of *Plasmodium falciparum*. Proc Natl Acad Sci U S A *106*, 9655-9660.
Sam-Yellowe, T.Y., Fujioka, H., Aikawa, M., and Messineo, D.G. (1995). *Plasmodium falciparum* Rhoptry Proteins of 140/130/110 kd (Rhop-H) Are Located in an Electron Lucent Compartment in the Neck of the Rhoptries. Journal of Eukaryotic Microbiology *42*, 224-231.
Sanchez, R., and Zhou, M.-M. (2009). The role of human bromodomains in chromatin biology and gene transcription. Curr Opin Drug Discov Devel *12*, 659-665.

Sanders, S.L., Jennings, J., Canutescu, A., Link, A.J., and Weil, P.A. (2002). Proteomics of the Eukaryotic Transcription Machinery: Identification of Proteins Associated with Components of Yeast TFIID by Multidimensional Mass Spectrometry. Molecular and Cellular Biology *22*, 4723.
Santos, J., Josling, G., Ross, P., Joshi, P., Orchard, L., Campbell, T., Schieler, A., Cristea, I., and Llinás, M. (2017). Red Blood Cell Invasion by the Malaria Parasite Is Coordinated by the PfAP2-I Transcription Factor. Cell Host and Microbe *21*, 731-741.e710.
Saraf, A., Cervantes, S., Bunnik, E.M., Ponts, N., Sardiu, M.E., Chung, D.W., Prudhomme, J., Varberg, J.M., Wen, Z., Washburn, M.P.*, et al.* (2016). Dynamic and Combinatorial Landscape of Histone Modifications during the Intraerythrocytic Developmental Cycle of the Malaria Parasite. Journal of proteome research *15*, 2787-2801.
Sautel, C.F., Cannella, D., Bastien, O., Kieffer, S., Aldebert, D., Garin, J., Tardieux, I., Belrhali, H., and Hakimi, M.A. (2007). SET8-mediated methylations of histone H4 lysine 20 mark silent heterochromatic domains in apicomplexan genomes. Mol Cell Biol *27*, 5711-5724.
Scherf, A., Hernandez-Rivas, R., Buffet, P., Bottius, E., Benatar, C., Pouvelle, B., Gysin, J., and Lanzer, M. (1998). Antigenic variation in malaria: in situ switching, relaxed and mutually exclusive transcription of var genes during intra-erythrocytic development in *Plasmodium falciparum*. EMBO J *17*, 5418-5426.
Schöffski, P., Blay, J.-Y., De Greve, J., Brain, E., Machiels, J.-P., Soria, J.-C., Sleijfer, S., Wolter, P., Ray-Coquard, I., Fontaine, C.*, et al.* (2010). Multicentric parallel phase II trial of the polo-like kinase 1 inhibitor BI 2536 in patients with advanced head and neck cancer, breast cancer, ovarian cancer, soft tissue sarcoma and melanoma. The first protocol of the European Organization for Research and Treatment of Cancer (EORTC) Network Of Core Institutes (NOCI). European Journal of Cancer *46*, 2206-2215.
Schrodinger, LLC (2015). The PyMOL Molecular Graphics System, Version 1.8.
Schwach, Schwach, F., Bushell, E., Gomes, A., Anar, B., Girling, G., Herd, C., Rayner, J., and Billker, O. (2015). PlasmoGEM, a database supporting a community resource for large-scale experimental genetics in malaria parasites. Nucleic acids research *43*, D1176-D1182.
Sebastian, M., Reck, M., Waller, C.F., Kortsik, C., Frickhofen, N., Schuler, M., Fritsch, H., Gaschler-Markefski, B., Hanft, G., Munzert, G.*, et al.* (2010). The Efficacy and Safety of BI 2536, a Novel Plk-1 Inhibitor, in Patients with Stage IIIB/IV Non-small Cell Lung Cancer Who Had Relapsed after, or Failed, Chemotherapy: Results from an Open-Label, Randomized Phase II Clinical Trial. Journal of Thoracic Oncology *5*, 1060-1067.
Sen, U., Saxena, H., Khurana, J., Nayak, A., and Gupta, A. (2018). *Plasmodium falciparum* RUVBL3 protein: a novel DNA modifying enzyme and an interacting partner of essential HAT protein MYST. Sci Rep *8*, 10917-10917.
Sharma, P., Wollenberg, K., Sellers, M., Zainabadi, K., Galinsky, K., Moss, E., Nguitragool, W., Neafsey, D., and Desai, S.A. (2013). An epigenetic antimalarial resistance mechanism involving parasite genes linked to nutrient uptake. Journal of Biological Chemistry.
Sheehy, S.H., Duncan, C.J., Elias, S.C., Choudhary, P., Biswas, S., Halstead, F.D., Collins, K.A., Edwards, N.J., Douglas, A.D., Anagnostou, N.A.*, et al.* (2012). ChAd63-MVA-vectored blood-stage malaria vaccines targeting MSP1 and AMA1: assessment of efficacy against mosquito bite challenge in humans. Molecular therapy : the journal of the American Society of Gene Therapy *20*, 2355-2368.
Shen, B., and Sibley, L.D. (2012). The moving junction, a key portal to host cell invasion by apicomplexan parasites. Curr Opin Microbiol *15*, 449-455.
Sherling, E.S., Knuepfer, E., Brzostowski, J.A., Miller, L.H., Blackman, M.J., and Ooij, C.v. (2017). The *Plasmodium falciparum* rhoptry protein RhopH3 plays essential roles in host cell invasion and nutrient uptake. eLife *6*, e23239.

Sidik, Sidik, S., Huet, D., Ganesan, S., Huynh, M.-H., Wang, T., Nasamu, A., Thiru, P., Saeij, J.P.J., Carruthers, V.*, et al.* (2016). A Genome-wide CRISPR Screen in *Toxoplasma* Identifies Essential Apicomplexan Genes. Cell *166*, 1423-1435.e1412.
Sierra-Miranda, M., Vembar, S.S., Delgadillo, D.M., Avila-Lopez, P.A., Herrera-Solorio, A.M., Lozano Amado, D., Vargas, M., and Hernandez-Rivas, R. (2017). PfAP2Tel, harbouring a non-canonical DNA-binding AP2 domain, binds to *Plasmodium falciparum* telomeres. Cell Microbiol *19*.
Sievers, F., Wilm, A., Dineen, D., Gibson, T.J., Karplus, K., Li, W., Lopez, R., McWilliam, H., Remmert, M., Söding, J.*, et al.* (2011). Fast, scalable generation of high-quality protein multiple sequence alignments using Clustal Omega. Mol Syst Biol *7*, 539-539.
Silberhorn, E., Schwartz, U., Loffler, P., Schmitz, S., Symelka, A., de Koning-Ward, T., Merkl, R., and Langst, G. (2016). *Plasmodium falciparum* Nucleosomes Exhibit Reduced Stability and Lost Sequence Dependent Nucleosome Positioning. PLoS Pathog *12*, e1006080.
Singh, B., and Daneshvar, C. (2013). Human Infections and Detection of *Plasmodium knowlesi*. Clinical Microbiology Reviews *26*, 165.
Singh, S., Alam, M.M., Pal-Bhowmick, I., Brzostowski, J.A., and Chitnis, C.E. (2010). Distinct External Signals Trigger Sequential Release of Apical Organelles during Erythrocyte Invasion by Malaria Parasites. PLOS Pathogens *6*, e1000746.
Sinha, A., Hughes, K.R., Modrzynska, K.K., Otto, T.D., Pfander, C., Dickens, N.J., Religa, A.A., Bushell, E., Graham, A.L., Cameron, R.*, et al.* (2014). A cascade of DNA-binding proteins for sexual commitment and development in *Plasmodium*. Nature *507*, 253-257.
Smith, J.D., Chitnis, C.E., Craig, A.G., Roberts, D.J., Hudson-Taylor, D.E., Peterson, D.S., Pinches, R., Newbold, C.I., and Miller, L.H. (1995). Switches in expression of *Plasmodium falciparum* var genes correlate with changes in antigenic and cytoadherent phenotypes of infected erythrocytes. Cell *82*, 101-110.
Spangenberg, T., Burrows, J.N., Kowalczyk, P., McDonald, S., Wells, T.N.C., and Willis, P. (2013). The Open Access Malaria Box: A Drug Discovery Catalyst for Neglected Diseases. PLOS ONE *8*, e62906.
Stafford, W.H.L., Günder, B., Harris, A., Heidrich, H.-G., Holder, A.A., and Blackman, M.J. (1996). A 22 kDa protein associated with the *Plasmodium falciparum* merozoite surface protein-1 complex. Molecular and Biochemical Parasitology *80*, 159-169.
Steegmaier, M., Hoffmann, M., Baum, A., Lenart, P., Petronczki, M., Krssak, M., Gurtler, U., Garin-Chesa, P., Lieb, S., Quant, J.*, et al.* (2007). BI 2536, a potent and selective inhibitor of polo-like kinase 1, inhibits tumor growth in vivo. Current biology : CB *17*, 316-322.
Strobl, J.S., Cassell, M., Mitchell, S.M., Reilly, C.M., and Lindsay, D.S. (2007). Scriptaid and suberoylanilide hydroxamic acid are histone deacetylase inhibitors with potent anti-*Toxoplasma gondii* activity in vitro. J Parasitol *93*, 694-700.
Strohner, R., Németh, A., Nightingale, K.P., Grummt, I., Becker, P.B., and Längst, G. (2004). Recruitment of the nucleolar remodeling complex NoRC establishes ribosomal DNA silencing in chromatin. Molecular and cellular biology *24*, 1791-1798.
Stubbs, J., Simpson, K.M., Triglia, T., Plouffe, D., Tonkin, C.J., Duraisingh, M.T., Maier, A.G., Winzeler, E.A., and Cowman, A.F. (2005). Molecular mechanism for switching of *P. falciparum* invasion pathways into human erythrocytes. Science *309*, 1384-1387.
Su, X.Z., Heatwole, V.M., Wertheimer, S.P., Guinet, F., Herrfeldt, J.A., Peterson, D.S., Ravetch, J.A., and Wellems, T.E. (1995). The large diverse gene family var encodes proteins involved in cytoadherence and antigenic variation of *Plasmodium falciparum*-infected erythrocytes. Cell *82*, 89-100.
Suarez, C., Volkmann, K., Gomes, A.R., Billker, O., and Blackman, M.J. (2013). The malarial serine protease SUB1 plays an essential role in parasite liver stage development. PLoS pathogens *9*, e1003811-e1003811.

Sullivan, W.J., Jr., Naguleswaran, A., and Angel, S.O. (2006). Histones and histone modifications in protozoan parasites. Cell Microbiol *8*, 1850-1861.
Sun, Z., Zhang, H., Chen, Z., Xie, Y., Jiang, H., Chen, L., Ding, H., Zhang, Y., Jiang, H., Zheng, M.*, et al.* (2017). Discovery of novel BRD4 inhibitors by high-throughput screening, crystallography, and cell-based assays. Bioorganic & Medicinal Chemistry Letters *27*, 2003-2009.
Supek, F., Bošnjak, M., Škunca, N., and Šmuc, T. (2011). REVIGO Summarizes and Visualizes Long Lists of Gene Ontology Terms. PLOS ONE *6*, e21800.
Suto, R.K., Clarkson, M.J., Tremethick, D.J., and Luger, K. (2000). Crystal structure of a nucleosome core particle containing the variant histone H2A.Z. Nature structural biology *7*, 1121-1124.
Swamy, L., Amulic, B., and Deitsch, K.W. (2011). *Plasmodium falciparum* var gene silencing is determined by cis DNA elements that form stable and heritable interactions. Eukaryotic cell *10*, 530-539.
Talbert, P.B., Ahmad, K., Almouzni, G., Ausio, J., Berger, F., Bhalla, P.L., Bonner, W.M., Cande, W.Z., Chadwick, B.P., Chan, S.W.*, et al.* (2012). A unified phylogeny-based nomenclature for histone variants. Epigenetics Chromatin *5*, 7.
Tallant, C., Valentini, E., Fedorov, O., Overvoorde, L., Ferguson, Fleur M., Filippakopoulos, P., Svergun, Dmitri I., Knapp, S., and Ciulli, A. (2015). Molecular Basis of Histone Tail Recognition by Human TIP5 PHD Finger and Bromodomain of the Chromatin Remodeling Complex NoRC. Structure *23*, 80-92.
Tarr, S.J., Withers-Martinez, C., Flynn, H.R., Snijders, A.P., Masino, L., Koussis, K., Conway, D.J., and Blackman, M.J. (2020). A malaria parasite subtilisin propeptide-like protein is a potent inhibitor of the egress protease SUB1. Biochem J *477*, 525-540.
Tawk, L., Lacroix, C., Gueirard, P., Kent, R., Gorgette, O., Thiberge, S., Mercereau-Puijalon, O., Ménard, R., and Barale, J.-C. (2013). A Key Role for *Plasmodium* Subtilisin-like SUB1 Protease in Egress of Malaria Parasites from Host Hepatocytes. Journal of Biological Chemistry *288*, 33336-33346.
Taylor, L.H., and Read, A.F. (1997). Why so few transmission stages? Reproductive restraint by malaria parasites. Parasitology today (Personal ed) *13*, 135-140.
Templeton, T.J., Iyer, L.M., Anantharaman, V., Enomoto, S., Abrahante, J.E., Subramanian, G.M., Hoffman, S.L., Abrahamsen, M.S., and Aravind, L. (2004). Comparative Analysis of Apicomplexa and Genomic Diversity in Eukaryotes. Genome Res *14*, 1686-1695.
Tham, W.-H., Healer, J., and Cowman, A.F. (2012). Erythrocyte and reticulocyte binding-like proteins of *Plasmodium falciparum*. Trends in Parasitology *28*, 23-30.
Thambirajah, A.A., Dryhurst, D., Ishibashi, T., Li, A., Maffey, A.H., and Ausio, J. (2006). H2A.Z stabilizes chromatin in a way that is dependent on core histone acetylation. The Journal of biological chemistry *281*, 20036-20044.
Thomas, J.A., Tan, M.S.Y., Bisson, C., Borg, A., Umrekar, T.R., Hackett, F., Hale, V.L., Vizcay-Barrena, G., Fleck, R.A., Snijders, A.P.*, et al.* (2018). A protease cascade regulates release of the human malaria parasite *Plasmodium falciparum* from host red blood cells. Nature microbiology *3*, 447-455.
Thomson, R., Beshir, K.B., Cunningham, J., Baiden, F., Bharmal, J., Bruxvoort, K.J., Maiteki-Sebuguzi, C., Owusu-Agyei, S., Staedke, S.G., and Hopkins, H. (2019). *pfhrp2* and *pfhrp3* Gene Deletions That Affect Malaria Rapid Diagnostic Tests for *Plasmodium falciparum*: Analysis of Archived Blood Samples From 3 African Countries. The Journal of infectious diseases *220*, 1444-1452.
Tibúrcio, M., Yang, A.S.P., Yahata, K., Suárez-Cortés, P., Belda, H., Baumgarten, S., van de Vegte-Bolmer, M., van Gemert, G.-J., van Waardenburg, Y., Levashina, E.A.*, et al.* (2019).

A Novel Tool for the Generation of Conditional Knockouts To Study Gene Function across the *Plasmodium falciparum* Life Cycle. mBio *10*, e01170-01119.
Tillo, D., and Hughes, T.R. (2009). G+C content dominates intrinsic nucleosome occupancy. BMC bioinformatics *10*, 442.
Toenhake, Toenhake, C., Fraschka, S., Vijayabaskar, M., Westhead, D., van Heeringen, S., and Bártfai, R. (2018). Chromatin Accessibility-Based Characterization of the Gene Regulatory Network Underlying *Plasmodium falciparum* Blood-Stage Development. Cell Host and Microbe *23*, 557-569.e559.
Tonkin, C.J., Carret, C.K., Duraisingh, M.T., Voss, T.S., Ralph, S.A., Hommel, M., Duffy, M.F., Silva, L.M.d., Scherf, A., Ivens, A.*, et al.* (2009). Sir2 Paralogues Cooperate to Regulate Virulence Genes and Antigenic Variation in *Plasmodium falciparum*. PLOS Biology *7*, e1000084.
Tonkin, M.L., Roques, M., Lamarque, M.H., Pugnière, M., Douguet, D., Crawford, J., Lebrun, M., and Boulanger, M.J. (2011). Host Cell Invasion by Apicomplexan Parasites: Insights from the Co-Structure of AMA1 with a RON2 Peptide. Science *333*, 463.
Trager, W., and Jenson, J.B. (1978). Cultivation of malarial parasites. Nature *273*, 621-622.
Trelle, M.B., Salcedo-Amaya, A.M., Cohen, A.M., Stunnenberg, H.G., and Jensen, O.N. (2009). Global histone analysis by mass spectrometry reveals a high content of acetylated lysine residues in the malaria parasite *Plasmodium falciparum*. Journal of proteome research *8*, 3439-3450.
Trucco, C., Fernandez-Reyes, D., Howell, S., Stafford, W.H., Scott-Finnigan, T.J., Grainger, M., Ogun, S.A., Taylor, W.R., and Holder, A.A. (2001). The merozoite surface protein 6 gene codes for a 36 kDa protein associated with the *Plasmodium falciparum* merozoite surface protein-1 complex. Molecular and Biochemical Parasitology *112*, 91-101.
Ukaegbu, U.E., Kishore, S.P., Kwiatkowski, D.L., Pandarinath, C., Dahan-Pasternak, N., Dzikowski, R., and Deitsch, K.W. (2014). Recruitment of PfSET2 by RNA Polymerase II to Variant Antigen Encoding Loci Contributes to Antigenic Variation in P. falciparum. PLOS Pathogens *10*, e1003854.
Valdes-Mora, F., Song, J.Z., Statham, A.L., Strbenac, D., Robinson, M.D., Nair, S.S., Patterson, K.I., Tremethick, D.J., Stirzaker, C., and Clark, S.J. (2012). Acetylation of H2A.Z is a key epigenetic modification associated with gene deregulation and epigenetic remodeling in cancer. Genome Res *22*, 307-321.
Vembar, S.S., Macpherson, C.R., Sismeiro, O., Coppée, J.-Y., and Scherf, A. (2015). The PfAlba1 RNA-binding protein is an important regulator of translational timing in *Plasmodium falciparum* blood stages. Genome Biology *16*, 212.
Verma, G., and Surolia, N. (2013). *Plasmodium falciparum* CENH3 is able to functionally complement Cse4p and its, C-terminus is essential for centromere function. Mol Biochem Parasitol *192*, 21-29.
Vivax Sporozoite, C. (2019). Transcriptome and histone epigenome of *Plasmodium vivax* salivary-gland sporozoites point to tight regulatory control and mechanisms for liver-stage differentiation in relapsing malaria. Int J Parasitol *49*, 501-513.
Volz, J., Carvalho, T.G., Ralph, S.A., Gilson, P., Thompson, J., Tonkin, C.J., Langer, C., Crabb, B.S., and Cowman, A.F. (2010). Potential epigenetic regulatory proteins localise to distinct nuclear sub-compartments in *Plasmodium falciparum*. Int J Parasitol *40*, 109-121.
Volz, J.C., Bartfai, R., Petter, M., Langer, C., Josling, G.A., Tsuboi, T., Schwach, F., Baum, J., Rayner, J.C., Stunnenberg, H.G.*, et al.* (2012). PfSET10, a *Plasmodium falciparum* methyltransferase, maintains the active var gene in a poised state during parasite division. Cell Host Microbe *11*, 7-18.

Voss, T.S., Healer, J., Marty, A.J., Duffy, M.F., Thompson, J.K., Beeson, J.G., Reeder, J.C., Crabb, B.S., and Cowman, A.F. (2006). A var gene promoter controls allelic exclusion of virulence genes in *Plasmodium falciparum* malaria. Nature *439*, 1004-1008.
Voss, T.S., Kaestli, M., Vogel, D., Bopp, S., and Beck, H.P. (2003). Identification of nuclear proteins that interact differentially with *Plasmodium falciparum* var gene promoters. Mol Microbiol *48*, 1593-1607.
Voss, T.S., Tonkin, C.J., Marty, A.J., Thompson, J.K., Healer, J., Crabb, B.S., and Cowman, A.F. (2007). Alterations in local chromatin environment are involved in silencing and activation of subtelomeric var genes in *Plasmodium falciparum*. Mol Microbiol *66*, 139-150.
Wang, H., Bloom, O., Zhang, M., Vishnubhakat, J.M., Ombrellino, M., Che, J., Frazier, A., Yang, H., Ivanova, S., Borovikova, L.*, et al.* (1999a). HMG-1 as a late mediator of endotoxin lethality in mice. Science *285*, 248-251.
Wang, H., Vishnubhakat, J.M., Bloom, O., Zhang, M., Ombrellino, M., Sama, A., and Tracey, K.J. (1999b). Proinflammatory cytokines (tumor necrosis factor and interleukin 1) stimulate release of high mobility group protein-1 by pituicytes. Surgery *126*, 389-392.
Wang, R., Li, Q., Helfer, C.M., Jiao, J., and You, J. (2012). Bromodomain protein Brd4 associated with acetylated chromatin is important for maintenance of higher-order chromatin structure. The Journal of biological chemistry *287*, 10738-10752.
Wang, W.-F., and Zhang, Y.-L. (2020). PfSWIB, a potential chromatin regulator for var gene regulation and parasite development in *Plasmodium falciparum*. Parasit Vectors *13*, 48.
Waterhouse, A.M., Procter, J.B., Martin, D.M.A., Clamp, M., and Barton, G.J. (2009). Jalview Version 2—a multiple sequence alignment editor and analysis workbench. Bioinformatics (Oxford, England) *25*, 1189-1191.
Weiss, G.E., Gilson, P.R., Taechalertpaisarn, T., Tham, W.-H., de Jong, N.W.M., Harvey, K.L., Fowkes, F.J.I., Barlow, P.N., Rayner, J.C., Wright, G.J.*, et al.* (2015). Revealing the sequence and resulting cellular morphology of receptor-ligand interactions during *Plasmodium falciparum* invasion of erythrocytes. PLoS pathogens *11*, e1004670-e1004670.
Wernimont, A., and Edwards, A. (2009). In situ proteolysis to generate crystals for structure determination: an update. PloS one *4*, e5094-e5094.
Wernimont, A.K., Amaya, M.F., Lam, A., Ali, A., Zhang, A.Z., Kenzina, L., Lin, Y.H., Mackenzie, F., Kozieradzki, I., Cossar, D.*, et al. Plasmodium falciparum* bromodomain-containing protein PF10_0328.
Wernimont, A.K., Loppnau, P., Knapp, S., Fonseca, M., Brennan, P.E., Dong, A., Walker, J.R., Arrowsmith, C.H., Edwards, A.M., Bountra, C.*, et al.* Crystal Structure of PF3D7_1475600, a bromodomain from *Plasmodium falciparum*.
Westenberger, S.J., Cui, L., Dharia, N., Winzeler, E., and Cui, L. (2009). Genome-wide nucleosome mapping of *Plasmodium falciparum* reveals histone-rich coding and histone-poor intergenic regions and chromatin remodeling of core and subtelomeric genes. BMC Genomics *10*, 610.
WHO (2019). The World malaria report.
Wickham, M.E., Culvenor, J.G., and Cowman, A.F. (2003). Selective Inhibition of a Two-step Egress of Malaria Parasites from the Host Erythrocyte. Journal of Biological Chemistry *278*, 37658-37663.
Wilde, M.L., Triglia, T., Marapana, D., Thompson, J.K., Kouzmitchev, A.A., Bullen, H.E., Gilson, P.R., Cowman, A.F., and Tonkin, C.J. (2019). Protein Kinase A Is Essential for Invasion of *Plasmodium falciparum* into Human Erythrocytes. mBio *10*.
Wilson, D.W., Crabb, B.S., and Beeson, J.G. (2010). Development of fluorescent Plasmodium falciparum for in vitro growth inhibition assays. Malaria Journal *9*, 152.
Withers-Martinez, C., Suarez, C., Fulle, S., Kher, S., Penzo, M., Ebejer, J.-P., Koussis, K., Hackett, F., Jirgensons, A., Finn, P.*, et al.* (2012). *Plasmodium* subtilisin-like protease 1

(SUB1): Insights into the active-site structure, specificity and function of a pan-malaria drug target. International Journal for Parasitology *42*, 597-612.
Woehlbier, U., Epp, C., Kauth, C.W., Lutz, R., Long, C.A., Coulibaly, B., Kouyaté, B., Arevalo-Herrera, M., Herrera, S., and Bujard, H. (2006). Analysis of antibodies directed against merozoite surface protein 1 of the human malaria parasite *Plasmodium falciparum*. Infection and Immunity *74*, 1313.
Wongsrichanalai, C., Pickard, A.L., Wernsdorfer, W.H., and Meshnick, S.R. (2002). Epidemiology of drug-resistant malaria. The Lancet Infectious Diseases *2*, 209-218.
Woychik, N.A., and Hampsey, M. (2002). The RNA Polymerase II Machinery: Structure Illuminates Function. Cell *108*, 453-463.
Wu, Q., Heidenreich, D., Zhou, S., Ackloo, S., Kramer, A., Nakka, K., Lima-Fernandes, E., Deblois, G., Duan, S., Vellanki, R.N.*, et al.* (2019). A chemical toolbox for the study of bromodomains and epigenetic signaling. Nat Commun *10*, 1915.
Wu, S.Y., Lee, A.Y., Hou, S.Y., Kemper, J.K., Erdjument-Bromage, H., Tempst, P., and Chiang, C.M. (2006). Brd4 links chromatin targeting to HPV transcriptional silencing. Genes Dev *20*, 2383-2396.
Xiao, B., Yin, S., Hu, Y., Sun, M., Wei, J., Huang, Z., Wen, Y., Dai, X., Chen, H., Mu, J.*, et al.* (2019). Epigenetic editing by CRISPR/dCas9 in *Plasmodium falciparum*. Proc Natl Acad Sci U S A *116*, 255-260.
Xie, S.C., Gillett, D.L., Spillman, N.J., Tsu, C., Luth, M.R., Ottilie, S., Duffy, S., Gould, A.E., Hales, P., Seager, B.A.*, et al.* (2018). Target Validation and Identification of Novel Boronate Inhibitors of the *Plasmodium falciparum* Proteasome. J Med Chem *61*, 10053-10066.
Xing, X., Zhang, L., Wen, X., Wang, X., Cheng, X., Du, H., Hu, Y., Li, L., Dong, B., Li, Z.*, et al.* (2014). PP242 suppresses cell proliferation, metastasis, and angiogenesis of gastric cancer through inhibition of the PI3K/AKT/mTOR pathway. Anticancer Drugs *25*, 1129-1140.
Yang, H., Wang, H., Czura, C.J., and Tracey, K.J. (2005). The cytokine activity of HMGB1. Journal of leukocyte biology *78*, 1-8.
Yang, S.Y. (2010). Pharmacophore modeling and applications in drug discovery: challenges and recent advances. Drug Discov Today *15*, 444-450.
Yap, A., Azevedo, M.F., Gilson, P.R., Weiss, G.E., O'Neill, M.T., Wilson, D.W., Crabb, B.S., and Cowman, A.F. (2014). Conditional expression of apical membrane antigen 1 in *Plasmodium falciparum* shows it is required for erythrocyte invasion by merozoites. Cellular microbiology *16*, 642-656.
Yasgar, A., Jadhav, A., Simeonov, A., and Coussens, N.P. (2016). AlphaScreen-Based Assays: Ultra-High-Throughput Screening for Small-Molecule Inhibitors of Challenging Enzymes and Protein-Protein Interactions. Methods Mol Biol *1439*, 77-98.
Yeoh, L.M., Goodman, C.D., Mollard, V., McFadden, G.I., and Ralph, S.A. (2017). Comparative transcriptomics of female and male gametocytes in *Plasmodium berghei* and the evolution of sex in alveolates. BMC Genomics *18*, 734.
Yeoh, S., O'Donnell, R.A., Koussis, K., Dluzewski, A.R., Ansell, K.H., Osborne, S.A., Hackett, F., Withers-Martinez, C., Mitchell, G.H., Bannister, L.H.*, et al.* (2007). Subcellular Discharge of a Serine Protease Mediates Release of Invasive Malaria Parasites from Host Erythrocytes. Cell *131*, 1072-1083.
Yin, H., Guo, Q., Li, X., Tang, T., Li, C., Wang, H., Sun, Y., Feng, Q., Ma, C., Gao, C.*, et al.* (2018). Curcumin Suppresses IL-1beta Secretion and Prevents Inflammation through Inhibition of the NLRP3 Inflammasome. Journal of immunology (Baltimore, Md : 1950) *200*, 2835-2846.

Yuda, M., Iwanaga, S., Kaneko, I., and Kato, T. (2015). Global transcriptional repression: An initial and essential step for *Plasmodium* sexual development. Proceedings of the National Academy of Sciences of the United States of America *112*, 12824-12829.
Yuda, M., Iwanaga, S., Shigenobu, S., Kato, T., and Kaneko, I. (2010). Transcription factor AP2-Sp and its target genes in malarial sporozoites. Mol Microbiol *75*, 854-863.
Yuda, M., Iwanaga, S., Shigenobu, S., Mair, G.R., Janse, C.J., Waters, A.P., Kato, T., and Kaneko, I. (2009). Identification of a transcription factor in the mosquito-invasive stage of malaria parasites. Mol Microbiol *71*, 1402-1414.
Zhang, M., Wang, C., Otto, T.D., Oberstaller, J., Liao, X., Adapa, S.R., Udenze, K., Bronner, I.F., Casandra, D., Mayho, M.*, et al.* (2018). Uncovering the essential genes of the human malaria parasite *Plasmodium falciparum* by saturation mutagenesis. Science *360*.
Zhang, Q., Huang, Y., Zhang, Y., Fang, X., Claes, A., Duchateau, M., Namane, A., Lopez-Rubio, J.J., Pan, W., and Scherf, A. (2011). A critical role of perinuclear filamentous actin in spatial repositioning and mutually exclusive expression of virulence genes in malaria parasites. Cell Host Microbe *10*, 451-463.
Zhang, Y., Liu, T., Meyer, C.A., Eeckhoute, J., Johnson, D.S., Bernstein, B.E., Nusbaum, C., Myers, R.M., Brown, M., Li, W.*, et al.* (2008). Model-based Analysis of ChIP-Seq (MACS). Genome Biology *9*, R137.
Zhou, M., Huang, K., Jung, K.-J., Cho, W.-K., Klase, Z., Kashanchi, F., Pise-Masison, C.A., and Brady, J.N. (2009). Bromodomain protein Brd4 regulates human immunodeficiency virus transcription through phosphorylation of CDK9 at threonine 29. J Virol *83*, 1036-1044.
Zilberman, D., Coleman-Derr, D., Ballinger, T., and Henikoff, S. (2008). Histone H2A.Z and DNA methylation are mutually antagonistic chromatin marks. Nature *456*, 125-129.
Zou, L.J., Xiang, Q.P., Xue, X.Q., Zhang, C., Li, C.C., Wang, C., Li, Q., Wang, R., Wu, S., Zhou, Y.L.*, et al.* (2019). Y08197 is a novel and selective CBP/EP300 bromodomain inhibitor for the treatment of prostate cancer. Acta Pharmacol Sin.

9. Appendices

Table 9.1 List of primers used in this study

Name	Target	Sequence
PCR primers		
HN47	PfBDP3 3' homology arm (KasI) Forward	AAAAAAGGCGCCAGTGCACATTGTGTATCCTCTTTTATATTT
HN48	PfBDP3 3' homology arm (BstAPI) Reverse	TATTATGCACCATATGCAACGGGCCCAATATATAGTTAAAAAAATG
HN52	PfBDP3 5' homology arm (BglII) Forward	AATAAAAGATCTGATGAGAACCTTATGAATAGTGACGATT
HN53	PfBDP3 5' homology arm (PstI) Reverse	ATATATCTGCAGCGGACGCTAATGCCATTACTCCAAAC
gRNA-3F	guide RNA Forward	ATTGTATATATATATATGACCCCG
gRNA-3R	guide RNA Reverse	AAACCGGGGTCATATATATATATA
MP27	HSP-70 5'UTR Forward	AAACAGAAGGGGCGAAATGG
MP28	HSP-70 5'UTR Reverse	GCAAGTTCAAGGGACTAAAATTCG
Test SP	PfBDP4 5' Forward	TTTCTTTTGTTTTTGTGTGAT

Test WT ASP	PfBDP4 5' wildtype Reverse	TCCATAGGTTCTTTTATGACA
loxPint ASP	PfBDP4 5' integration Reverse	ATATATGTATCTATTTATTCAAAAGTCT
MP421	PfBDP3 Forward	GCATACTAGTGAGGGTAATGGT
MP422	PfBDP3 wildtype Reverse	TGTAATAAGAATCTGTAGGAAAGA
HN41	PfBDP3 5' integration Reverse	GCAGCGGCATAATCTGGAAC
qPCR primers		
HN_qPCR_5	PfBDP4 intact Forward	CTCGTCAACTAAGCCTTTTTCCGGG
HN_qPCR_7	PfBDP4 intact Reverse	AAGTTCATAAAGGCTGCCGCATACC
MP31	HSP-70 CDS Forward	GGTATTCCACCTGCACCAAGAA
MP32	HSP-70 CDS Reverse	CAGCCGTAACGTTTAAGATACCGT
MP37	Casein Kinase 5'UTR Forward	TATATTCATGTCATGCACTCTTCCC
MP38	Casein Kinase 5'UTR Reverse	TTAAGTCAGGCGTTCTTAGAAATCTTT
MP39	Casein Kinase CDS Forward	TGGTGTACCTAAAGTATATTGGTACGGT
MP40	Casein Kinase CDS Reverse	AAGGGATGGGCCTAATAAATCAA
MP65	ETRAMP-10 5'UTR Forward	AAGTATACATTTGTCCGCCGAAA
MP66	ETRAMP-10 5'UTR Reverse	TGCATACAAGAACGACATTGAAATT
MP67	ETRAMP-10 CDS Forward	TTCCGTAGCTTCTGTTCTCGCT
MP68	ETRAMP-10 CDS Reverse	CCAAAACCTACACCAGCACCTAT
MP94	SBP 5'UTR Forward	GTATTATTATTATATACGTATCAATGTATGATC
MP95	SBP 5'UTR Reverse	ATGTAACATATGTATCATTATAAAGGGA

MD93	SBP CDS Forward	TTAGCCGACGAACCAACACA
MD94	SBP CDS Reverse	TTCGGTTGTCTCTGGTACTGCA
MP61	REX 5'UTR Forward	AATATTATAAAATATTAAAATTTTCTTGTATTCCT
MP62	REX 5'UTR Reverse	ACATATATATATAATATGTAAAAGAACGTGCA
MP63	REX CDS Forward	AAGATATGCAAAGCCCATTTGATT
MP64	REX CDS Reverse	GGGAGCAAAGATTGTGTACTTACGA
MP123	MSP-2 5'UTR Forward	GATCAAAATAGAAAATCATGTGCCATA
MP124	MSP-2 5'UTR Reverse	TGATCATCAGAACATCCACCATTAT
MP25	MSP-2 CDS Forward	TCCTGTACCTTTATTCTCTGGTG
MP26	MSP-2 CDS Reverse	CAAGCTGAAAATTCTGCTCC
MP57	EBA-175 5'UTR Forward	GATACAATTTGAATTACGTCATTCCA
MP58	EBA-175 5'UTR Reverse	TCTTATTTATTACTTTATTTGGTTTTCCTTGT
MP59	EBA-175 CDS Forward	GAACGGAAACTCGTACGGATGA
MP60	EBA-175 CDS Reverse	CTCTCCTACACTTTGTTGTGGATTCT
MP41	CSP 5'UTR Forward	GAGGGGTAAAGGGGGGCTTAA
MP42	CSP 5'UTR Reverse	AACATTATATGCTTCCTTAAGAACATATAGTGAAT
MP43	CSP CDS Forward	TCACTTGGAGAAAATGATGATGGA
MP44	CSP CDS Reverse	CCATCCGCTGGTTGCTTTA
MP45	SSP-2 5'UTR Forward	TTTTTACATGTATAGTGAATGAGGTGTCCT
MP46	SSP-2 5'UTR Reverse	TCAGATTTATTCAAACGCATGCTG
MP47	SSP-2 CDS Forward	CCTTCTAATGGATTGTTCTGGAAGT

MP48	SSP-2 CDS Reverse	TTTCATAGCTAGAGGTACTGCATGG
MP154	FIKK 5'UTR Forward	GAATCATGCGTACCAACTATAGGA
MP155	FIKK 5'UTR Reverse	CTATTGGTGTATATTCACGTTTTCC
MP156	FIKK CDS Forward	TGAGAAAAGCAAATTGAGTACTTTTAA
MP157	FIKK CDS Reverse	ATCTGGGGGTCCTACGATATAT

Table 9.2 Antibodies used in this study

Antibody	Western blot	ChIP	Source (catalogue number)
Primary antibodies			
Mouse anti-Ty1	1 in 10,000	5 µg	Sigma (SAB4800032)
Rabbit anti-Ty1		2 µg	GenScript (A01004)
Rabbit anti-Aldolase	1 in 2,500		Abcam (ab207494)
Rabbit anti-Histone 3	1 in 2,500		Abcam (ab1791)
Rat anti-HA	1 in 2,500		Roche (11867423001)
Secondary antibodies			
Goat anti-mouse IgG HRP	1 in 10,000		Invitrogen (62-6520)
Goat anti-rabbit IgG HRP	1 in 10,000		Invitrogen (65-6120)
Goat anti-rat IgG HRP	1 in 2,500		Abcam (ab97057)
Goat anti-mouse IgG Alexa Fluor 488	1 in 5,000		Invitrogen (A11001)

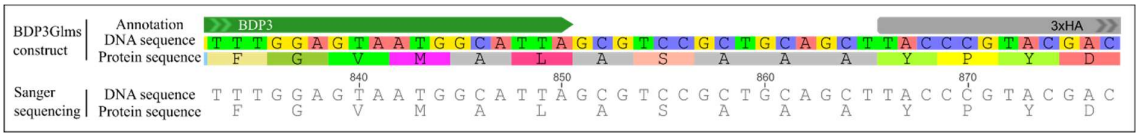

Figure 9.1 Sanger sequencing for donor plasmid of BDP3*glmS* parasite line indicating that HA was in frame with

Table 9.3 Genes enriched with PfBDP4 upstream. Genes overlapped with AP2-I and PfBDP1 highlighted in yellow.

PF3D7_0104200	PF3D7_0416800	PF3D7_0618500	PF3D7_0811000	PF3D7_0931300	PF3D7_1037000
PF3D7_0105900	PF3D7_0417200	PF3D7_0619400	PF3D7_0813100	PF3D7_0931600	PF3D7_1037400
PF3D7_0106000	PF3D7_0418400	PF3D7_0620400	PF3D7_0813200	PF3D7_0932200	PF3D7_1037900
PF3D7_0106800	PF3D7_0419300	PF3D7_0621100	PF3D7_0814900	PF3D7_0934200	PF3D7_1041300
PF3D7_0203600	PF3D7_0422300	PF3D7_0624500	PF3D7_0815400	PF3D7_0934800	PF3D7_1103800
PF3D7_0204100	PF3D7_0423400	PF3D7_0626100	PF3D7_0817800	PF3D7_0935500	PF3D7_1105000
PF3D7_0206300	PF3D7_0423700	PF3D7_0626400	PF3D7_0817900	PF3D7_0935800	PF3D7_1105100
PF3D7_0206800	PF3D7_0500100	PF3D7_0627300	PF3D7_0818200	PF3D7_1000100	PF3D7_1107100
PF3D7_0207000	PF3D7_0501500	PF3D7_0628100	PF3D7_0819700	PF3D7_1001700	PF3D7_1108400
PF3D7_0207400	PF3D7_0503400	PF3D7_0630400	PF3D7_0820200	PF3D7_1002900	PF3D7_1108600
PF3D7_0207500	PF3D7_0503600	PF3D7_0630600	PF3D7_0820300	PF3D7_1003000	PF3D7_1110100
PF3D7_0207600	PF3D7_0508000	PF3D7_0631000	PF3D7_0821000	PF3D7_1003600	PF3D7_1112900
PF3D7_0207700	PF3D7_0508900	PF3D7_0700100	PF3D7_0823200	PF3D7_1004200	PF3D7_1113300
PF3D7_0208500	PF3D7_0510200	PF3D7_0702700	PF3D7_0826400	PF3D7_1007700	PF3D7_1115100
PF3D7_0209600	PF3D7_0510500	PF3D7_0703600	PF3D7_0828900	PF3D7_1008100	PF3D7_1115800
PF3D7_0211600	PF3D7_0510900	PF3D7_0704300	PF3D7_0830100	PF3D7_1008700	PF3D7_1116100
PF3D7_0214900	PF3D7_0511200	PF3D7_0704800	PF3D7_0830400	PF3D7_1010700	PF3D7_1117400
PF3D7_0218000	PF3D7_0511600	PF3D7_0705900	PF3D7_0831600	PF3D7_1011000	PF3D7_1120200
PF3D7_0218100	PF3D7_0515700	PF3D7_0706400	PF3D7_0831700	PF3D7_1011400	PF3D7_1121000
PF3D7_0219400	PF3D7_0515900	PF3D7_0706800	PF3D7_0831800	PF3D7_1012200	PF3D7_1121300
PF3D7_0219600	PF3D7_0518200	PF3D7_0707300	PF3D7_0900100	PF3D7_1012300	PF3D7_1123100
PF3D7_0220300	PF3D7_0518300	PF3D7_0708700	PF3D7_0903300	PF3D7_1013000	PF3D7_1124200
PF3D7_0220800	PF3D7_0519200	PF3D7_0709800	PF3D7_0903600	PF3D7_1013200	PF3D7_1124600
PF3D7_0223500	PF3D7_0519900	PF3D7_0710600	PF3D7_0903700	PF3D7_1014900	PF3D7_1125000
PF3D7_0300100	PF3D7_0522400	PF3D7_0713700	PF3D7_0904700	PF3D7_1015700	PF3D7_1125600

PF3D7_0301800	PF3D7_0523900	PF3D7_0713800	PF3D7_0905400	PF3D7_1019100	PF3D7_1126200
PF3D7_0302500	PF3D7_0525400	PF3D7_0714000	PF3D7_0905500	PF3D7_1019400	PF3D7_1127100
PF3D7_0303200	PF3D7_0526200	PF3D7_0716300	PF3D7_0907200	PF3D7_1019500	PF3D7_1128900
PF3D7_0305200	PF3D7_0526600	PF3D7_0717500	PF3D7_0907900	PF3D7_1021800	PF3D7_1129300
PF3D7_0305600	PF3D7_0527700	PF3D7_0717600	PF3D7_0908400	PF3D7_1022200	PF3D7_1132800
PF3D7_0306000	PF3D7_0528300	PF3D7_0718100	PF3D7_0908500	PF3D7_1022700	PF3D7_1133000
PF3D7_0308100	PF3D7_0529900	PF3D7_0718300	PF3D7_0911000	PF3D7_1022800	PF3D7_1133200
PF3D7_0312400	PF3D7_0530300	PF3D7_0720500	PF3D7_0911200	PF3D7_1023000	PF3D7_1133800
PF3D7_0314000	PF3D7_0532100	PF3D7_0720600	PF3D7_0911800	PF3D7_1023900	PF3D7_1135400
PF3D7_0314800	PF3D7_0601800	PF3D7_0721400	PF3D7_0914300	PF3D7_1024000	PF3D7_1135900
PF3D7_0319400	PF3D7_0604200	PF3D7_0722200	PF3D7_0915000	PF3D7_1027300	PF3D7_1136200
PF3D7_0320900	PF3D7_0607600	PF3D7_0724600	PF3D7_0916000	PF3D7_1028600	PF3D7_1136500
PF3D7_0321400	PF3D7_0609900	PF3D7_0725400	PF3D7_0916800	PF3D7_1028800	PF3D7_1138500
PF3D7_0324900	PF3D7_0610400	PF3D7_0725500	PF3D7_0918000	PF3D7_1029800	PF3D7_1139900
PF3D7_0404400	PF3D7_0611600	PF3D7_0727400	PF3D7_0919900	PF3D7_1030200	PF3D7_1140100
PF3D7_0405900	PF3D7_0612300	PF3D7_0728400	PF3D7_0922200	PF3D7_1031200	PF3D7_1140200
PF3D7_0407800	PF3D7_0612700	PF3D7_0801800	PF3D7_0924300	PF3D7_1031300	PF3D7_1142100
PF3D7_0408000	PF3D7_0613400	PF3D7_0802800	PF3D7_0924500	PF3D7_1033200	PF3D7_1142900
PF3D7_0409800	PF3D7_0613800	PF3D7_0803300	PF3D7_0925300	PF3D7_1033900	PF3D7_1143200
PF3D7_0410800	PF3D7_0614100	PF3D7_0803800	PF3D7_0926200	PF3D7_1034600	PF3D7_1143500
PF3D7_0413500	PF3D7_0615500	PF3D7_0805500	PF3D7_0926600	PF3D7_1035200	PF3D7_1145400
PF3D7_0414700	PF3D7_0616600	PF3D7_0806400	PF3D7_0927300	PF3D7_1035400	PF3D7_1202200
PF3D7_0416100	PF3D7_0617800	PF3D7_0809900	PF3D7_0927500	PF3D7_1035700	PF3D7_1203000
PF3D7_0416500	PF3D7_0618000	PF3D7_0810300	PF3D7_0930300	PF3D7_1035900	PF3D7_1205300
PF3D7_1206300	PF3D7_1321200	PF3D7_1368900	PF3D7_1457200	PF3D7_1252100	
PF3D7_1206800	PF3D7_1321500	PF3D7_1373500	PF3D7_1457900	PF3D7_1300100	
PF3D7_1207000	PF3D7_1322200	PF3D7_1401600	PF3D7_1459400	PF3D7_1303300	

PF3D7_1208900	PF3D7_1323700	PF3D7_1402200	PF3D7_1460600	PF3D7_1305000
PF3D7_1209900	PF3D7_1324100	PF3D7_1406800	PF3D7_1462700	PF3D7_1306000
PF3D7_1210100	PF3D7_1324900	PF3D7_1409300	PF3D7_1464400	PF3D7_1306300
PF3D7_1215000	PF3D7_1325700	PF3D7_1409400	PF3D7_1465000	PF3D7_1355800
PF3D7_1217500	PF3D7_1327400	PF3D7_1410400	PF3D7_1466300	PF3D7_1356100
PF3D7_1217800	PF3D7_1328100	PF3D7_1410700	PF3D7_1466400	PF3D7_1356300
PF3D7_1221100	PF3D7_1328200	PF3D7_1411100	PF3D7_1466500	PF3D7_1357000
PF3D7_1221300	PF3D7_1328300	PF3D7_1412000	PF3D7_1468100	PF3D7_1358700
PF3D7_1222300	PF3D7_1330400	PF3D7_1416200	PF3D7_1468200	PF3D7_1359700
PF3D7_1222700	PF3D7_1330500	PF3D7_1422200	PF3D7_1468500	PF3D7_1443100
PF3D7_1223000	PF3D7_1330700	PF3D7_1422500	PF3D7_1475000	PF3D7_1443300
PF3D7_1224100	PF3D7_1331700	PF3D7_1425300	PF3D7_1308800	PF3D7_1445000
PF3D7_1224500	PF3D7_1332300	PF3D7_1426700	PF3D7_1309200	PF3D7_1446600
PF3D7_1226600	PF3D7_1332600	PF3D7_1427700	PF3D7_1315300	PF3D7_1447100
PF3D7_1227000	PF3D7_1333700	PF3D7_1428000	PF3D7_1317000	PF3D7_1449100
PF3D7_1227600	PF3D7_1335100	PF3D7_1431400	PF3D7_1320100	PF3D7_1451300
PF3D7_1228600	PF3D7_1337700	PF3D7_1432200	PF3D7_1361900	PF3D7_1451700
PF3D7_1232600	PF3D7_1338700	PF3D7_1432300	PF3D7_1362000	PF3D7_1247500
PF3D7_1233300	PF3D7_1339700	PF3D7_1432900	PF3D7_1363900	PF3D7_1355100
PF3D7_1233600	PF3D7_1339900	PF3D7_1433400	PF3D7_1364100	PF3D7_1442400
PF3D7_1235200	PF3D7_1342100	PF3D7_1435200	PF3D7_1366500	PF3D7_1449200
PF3D7_1236900	PF3D7_1343000	PF3D7_1435800	PF3D7_1451800	
PF3D7_1237700	PF3D7_1343200	PF3D7_1436200	PF3D7_1452000	
PF3D7_1238000	PF3D7_1344200	PF3D7_1437000	PF3D7_1455600	
PF3D7_1238700	PF3D7_1344400	PF3D7_1437300	PF3D7_1456000	
PF3D7_1242500	PF3D7_1345500	PF3D7_1438400	PF3D7_1456800	
PF3D7_1242800	PF3D7_1346400	PF3D7_1439400	PF3D7_1306400	

PF3D7_1243000	PF3D7_1346900	PF3D7_1439600	PF3D7_1307600
PF3D7_1243600	PF3D7_1350600	PF3D7_1440100	PF3D7_1307900
PF3D7_1244700	PF3D7_1351700	PF3D7_1440700	PF3D7_1359800
PF3D7_1246200	PF3D7_1353600	PF3D7_1441200	PF3D7_1360800
PF3D7_1246400	PF3D7_1354900	PF3D7_1441600	PF3D7_1361700